

INFORMATION TO USERS

This manuscript has been reproduced from the microfilm master. UMI films the text directly from the original or copy submitted. Thus, some thesis and dissertation copies are in typewriter face, while others may be from any type of computer printer.

The quality of this reproduction is dependent upon the quality of the copy submitted. Broken or indistinct print, colored or poor quality illustrations and photographs, print bleedthrough, substandard margins, and improper alignment can adversely affect reproduction.

In the unlikely event that the author did not send UMI a complete manuscript and there are missing pages, these will be noted. Also, if unauthorized copyright material had to be removed, a note will indicate the deletion.

Oversize materials (e.g., maps, drawings, charts) are reproduced by sectioning the original, beginning at the upper left-hand corner and continuing from left to right in equal sections with small overlaps. Each original is also photographed in one exposure and is included in reduced form at the back of the book.

Photographs included in the original manuscript have been reproduced xerographically in this copy. Higher quality 6" x 9" black and white photographic prints are available for any photographs or illustrations appearing in this copy for an additional charge. Contact UMI directly to order.

UMI[®]

**Bell & Howell Information and Learning
300 North Zeeb Road, Ann Arbor, MI 48106-1346 USA
800-521-0600**

NOTE TO USERS

This reproduction is the best copy available.

UMI

A Calendering Model for Cross-Direction Control

by

Dariusz Włodzimierz Kawka

Department of Chemical Engineering

McGill University

Montreal

January 1998

**A thesis submitted to the Faculty of Graduate Studies and Research
in partial fulfillment of the requirements for the
degree of Doctor of Philosophy**

© D.W. Kawka, January 98



National Library
of Canada

Acquisitions and
Bibliographic Services

395 Wellington Street
Ottawa ON K1A 0N4
Canada

Bibliothèque nationale
du Canada

Acquisitions et
services bibliographiques

395, rue Wellington
Ottawa ON K1A 0N4
Canada

Your file *Votre référence*

Our file *Notre référence*

The author has granted a non-exclusive licence allowing the National Library of Canada to reproduce, loan, distribute or sell copies of this thesis in microform, paper or electronic formats.

The author retains ownership of the copyright in this thesis. Neither the thesis nor substantial extracts from it may be printed or otherwise reproduced without the author's permission.

L'auteur a accordé une licence non exclusive permettant à la Bibliothèque nationale du Canada de reproduire, prêter, distribuer ou vendre des copies de cette thèse sous la forme de microfiche/film, de reproduction sur papier ou sur format électronique.

L'auteur conserve la propriété du droit d'auteur qui protège cette thèse. Ni la thèse ni des extraits substantiels de celle-ci ne doivent être imprimés ou autrement reproduits sans son autorisation.

0-612-44473-2

Canada

ABSTRACT

A dynamic model of the calendering of paper which incorporates relationships for both roll local thermal deformation and the stress-strain behaviour of paper in and after the nip was developed, validated, then used to demonstrate its application to model predictive control of calendering. The experimental determination of the stress-strain behaviour of paper included documenting the effect of initial temperature and moisture content as well as process parameters, and was expressed as the in-nip calendering equation. The rheological behaviour of commercial newsprint made from thermomechanical pulp was found to be a strong nonlinear function of temperature and moisture content over the wide range of 20 to 80 °C and 1 to 14% moisture.

A simplified model for the transient local deformation of a calender roll in response to a local cross-machine (CD) control action was determined and validated against the previous complete numerical analysis solution for a variety of roll designs and thermal boundary conditions. This model, appropriate for use in real-time control, was shown to be effective in seeking a compromise between the conflicting CD control objectives of large roll deformation, fine CD resolution and fast control response time.

From the above two elements a dynamic model of the calendering process was developed by appropriate combination of the model of transient local calender roll deformation with the in-nip calendering equation used to estimate, at a specific CD position, in-nip strain from permanent strain. Use of the model shows that paper response to a control action is highly sensitive to local nip load and to temperature and moisture content of the paper. After validation with published measurements on an industrial calender, the effectiveness of this model for minimizing thickness nonuniformity in the CD dimension through implementation of model predictive control of calendering was demonstrated. For a multi-roll calender stack of industrial specifications this demonstration showed an impressive reduction in CD control response time through use of multi-step control action. This model opens the prospect of a significant industrial innovation through the introduction of model predictive control to the difficult problem of CD control of calendering.

Résumé

Un modèle dynamique du calandrage du papier, comprenant des équations à la fois pour la déformation thermique locale du rouleau et pour le comportement contrainte-déformation du papier à l'intérieur et à la sortie de la pince, a été développé, validé puis utilisé pour être appliqué à la commande prédictive du calandrage. La détermination expérimentale du comportement contrainte-déformation du papier comprend l'étude de l'influence des conditions initiales de température et d'humidité, et a été traduite dans l'équation de la pince de calandrage. Nous avons constaté que le comportement rhéologique de papier journal commercial fait de pâte thermomécanique est une fonction fortement non-linéaire de la température et de l'humidité, pour des températures variant de 20 à 80°C et des taux d'humidité de 1 à 14%.

Un modèle simplifié pour la déformation transitoire locale du rouleau de calandrage en réponse à une action de contrôle local dans le sens travers a été déterminé puis validé par rapport à la solution numérique complète pour plusieurs types de rouleaux et différentes conditions thermiques aux limites. Ce modèle, approprié pour un contrôle en sens travers et en temps réel, peut aider à trouver un compromis entre la déformation importante du rouleau, la haute résolution en sens travers et le temps de réponse rapide.

De ces deux éléments a été développé un modèle dynamique du procédé de calandrage, par la combinaison du modèle de déformation locale transitoire du rouleau de calandrage et de l'équation de la pince de calandrage utilisée pour estimer, à une position sens travers donnée, la déformation dans la pince en fonction de la déformation permanente. L'utilisation de ce modèle indique que la réponse du papier à une action de contrôle est très sensible à la force locale de la pince ainsi qu'à la température et l'humidité du papier. Après la validation par des mesures effectuées sur une calandre industrielle, l'efficacité de ce modèle pour minimiser la non-uniformité de l'épaisseur dans le sens travers par l'utilisation de commande prédictive a été prouvée. Pour une calandre à plusieurs rouleaux de spécifications industrielles, nous avons montré qu'il est possible d'obtenir une réduction impressionnante du temps de réponse pour le contrôle du sens travers grâce à une action de contrôle multi-pas. Ce modèle ouvre la voie à des améliorations industrielles significatives grâce à l'introduction d'une méthode de commande prédictive pour le difficile problème du contrôle du calandrage en sens travers.

ACKNOWLEDGMENTS

First, I would like to thank my advisors, Drs. R.H. Crotagino and W.J.M. Douglas, for their continued technical and financial support, without which this thesis would not have been possible.

I wish to thank the electronics and machine shop staffs at the Department of Chemical Engineering, McGill University, and at the Pulp and Paper Research Institute of Canada in Pointe Claire for their involvement in the design, manufacture and debugging of the complex experimental equipment. I also wish to thank Dr. R. Vyse from Mesaruex Corp. for his help in arranging a loan of the induction heaters.

I would like to acknowledge role of my colleagues and friends for their moral support and encouragement: A. Bieniasiewicz, J.P. Bernie, J.F. Bond, A. Boryniec, T.C. Browne, M. Dixit, C. Dolan, Mr. J. Dumont, J. Hamel, S.J. Hashemi, Irena and Witold Machejko, the Miskurka family, T. Murray, the Pienkowski family, M. van Spall, B. Stone.

Not to be forgotten, I would like to thank my parents and my wife, Dorota, for their moral support and understanding during this part of our life. Without them I would not have been able to complete this project.

I would like to thank all the people who had direct or indirect involvement in the completion of this research project. Hopefully, I have not omitted anyone; if I have, please accept my apologies.

FIGURES

<u>Figure 2.1:</u>	CD caliper control system on calender, induction heaters.	6
<u>Figure 2.2:</u>	Definition of characteristic width of roll deformation, W_{dr}	22
<u>Figure 2.3:</u>	Comparison of results: heated rolls with heating and cooling control jets	
	a) Effect of roll radius and shell thickness on peak roll deformation	
	b) Effect of roll radius and shell thickness on deformation time constant	
	Data: numerical simulation of Journeaux [42]	23
<u>Figure 3.1:</u>	Preconditioning rewinding enclosure.	27
<u>Figure 3.2:</u>	Paper sorption and desorption	28
<u>Figure 3.3:</u>	Facility for conditioned air.	32
<u>Figure 3.4:</u>	Steam flow control.	33
<u>Figure 3.5:</u>	Controlled environment calender.	35
<u>Figure 3.6:</u>	Overall view of the experimental calender	35
<u>Figure 3.7:</u>	Roll displacement sensors.	36
<u>Figure 3.8:</u>	On-line caliper gauge 296 mm after the nip.	37
<u>Figure 3.9:</u>	Induction heater and temperature sensors.	39
<u>Figure 3.10:</u>	Typical displacement sensor output (data from Exp.8 runs #e (with paper) and #0e (without paper)).	44
<u>Figure 3.11:</u>	Effect of air temperature and humidity on paper temperature and moisture content.	47
<u>Figure 3.12a:</u>	Air temperature during preconditioning, nominal air temperatures of 40, 60 and 80 °C. (data from Exp. 8, Exp. 13 and Exp. 14 - preconditioning)	48
<u>Figure 3.12b:</u>	Air relative humidity during preconditioning, nominal air humidity of 9.2, 32 (30) and 86%. (data from Exp.14 - preconditioning)	48
<u>Figure 3.12c:</u>	Paper speed during preconditioning. (data from Exp.14 - preconditioning)	49
<u>Figure 3.13:</u>	Displacement sensor output, "long experiment" for the paper and roll temperature 40 °C. $V=90$ m/min, $L=95$ kN/m. $t=20$ min (data from Exp.8 runs 0b and 0b' - before and after the whole experiment)	51
<u>Figure 3.14:</u>	Displacement sensor output, "short experiment" for paper and roll temperature 40 °C. $V=90$ m/min, $L=95$ kN/m. $t=8$ min. (data from Exp.8 runs #0a and #0e)	52
<u>Figure 3.15:</u>	Paper thickness profile before and after calendering. (data from Exp.25 run #h)	55

<u>Figure 3.16a:</u>	Paper temperature profiles. nominal temperatures of 30, 40, 50 and 80 °C. (data from Exp.8 run #e, Exp.13 run #f, Exp.14 run #e and Exp.24 run #m)	56
<u>Figure 3.16b:</u>	Paper moisture content profiles. nominal moisture contents of 2, 6 and 12% (data from Exp.8 run #e, Exp.14 run #f and Exp.25 run #m)	56
<u>Figure 4.1:</u>	Experimental combinations of paper temperature and moisture content.	58
<u>Figure 4.2:</u>	Combinations of calendering variables for 760 experiments	59
<u>Figure 4.3:</u>	SYSTAT estimates of paper strain.	62
<u>Figure 4.4:</u>	Residual error-paper strain relation.	63
<u>Figure 4.5:</u>	Residual error-calendering parameter relations for initial bulk, line load, and speed	64
<u>Figure 4.6:</u>	Residual error-calendering parameter relations for roll radius, sheet temperature and moisture content.	65
<u>Figure 4.7:</u>	Effect of load on strain: $Bi= 2.22 \text{ cm}^3/\text{g}$, $R= 0.355 \text{ m}$, $M= 4.1\%$, $\Theta= 24.5 \text{ }^\circ\text{C}$, all speeds	66
<u>Figure 4.8:</u>	Effect of load on strain: $Bi= 2.33 \text{ cm}^3/\text{g}$, $R= 0.355 \text{ m}$, $M= 12.5\%$, $\Theta= 24.9 \text{ }^\circ\text{C}$, all speeds.	66
<u>Figure 4.9:</u>	Effect of load on strain: $Bi= 2.31 \text{ cm}^3/\text{g}$, $R= 0.355 \text{ m}$, $M= 7.8\%$, $\Theta= 21.7 \text{ }^\circ\text{C}$, all speeds.	67
<u>Figure 4.10:</u>	Effect of load on strain: $Bi= 2.39 \text{ cm}^3/\text{g}$, $R= 0.355 \text{ m}$, $M= 13.7\%$, $\Theta= 24.1 \text{ }^\circ\text{C}$, all speeds.	67
<u>Figure 4.11:</u>	Effect of load on strain: $Bi= 2.23 \text{ cm}^3/\text{g}$, $R= 0.355 \text{ m}$, $M= 2.1\%$, $\Theta= 27.3 \text{ }^\circ\text{C}$, all speeds.	68
<u>Figure 4.12:</u>	Effect of load on strain: $Bi= 2.23 \text{ cm}^3/\text{g}$, $R= 0.355 \text{ m}$, $M= 1.8\%$, $\Theta= 30.1 \text{ }^\circ\text{C}$, all speeds.	68
<u>Figure 4.13:</u>	Effect of load on strain: $Bi= 2.34 \text{ cm}^3/\text{g}$, $R= 0.355 \text{ m}$, $M= 9.0\%$, $\Theta= 28.1 \text{ }^\circ\text{C}$, all speeds.	69
<u>Figure 4.14:</u>	Effect of load on strain: $Bi= 2.27 \text{ cm}^3/\text{g}$, $R= 0.355 \text{ m}$, $M= 5.2\%$, $\Theta= 38.8 \text{ }^\circ\text{C}$, all speeds.	69
<u>Figure 4.15:</u>	Effect of load on strain: $Bi= 2.28 \text{ cm}^3/\text{g}$, $R= 0.355 \text{ m}$, $M= 1.9\%$, $\Theta= 48.4 \text{ }^\circ\text{C}$, all speeds.	70
<u>Figure 4.16:</u>	Effect of load on strain: $Bi= 2.30 \text{ cm}^3/\text{g}$, $R= 0.355 \text{ m}$, $M= 6.4\%$, $\Theta= 46.3 \text{ }^\circ\text{C}$, all speeds.	70
<u>Figure 4.17:</u>	Effect of load on strain: $Bi= 2.29 \text{ cm}^3/\text{g}$, $R= 0.355 \text{ m}$, $M= 3.8\%$, $\Theta= 59.0 \text{ }^\circ\text{C}$, all speeds.	71
<u>Figure 4.18:</u>	Effect of load on strain: $Bi= 2.24 \text{ cm}^3/\text{g}$, $R= 0.355 \text{ m}$, $M= 1.6\%$, $\Theta= 49.3 \text{ }^\circ\text{C}$, $S= 300 \text{ m/min}$.	71
<u>Figure 4.19:</u>	Effect of load on strain: $Bi= 2.30 \text{ cm}^3/\text{g}$, $R= 0.355 \text{ m}$, $M= 1.3\%$, $\Theta= 73.4 \text{ }^\circ\text{C}$, all speeds.	72
<u>Figure 4.20:</u>	Effect of load on strain: $Bi= 2.28 \text{ cm}^3/\text{g}$, $R= 0.355 \text{ m}$, $M= 3.3\%$, $\Theta= 39.6 \text{ }^\circ\text{C}$, all speeds.	72

<u>Figure 4.21:</u>	Effect of load on strain: $Bi= 2.25 \text{ cm}^3/\text{g}$, $R= 0.355 \text{ m}$, $M= 7.0\%$, $\Theta= 29.0 \text{ }^\circ\text{C}$, all speeds.	73
<u>Figure 4.22:</u>	Effect of load on strain: $Bi= 2.3 \text{ cm}^3/\text{g}$, $R= 0.355 \text{ m}$. $M= 10.3\%$, $\Theta= 25.9 \text{ }^\circ\text{C}$, all speeds.	73
<u>Figure 4.23:</u>	Effect of load on strain: $Bi= 2.17 \text{ cm}^3/\text{g}$, $R= 0.355 \text{ m}$, $M= 1.3\%$, $\Theta= 27.8 \text{ }^\circ\text{C}$, all speeds.	74
<u>Figure 4.24:</u>	Effect of load on strain: $Bi= 2.22 \text{ cm}^3/\text{g}$. $R= 0.355 \text{ m}$. $M= 4.5\%$, $\Theta= 27.6 \text{ }^\circ\text{C}$. all speeds.	74
<u>Figure 4.25:</u>	Effect of load on strain: $Bi= 2.22 \text{ cm}^3/\text{g}$, $R= 0.355 \text{ m}$. $M= 3.5\%$, $\Theta= 28.3 \text{ }^\circ\text{C}$. all speeds.	75
<u>Figure 4.26:</u>	Effect of load on strain: $Bi= 2.21 \text{ cm}^3/\text{g}$, $R= 0.355 \text{ m}$. $M= 1.3\%$, $\Theta= 47.3 \text{ }^\circ\text{C}$. all speeds.	75
<u>Figure 4.27:</u>	Effect of load on strain: $Bi= 2.29 \text{ cm}^3/\text{g}$, $R= 0.355 \text{ m}$. $M= 3.2\%$, $\Theta= 60.1 \text{ }^\circ\text{C}$. all speeds.	76
<u>Figure 4.28:</u>	Effect of load on strain: $Bi= 2.26 \text{ cm}^3/\text{g}$. $R= 0.355 \text{ m}$. $M= 4.9\%$. $\Theta= 45.9 \text{ }^\circ\text{C}$. all speeds.	76
<u>Figure 4.29:</u>	Effect of load on strain: $Bi= 2.30 \text{ cm}^3/\text{g}$. $R= 0.202 \text{ m}$. $M= 2.2\%$. $\Theta= 30.2 \text{ }^\circ\text{C}$. all speeds.	77
<u>Figure 4.30:</u>	Effect of load on strain: $Bi= 2.4 \text{ cm}^3/\text{g}$. $R= 0.202 \text{ m}$. $M= 11.8\%$, $\Theta= 30.6 \text{ }^\circ\text{C}$, all speeds.	77
<u>Figure 4.31:</u>	Effect of load on strain: $Bi= 2.28 \text{ cm}^3/\text{g}$, $R= 0.202 \text{ m}$, $M= 2.2\%$, $\Theta= 60.1 \text{ }^\circ\text{C}$, all speeds.	78
<u>Figure 4.32:</u>	Effect of load on strain: $Bi= 2.35 \text{ cm}^3/\text{g}$, $R= 0.202 \text{ m}$, $M= 8.4\%$, $\Theta= 31.7 \text{ }^\circ\text{C}$, all speeds.	78
<u>Figure 4.33:</u>	Effect of load on strain: $Bi= 2.22 \text{ cm}^3/\text{g}$, $R= 0.202 \text{ m}$. $M= 5.2\%$, $\Theta= 29.3 \text{ }^\circ\text{C}$. all speeds.	79
<u>Figure 4.34:</u>	Effect of load on strain: $Bi= 2.24 \text{ cm}^3/\text{g}$, $R= 0.202 \text{ m}$. $M= 2.6\%$, $\Theta= 32.6 \text{ }^\circ\text{C}$. all speeds.	79
<u>Figure 4.35:</u>	Effect of load on strain: $Bi= 2.30 \text{ cm}^3/\text{g}$. $R= 0.202 \text{ m}$. $M= 3.5\%$, $\Theta= 58.4 \text{ }^\circ\text{C}$, all speeds.	80
<u>Figure 4.36:</u>	Effect of load on strain. Best fit lines with upper and lower 95% confidence limits	80
<u>Figure 4.37:</u>	Effect of load on strain. Best fit lines with upper and lower 95% confidence limits	81
<u>Figure 4.38:</u>	Effect of load on strain. Best fit lines with upper and lower 95% confidence limits	81
<u>Figure 4.39:</u>	Effect of load on strain. Best fit lines with upper and lower 95% confidence limits	82
<u>Figure 4.40:</u>	Effect of load on strain. Best fit lines with upper and lower 95% confidence limits	82
<u>Figure 4.41:</u>	Effect of load on in-nip strain.	91
<u>Figure 4.42:</u>	Effect of load on in-nip strain.	92
<u>Figure 4.43:</u>	Effect of load on in-nip strain.	93

<u>Figure 4.44:</u>	Effect of load on in-nip strain.	94
<u>Figure 4.45:</u>	Effect of load on in-nip strain.	95
<u>Figure 4.46:</u>	Effect of load on in-nip strain.	96
<u>Figure 4.47:</u>	Effect of load on in-nip strain: $\Theta = \sim 21.8$ °C, M= ~7.8%, R= 0.355 m, all speeds.	98
<u>Figure 4.48:</u>	Effect of moisture content on thickness of uncalendered paper a) $\Theta = \sim 30$ °C b) $\Theta = \sim 40$ °C	102
<u>Figure 4.49:</u>	Effect of moisture content on thickness of uncalendered paper: $\Theta = \sim 60$ °C	103
<u>Figure 4.50:</u>	Effect of temperature on thickness of uncalendered paper: M= 1.8%	103
<u>Figure 4.51:</u>	Effect of temperature on thickness of uncalendered paper a) M= ~3.1% b) M= ~4.3%	104
<u>Figure 4.52:</u>	Effect of moisture content and line load on paper strain R= 0.355 m, $\Theta = 23.5$ °C, S= 90 m/min	107
<u>Figure 4.53:</u>	Effect of moisture content and line load on paper strain R= 0.355 m, $\Theta = 23.5$ °C, S= 180 m/min	108
<u>Figure 4.54:</u>	Effect of moisture content and line load on paper strain. R= 0.355 m, $\Theta = 23.5$ °C a) S= 500 m/min b) S= 900 m/min	109
<u>Figure 4.55:</u>	Effect of moisture content and line load on paper strain. R= 0.355 m, $\Theta = \sim 30$ °C a) S= 180 m/min b) S= 500 m/min	110
<u>Figure 4.56:</u>	Effect of moisture content and line load on paper strain. R= 0.202 m, $\Theta = \sim 30$ °C, S= 90 m/min	111
<u>Figure 4.57:</u>	Effect of moisture content and line load on paper strain. R= 0.202 m, $\Theta = \sim 30$ °C, S= 300 m/min	112
<u>Figure 4.58:</u>	Effect of temperature and line load on paper strain, R= 0.355 m, M= ~1.8% a) S= 90 m/min b) S= 500 m/min	113
<u>Figure 4.59:</u>	Effect of temperature and line load on paper strain, R= 0.355 m, M= ~4.1% a) S= 180 m/min b) S= 500 m/min	114

<u>Figure 4.60:</u>	Effect of paper moisture content on permanent strain at three levels of paper temperature, Crotogino and Pye data. Pulp and Paper Research Institute of Canada	115
<u>Figure 4.61:</u>	Effect of moisture content and load on paper in-nip strain. all speeds	
	a) $R= 0.355 \text{ m}$, $\Theta= \sim 48 \text{ }^\circ\text{C}$	
	b) $R= 0.202 \text{ m}$, $\Theta= \sim 60 \text{ }^\circ\text{C}$	117
<u>Figure 4.62</u>	Effect of moisture content on in-nip strain. $R= 0.356 \text{ m}$. $\Theta= 27 \text{ to } 30 \text{ }^\circ\text{C}$.	
	a) $L= 20 \text{ kN/m}$. $S= 90 \text{ m/min}$	
	b) $L= 40 \text{ kN/m}$. all speeds	120
<u>Figure 4.63:</u>	Effect of moisture content on in-nip strain, $R= 0.202 \text{ m}$. $\Theta= 29 \text{ to } 32 \text{ }^\circ\text{C}$, all speeds.	
	a) $L= 40 \text{ kN/m}$	
	b) $L= 95 \text{ kN/m}$	121
<u>Figure 4.64:</u>	Effect of moisture content on in-nip strain, $R= 0.202 \text{ m}$. $L= 210 \text{ kN/m}$. $\Theta= 29 \text{ to } 32 \text{ }^\circ\text{C}$, all speeds.	122
<u>Figure 4.65:</u>	Effect of temperature on in-nip strain. $R= 0.356 \text{ m}$. $L= 135 \text{ kN/m}$. $M= 1.1 \text{ to } 2.2 \%$. all speeds.	122
<u>Figure 4.69:</u>	Effect of line load on density ratio, $R= 0.356 \text{ m}$. all speeds	
	a) $\Theta= 38.8 \text{ }^\circ\text{C}$, $M= 5.2\%$	
	b) $\Theta= 73.4 \text{ }^\circ\text{C}$, $M= 1.3\%$	127
<u>Figure 4.70:</u>	Effect of line load on density ratio, $R= 0.202 \text{ m}$. all speeds	
	a) $\Theta= 29.5 \text{ }^\circ\text{C}$, $M= 5.2\%$	
	b) $\Theta= 30.6 \text{ }^\circ\text{C}$, $M= 11.8\%$	128
<u>Figure 4.71:</u>	SYSTAT estimates of the permanent paper strain: Master creep equation	133
<u>Figure 4.72:</u>	Residual error vs. permanent strain: Master creep equation	133
<u>Figure 4.73:</u>	SYSTAT estimates of the in-nip paper strain: Master creep equation	134
<u>Figure 4.74:</u>	Residual error vs. in-nip strain: Master creep equation	134
<u>Figure 4.75:</u>	Effect of line load on strain, all speeds. Master creep and calendering equations	137
<u>Figure 4.76:</u>	Effect of line load on strain, all speeds. Master creep and calendering equations	138
<u>Figure 4.77:</u>	Effect of line load on strain, all speeds. Master creep and calendering equations	139
<u>Figure 4.78:</u>	Effect of line load on strain, all speeds. Master creep and calendering equations	140
<u>Figure 4.79:</u>	Effect of line load on strain, all speeds. Master creep and calendering equations	141

<u>Figure 4.80:</u>	Relationship between permanent and in-nip strain a) $\Theta = 25$ to 33 °C, all loads and moisture contents b) $M = 1.3$ to 2.3% , all loads and temperatures	147
<u>Figure 5.1:</u>	Effect of roll geometry on peak roll deformation Data: numerical simulation of Journeaux [42] Lines: Equations 5.2 and 5.3	155
<u>Figure 5.2:</u>	Effect of roll geometry on characteristic deformation width Data: numerical simulation of Journeaux [42] Lines: Equations 5.4 and 5.5	158
<u>Figure 5.3:</u>	Effect of roll geometry on deformation index Lines: Equations 5.7 and 5.8	161
<u>Figure 5.4:</u>	Effect of roll geometry on deformation time constant Data: numerical simulation of Journeaux [42] Lines: Equations 5.9 and 5.10	163
<u>Figure 5.5a:</u>	Effect of roll geometry on $(\Delta r_{\text{peak}})_{\text{heated}} / (\Delta r_{\text{peak}})_{\text{unheated}}$	165
<u>Figure 5.5b:</u>	Effect of roll geometry on $(I_D)_{\text{heated}} / (I_D)_{\text{unheated}}$	165
<u>Figure 5.5c:</u>	Effect of roll geometry on $\tau_{\text{heated}} / \tau_{\text{unheated}}$	165
<u>Figure 5.6:</u>	Local roll deformation for unheated rolls a) simulation results, present study b) numerical results, Journeaux [42]	167
<u>Figure 5.7:</u>	Local roll deformation for heated rolls a) simulation results, present study b) numerical results, Journeaux [42]	168
<u>Figure 5.8:</u>	Local roll deformation for unheated and heated rolls after 10 minutes a) simulation results, present study b) numerical results, Journeaux [42]	173
<u>Figure 6.1:</u>	Simulation of multi-nip calendering	179
<u>Figure 6.2:</u>	Procedure for simulation of multi-nip calendering	181
<u>Figure 6.3:</u>	Effect of initial nip load on paper response: single nip control action $L = 25$ to 210 kN/m, $\Theta = 30$ °C, $M = 8\%$, other parameters as listed in Table 6.1.	186
<u>Figure 6.4:</u>	Effect of initial nip load on paper response after 25 minutes: single nip control action. $L = 25$ to 210 kN/m, $\Theta = 30$ °C, $M = 8\%$, other parameters as listed in Table 6.1.	187
<u>Figure 6.5:</u>	Effect of moisture content on paper response: single nip control action. $L = 65$ kN/m, $\Theta = 30$ °C, $M = 2$ to 12% , other parameters as listed in Table 6.1.	188

<u>Figure 6.6:</u>	Effect of moisture content and temperature on paper response after 25 minutes: single nip control action. a) $\Theta = 30\text{ }^{\circ}\text{C}$, $M = 2$ to 12% , b) $\Theta = 30$ to $80\text{ }^{\circ}\text{C}$, $M = 2\%$, $L = 65\text{ kN/m}$, other parameters as listed in Table 6.1.	189
<u>Figure 6.7:</u>	Effect of temperature on paper response: single nip control action $L = 65\text{ kN/m}$, $\Theta = 30$ to $80\text{ }^{\circ}\text{C}$, $M = 2\%$, other parameters as listed in Table 6.1.	190
<u>Figure 6.8:</u>	Effect of temperature and moisture content on paper response: single nip control action. $L = 65\text{ kN/m}$, $\Theta = 50\text{ }^{\circ}\text{C}$, $M = 6$ to 10% , other parameters as listed in Table 6.1.	192
<u>Figure 6.9:</u>	Comparison of single and two-step actuator change on speed of paper response: single nip control action $L = 65\text{ kN/m}$, $\Theta = 50\text{ }^{\circ}\text{C}$, $M = 6\%$, other parameters as listed in Table 6.1.	194
<u>Figure 6.10:</u>	Single calender stack for simulation	197
<u>Figure 6.11:</u>	Effect on final paper bulk of location of control actuator. Case 1	199
<u>Figure 6.12:</u>	Effect on final paper bulk of location of control actuator. Cases 2 and 3	201
<u>Figure 6.13:</u>	Measured and predicted effect of control actuator position: single stack a) simulation results, present study b) experimental results, industrial calender. Journeaux et al. [42, 43]	204
<u>Figure 6.14:</u>	Double calender stack for simulation	205
<u>Figure 6.15:</u>	Simulation of effectiveness of calendering: double calender stack	206
<u>Figure 6.16:</u>	Comparison of single and two-step actuator change on speed of paper response: single stack.	208

TABLES

<u>Table 3.1:</u>	Calendering conditions	46
<u>Table 4.1:</u>	In-nip coefficients for the calendering equation, present study.	83
<u>Table 4.2:</u>	In-nip coefficients for the calendering equation. Browne et al. [6, 7]	83
<u>Table 4.3:</u>	Permanent coefficients for the calendering equation, present study.	87
<u>Table 4.4:</u>	Permanent coefficients for the calendering equation, from Crotogino et al. (1, 2, 3) and Browne et al. (4)	87
<u>Table 4.5:</u>	Calendering coefficients for narrower range of nip loads, present study. a) permanent coefficients b) in-nip coefficients	97
<u>Table 4.6:</u>	Distribution of data according to calendering equation upper limit, narrow and full data sets.	99
<u>Table 4.7:</u>	In-nip coefficients for the nonlinear portion of the calendering equation, 386 data points.	100
<u>Table 4.8:</u>	Parameters of correlation for uncalendered paper thickness. Equation 4.8.	105
<u>Table 4.9:</u>	In-nip coefficients for Equation 4.10.	123
<u>Table 4.10:</u>	In-nip coefficients for Equation 4.10 modified with Equation 4.11	124
<u>Table 4.11:</u>	In-nip calendering coefficients, Experiments 8 to 30 a) the calendering equation b) Equation 4.10	125
<u>Table 4.12:</u>	In-nip coefficients for Equation 4.12.	126
<u>Table 4.13:</u>	Permanent coefficients for the master creep equation, present study.	131
<u>Table 4.14:</u>	Permanent coefficients for the master creep equation a) Colley and Peel (1) and Kerekes (2) b) Browne et al.	131
<u>Table 4.15:</u>	In-nip coefficients for the master creep equation, present study.	132
<u>Table 4.16:</u>	In-nip coefficients for the master creep equation a) Colley and Peel b) Browne et al.	132
<u>Table 4.17:</u>	Permanent coefficients for the master creep equation, $\rho_{p_max} = 1.32 \text{ g/cm}^3$.	143
<u>Table 4.18:</u>	Coefficients for Equation 4.19 a) present study a) Browne et al. data	145

<u>Table 4.19</u>	Coefficients for Equation 4.20	146
<u>Table 5.1:</u>	Coefficients for Equation 5.2, unheated rolls	156
<u>Table 5.2:</u>	Coefficients for Equation 5.3, internally heated rolls	157
<u>Table 5.3:</u>	Coefficients for Equation 5.10, internally heated rolls	159
<u>Table 5.4:</u>	Coefficients for Equation 5.15, internally heated rolls	163
<u>Table 6.1:</u>	Parameters for simulation of single-nip calendering	185
<u>Table 6.2:</u>	Parameters for single calender stack simulation, Case 1.	197
<u>Table 6.3:</u>	Parameters for single calender stack simulation, Cases 2 and 3.	200
<u>Table A1.1:</u>	Paper sorption and desorption, TMP newsprint	224
<u>Table A1.2:</u>	Command log input to SYSTAT, calendering equation	226
<u>Table A1.3:</u>	SYSTAT output, calendering equation	227
<u>Table A1.4:</u>	Experimental results: TMP newsprint	228

NOMENCLATURE

The number in parentheses gives the Chapter where the variable is defined.

a	Curve fitting coefficient (2.3)
a_0, a_r	Coefficients for peak deformation equation, heated roll (5.2)
a_0, a_{s1}, a_{s2}, a_t	Coefficients for peak deformation equation, unheated roll (5.2)
$a_{M2n}, a_{M20}, a_{MIL}, a_{M\Theta}$	Coefficients for modified calendering equation (4.4)
$A_2, a_{02}, a_{L2}, a_{S2},$	Coefficients for density equation (4.4)
$a_{R2}, a_{M2}, a_{\Theta2}$	Coefficients for density equation (4.4)
$A_{ij} - a_{ij}$	Calendering equation coefficients (2.3)
	Subscript:
	i : O offset, L load, S speed, R radius, Θ temperature.
	M moisture content, P pressure, t time
	j : n in-nip, p permanent
b_0, b_{S1}, b_{S2}, b_r	Coefficients for deformation time constant equation (5.4)
B_i	Initial bulk, cm^3/g (2.3)
B_n	In-nip bulk, cm^3/g (2.3)
B_p	Permanent bulk, cm^3/g (2.3)
BW	Basis weight, g/m^2 (6.2)
c	Curve fitting coefficient (2.3)
C	Roll material property (2.5)
c_0, c_s	Coefficients for characteristic deformation width equation (5.3)
$c_\varepsilon, c_0, c_L, c_M, c_\Theta$	Curve fitting coefficients (4.6)
CD	Cross-machine direction (1)
d	Jet nozzle diameter, mm (5.1.1)
E_m	Roll material property (2.4)
$E = \delta\sigma / \delta\varepsilon$	Young's modulus (2.3)
$F(\varepsilon)$	Shape factor (2.3)
i	Specific nip number, $i = 1, 2, \dots, n-1$ (6.2)
l_D	Calender control deformation index, $\text{mm}/\mu\text{m}$ (2.5)
k	Roll material property (2.5)
L	Line load, kN/m (2.3)
L_{avg}	Average line load, kN/m (6.2)
L_j	Initial local load for a specific nip, kN/m (6.2)
$L(t)$	Nip load profile, kN/m (6.2)
M	Paper moisture content, % (2.3)
M_{initial}	Initial moisture content of paper, % (6.2)
M_i	Local moisture content of paper entering each nip, % (6.2)
MD	Machine direction (1)
n	Number of rolls in the stack (6.2)
P_{line}	In-nip applied line pressure, MPa (2.3)
P	In-nip maximum pressure, Mpa (4.5)

r	Roll radius, mm (2.5)
r_p	Radial position (2.5)
r_i	Specific roll radius, mm (6.2)
R	Average roll radius, m (2.3)
$R\text{-squared}$	Coefficient of correlation (4.1)
s	Shell thickness, mm (2.5)
s_i	Specific shell thickness, mm (6.2)
s_r	Roll stress (2.5)
S	Calendering speed, m/min (2.3)
S_j	Jet-to-jet separation, mm (5.1.1)
$S.E.$	Standard error (4.1)
t	Dwell time, sec (4.5)
t_i	Uncalendered paper caliper, μm (4.2)
t_0, t_M, t_Θ	Coefficients for uncalendered paper caliper equation (4.2)
T	Total data acquisition time, s (3.2)
TMP	Thermo-mechanical pulp (1)
u, u_0	Upper roll average position, μm (3.2)
u_r, u_z	Radial and axial roll displacements, μm (2.5)
v, v_0	Lower roll average position, μm (3.2)
$W_{\Delta r}$	Characteristic width of deformation, mm (2.5)
W	Sheet width, m (6.2)
z	Roll axial position (2.5)
α	Roll material property (2.5)
Δr_{peak}	Peak roll deformation at steady state, μm (2.5)
$\Delta r(t)$	Transient roll deformation, μm (2.5)
ϵ_n	In-nip strain (2.3)
$\epsilon_n(t)$	In-nip strain after control (6.2)
ϵ_{n0}	Initial in-nip strain (6.2)
ϵ_p	Permanent strain (2.3)
$\epsilon_{rr}, \epsilon_{zz}, \epsilon_{qq}, \epsilon_{rz}$	Roll strain (2.5)
Θ	Temperature, $^{\circ}\text{C}$ (2.3)
Θ_i	Local paper temperature entering each nip, $^{\circ}\text{C}$ (6.2)
Θ_{initial}	Initial paper temperature, $^{\circ}\text{C}$ (6.2)
$\Theta(r_p, z, t)$	Temperature distribution within the roll, $^{\circ}\text{C}$ (2.5)
μ_2	Nip intensity for density equation (4.4)
μ_n	In-nip calendering intensity (2.3)
μ_p	Permanent calendering intensity (2.3)
μ_n	In-nip calendering intensity without load term (6.2)
v_m	Roll material property (2.5)
ρ	Paper density, q/cm^3 (4.4)
ρ_i	Initial paper density, q/cm^3 (4.5)
$\rho_n, \rho_{\text{max}}$	Maximum in-nip and permanent paper density, q/cm^3 (4.5)
τ	Deformation time constant, min (2.5)

Table of Contents

Acknowledgments	
Abstract	
Resume	
Figures	
Tables	
Nomenclature	
1. Introduction	1
2. Literature review	
2.1 Control of the calendering process	4
2.2 Factors involved in a model of calendering	9
2.3 Stress-strain behaviour of paper during and after calendering	10
2.4 Heat transfer aspect of a model	18
2.5 Local temperature and thermal expansion of a calender roll	19
2.6 Summary	24
3. Experimental procedure and equipment	
3.1 Overall mechanical design	26
3.1.1 Preconditioning and rewinding enclosure	27
3.1.2 Facility for controlling air humidity and temperature	31
3.1.3 Controlled environment calender	34
3.2 Data acquisition and processing systems	42
3.3 Experimental conditions	46
4. Experimental results	58
4.1 The calendering equations	59
4.1.1 Effect of nip load on radius and load coefficients	89
4.2 Effect of moisture content and temperature on uncalendered paper thickness	100
4.3 Effect of moisture content and temperature on paper strain	105
4.4 Modified calendering equation	118
4.5 Master creep equation	129
4.6 Relationship between permanent and in-nip strain	144
4.7 Conclusions	148

5.	Thermal deformation of the calender roll	
5.1	Transient and steady state local heat transfer and roll deformation	150
	5.1.1 Introduction	150
	5.1.2 Factors governing roll thermal differentiation	152
5.2	Peak roll deformation at steady state	154
5.3	Width of roll deformation at steady state	157
5.4	Roll deformation index	159
5.5	Roll deformation time constant	162
5.6	Comparison of unheated and heated calender rolls	164
5.7	Simulation of dynamic roll deformation	166
5.8	Conclusions	175
6.	Simulation of the calendering process	
6.1	Introduction	177
6.2	Calculation procedure for simulation of calendering	180
6.3	Simulation of single nip calendering	185
	6.3.1 Effect of calendering parameters on control response	185
	6.3.2 Model predictive control: Single nip calendering	193
6.4	Simulation of multi-nip calendering	195
	6.4.1 Single calender stack	195
	6.4.2 Double calender stack	205
	6.4.3 Model predictive control: Multi-nip calendering	207
6.5	Summary and conclusions	208
7.	Conclusions	
7.1	Contributions to knowledge	211
7.2	Suggestions for future study	214
	References	216
	Appendixes	
A1	Raw data and results of non-linear regression analysis	223
A2	Computer program for data acquisition and control: facility for controlled air temperature and humidity and preconditioning chamber	245
A3	Computer program for data acquisition and control: environment controlled calender	264

1 Introduction

Uniformity of paper thickness and surface properties is a key factor determining the end-use performance of paper. Nonuniformity in sheet thickness causes variation in reel hardness, and thus problems with roll structure during the winding process as well as when paper is rewound and cut into narrow rolls. Those variations are also the major source of sheet breaks in printing presses, causing loss of production. Lack of uniformity in surface properties, roughness and gloss, which are often related to paper thickness variations, lead to nonuniform quality of images printed on paper.

Calendering is for many grades of paper the final papermaking operation, and thus the last processing step where nonuniformity of paper properties can be controlled both in its direction of travel in the paper machine, the machine direction (MD), and in the direction across the width of the machine, the cross-machine direction (CD).

A calender is effectively a rolling mill, a vertical stack of two or more cast iron rolls machined to a very high quality of uniformity. The rough and bulky paper, product of the preceding steps in the papermaking process enters the top calender nip and proceeds down through successive nips between each pair of rolls in the stack. High pressure imposed on the paper in these nips permanently deforms the wood fibres both on the surface and inside the paper, reducing sheet roughness and thickness. Passing from top to bottom of the calender the sheet becomes progressively thinner and smoother, which improves the quality of the end product. Sheet thickness is typically reduced by about 30 to 60% in calendering.

Improvement in the uniformity of paper properties in the CD dimension is achieved by adjustment in local nip load and/or temperature distribution. MD variation, usually changing slowly, is controlled by altering the average calendering load using rolls with hot water circulation, variable crown or selective hydraulic loading adjustment. The response action in this type of control is quick, so real-time MD calender control is straightforward.

The much more difficult reduction in nonuniformity of paper thickness in the CD dimension is accomplished by adjustment in local roll radius, and consequently the CD profile of local nip load on the paper by manipulating the CD profile of local roll temperature [16, 38, 53, 58, 63]. Arrays of locally adjustable impinging air jets, induction coils or infrared heaters are used as the control actuators to change local roll temperature, thereby changing local nip load and the extent of compression of the paper. Because the reaction time for thermal control is relatively long while sheet speed is high, the difficult challenge in CD control of calendering is to minimize the delay in control action.

CD variation in paper temperature and moisture content from conditions of the drying process affect not only the rheological properties of the paper but also the CD profile of roll surface temperature. Varying roll temperature alters the local roll diameter, and thus the CD distribution of local nip pressure which controls thickness reduction in the nip. Nip load along with roll radius and machine speed define the magnitude and duration of the pressure pulse in the nip, while the properties of paper determine its response to this pulse. Physical problems related to CD control include calender roll grinding accuracy, crowning, roll deflection and wear.

The complex interaction of calendering parameters, control variables and their effect on the thickness profile have been understood qualitatively by calender operators who first used manual control, now commonly closed-loop control, to adjust the CD profiling system. Current practice is to use closed-loop automatic CD control of the paper thickness profile and thus of reel building, thereby reducing system response time, improving paper quality, increasing productivity and minimizing waste. Accurate paper thickness sensors, fast signal processing and more powerful actuator systems of better CD resolution led to improved CD control systems.

As for the system being controlled, by far the slowest element to respond to change is the calender itself because of the high thermal inertia of the heavy rolls. For systems difficult to control through having elements of greatly divergent time constants, an approach intrinsically superior to feedback control is model predictive control, which can allow for the dynamic response of the calender. However use of model predictive control

requires a precise description of the system behaviour, which in this case means of what occurs in the nip of the calender. Determination of that description of the behaviour of paper in the nip of a calender in order to construct a model predictive control of calendering has been the goal of two preceding theses, Journeaux [42] and Browne [7], and of the present thesis.

In the first stage Journeaux [42] focused on relationship between thermal roll deformation, resulting from heat transfer provided by an actuator system, and the CD radius profile, which was obtained for a variety of roll designs and thermal boundary conditions. Next, Browne [7] determined the permanent and in-nip CD local thickness reduction as a function of the local calendering variables, that is, contributed the in-nip calendering equation. However, this was done only for the ambient conditions of two key variables, paper temperature and moisture content.

The permanent and in-nip versions of the calendering equation allow calculation of the desired local load distribution, corresponding to a local roll deformation. Availability of an in-nip calendering equation enables calculation of the control response to a local change in paper thickness as a function of local thermal deformation of the calender roll. However, in order that this can be done over the range of industrially relevant conditions requires that the in-nip calendering equation incorporate the effects of paper temperature and moisture content.

The objective of the present step of the project is to determine the effect of paper temperature and moisture content on the in-nip behaviour of paper, to assemble the existing information into a comprehensive dynamic model and to demonstrate the use of this knowledge in the CD control of calendering by model predictive control. Achieving this objective involved the design and construction of a controlled environment calendering facility, a modified version of the equipment used in the second stage of the project. An extensive experimental program was required for the measurement of in-nip paper thickness under wide ranging calendering conditions. Development and testing of a comprehensive dynamic simulation for model predictive control completed the present work.

2 Literature review

2.1 Control of the calendering process

Paper thickness reduction in the nip of a calender is affected primarily by nip load, machine speed, roll diameter, paper and calender roll temperature, paper moisture content and initial bulk (specific volume). Crotagino [15] compiled a comprehensive review of the parameters affecting calendering. Nip load is the most effective parameter for calendering paper. The thickness reduction that accompanies increasing nip load also increases paper surface smoothness and gloss but may decrease paper strength. Temperature, the second most effective parameter, makes the paper web more plastically deformable and pliable, so paper structure is more predisposed to change. Similarly, increasing its moisture content makes paper more sensitive to calendering. However, moisture content higher than 15 to 20% can result in calendering blackening. Moreover, only up to about this level of moisture content, depending on temperature, does permanent deformation increase with paper moisture content. High temperature and moisture content also increase paper sensitivity to disturbances such as temperature and moisture streaks. On the other hand higher paper temperature or/and moisture content allows a specific calendering effect to be achieved at a lower nip load with correspondingly reduced loss in paper strength. The initial bulk describes the potential for compression of the paper up to the limit beyond which no further bulk reduction is possible. Passing through successive nips from top to bottom of the calender stack the web becomes thinner and more resistant to further compression. Roll diameter affects the length and surface area of the nip, which thereby alters the calendering dwell time and the distribution of nip load. Machine speed likewise affects calendering through controlling the dwell time in the nip.

A typical paper machine calender consists of a vertical stack of from two to eight chill cast iron rolls. Roll diameters vary from approximately 300 mm for old paper machines to 800 mm for modern, fast machines. The pressure in the nip, or the nip load, that is provided by the gravity loading from the weight of the rolls may be augmented or relieved at intermediate positions in the stack. The great variety of types of rolls used in

industrial calenders can be divided into three major groups, i.e. solid rolls, heat transfer rolls, and variable crown rolls.

The solid rolls used on older calender stacks are not common in newer installations. The only advantage, the higher nip load associated with the weight of these rolls, has become a disadvantage with the larger roll diameters used in newer calenders where the weight of solid rolls can be excessive. Consequently solid rolls in existing calender stacks are being replaced by heat transfer or variable crown rolls.

Heat transfer rolls are internally heated to promote bulk and roughness reduction of paper. The simplest design is the center-bored roll with steam passing through the core as the heating fluid. Typically the heat transfer rate for this type of roll is relatively low, a consequence of the limited internal area available for heat transfer with the thick shell. On modern calender stacks this type of design is being replaced by the more sophisticated double walled and peripherally bored rolls. The advantage of these rolls is their much larger internal heat transfer area and thinner effective shell thickness, both of which increase the heat transfer rate. The heating fluid, most typically pressurised hot water, is passed through the heating channel at high velocity, ensuring an axially uniform temperature profile.

Variable crown rolls typically consist of hollow shells supported across the entire width of the roll on hydraulic or hydrostatic bearing systems. Externally applied force is transferred through the shell and the hydraulic support elements to the stationary central beam. This design allows compensation for the tendency of the bottom roll, the king roll, to sag under its own weight and that of the roll above it. Another application for the variable crown roll is to use additional load applied through its bearing housings in order to prevent roll bending. The several designs of variable crown roll differ primarily in the choice of internal hydraulic loading system.

A type not considered here is the soft calender roll. Although this version of roll was developed originally for off-line super calenders or gloss calenders, recently it is being used increasingly for on-machine, temperature gradient calendering. Synthetic polymers,

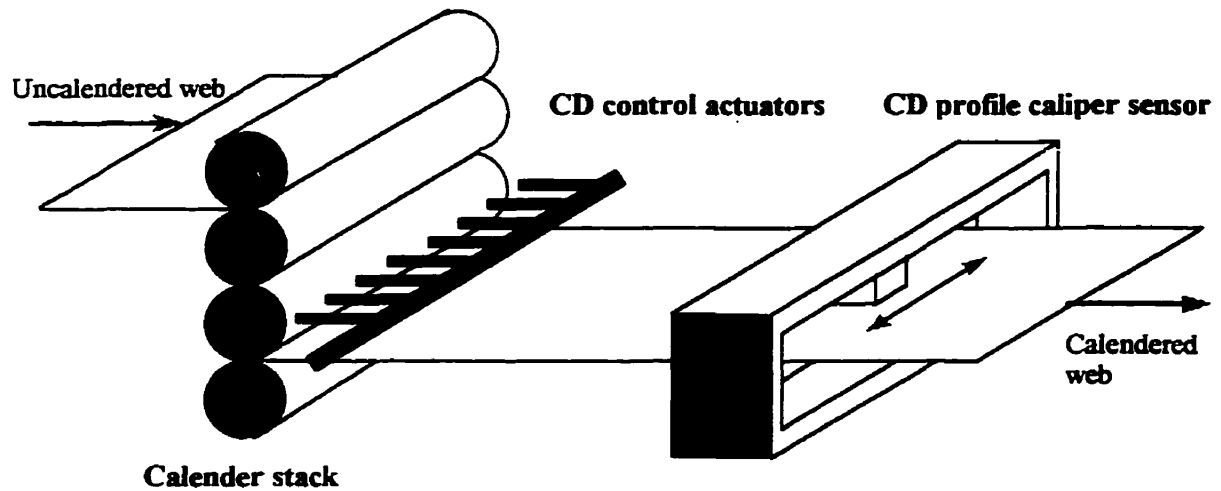


Figure 2.1: Calender CD caliper control system with impingement air jets

rubber or paper under extremely high radial compression is used as the soft cover for the roll.

The actuator systems most commonly used to control the local variation in CD paper thickness profile are air showers and induction heaters, with the latter being the predominant industrial practice now. Arrays of air jets or induction pads placed along the width of calender rolls constitute the calendering control elements, Figure 2.1. Development of precise, continuous and direct on-line thickness measurement enabled introduction of automatic CD control of calendering. Caliper sensors with fast signal processing and very good resolution, $\pm 1 \mu\text{m}$, are interfaced with the actuator systems through a process control computer [20]. CD control system architecture now captures snapshots of the raw sensor data and position of the measurement scanner head for sending to the profile transformation module using a high speed serial link. The high speed of the data processing and of the inner control loops of the scanner system now enables

high resolution of spatially-aligned profiles from up to 480 measurement zones, a significant increase from the 60 zones of older systems [69]. The larger sample allows more precise alignment of the CD profile, which in turn permits identification and elimination of previously invisible process problems, i.e. fine streaks.

This high resolution data link permits adoption of advanced profile processing and control techniques. Thus adaptive profile estimation can be used to identify the persistent CD high-resolution profile by eliminating short term variation, usually measurement noise. This uncontrollable variation is eliminated by digital filtration schemes. Use of non-linear, adaptive controllers allows fast and precise control of paper thickness, with faster recovery after upsets and breaks. Profile transformation algorithms allow for precise alignment of actuator position with the profiles. The power of inductive heating systems has been doubled from about 2 to 4 kW/zone while the width of control zones has been reduced from 120 mm to 75 mm [53]. Journeaux [42] show that axial heat conduction in the roll makes this 75 mm wide control zone the narrowest achievable control of roll deformation. These high power heating systems allow raising the roll temperature from 40 to 60 °C , with resulting local roll deformation being up to 15 µm at steady state [42, 52]. To further enhance the effectiveness of CD control of calendering, a heating/cooling control can be exercised on more than one roll, thus giving more control over final uniformity of CD thickness profile.

Closed-loop feedback control is the strategy currently used in CD sheet thickness profiling. When the controlled variable, paper caliper as measured after calendering by a traversing sensor, starts deviating from the set-point the error signal generated initiates corrective action regardless of the source or type of disturbance. However the calender is so massive that it requires 10 to 30 minutes to react. With the high speed of modern paper machines, up to 1500 m/min, feedback control of calendering requires either excessive time to settle if a strong control action is used to minimize the time that the local caliper is off specification, or else allows extended time off specification if a restrained control action is used to avoid overshooting. Although new CD control systems provide a significant reduction of

this response time, with reduced overshooting, corrective action still requires 8 to 10 minutes [37, 69].

A 9 meter wide newsprint machine running at 1100 m/min produces about 30 tonnes/hour; if the control system requires 10 minutes to arrive at 95% of the target variation, about 5 tonnes of substandard paper will have been made. Two possibilities for improved control system response are: reduction in response time by reducing roll thermal inertia or improvement in the effectiveness of the control action. The thermal inertia of calender rolls has already been reduced to the limit permitted by roll bending and other mechanical considerations. Improvement of control effectiveness requires the ability to predict the future behaviour of the system in response to various process and control variables.

Model predictive control (MPC) is an advanced control strategy which uses an explicit dynamic model of the process to predict, based on past control outputs, the effect on the process output of future actions of the manipulated variable. The future moves of the manipulated variable are selected such that the predicted response has desired characteristics. The behaviour of the process is considered over a certain prediction horizon which is a design parameter that influences control system performance and is usually longer than any process time delay. One sampling period after the application of the current control action, the predicted response is compared with the actual response given by measure system. Using corrective feedback action for any errors between actual and predicted response, the entire sequence of calculation is then repeated at each sampling instant with the horizon moved by one time interval. The future outputs predicted by the internal dynamic model may be displayed to provide operator confidence in the effectiveness of the control system and to allow transparent on-line tuning. Corrective action is taken through automatic adjustment of the individual actuators.

The MPC strategy has found wide acceptance in the chemical process industry over last decade for its high performance capability of managing difficult to control systems without expert interventions for long periods of time [26]. MPC is the best solution for multivariable processes with very dynamic and unpredictable changes in process conditions and with large dead times. The popularity of this control strategy in the pulp and paper industry is increasing

steadily, especially in combination with adaptive control strategy [21, 22, 28, 71]. Model predictive control would be highly advantageous for CD control of paper caliper through the ability to predict the dynamic response of the calender.

The MPC strategy would allow prediction of local CD caliper for a number of future time steps, thereby compensating for the large time delays typical of the calendering process. In combination with both feedback and feedforward compensation, MPC could produce a much more effective and robust control system than any of the current strictly feedback systems for CD caliper profiling.

The accuracy, robustness and stability of the MPC approach requires having a precise model of the process [26, 72]. For control by MPC of the CD local thickness of paper, the process for which a precise model is required is of the behaviour of paper to CD local conditions in the nip between calender rolls. The absence of knowledge of the behaviour of paper to local in-nip conditions has been the obstacle to the adoption of model predictive control to this difficult control problem.

2.2 Factors involved in a model of calendering

Consideration of the evolution of progress in CD control of calendering starts with Haglund [31], who proposed a numerical model to describe the effect of CD variation of calendering variables and of initial paper properties on the thickness profile of the outgoing sheet. The local CD calendering conditions were linked using the line pressure distribution, the resulting calender roll deflection and local roll deformation. This procedure requires conversion from the measurable applied line pressure, P_{line} , to the resulting pressure distribution in a calender nip. Robertson and Haglund [30] showed that the relationships for permanent and in-nip paper strain proposed by Peel and co-workers [11, 12] could be applied to a rolling nip using a method developed by Mardon et al. [59] which related the maximum pressure in the nip, P_{max} , to the line pressure. This procedure is implicit and requires a large amount of experimental data. For this reason Haglund used

the simplification suggested by Robertson and Haglund, where the pressure pulse in the nip is approximated by a rectangular pulse. Their model predicted that successful calender control would require change in the local roll radius equal or less than 1 μm .

Derezinski [19] used the approach of Haglund et al. to develop a model of a complete calender stack, incorporating the effect of heat transfer within the calender stack on the local roll deformation and resulting local thickness correction. As in the previous analysis, difficulties were encountered in describing the line pressure distribution along the calender nip as a function of local sheet thickness and calender roll diameter.

According to Lyne et al.[57] and Robertson et al.[30] development of a complete model of the calendering process should contain the following elements:

- a local model for a single cross-machine position in an ideal calender nip,
- the local pressure increase and accompanying compressive effect caused by varying calender roll radius profile
- the effect of paper web moisture content and temperature on web compression given a constant diameter profile,
- the relationship between temperature distribution and diameter profile in a calender roll,
- the change in roll temperature distribution due to excess heat generation and heat transfer effect,
- the amount of control over roll temperature distribution exercisable with an available actuator system.

Finally, this model should be extended taking into account roll crowns and deflection as well as a multi-nip calender stack.

2.3 Stress-strain behaviour of paper during and after calendering

Chapman and Peel [11] investigated the effect of a pressure pulse on paper thickness using a platen press. They derived empirical relationships, the master creep equations, for compressed and recovered paper thickness as functions of maximum

pressure and pulse duration. The shortest pulse duration was about 6 ms, which is an order of magnitude or more greater than the dwell time in a commercial calender, and the pressures applied were fairly constant over that duration. Thereby their results describe more the deformation characteristics of paper than the response to a calendering pulse. The work was extended by Colley and Peel [12] to include the effect of paper temperature and moisture content. In neither study was the effect of successive compression investigated.

Kerekes et al. [47, 49] modified these relationships to predict directly the thickness reduction in a calender in terms of the more easily measured nip load, roll radius and machine speed rather than maximum pressure and pulse duration. Predictions were based on assumptions regarding the viscoelastic behaviour of paper and were verified using a laboratory-scale calender at speeds approaching industrial values.

Haglund and Robertson [30] used optical methods to measure paper thickness in the nip of a small laboratory calender run at low speeds. Compared to industrial practice their roll diameters and sheet speeds were both extremely small, thus limiting the applicability of their results. However their results showed, in agreement with Colley and Peel, that while initial density had an effect on thickness reduction, initial thickness did not. They suggested therefore modification of the master creep equations to include the effect of initial density on permanent and in-nip paper strain:

$$\epsilon_{n,p} = 0.5 (1 - \rho_i / \rho_{n,p_max}) [1 + \tanh(\mu_{n,p})] \quad [\text{Eq. 2.1}]$$

for which the permanent and in-nip calendering intensities, μ_p and μ_n , are defined as:

$$\mu_{n,p} = a_{0,n,p} + a_{L,n,p} \log_{10} L + a_{S,n,p} \log_{10} S + a_{R,n,p} \log_{10} R + a_{M,n,p} M + a_{\Theta,n,p} \Theta \quad [\text{Eq. 2.2}]$$

where ρ_{n_max} and ρ_{p_max} are the maximum density obtainable either in or after the nip, g/cm^3 , ρ_i is the initial paper density, g/cm^3 , and thus the inverse of initial paper bulk

(specific volume) B_i , L is the nip load, kN/m, S is the machine speed, m/min, R is the roll radius, m, Θ is the paper temperature, °C, and M is the moisture content, %. $a_{0\ n,p}$, $a_{L\ n,p}$, $a_{S\ n,p}$, $a_{R\ n,p}$, $a_{M\ n,p}$ and $a_{\Theta\ n,p}$ are regression coefficients. The permanent and in-nip versions of the master creep equation provide strain relative to initial bulk, thereby enabling both versions of Equation 2.1 to be used successively for multiple nips.

Crotogino et al. [14, 17, 18] proposed a comprehensive calendering equation, an empirical relationship for permanent bulk reduction in terms of web speed, roll radius, nip load and the initial paper properties: initial bulk, sheet temperature and sheet moisture content. The fractional reduction in permanent bulk defines the strain, ϵ_p :

$$\epsilon_p = \frac{B_i - B_p}{B_i} \quad [\text{Eq. 2.3}]$$

where B_i and B_p are initial and permanent recovered bulks, bulk being the ratio of thickness to basis weight. Since the CD and MD paper dimensional changes in calendering were shown to be negligible [2, 27, 29, 54], i.e. less than 1% for the most severe calendering conditions, basis weight remains essentially constant during the process. Thereby ϵ_p as defined by Equation 2.3 is the strain, positive for thickness reduction:

$$\epsilon_p = A_p + \mu_p B_i \quad [\text{Eq. 2.4}]$$

for which the calendering intensity μ_p , is defined as for the master creep equation:

$$\mu_p = a_{0p} + a_{Lp} \log_{10} L + a_{Sp} \log_{10} S + a_{Rp} \log_{10} R + a_{Mp} M + a_{\Theta p} \Theta \quad [\text{Eq. 2.5}]$$

This calendering equation has been used extensively to calculate the cross-direction average thickness reduction as a function of CD average calendering variables [14, 17, 18, 33, 34, 74].

Browne et al. [6, 7] determined a calendering equation for in-nip conditions, thereby providing also a quantitative description of the viscoelastic behaviour of paper in and immediately after the nip in calendering, what contributed a significant advance. This information was obtained by measuring paper thickness in and immediately after the nip under precisely known nip load for industrial conditions using a laboratory calender with a web only 70 mm wide. With all other conditions in the industrial range, calendering for a narrow width enabled maintaining constant radius and pressure profiles across the width of the calender, thereby enabling precise determination of in-nip conditions. Their calender [4, 5, 7], which in modified version was used in the present study, was effectively of a differential CD slice of an industrial calender designed to enable measurement of CD local values of the calendering conditions and in-nip strain. From this data they obtained an in-nip calendering equation, complementing the permanent version of the calendering equation. Their results [6, 7] established the validity of the calendering equation of the form of Equations 2.3 to 2.5 for quantitative description of in-nip strain ϵ_n as:

$$\epsilon_n = A_n + \mu_n B_i \quad [\text{Eq. 2.6}]$$

where:

$$\mu_n = a_{0n} + a_{Ln} \log_{10} L + a_{Sn} \log_{10} S + a_{Rn} \log_{10} R \quad [\text{Eq. 2.7}]$$

The dependence of in-nip strain on sheet temperature and moisture content was not determined by Browne et al. [6, 7] as all experiments were made at ambient conditions. Thus Equations 2.6 and 2.7 do not contain terms for temperature and moisture content, the effect of these variables being included in the curve-fitting coefficient a_{0n} , Equation 2.7.

Equations 2.4 and 2.6 are valid between the limits:

$$-A_{p,n} / \mu_{p,n} \leq B_i \leq (1 - A_{p,n}) / 2\mu_{p,n} \quad [\text{Eq. 2.8a}]$$

Outside these limits a new set of equations must be used:

$$\varepsilon_{p,n} = 0 \quad \text{if} \quad B_i < A_{p,n} / \mu_{p,n} \quad \text{[Eq. 2.8b]}$$

$$\varepsilon_{p,n} = (1 - A_{p,n})^2 / 4B_i \mu_{p,n} \quad \text{if} \quad B_i > (1 - A_{p,n}) / 2\mu_{p,n} \quad \text{[Eq. 2.8c]}$$

The lower limit is the point below which, for the specific calendering nip intensities $\mu_{p,n}$, no further bulk reduction will occur. Below this limit both versions of the calendering equation, which are the result of empirical curve fitting, would predict the impossibility of final bulk B_p being larger than initial bulk B_i . The upper limit of applicability of the calendering equations is the point beyond which an increase in initial bulk has no measurable effect on bulk reduction. Above this point the calendering equation would predict the final bulk B_i as a parabolic function of B_i , which is not true.

Those limits are particularly important for the in-nip calendering equation for which strain was shown by Browne et al. [7] to be generally above the upper limit of the calendering equation. The lower limit is relevant only for very light calendering conditions for which, a result of the viscoelastic behaviour of paper, there is no permanent deformation of the paper. Browne et al. [6, 7] established that although the relationship between permanent paper strain and the logarithm of nip load is essentially linear over the industrially relevant range of loads, this is not so for in-nip strain. Only for loads lighter than industrial practice is the in-nip compression of paper mostly elastic, with the sheet subsequently recovering most of its thickness.

Coefficients for the permanent and in-nip equations are different. While in-nip strain concerns the material behaviour under rapid compression only, permanent strain reflects the final deformation after two very different processes - first extremely rapid compression, then expansion to a 24-hour equilibrium state. Thus the coefficients of the equations for in-nip and permanent strain are independent measures of different aspects of rheological behaviour which must each be determined experimentally. These coefficients are dependent on the furnish used (i.e. the wood species, pulping conditions, etc.) and to some extent on the papermaking operations before calendering. Because both the permanent and in-nip versions

of the calendering equation express strain relative to initial bulk, the calendering equation treatment may be applied successively for multiple nips, with the final bulk from the previous nip serving as the new initial bulk.

The relationship for in-nip strain obtained by Browne et al. [6, 7] is valid for a very narrow range of initial bulk. Due to this limited range the dependence of the coefficients on initial bulk could not be determined with statistical reliability. To account for this effect Browne and Kawka [10] performed experimental measurements for TMP paper in ambient temperature and relative humidity with this same laboratory calender. These results show that for a specific nip load, in-nip strain is essentially independent of initial bulk. By contrast they again found a large effect of initial bulk on permanent strain, in agreement with Crotogino [14]. Thus a dense compact sheet recovers more completely after calendering than one of low density which experiences greater in-nip deformation.

The effect of furnish on in-nip calendering coefficients, not investigated in the Browne et al. study, requires exploration in order to provide the basis for extending the potential of the MPC concept to mills making paper from furnishes other than TMP. Previous studies [33] have shown that the permanent version of the calendering equation and the master creep equation hold for various types of paper but with different sets of coefficients.

Browne et al. [6, 7] also obtained a convenient relationship between permanent and in-nip strain, thus verifying the earlier suggestion of Ionides et al. [39] made on theoretical considerations. Using a Poisson model of fiber distribution inside the paper and an exponential relationship for stress-strain behaviour of paper, Ionides et al. argued that a simple linear function should relate a specific permanent strain to an unknown in-nip strain:

$$\varepsilon_n = a + c\varepsilon_p \quad [\text{Eq. 2.10}]$$

The Browne et al. results showed that Equation 2.10 fits the experimental data relatively well only for permanent strain higher than about 0.20. To cover their full set of permanent

strain data with strain ranging from 0 to 0.45, an nonlinear function is required. Accordingly, they proposed a logarithmic fit:

$$\varepsilon_n = a + c \log_{10} \varepsilon_p \quad [\text{Eq. 2.11}]$$

The concept of an ε_n - ε_p relation will be further examined in the present study.

Timms [74] reported optimisation of industrial calender performance and troubleshooting of problems using the permanent version of the calendering equation obtained using inexpensive laboratory results instead of more costly machine trials. Hamel et al. [34] used the calendering equation to calculate the nip load distribution from the recovered thickness profile of paper calendered at low speeds. Although this procedure is useful for locating misaligned or poorly ground rolls it provides no information about the nip shape or paper thickness in the nip. As this approach does not provide a link between roll radius profile and final thickness profile it cannot therefore yield an in-nip stress-strain relationship or be used to build a dynamic model of calendering.

Aside from empirical descriptions of paper strain during and after calendering a number of theoretical descriptions of paper response to a compressive stress have appeared. Based on work by May et al. [60], Hunter [39] and Alblas and Kuipers [1], Kerekes [48] predicted that the pressure pulse in a calender nip would be basically parabolic but somewhat skewed due to the time-dependent response of paper. However this model is based on the assumption that permanent paper deformation is small compared to the initial thickness, a poor approximation as permanent strain is often in the range of 30 to 60%.

Rodal [70] proposed separating the compressive stress-strain curve for paper into three more or less distinct phases. Under low load Hooke's law applies and Young's modulus, $E = \delta\sigma / \delta\varepsilon$, is a constant. At intermediate load the fibre network does not just deform but begins to collapse, leading to a much lower modulus $\delta\sigma / \delta\varepsilon$. Finally, large loads result in little additional strain as the fibres themselves collapse; here the Young's modulus E approaches infinity as the stress-strain curve becomes vertical. These three

regimes are integrated by using a version of Hooke's law modified by a nonlinear term $F(\epsilon)$:

$$\sigma = \epsilon E F(\epsilon) \quad [\text{Eq. 2.12}]$$

The stress-strain curve "shape factor" $F(\epsilon)$ is further decomposed into two additive parts, one due to buckling of the fiber network, one to collapse of individual fibres, which are then derived in terms of a critical strain ϵ_N at which buckling of the fibre network begins. The model fits literature data in the high stress regimes but requires estimated values for critical strain and several other parameters. Rodal noted that the best results are obtained when calendering in the low modulus region, which is not the region of prime industrial importance.

Based on the assumption that there are two compressive regimes, one due to fibre network collapse, the other due to fibre crushing, Osaki et al. [45, 46] derive separate stress-strain relationships for the two regimes using statistical descriptions of fibre distributions. Supporting tests were performed in a platen press at compression rates up to only $0.085 \mu\text{m/ms}$, extremely low relative to typical industrial rate is $50 \mu\text{m/ms}$.

Browne et al. [7, 9] used the Burger model, a combination of elastic and viscous elements, to describe the viscoelastic behaviour of paper during calendering. However model parameters were shown to be not material properties but strong functions of the process parameters. Typical scales for roughness and structure of the TMP newsprint investigated were found to be similar to the dimensions of the gap and length of the nip [8]. Taking into account that fibre compressibility depends on coarseness, a sheet made of a stack of such different fibre types acts as a stack of mechanical elements, each with its own stiffness properties. They established that with this non-uniform, non-homogenous structure in the plane of the sheet and in its thickness dimension, paper behaviour under compression in the nip of a calender cannot be described by a linear viscoelastic model.

2.4 Heat transfer aspects of a model

Kerekes [50] proposed simplified equations to predict the temperature distribution in a sheet under transient heat transfer during calendering for three specific cases: the sheet in a nip, in contact with a roll, and in an unsupported draw. His simulations show that a high speed calender, over 600 m/min, heat transfer in the nip to a sheet initially at 52 °C from a heated roll with surface temperature in the range 72 to 83 °C penetrates only a fraction of sheet thickness. Thus paper passing through a nip with 20 to 30 °C temperature difference between the roll surface and the paper is heated substantially at the surface while the center of the web remains unheated, thus creating large thickness dimension temperature gradients. Only at a machine speed as low as 200 m/min would the heat penetrate in the nip to the centerline of a sheet. At high speeds, moreover, heat transfer in the nip was shown to be a substantial portion of the total heat transfer between the roll and the sheet, being as high as 1/5 to 1/3 of the total. This distribution of roll-to-paper heat transfer is particularly impressive because the nip dwell time is only about 1% of the total roll-sheet contact time. Another important implication from Kerekes' work is that there is no heat conduction between rolls in a high speed calender stack as they are totally insulated from each other by the paper. Such downward conduction in the stack from upper heated rolls to lower unheated rolls would occur only at calender speeds less than 200 m/min. Comparison of predicted and experimentally measured temperatures showed good agreement when a small moisture evaporation effect was taken into account.

Roll to sheet heat transfer is governed by the paper thermal conductivity and its contact resistance with the roll surface. Based on experimental measurements, Kerekes [51] proposed a model involving these two resistances. His results show that the heat conduction characteristics of paper change dramatically in a calender nip. As the sheet is consolidated by calendering, the roll-to-paper heat transfer rate increases significantly as a result of the changing material properties of paper. In the initial stages of compression in the nip, heat transfer is limited by the sheet surface roughness. As the paper becomes smoother with further compression the roll to sheet contact resistance decreases, thereby

increasing the heat transfer rate. Two other factors contributing to an increased heat transfer rate in the nip are decreased thickness of the sheet and increased thermal conductivity as the air providing the good thermal insulation characteristic of paper is squeezed out.

The above findings are in general agreement with the calculations by Keller [45, 46] for heat transfer between a hot metal roll and paper which he based on measured paper-roll temperature differences under a range of conditions encompassing industrial practice. Keller's results show the strong effect of nip pressure on heat conduction due to the reduction in paper porosity in the nip. With other parameters fixed, the calender nip transfers less heat at light than heavy loads. Keller also found a much higher heat transfer rate for coated than uncoated paper, a consequence of the differences in density, surface smoothness and material properties that reflect the difference in these properties between fibres and mineral pigments and the reduced porosity from coating.

Based on an earlier model for convective heat transfer from a single heated calender roll in still air Hamel and Dostie [35] derived a model for computing heat transfer from a stack of rolls operating in more realistic conditions. Convective heat transfer was found to be affected by the presence of the adjacent roll. Their model can be used to determine the heat balance in high temperature calendering, for modelling of heat transfer in calendering, and to evaluate heat transfer from hot calender rolls to paper.

2.5 Local temperature and thermal expansion of a calender roll

An essential element of any CD calender control system is the ability to predict the roll radius deformation, and thus the calender nip profile, due to a specific heating/cooling CD profile from a control actuator. Through extension of the measurement by Pelletier et al. [67, 68] of local heat transfer for a calender roll with heating or cooling impinging air jets as the control actuator, Journeaux [42] obtained the associated transient and steady state aspects of the CD profile of local radius of a calender roll. The basis of the latter study, where finite

volume and finite element numerical methods were used to predict for a variety of roll designs the CD local roll deformation profile due to a CD local heat flux profile is now summarized.

The Fourier equation for unsteady-state heat transfer without heat generation is,

$$\frac{1}{r_p} \frac{\partial}{\partial r_p} \left(r_p k \frac{\partial \Theta}{\partial r_p} \right) + \frac{\partial}{\partial z} \left(k \frac{\partial \Theta}{\partial z} \right) = \rho C \frac{\partial \Theta}{\partial t} \quad [\text{Eq. 2.13a}]$$

which at steady state is,

$$\frac{1}{r_p} \frac{\partial}{\partial r_p} \left(r_p k \frac{\partial \Theta}{\partial r_p} \right) + \frac{\partial}{\partial z} \left(k \frac{\partial \Theta}{\partial z} \right) = 0 \quad [\text{Eq. 2.13b}]$$

where r_p and z are radial and axial position along the roll, Θ is temperature, t is time, with k and C the material properties. The corresponding equations for stress σ_r in the roll are

$$\frac{1}{r_p} \frac{\partial (r_p \sigma_{rr})}{\partial r_p} + \frac{\partial \sigma_{rz}}{\partial z} + \frac{1}{r} \sigma_{\theta\theta} = 0 \quad [\text{Eq. 2.14}]$$

The stress-strain relationships are given in terms of the roll material properties E , ν_m and α as

$$\sigma_{rr} = \frac{E\nu}{(1+\nu_m)(1-2\nu_m)} (\epsilon_{rr} + \epsilon_{zz} + \epsilon_{\theta\theta}) + \frac{E}{(1+\nu_m)} \epsilon_{rr} - \frac{E\alpha\Theta}{(1-2\nu_m)} \quad [\text{Eq. 2.15}]$$

where the roll strain components ϵ_{rr} , ϵ_{zz} , $\epsilon_{\theta\theta}$ and ϵ_{rz} are related to the radial and axial displacements, u_r and u_z by Equation 2.16:

$$\begin{aligned} \epsilon_{rr} &= \frac{\partial u_r}{\partial r_p} & \epsilon_{zz} &= \frac{\partial u_z}{\partial z} \\ \epsilon_{\theta\theta} &= \frac{u_r}{r_p} & \epsilon_{rz} &= \frac{1}{2} \left(\frac{\partial u_r}{\partial z} + \frac{\partial u_z}{\partial r_p} \right) \end{aligned}$$

[Eq. 2.16]

With the applicable boundary conditions they solved Equations 2.13b through 2.16 simultaneously using finite element methods to arrive at the steady state solution. In the unsteady state case, the necessary additional relationship for elastic deformation of a shell in plane strain is:

$$u_r = \frac{\alpha}{r_p(1-\nu_m)} \left\{ (1+\nu_m) \int_{r_i}^{r_p} \Theta r_p dr_p + \frac{(1-3\nu_m)r_p^2 + (1+\nu_m)r_i^2}{r_o^2 - r_i^2} \int_{r_i}^{r_o} \Theta r_p dr_p \right\} \quad [\text{Eq. 2.17}]$$

where the temperature distribution $\Theta(r_p, z, t)$ was obtained by solving Equation 2.13 using finite volume methods. Equation 2.17 was then used to calculate the roll deformation profile u , a function of z and t . Steady and unsteady state solutions were verified with published results. From these numerical solutions they determined for a variety of roll designs the maximum value of $u(z, t)$, denoted Δr_{peak} , and a characteristic width of deformation.

As characteristic width of deformation $W_{\Delta r}$, Journeaux [42] used the definition first proposed by Verkasalo [75], i.e. the z -direction width over which $\Delta r \geq \Delta r_{\text{peak}} / 3$, Figure 2.2. As the results of Journeaux show that the local roll deformation approximates a normal distribution, the above definition of deformation width corresponds to $W_{\Delta r} = 1.48 \sigma$.

For effective CD calender control it is desirable to maximize Δr_{peak} while minimizing $W_{\Delta r}$. Accordingly Journeaux defined the calender control deformation index $I_D = W_{\Delta r} / \Delta r_{\text{peak}}$, the width of deformation (in mm) per micrometer of peak radial deformation. With a low I_D index being desirable, Journeaux reports values ranging from a high of 86 mm/ μm for a large radius, thick-walled internally heated roll to a low of 35 mm/ μm for a small radius, thin-walled unheated roll. Thus for a given radial deformation, the control action will be felt over a narrower width with the latter type of roll.

Journeaux [42] also demonstrated that their exact solution for the local deformation of roll radius $\Delta r(t)$ in response to a particular local heat flux could be approximated as a

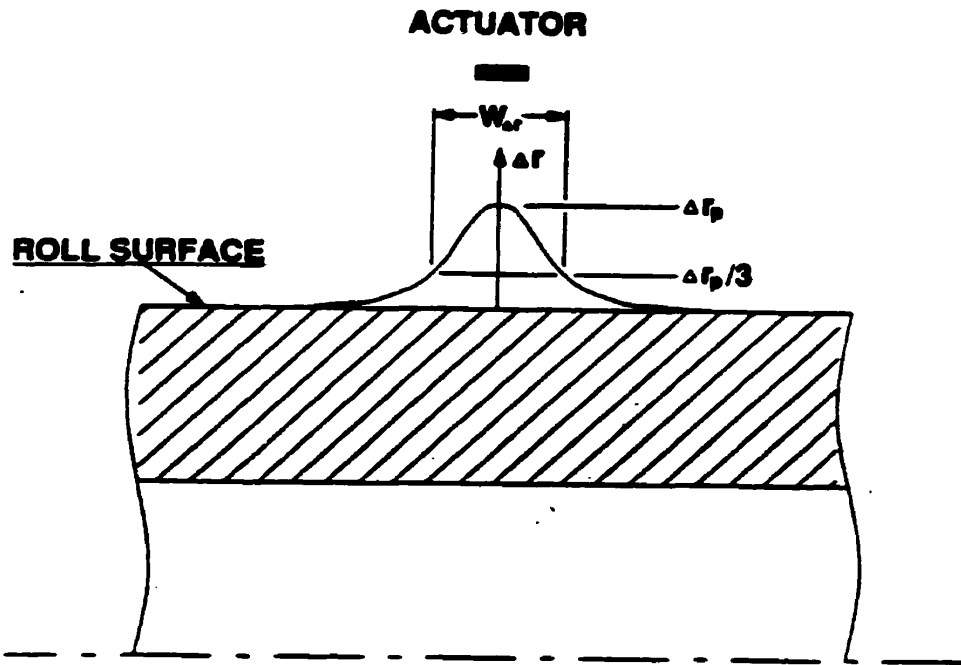


Figure 2.2: Definition of characteristic width of roll deformation, $W_{\Delta r}$

simple two-parameter exponential decay, a procedure particularly suitable for real-time control:

$$\Delta r(t) = \Delta r_{peak} (1 - e^{-t/\tau}) \quad [\text{Eq. 2.18}]$$

where:

- Δr_{peak} - peak roll deformation at steady state [mm]
- τ - deformation time constant [min]
- t - time [min]

In a comparison of $\Delta r(t)$ at $t = 10$ minutes, Journeaux showed that the largest deformation is given by thin shelled unheated rolls, this advantage indicating that for such rolls the advantage of a larger steady state deformation Δr_{peak} is more important than their slower deformation time constant τ . Thus according to Journeaux the most effective type of roll on

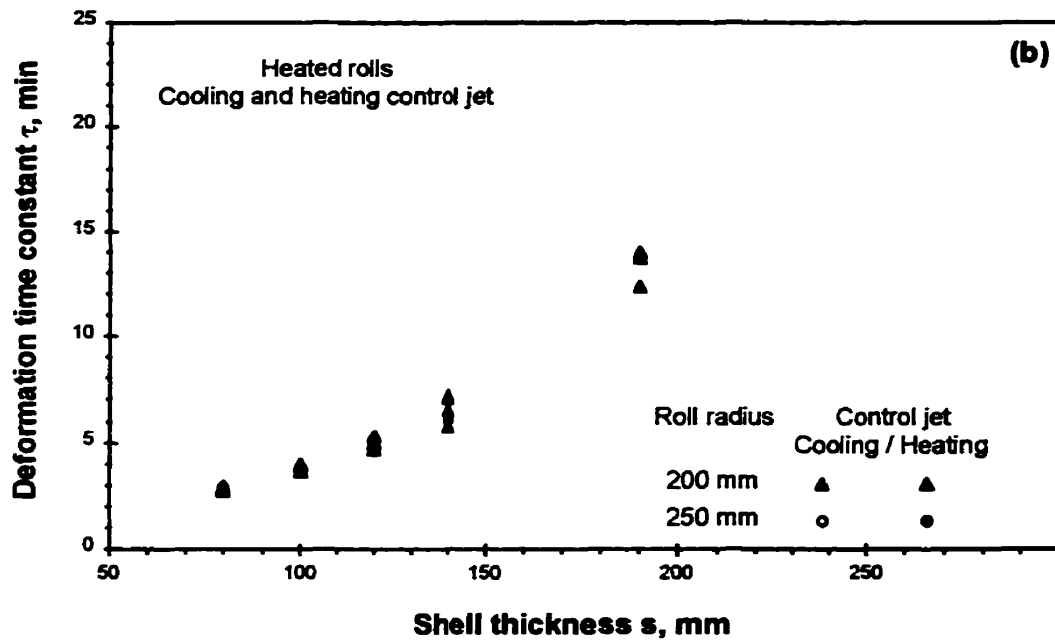
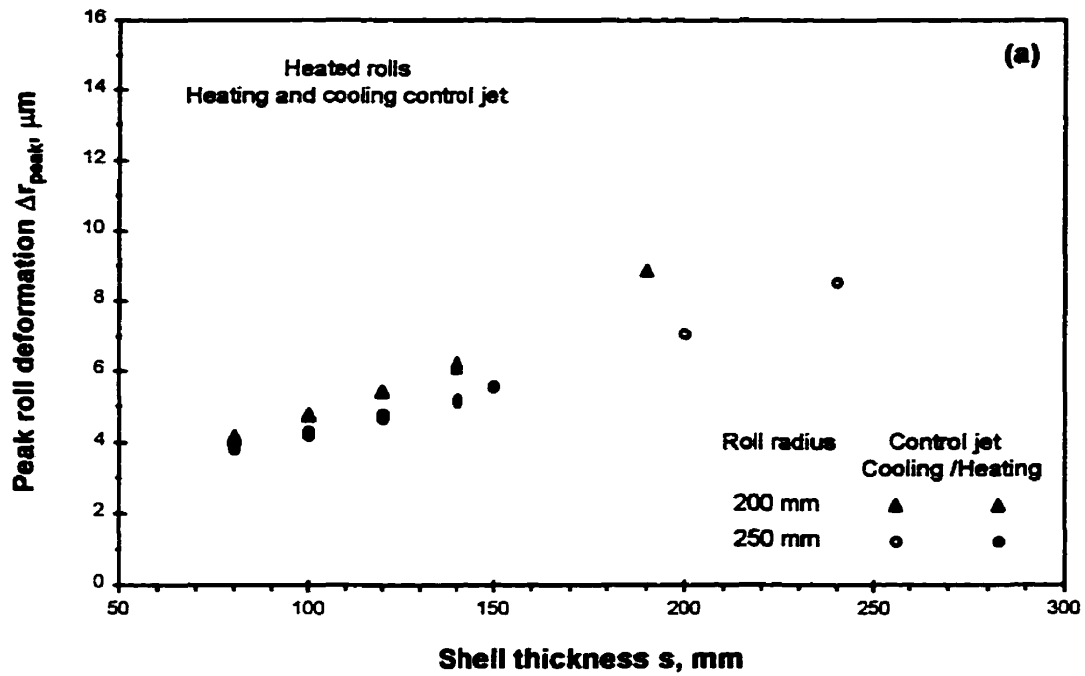


Figure 2.3: Comparison of results: heated rolls with heating and cooling control jets

- a) Effect of roll radius and shell thickness on peak roll deformation
- b) Effect of roll radius and shell thickness on deformation time constant

Data: numerical simulation of Journeaux [42]

which to place the control actuator for quick initial response, large radial deformation and small width of deformation is a thin-walled unheated roll.

As Journeaux demonstrated his numerical solution with the control actuator as either one heating jet in an array of cooling jets or the opposite, one cooling jet in an array of heating jets, there is the question of the equivalence or non-equivalence of the control actuator providing a local heating or cooling flux. With internally unheated rolls, the effect of heating and cooling control action on steady state roll deformation is always equivalent because the boundary conditions are symmetric. This equivalence does not exist for internally heated rolls, where the boundary conditions are unsymmetric because the radial heat flux within the rolls is always outward from the heated core whereas the direction of heat flux at the roll surface reverses with a switch between heating and cooling control action. However the results of Journeaux [42] showed that for conditions of industrial relevance the absolute magnitude of thermal roll deformation for heating or cooling control jets is generally indistinguishable, Figure 2.3a, as it the case also for the deformation time constant, Figure 2.3b. Thus there is no need to distinguish between heating or cooling control action.

In summary, the CD roll deformation profile due to a CD heat flux profile can be calculated using finite element and finite volume methods, the effectiveness of a given control action on a variety of roll designs can be estimated using the deformation index I_D , and the dynamic characteristics can be approximated with a two-parameter exponential relation based on the steady state peak deformation Δr_{peak} and the deformation time constant τ .

2.6 Thesis objectives

Most of the elements for a CD local in-nip calendering model now exist. The control algorithms and powerful actuator systems are available [3, 16, 32, 38, 52, 53, 63] as well as the precise on-line caliper sensors. The relationship between the heat flux profile and the resulting roll radius profile is known [42]. What is incomplete is the effect of local

temperature and moisture content on the local in-nip behaviour of paper during calendering, which is necessary for establishing as a function of all calendering parameters the relationship between nip shape and nip pressure distribution, i.e. a reliable stress-strain model for paper in the calender nip. This in-nip stress-strain model incorporating the effects of the key variables of paper temperature and moisture content is an essential element for developing a comprehensive dynamic model of the calendering process.

The objective of the present work is to provide this relation, to assemble the existing knowledge into a comprehensive dynamic calendering model suitable for model predictive control, and to demonstrate its use for incorporation into a superior calender control system.

3 Experimental procedure and equipment

3.1 Overall mechanical design

The calendering equipment of Browne et al. [4 to 7], designed to reproduce industrial conditions of nip load, roll radius, and machine speed while allowing accurate measurement of the separation distance between the rolls, was modified to provide a unique controlled environment calendering facility. With this facility the web temperature and web moisture content are independently controllable over a quite extended range, 20 to 80°C, 1% to 14% moisture. The strategy of the present research requires that all sources of cross-machine and machine direction variation in web temperature and moisture content as well as cross-machine direction thickness variation be minimised. This objective was achieved by preconditioning an entire roll of paper to a particular temperature and moisture content, then maintaining it at those precise conditions while calendering it between narrow rolls at the same temperature as the paper. Measurable error due to roll bending or bearing deflection was eliminated through use of a face width of calender rolls of only 75 mm, with maximum paper width of 70 mm. This particular combination of calender and paper dimensions provided a good compromise between minimising width while maintaining sufficient web strength.

The new experimental calendering equipment consists of three basic elements: (1) a facility for bringing a complete roll of paper to a specific temperature and moisture content in advance of calendering, (2) the controlled environment calender, (3) a facility for producing air conditioned to a temperature and humidity independently controllable over a wide range for use in both the preconditioning chamber and the controlled environment hoods of the calender.

3.1.1 Preconditioning and rewinding chamber

A stand-alone preconditioning and rewinding enclosure, 3 m long x 1 m wide x 1.8 m high, Figure 3.1, was designed to allow reels of paper one meter in diameter, comprising a length of about 6 km, to be pre-conditioned by rewinding slowly in an atmosphere of controlled temperature and relative humidity. The roll being unwound is shown in the left, that being wound on the right. In this slow rewinding chamber a total exposed length of 15 meters of paper was achieved by passing the web back and forth the 1.5 m of vertical spacing between two sets of 9 idle rolls of 51 mm diameter, as seen in Figure 3.1. The sheet wraps each idler effectively 180 degrees. The surface of the idler rolls was roughened during manufacturing, minimising the possibility of slip between the sheet and idler. All sides of this enclosure except the floor were insulated with 38 mm

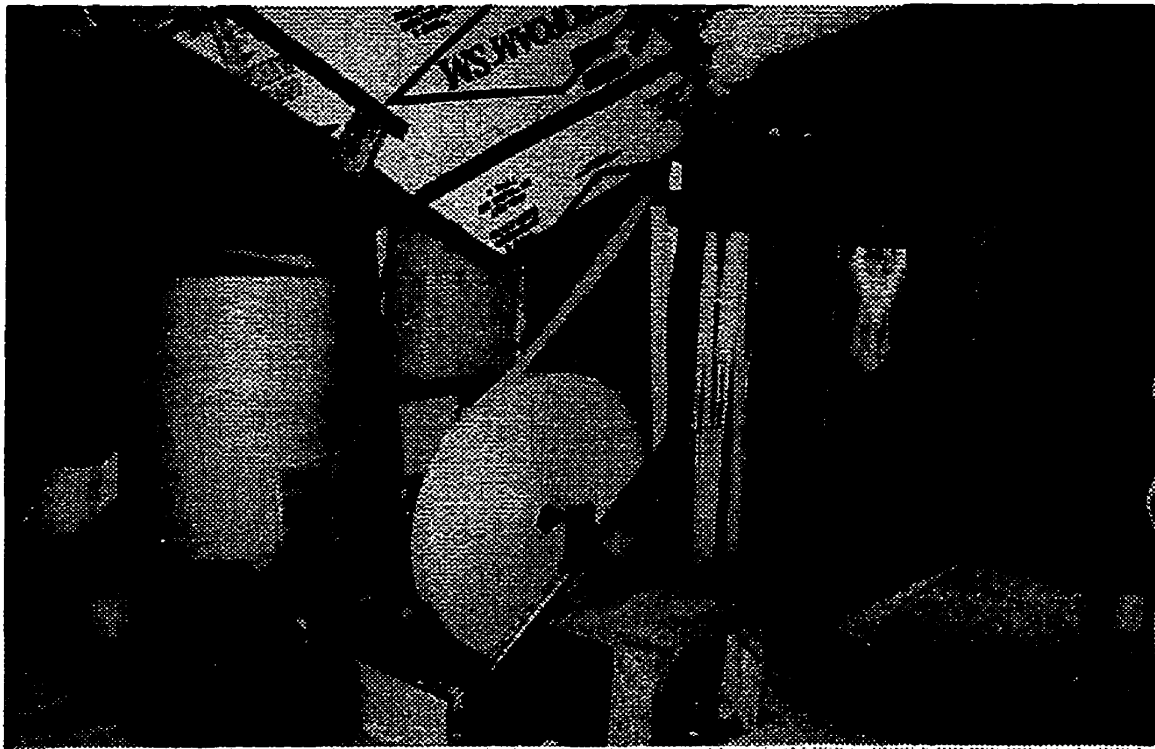


Figure 3.1: Preconditioning rewinding enclosure.

slabs of polyurethane in order to insulate the enclosure from the room environment.

An optical sensor measuring the rotational speed of an idler roll, and thus the paper web speed, was used to adjust the variable speed 0.5 HP D.C. motor drive which was connected with the shaft of the wind-up roll through a gear set with an overall ratio of 50:1. The sensor consists of a 20 mm diameter shiny disk with 250 small holes drilled along its circumference, thereby generating 250 square wave cycles per rotation. With the idler roll connected to the disk through the 4:1 ratio gear set, each idler roll rotation generated 1000 square wave cycles. Each rotation of this 50.8 mm diameter idler roll corresponds to a sheet length of 160 mm. Pulses were counted using the counter/timer function on the A/D computer board. The sheet speed is given by pulse count / time.

The paper rewinding speed was controlled at 1.7 m/min by the PID loop in the control program so that the web was exposed to the conditioned air for about 9 minutes. A manual control option was used at the beginning of the rewinding process to align the position of the reel on the unwind stand. Complete rewinding of 1m diameter

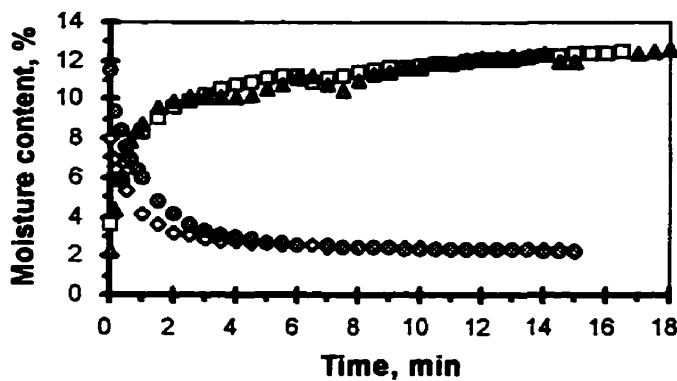


Figure 3.2: Paper sorption and desorption

reel took about 84 hours. The measurements at about 40 °C of Figure 3.2 established that this contact time provided about a 90% approach to the target paper moisture content. Various measurements, most recently those of Hashemi et al. [36], establish that the diffusivity of moisture in paper

drops precipitously at low moisture content. Thus it was not surprising that the paper had to be run a second time through the conditioning chamber to achieve the low moisture content of 1 to 2%, especially for a low paper temperature of 20 to 30 °C. Data displayed on Figure 3.2 were collected using TMP newsprint, 70 mm x 100

mm, placed in a sealed controlled environment enclosure, 0.15 m x 0.15 m x 0.1 m high, which was linked with the facility for the conditioned air described in Section 3.1.2. With air at 0.5 CFM at a specific temperature and humidity circulating through this conditioning chamber, a microprocessor based BSP-901 Continuous Moisture Analyser, described in Section 3.3, was used to measure the transient change in moisture content of the sheet. These measurements were performed at 40 °C and at two levels of relative humidity, 80 to 90% for sorption, 5 to 8% for desorption. The results are tabulated in Appendix A1.

With the objective of operating the paper conditioning chamber at from 20 to 80 °C and at levels of absolute humidity up to 0.3 kg water/ kg air, which is about 4 times that of saturated air at 20 °C, it was necessary to insulate conditioning chamber well. All sides of this enclosure except the floor were insulated with 38 mm thick slabs of polyurethane. Also a heating and air circulation system was provided to achieve uniform temperature within. Air temperature inside the rewinding chamber was controlled at three locations with custom-built heating units. Located close to both the unwind and windup stands are units consisting of a manually controlled, variable speed heavy-duty fan of range 0 to 2.8 m³/min (100 CFM) with a compact, powerful (1.74 kW) 30 mm diameter spiral heating element mounted at each fan outlet. The third unit was a 1.74 kW heating element placed at the air inlet to the conditioning chamber from the specially designed facility for providing air of controlled humidity and temperature. Each heater had a computer controlled voltage supply. The temperatures at each of these three locations were measured in range 0 to 100 °C with an accuracy of ±0.1 °C using Platinum type-100 RTD thermocouple. The air exhaust return to the conditioning unit was located in the lower, right corner at the back of the chamber.

This rewinder heating system was controlled by a computer program using three PID algorithms to control air temperature by independently varying the power supply for each heating unit from 0 to 220 VAC. Experience established that typically only the unwind and wind-up stand heating units were needed, the third heating unit generally being switched off by the control program. For safety reasons and to prevent a burnout

without air flow, a protective on/off switch installed on the main 220 VAC heating element line turned the heater power off when the blower power supply was off.

The humidity of the air in the paper conditioning chamber, supplied from the air conditioning facility, was monitored using an accurate dew point hygrometer. To avoid moisture condensation internally, the sensor head was placed inside the chamber while the remaining electronics box, very sensitive to high temperature and humidity, was kept outside. A small pump provided the flow through the sensor head of the air to be monitored.

Sheet tension, which influences windup reel hardness, was controlled automatically by a simple device comprising two limit switches and the dancing idler roll installed immediately after the unwind stand. When tension exceeded the control limits an electric signal from one of the limit switches was sent to a small 75 RPM stepper motor mounted on a general purpose winch. The force on the brake on the unwind stand was thereby adjusted to maintain the target sheet tension. A photoelectric sensor just before the windup stand, which sensed the presence of paper by measuring reflected light, turned off the power supply for the rewinder and tension control motors when the rewinding of a roll was complete or the sheet broke.

After being placed on the unwind stand of the rewinding chamber the position of a new roll was carefully aligned so as to provide the required path of the web threaded through the idler rolls and the impingement nozzles. The manual mode of the rewinder speed controller was used for that purpose. Once set up correctly, the rewinding chamber was tightly sealed with tape to prevent heat or moisture loss during rewinding and the rewinder heating system was turned on to provide the required temperature.

While the conditioning chamber was being brought up to temperature the conditioned air facility, described in Section 3.1.2, was set to provide air at the desired temperature and humidity. After the target conditions were obtained the conditioned air was then directed to the rewinding chamber. The time required to bring the whole system

to 90% of the required air humidity and temperature ranged from 2 hours for low temperature and ambient humidity, to 12 hours for high temperature and high humidity.

3.1.2 Facility for controlling air humidity and temperature

Conditioned air for both the paper preconditioning chamber and the controlled environment hoods of the calender was provided by a specially designed facility for independent control of these variables. The required operating ranges are 20 to 80 °C and 2 to 98% relative humidity in order to calender paper over the moisture range of 1 to 14% over this temperature range. Purchase of a commercial unit was rejected not just for its high price but because the quality and reliability of control over the very wide range required was uncertain, a fact frustratingly familiar to researchers requiring precisely controlled environment rooms even at a single value of humidity and temperature. The overall view, Figure 3.3, shows the five major parts: humidifier, dehumidifier, duct heater, water cooler and precision humidity and temperature sensors. Air was circulated within this facility at a constant flow rate of 2.8 m³/min (100 CFM) and was circulated to the paper preconditioning chamber by a variable speed heavy-duty fan at a rate in the range 0 to 2.8 m³/min (100 CFM).

The custom-built humidifier providing steam at 0 to 2.3 kg / hour consisted of a water container, which is filled to a constant level and heated with an electric immersion heater. The 4 kW, 220 VAC power supply was manually adjusted.

The air humidity was reduced by a modified Cargocaire HC-150-I dehumidifier with a desiccant honeycomb structure wheel charged with titanium enhanced silica gel. Rotation of the desiccant wheel through the regeneration position allowed for continuous desiccant regeneration using stream of a reactivation heated air. Continuous regeneration of the desiccant allowed for uninterrupted dehumidification. The level of moisture removal by this dehumidification was varied manually by adjusting the temperature of the

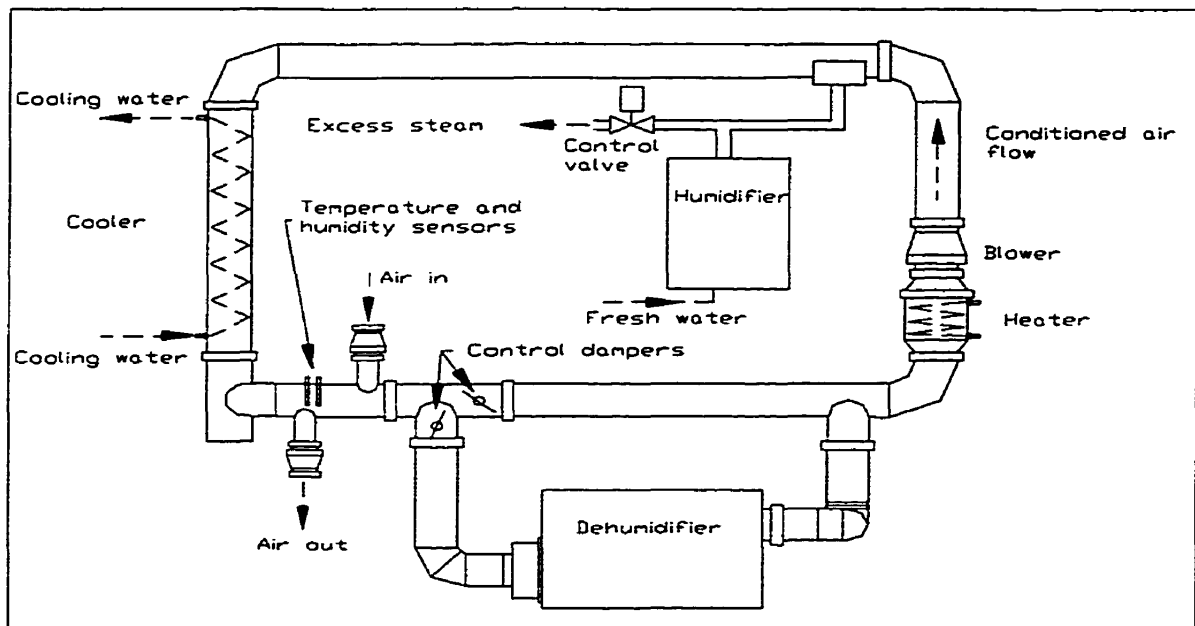


Figure 3.3: Facility for conditioned air.

regeneration air between 20 to 146 °C. Flow of the conditioned air through the dehumidifier was adjusted manually from 0 to 2.8 m³/min (100 CFM) using two air duct dampers installed upstream of the dehumidifier.

The conditioned air humidity was measured using a microprocessor based Vaisala HMP 230 series transmitter which incorporated a thin-film Humicap H-sensor. The humidity measuring range was 0 to 100% RH with an accuracy of ±1% of the reading from 0 to 90% RH and ±2% from 90 to 100% RH. The sensor response time (90% of target humidity) in still air at 20 °C was about 15 s. Temperature was measured in range 0 to 100 °C with an accuracy of ±0.1 °C using platinum type-100 RTD thermocouples.

A custom written program was used for data acquisition, control and processing (Appendix A2). Two PID algorithms were incorporated in the computer program to control air humidity and temperature independently, no decoupling terms were used to account for the interaction between these two variables. The humidity was controlled by



Figure 3.4: Steam flow control.

adding steam to the dehumidified air. This was accomplished with a computer controlled, motorized two-way valve (Figure 3.4), which discharged the excess steam from the manually controlled steam generator. The target temperature was obtained with a second PID loop controlling the power supply of the 2 kW duct heater, which worked against the water cooled exchanger. This cooler was controlled manually by adjusting the cooling

water flow. Using that simple control strategy this custom-built air conditioner was able to supply any combination of air relative humidity from 2% to 98%, with air temperature from 20^o to 80^o C, thereby providing sheet moisture content in the range of 1 to 14% for paper of this temperature range.

3.1.3 Controlled environment calender

The controlled environment calender, Figures 3.5 and 3.6, was designed to process continuous webs of paper up to 6 km long from reels up to 1 m diameter at speeds to 1000 m/min through a single calender nip between controlled temperature rolls and in an atmosphere of controlled temperature and relative humidity. To achieve controlled environment calendaring, several constant temperature and humidity enclosures were built around key parts of the calender. These hoods maintained constant temperature and moisture content of the sheet from a reel of preconditioned paper, before and during the paper passing from the unwind stand to the nip. These enclosures were supplied with air from the same controlled supply as used for the paper preconditioning enclosure.

The controlled environment calender stack consisted of two hard rolls, supported in a stiffened frame designed to withstand the high nip loads. The basic facility was as described by Browne et al. [4 to 7], with the major modification to convert it to a controlled environment calender. Nip loads were varied using a hydraulic pump and cylinder which pulled down on the upper roll supporting arm. This configuration achieved nip loads up to 210 kN/m while minimizing the bending load applied to the main calender stand and thus the movement of the upper roll relative to the displacement sensors. The hydraulic system could also be used for nip relief, allowing loads less than those due to gravity loading from the mass of the upper roll. The load cell for measuring nip load was placed under the hydraulic cylinder clevis.

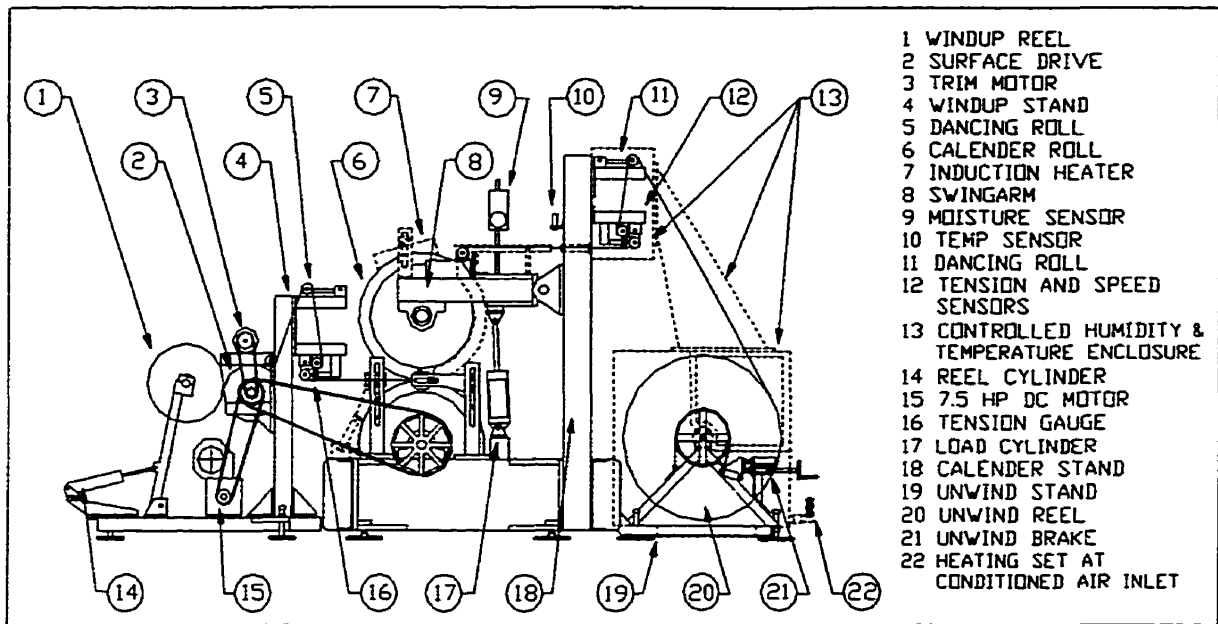


Figure 3.5: Controlled environment calender.



Figure 3.6: Overall view of the experimental calender

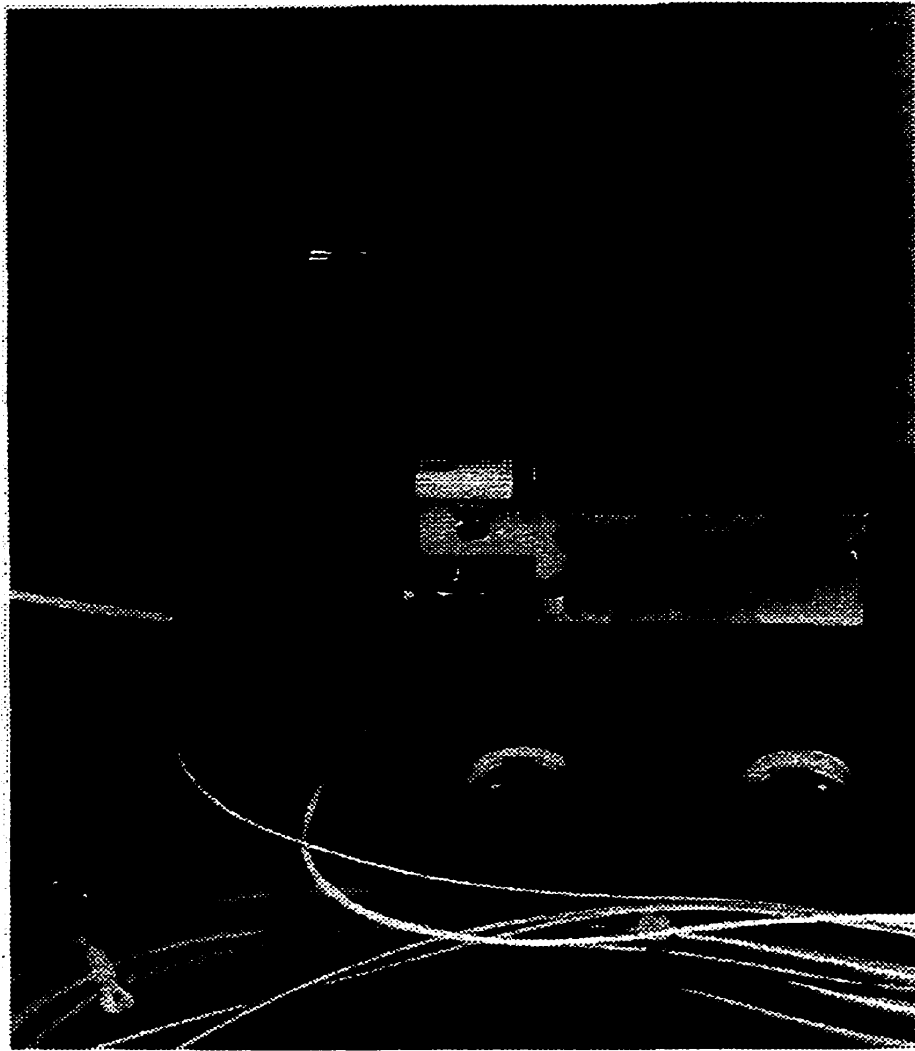


Figure 3.7: Roll displacement sensors.

Three pairs of rolls were provided, of diameters 404, 508 and 711 mm. A shoulder machined into the side of each roll, Figure 3.7, served as the target for two non-contact Kaman KD-2300 series inductive type sensors which react to the presence of a metallic mass. Signals from these displacement sensors recording the position of both rolls relative to the fixed calender base were used to calculate the nip gap, i.e. the in-nip paper

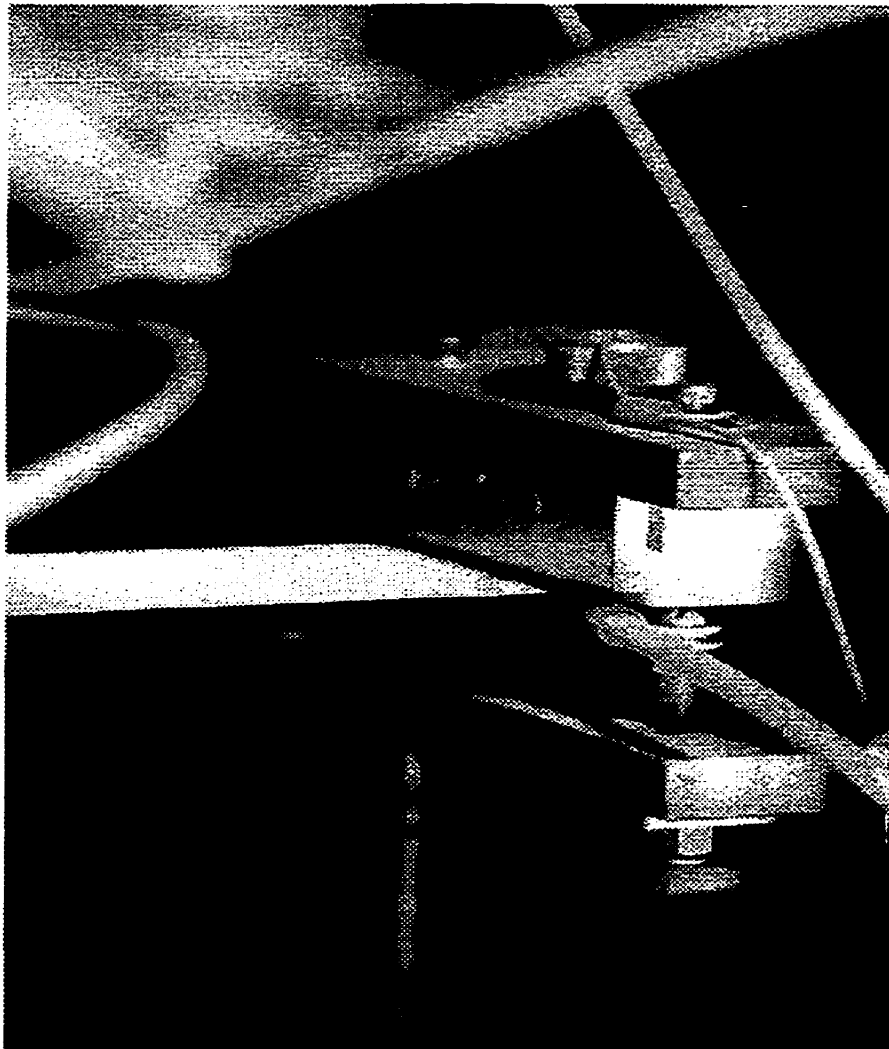


Figure 3.8: On-line caliper gauge 296 mm after the nip.

thickness, with a target resolution of $\pm 1 \mu\text{m}$ over the range of 0 to 500 mm, regardless of calender speed.

Paper caliper was also measured at two other positions, 296 mm and 1050 mm after the nip, using inductive sensors placed in a ceramic anvil, Figure 3.8. The target for each sensor was an aluminium disc, 10 mm diameter, carried in the floating head of a

modified industrial caliper gauge. Since these sensors involve a contact element, some bounce occurs under certain conditions.

The lower roll of the calender was driven by a 7.5 HP DC motor through an idler shaft, which also served as a surface drive roll for the windup reel. A tachometer installed on the main drive motor permitted calculation of surface speed of the lower (driven) calender roll, the in-nip sheet speed as used for all calculations.

Two other devices, before and after the nip, were used to measure sheet speed at two more points in order to compute the change in sheet speed from the unwind stand to the winder for each set of calendering conditions. These measurements provided necessary information to calculate the machine-direction strain imposed by the calender. The design and principle of operation of these speed measuring devices were similar to the one used to control paper speed in the preconditioning chamber. An optical sensor facing the idler roll covered with 10 alternating strips of matte black paint and shiny aluminium tape responded by generating a square wave. Since the diameter of the idlers, both before and after the nip, was 63.35 mm, each idler roll rotation corresponds to a sheet length of 199 mm and generates 10 cycles of a square wave. The output was filtered using a Schmidt trigger, the pulses being counted with the counter/timer function on the A/D computer board. The number of pulses in a given time, divided by the pulses per rotation, multiplied by the idler circumference, is proportional to the sheet speed at that idler. Comparison of the speed before and after the nip gave the speed increase, i.e. the MD stretch.

To minimise the possibility of slip between the sheet and idler, the idlers were roughened by sandblasting and were installed so that the sheet wrap was a full 180 degrees. Pulse counting using A/D counter function was initiated sequentially for the two counters just before the start of acquisition of the in-nip thickness data. The counters were stopped in the same sequence immediately after the end of the in-nip data acquisition. The MD stretch data was thus typically computed over a distance of about 17 meters, or about 1000 pulses from each sensor.

Sheet tension, another factor influencing sheet stretch, was measured before and after the nip using two identical load cells mounted under an idler roll. Control of sheet tension on the unwind side of the nip was provided by an external drum brake adjusted manually with a handscrew. Sheet tension on the wind-up side of the nip was controlled by a small DC motor driving a differential gearbox built into the idler shaft; this gearbox and motor allowed the web speed at the windup reel to be varied slightly relative to the speed at the calender roll, resulting in fine control of the sheet tension. The target tension on both sides of the nip was set at 600 N/m.

Temperature of the calender rolls was controlled by induction heaters, on loan from Measurex Corp. One induction heating coil per roll and one power module per coil, both rated at 4 kW, were installed, Figure 3.9. The induction coil covered a distance of



Figure 3.9: Induction heater and temperature sensors.

about 350 mm along the roll surface. The heat-up stage was carried out with the rate of surface temperature increase limited to about 1 °C/min, thus requiring about one hour to heat the rolls to the maximum calendering temperature of 80 °C. The slow heating rate avoided the build up of excessive thermal stresses which could seriously damage the roll.

In order to bring both calender rolls to the same temperature as the sheet, prior to each experiment the rolls were rotated to give a very slow speed, only 5 m/min, while the roll temperature was raised slowly. The time required for the roll warm-ups ranged from 30 minutes for small rolls and a temperature of 30 °C, to 3 hours for large rolls and a temperature of 80 °C.

With roll speeds to 2500 rpm, both sides of the rolls were insulated in order to minimise heat loss. Induction heating requirements were thereby lowered and roll surface temperature control was improved as well. The cross-machine direction variation in roll surface temperature was monitored by a thermocouple-type sensor which measured directly the temperature difference between the roll surface centre and edges. Tests established that with the roll surface temperature steady at 80 °C, the maximum variation over the 75 mm CD roll dimension was about 1.5 °C.

The temperature of the air inside the calender hoods, provided from the conditioned air supply facility, was controlled at two locations by a heating system similar to that described for the rewinding facility. One heating set, a spiral heating element and variable speed heavy-duty fan, was placed in the upper part of the hoods. The other unit, a heating element only, was located inside the inlet of the air supply system at the unwind stand. The specifications for the above heating sets were the same as described for the rewinder heating sets. The temperatures in each of these locations were measured to an accuracy of ± 0.1 °C over 0 to 100 °C, using platinum type-100 RTD thermocouples.

Sheet moisture content and temperature were monitored continuously using infra-red type sensors. The moisture measuring range of a microprocessor based BSP-901 Continuous Moisture Analyser was 0 to 80% with an accuracy of $\pm 0.1\%$ of the reading over the whole range. The response time (90% of target value) of the humidity sensor was

about 0.15 s. The range of the OMEGA OS62-MVC non-contact temperature measurement system was 0 to 538 °C with an accuracy of ± 1 °C of the reading, with response time (95% of target value) was 0.8 s. Both sensors were installed so that the measurements were made just prior to the sheet entering the calender nip, by about 0.08 s for a sheet speed of 950 m/min and a 404 mm diameter roll, and by about 1 s for 90 m/min sheet speed and a 711 mm diameter roll.

Most operations of the controlled environment calender were fully automated. The computer data acquisition system recorded and displayed sheet tension and speed before and after the nip, upper and lower roll surface temperature and their positions relative to a fixed point, CD variation in upper roll surface temperature, nip load, paper caliper at two positions immediately after the nip, and sheet temperature and moisture content immediately before the nip. The acquisition rate was keyed to sheet speed and roll radius in order to keep the distance along the sheet between samples approximately constant. With about 150 to 200 data points acquired per roll revolution, over a total of 10 to 15 roll revolutions, the acquisition rate was about 2000 Hz for a 404 mm diameter roll with 1000 m/min sheet speed, about 200 Hz with a 711 mm diameter roll at 90 m/min. In this way the data were taken while about 17 m of paper were calendered, as is detailed later. Calender speed and thus sheet speed was controlled using a PID loop in software, which sent a 0 to 10 V signal to a modified controller of the main motor drive. Sheet tension after the nip was controlled in the same way by sending a correction signal to a similar controller of the trim motor. Nip load was controlled by a PID loop which adjusted a pressure regulator in the hydraulic circuit supplying the load cylinder. The calender heating system was controlled by the same computer program as the rewinder heating system. Sheet tension before the nip and roll surface temperature were controlled manually in response to the displayed value.

3.2 Data acquisition and processing systems

With the objective of providing reliable information on paper behaviour in the calender nip, treatment of the output from the roll displacement gauges to give the paper in-nip thickness was the key data processing concern. The central aspect was the relationship between the position of each roll and appropriate displacement sensor. Calibration of these gauges was essential for reliable in-nip paper thickness measurement.

Neither the lower nor the upper roll remain fixed relative to the displacement sensor during use. The presence of paper in the nip alters the position of the upper roll without affecting the lower roll. However, an imperfection in design of the roll bearings allows vertical movement of both rolls. The amount of displacement depends on roll speed and nip load, which have opposing effects. At constant load, hydrodynamic forces between the ball bearings and race cause the roll to lift. At constant speed, load causes the roll to drop by forcing grease out from the lower ball races in the bearings. Although these effects concern mostly the lower roll, the position of both rolls was affected because the upper roll rides on the lower one.

In the case of the lower roll, increasing speed at constant load from the lowest to highest (90 to 900 m/min) could lift the roll as much as 10 μm . By keeping speed constant and increasing the load from the lowest to highest (15 to 210 kN/m), the roll could be pushed down as much as 15 μm . Such disturbances, while negligible on the scale of a 0.4 to 0.7 m diameter roll, are large relative to in-nip paper thickness of 30 to 40 μm .

Measurement of roll separation and thus in-nip paper thickness was further complicated by the slight eccentricity, relative to the bearing axes, of the surfaces and shoulders of all rolls used in the present study. The roll generates a sinusoidal wave of period and amplitude equal to the period of roll rotation and magnitude of the eccentricity, which affects the output from the displacement gauges. The eccentricities of the roll surface and roll shoulders are identical as to phase and comparable in amplitude, ranging from 25 to 40 μm . The position of the upper roll, riding on the lower roll, is even more

disturbed, being determined by the sum of the amplitudes and the relative angular position of both rolls. Again the effect of such eccentricities, small in the scale of the roll, are enormous relative to in-nip paper thickness.

To overcome the above problems two displacement sensors were used, one per roll, to accurately measure the sensor-roll surface distance. The distance between the rolls thus corresponded to the sum of the distances from the gauges to those rolls. For constant paper speed and nip load the displacement due to roll bearing imperfection was likewise constant, so the in-nip paper thickness was the difference between the roll separation without paper in the nip, and that measured with paper.

The effect of roll eccentricity was eliminated by averaging the measured sensor-to-roll distances over 10 to 15 roll revolutions, the number of revolutions used depending on paper speed and roll radius. Since the acquisition rate was keyed to those parameters, the in-nip paper thickness was an average over about 17 m of paper, these measurements being taken over a period of about 1.1 to 11.3 s.

For two runs, one with paper and the other without, Figure 3.10 shows typical outputs from both displacement sensors, obtained as a function of the elapsed time t normalised relative to the total acquisition time T . Data for both readings were collected at the same nominal line load, 95 kN/m, and same nominal speed, 90 m/min. The lower roll eccentricity of approximately 38 μm is easily visible. The slightly more deflected position of the upper roll, in the range 55 to 60 μm , reflects the combination of the upper and lower roll eccentricities.

All outputs from the controlled environment calender sensors were collected by two 12 bit analog-to-digital conversion boards installed at a 386 DX-33 based PC computer. Simple RC filters with a cut-off frequency of 34 Hz were used to eliminate interference from 60 Hz supply circuits for all analog outputs to be digitised. After digitization each signal was initially processed by taking the moving average which replaces each data point with the average of the four preceding points. The original set of 2048 data were thus reduced to 512 as only every fourth point need be saved. This

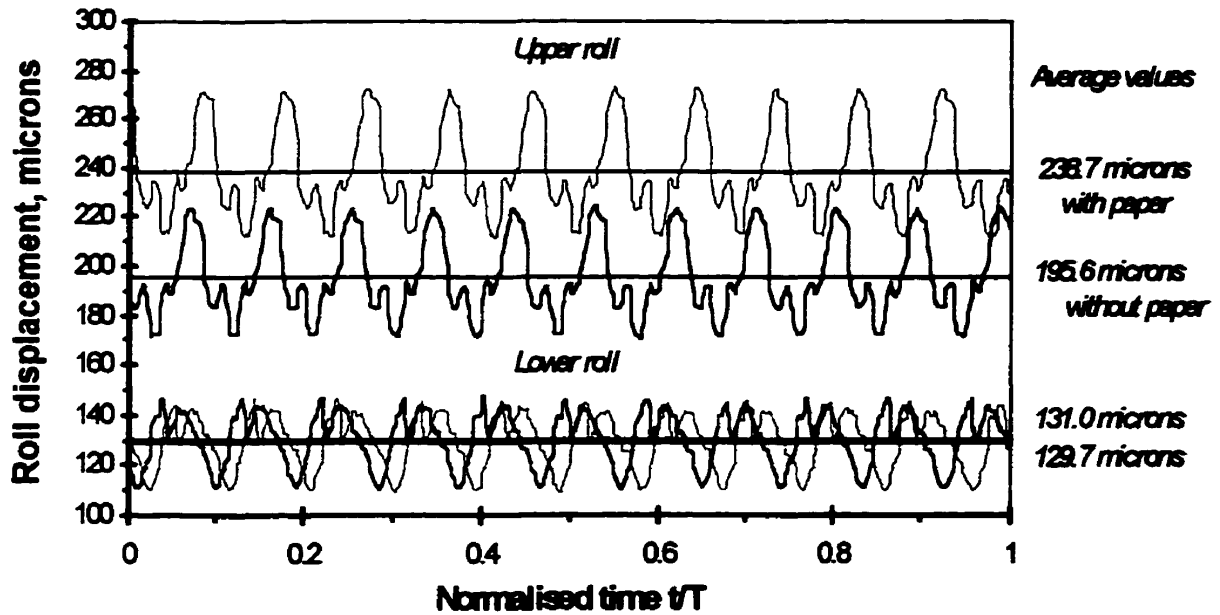


Figure 3.10: Typical displacement sensor output
 (data from Exp.8 runs #e (with paper) and #0e (without paper)).

processing was performed on each signal. The equipment was controlled using the digital input/output ports as well as the digital-to-analog conversion feature of the boards. A custom written program was used for data acquisition, control and initial processing (Appendix A3).

Finally, the in-nip paper thickness was calculated using the following equation:

$$t_n = (u - u_0) + (v - v_0) = (u + v) - (u_0 + v_0)$$

where:

- v - average position of the lower roll with paper (average of 512 data points)
- v₀ - average position of the lower roll without paper (average of 512 data points)
- u - average position of the upper roll with paper (average of 512 data points)

u_0 - average position of the upper roll without paper (average of 512 data points)

For the example shown in Figure 3.10, the upper roll was deflected by the presence of paper in the nip from its average position, $u_0 = 195.6 \mu\text{m}$ measured from a fixed reference point, to a new position $u = 238.7 \mu\text{m}$ as measured from the same reference point. At the same time average position of the lower roll, measured from a different but likewise fixed reference point was changed from $v_0 = 112.9 \mu\text{m}$ without paper to $v = 111.2 \mu\text{m}$ with paper. The average in-nip paper thickness was therefore:

$$t_n = (u - u_0) + (v - v_0) = (238.7 - 195.6) + (129.7 - 131.0) = 43.1 - 1.3 = 41.8 \mu\text{m}$$

The small displacement of the lower roll, only $-1.3 \mu\text{m}$, resulted primarily from the two measurements, one with paper and one without, being taken about 4 minutes apart at slightly different nip loads, even though the nominal nip loads were the same. Another factor affecting the roll displacement readings was that this data set was collected during the experiment for paper moisture content 5% and temperature $40 \text{ }^\circ\text{C}$. To maintain that constant temperature at the nip, the calender rolls were heated, which in turn could result in a small difference in position reading due to thermal deformation of the rolls.

Roll eccentricity also altered the output from the load cell, which controls the nip load, because the rotating rolls act to lift the upper arm. Varying nip load ($\pm 1 \text{ kN/m}$) caused varying paper speed ($\pm 5 \text{ m/min}$) by distorting the DC drive load. Variation in speed in turn changed the paper tension at the unwind stand, which was controlled manually. For low values of nip load, which required relief from the loading system, a small oscillation of the paper web resulted. Web oscillation affected outputs from the paper moisture analyser ($\pm 10\%$ of reading) and, to a much smaller extent, the paper temperature sensor (± 1 to 2% of reading) because both instruments were sensitive to distance from the sheet. All of the above disturbances were sinusoidal and were eliminated by averaging over the same distance as with the roll displacement gauges.

3.3 Experimental conditions

All experiments were performed using an Eastern Canadian newsprint supplied by the Abitibi-Price Company mill at Stephenville, Newfoundland, made from thermo-mechanical pulp (TMP) and of basis weight 48.8 g/m². Three master rolls of paper, each 1.492 m wide and 1.09 m in diameter, were slit into 64 narrow rolls of width 70 mm. Each test roll was preconditioned to a specific paper moisture content and temperature, then maintained at these conditions while run in the environment controlled calendering facility.

The in-nip and permanent paper thickness after calendering were determined using a full factorial experimental design. Experiments were performed for a wide selection of calendering conditions and for a range of paper moisture content and paper temperature well beyond that of any reported study. Several replicates were obtained at selected calendering conditions. The in-nip and permanent strain computed from experimental data were used to obtain the parameters for the full versions of both master creep and calendering equations. Experimental conditions are shown in Table 3.1.

All paper properties except the initial thickness were measured after conditioning for 24 hours at 23 °C and 50% relative humidity. Initial thickness, and consequently initial

Table 3.1: Calendering conditions.

Load, kN/m	15, 30, 40, 95, 135, 175 and 210
Paper speed, m/min	90, 180, 300, 500 and 950
Roll radius, mm	202 and 355
Paper temperature, °C	20, 30, 40, 50, 60 and 75
Paper moisture content, %	2 to 14
Initial bulk, cm ³ /g	2.16 to 2.35

bulk of the uncalendered paper, was measured just prior to calendering. Initial paper thickness was affected not only by its temperature and moisture content, but also to a lesser degree by a slight stretching as it passed through the set of the rewinder idler rolls. Although kept to a minimum, some tension was required to maintain good tracking of the web and good build-up of the windup reel, especially its hardness. The initial bulk, different for each combination of paper temperature and moisture content, was determined at those exact conditions just before calendering.

From literature data [55, 56] an initial estimate was made of the air humidity required to achieve the target moisture level. Figure 3.11 shows initial settings for the 10 combinations of the air temperature and humidity used for the calendering experiments. When a low level of air humidity was used, the measured paper moisture content was almost identical to that estimated. However, at higher levels of humidity the measured moisture content was considerably lower than that estimated, especially at higher temperatures. The discrepancy resulted from the humidity of the air with which the paper

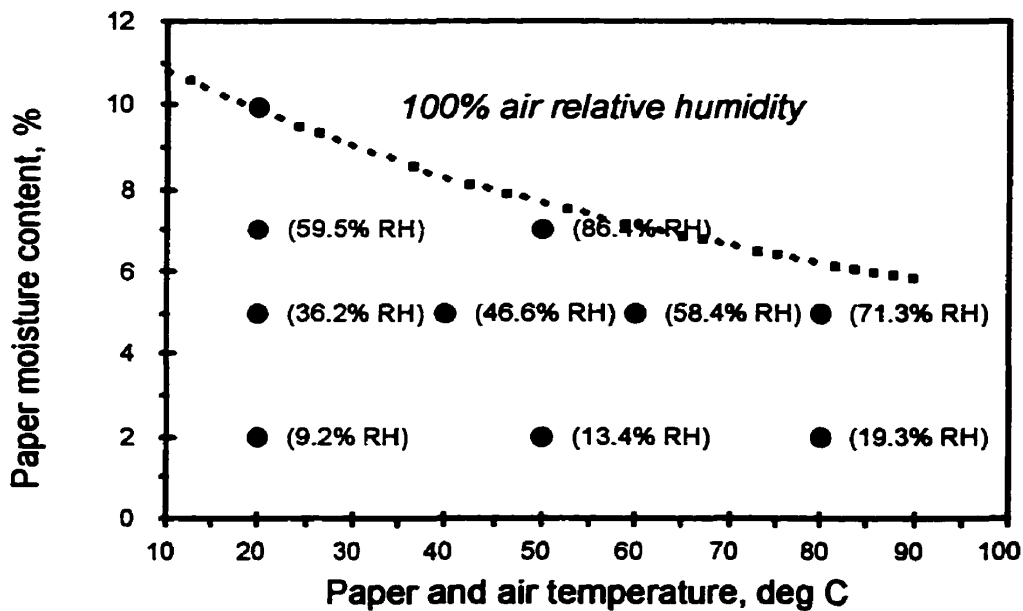


Figure 3.11: Effect of air temperature and humidity on paper temperature and moisture content.

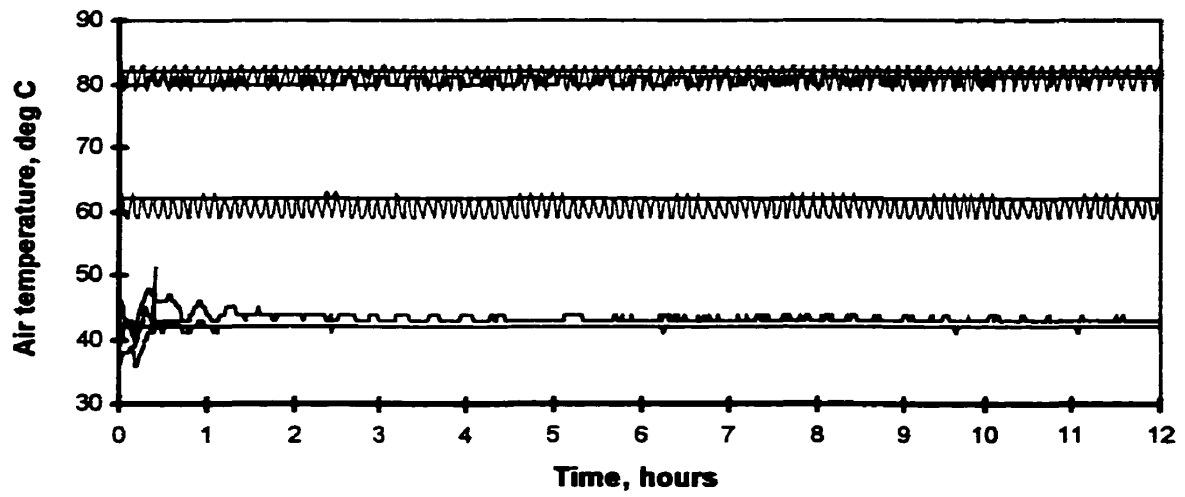


Figure 3.12a: Air temperature during preconditioning, nominal air temperatures of 40, 60 and 80 °C, for Experiments 8, 13 and 14

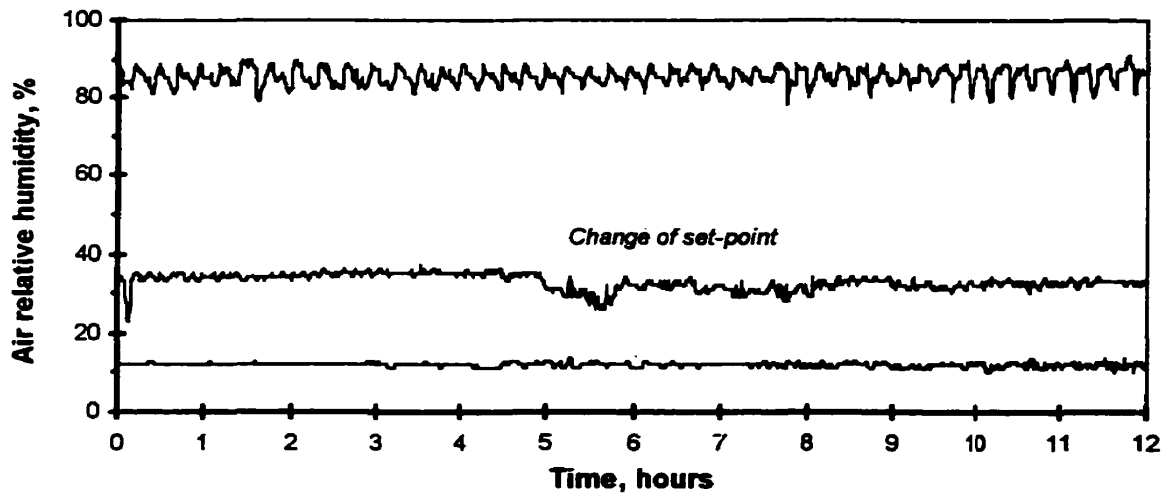


Figure 3.12b: Air relative humidity during preconditioning, nominal air humidity of 9.2, 32(30) and 86 %, for Experiments 21, 24 and 25

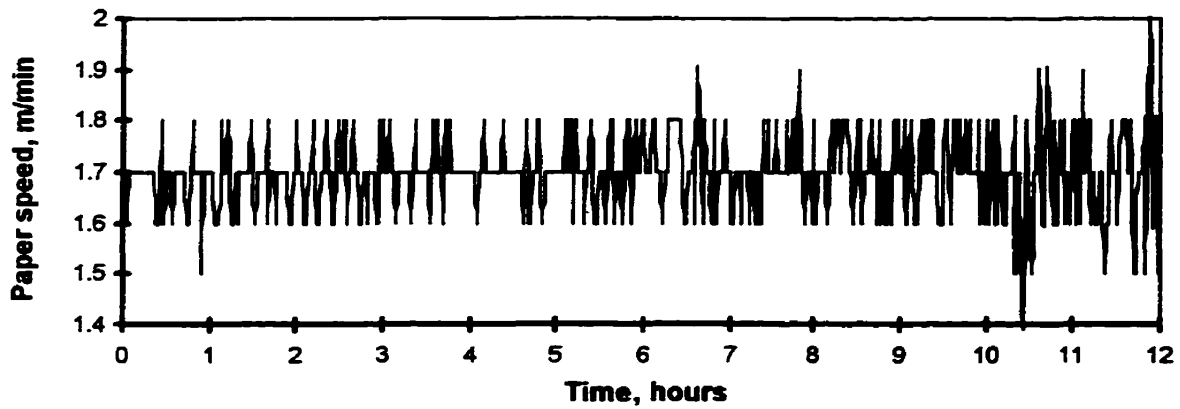


Figure 3.12c: Paper speed during preconditioning for Experiment 14

was equilibrated being lowered due to moisture loss by water condensation inside unheated parts of the air supply system, there being about 8 m between the facility for the conditioned air and the rewinding chamber. The conditioned roll was moved from the preconditioning chamber to the unwind stand of the controlled environment calender enclosure. Conditions there were maintained constant with the common facility for conditioned air, as previously detailed. The calender heating system ensured that roll temperature matched the sheet temperature precisely throughout the experiment. Records of monitoring these variables for a range of conditions are shown in Figures 3.12a to 3.12c. For each of these cases, four temperatures are shown on Figure 3.12a, i.e. at the conditioned air facility, and at three locations inside the rewinder chamber.

All sensors were allowed to warm up for a minimum of 2 hours. This time was used to measure the initial paper thickness at the constant air temperature and humidity, using a standard electronic micrometer. In order to maintain a specific paper temperature and moisture content constant during this procedure, these measurements were performed in one of the environment controlled hoods of the calender. Paper thickness was determined at 60 points in three rows of 20 each along the machine direction of the web,

over a length of about 1.5 m, one row along the centre-line of the 70 mm wide sheet, and the other two at 15 mm from each edge.

Once the rolls reached the required temperature, paper from the preconditioned roll was threaded through the calender. Under computer control of the main motor, sheet speed was increased slowly to 90 m/min under a 90 kN/m load while the tracking and tension of the sheet were checked. The calender was then speeded up to the desired value and the target nip load applied. When speed and tension were reasonably stable, the complete set of sensors was scanned 2048 times at the rate described in the previous section. The location in the wound roll corresponding to the data set was marked using slips of paper inserted in the winder nip.

The above process was then repeated at the same sheet speed for a sequence of 5 or 6 nip loads, ending each such sequence with a repeat of the initial value of load. Immediately after the data for a complete load sequence was obtained and saved to disk, the paper was cut and a similar set of data, this time without paper in the nip, was obtained for the identical sequence of line loads. This procedure enabled calculation of the calibration offset (u_0+v_0) required to determine in-nip paper thickness, as described in the previous section. This entire procedure was then repeated to cover each of the five sheet speeds.

Usually sheet speed was increased successively from 90 to 950 m/min. The load sequence differed slightly between the calendering speeds in order to maintain about the same range of calendering intensity, which depends primarily on speed and nip load. Thus for higher speed, more higher loads were used. For example, at the slowest speed of 90 m/min the load sequence was: 95, 135, 40, 175 and 95 kN/m but at the highest speed of 950 m/min the load sequence was changed to: 175, 135, 210, 95, 210 and 175 kN/m. It required 20 to 30 minutes to complete a set of experiments for all combinations of speed and nip load but for one paper moisture content- temperature condition.

Such a time consuming experimental approach was required because the thermal deformation of the roll depends on the temperature distribution inside the roll. As heat loss

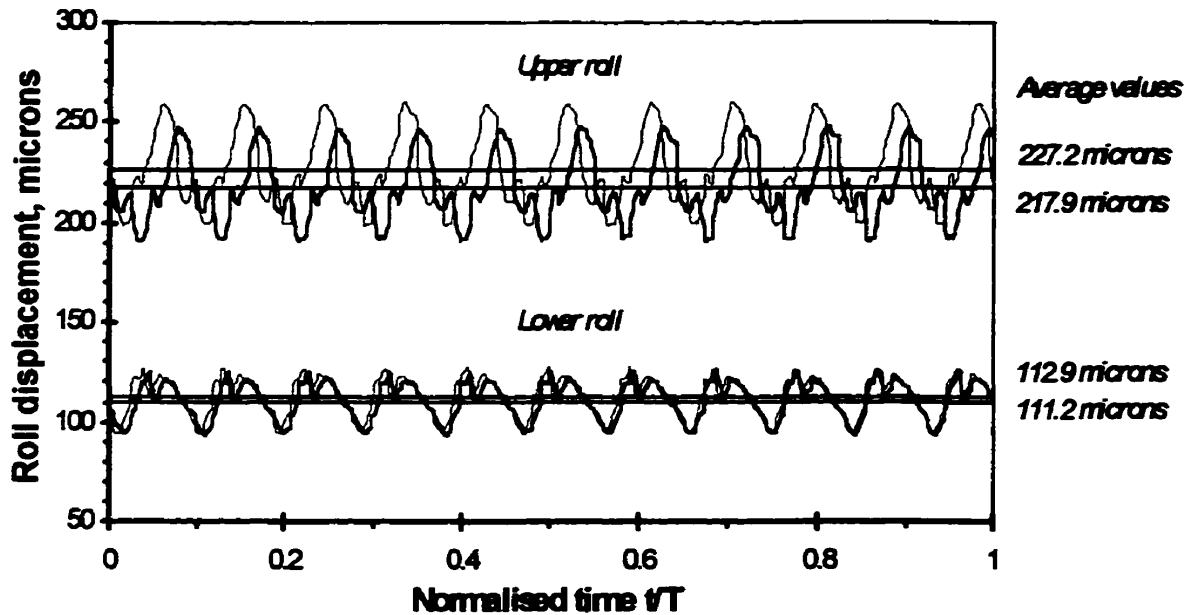


Figure 3.13: Displacement sensor output, “long experiment” for paper and roll
 temperature 40 °C, S= 90 m/min, L= 95 kN/m, T= 20 min
 (data from Exp.8 runs 0b and 0b’ - before and after the whole experiment)

from the rolls is speed dependent, quite apparent at 500 and 900 m/min, the distance between rolls varied during a long experiment. Roll separation measured without paper in the nip first at the beginning and then at the end of the 20 to 30 minute experiment differed by up to 15 μm for roll surface temperature of 80 °C.

Figure 3.13 shows readings from the displacement sensors obtained for base runs, i.e. without paper in the nip, during an experiment for the paper temperature and moisture content of 40 °C and 5%. The readings taken twice, just before the beginning and just after the end of the experiment were collected at the same nominal speed, 90 m/min, and same nominal nip load, 95 kN/m. The average values of position of the rolls measured from fixed reference points is seen to change between these readings. For the lower roll this

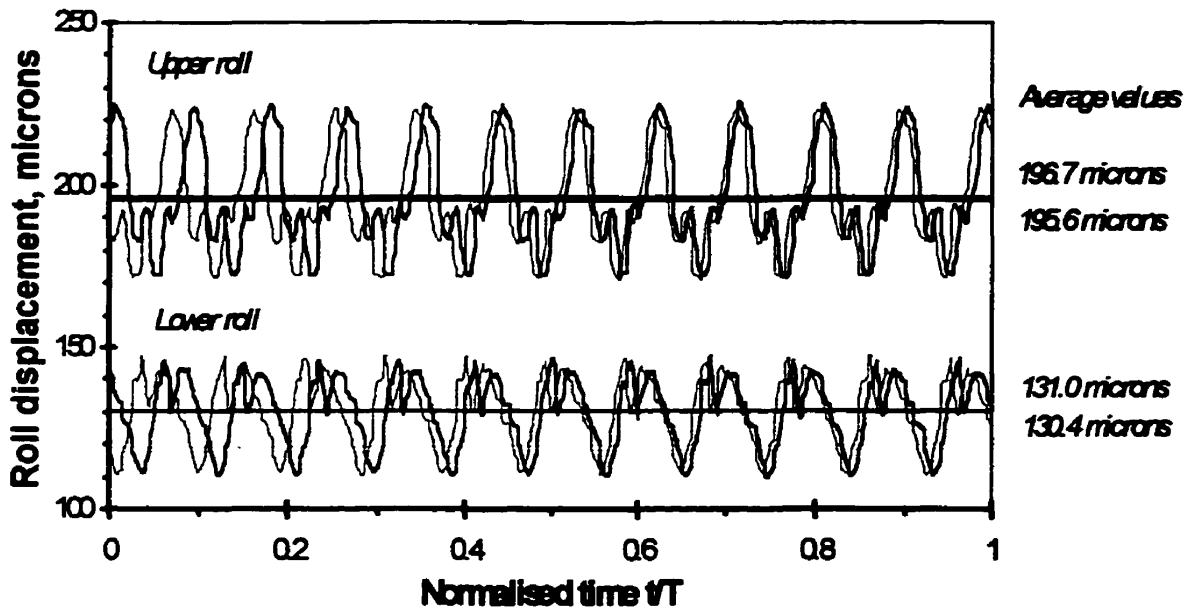


Figure 3.14: Displacement sensor output, “short experiment” for paper and roll
 temperature 40 °C, S= 90 m/min, L= 95 kN/m, T= 5 min.
 (data from Exp.8 runs #0a and #0e)

difference was small, changing from 112.9 μm to 111.2 μm , by only -1.7 μm . However the upper roll position changed from 217.9 μm to 227.2 μm , by 9.7 μm . In summary the calibration offset ($v_o + u_o$), required for the in-nip paper thickness calculation, differed over the long experiment by 11.4 μm . This difference was due to thermal deformation of the calender roll occurring during long experiments. As speed varied, and roll heat loss varied with speed, roll heating had to be varied accordingly. Thus the roll experienced unsteady state conditions, so roll thermal deformation varies and produces this effect. With the calibration effect, $v_o + u_o$, varying in this case by 11.4 μm over a long experiment, only the first 8 such long experiments were done for the calendering measurements reported here. The only way to obtain reliable measurements of in-nip paper caliper was to use a succession of short experiments, each without paper, before and

after each such sub-set. In this way any variations in the roll temperature were negligibly small (Figure 3.14).

The data in Figure 3.14 were obtained during an experiment which differed from those in Figure 3.13 only in that the time interval between taking the two base readings was about 4 minutes instead of 30 minutes. With the short time between base readings the difference in average values of roll position from fixed reference points was minimal for both rolls: $-0.6 \mu\text{m}$ for the lower roll and $1.1 \mu\text{m}$ for the upper one. The change in the calibration offset ($v_o + u_o$) for both base readings was only $1.7 \mu\text{m}$, a very acceptable value. The value used for $v_o + u_o$ was the average of these "before" and "after" determinations, hence is within $0.9 \mu\text{m}$ of the two limiting values.

As the unsteady state roll conditions due to the interaction of convection heat loss, variable roll rpm and compensating roll heating that the rolls experienced were of much more limited scope over 5 than 30 minutes operation, greatly reducing the variable roll deformation, the approximately 5 minutes interval between recording the base readings was adopted as standard procedure.

Taking advantage of the fact that each load sequence began and ended with the same value of load, each set of data for a particular paper speed was evaluated after the end of the experiment. If the in-nip paper thickness calculated using the first and the last data points, measured at almost identical conditions, differed more than $2 \mu\text{m}$, the entire set of data obtained for that speed was discarded and the experiment repeated.

A second advantage of the above procedure was in helping to solve a problem arising from the difficulty in aligning the load cylinder perfectly with the machine-direction centreline of the paper. This effect resulted in a slight twist of the calender stand whenever the loading system switched from providing load to relief. As the frame twisted the position of the upper roll was moved slightly, resulting in about $3 \mu\text{m}$ difference in the displacement sensor reading since it faced a different circumference of the upper roll shoulder. The solution to that problem was taking the measurement of roll separation with and without paper in the nip at the same load and speed. Although initial experiments

performed by Browne [5 to 7] at ambient air temperature and humidity showed that the above procedure was insensitive to roll speed, this procedure could introduce an error now because of the varying thermal deformation of the rolls which, as noted above, depends on roll speed. Since the switch between loading and relieving mode occurs when nip load is decreased below 40 kN/m (the nip load from the weight of the upper roll was 11 to 31 kN/m) the number of experiments performed for loads below 40 kN/m was reduced to minimum.

Once all experiments for one combination of paper temperature and moisture content were completed, the raw data were immediately processed using the same computer used for calendering control and as well, the measurement of the thickness profile of the uncalendered paper was repeated.

From the reel of calendered paper the samples from the marked sections corresponding to each combination of conditions were then collected. From these lengths, of about 17 m as noted earlier, samples were cut to a length equal to one circumference of the particular calender roll, thereby averaging out any small machine direction variation due to roll crowns or eccentricities. For each constant speed part of the experiment there would be 5 or 6 samples, so for a specific paper moisture content and temperature there were typically 27 or 28 samples for a complete sequence. With 30 full experiments performed, in all 760 samples were processed. These samples were moved to the environment controlled room to be conditioned for 24 hours at 23 °C and 50% relative humidity.

The thickness of all calendered samples was measured according to TAPPI Standard 411 (CPPA standard D.4) using a standard electronic micrometer, at 36 points in three rows of 12 along the machine direction of each strip (one row in the centre of the 70 mm wide sheet, the other two rows at 15 mm from each edge). Where the average cross-direction variation in the recovered thickness exceeded 3 μm , the data were discarded, the roll alignment was checked and the experiment repeated; otherwise the

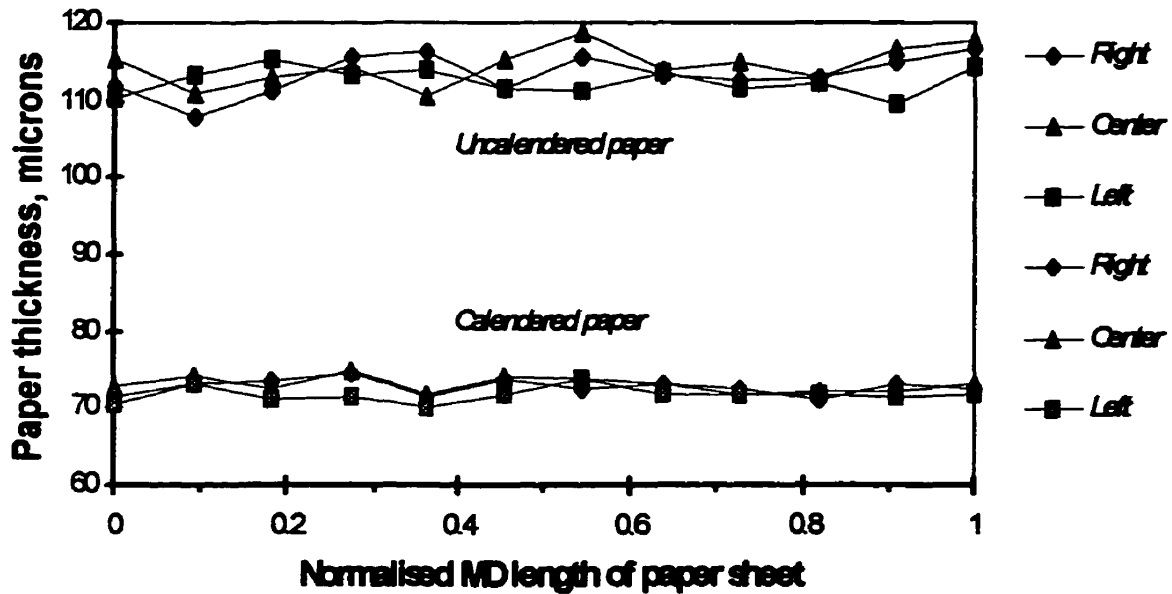


Figure 3.15: Paper thickness profile before and after calendaring.
(data from Exp.25 run #h)

average of all 36 measurements was used as the permanent paper thickness after calendaring.

Typical thickness profiles of the uncalendered and calendered paper are shown on Figure 3.15 as a function of the paper length normalised by dividing by the roll circumference. These data for both calendered and uncalendered paper were obtained for paper temperature and moisture content of 30 °C and 12%, the sheet was calendered at 180 m/min between 202 mm diameter rolls under a line load of 175 kN/m. The average value of the uncalendered paper thickness was 113.4 μm (STD= 2.35 μm), and after calendaring, 72.5 μm (STD= 1.12 μm). The apparent improvement in both machine and cross-machine thickness profiles obtained after calendaring should be interpreted with

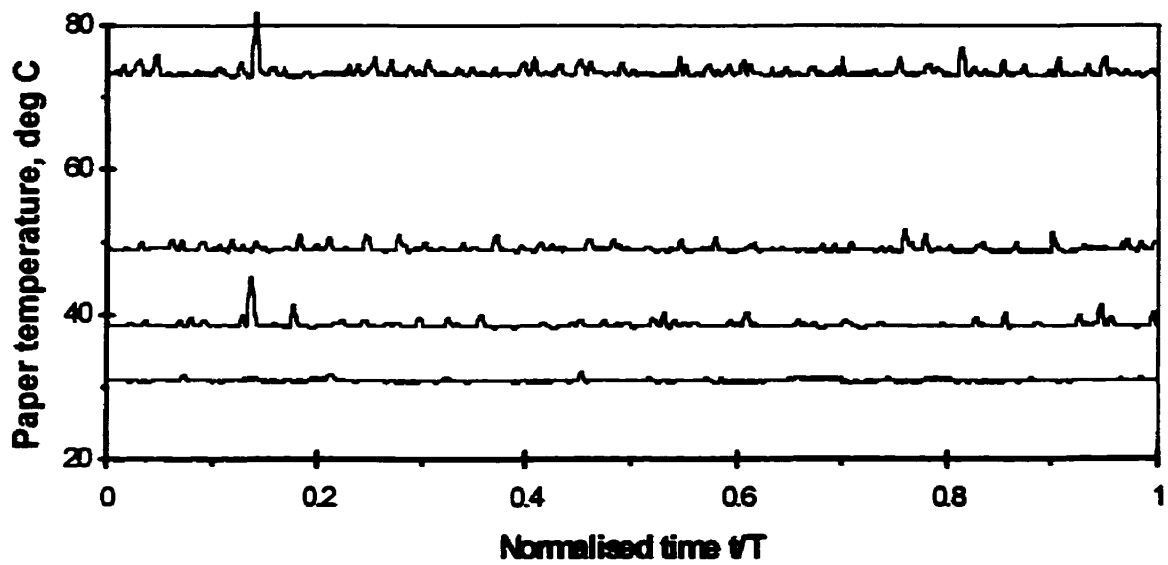


Figure 3.16a: Paper temperature profiles, nominal temperatures of 30, 40, 50 and 80 °C.
 (data from Exp.8 run #e, Exp.13 run #f, Exp.14 run #e and Exp.24 run #m)

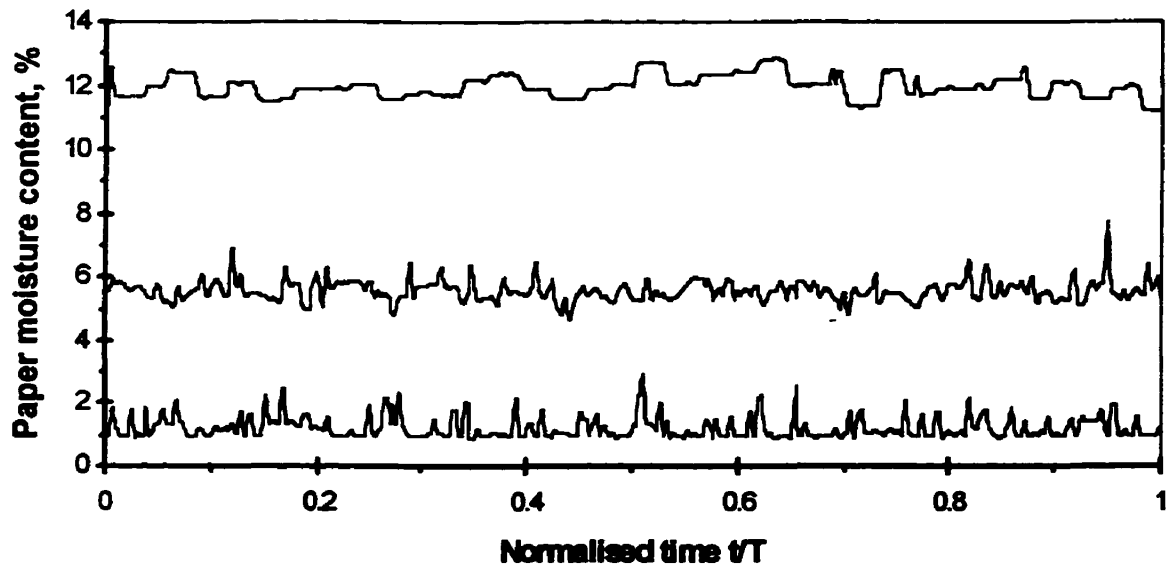


Figure 3.16b: Paper moisture content profiles, nominal moisture contents of 2, 6 and 12%
 (data from Exp.8 run #e, Exp.14 run #f and Exp.25 run #m)

caution. Although both samples were taking from the same roll, they came from a quite different part of that roll.

The first set of experiments, which was performed for a total of 23 combinations of paper temperature and moisture content, were made with the 355 mm rolls. Once a full set of data had been acquired, the pair of 202 mm rolls was installed and data for seven combinations of paper temperature and moisture content were acquired. Figure 3.16a and Figure 3.16b display machine direction variations in paper temperature and moisture content obtained during various experiments.

4 Experimental results

The experimental work focused on measurements of the in-nip and permanent paper strain as paper was calendered under wide selection of industrially relevant conditions. This program involved over 22 combinations of paper temperature and moisture content (30 sets of experiments with combinations of calendering load, speed and roll radius). All combinations of the latter are shown on Figure 4.1.

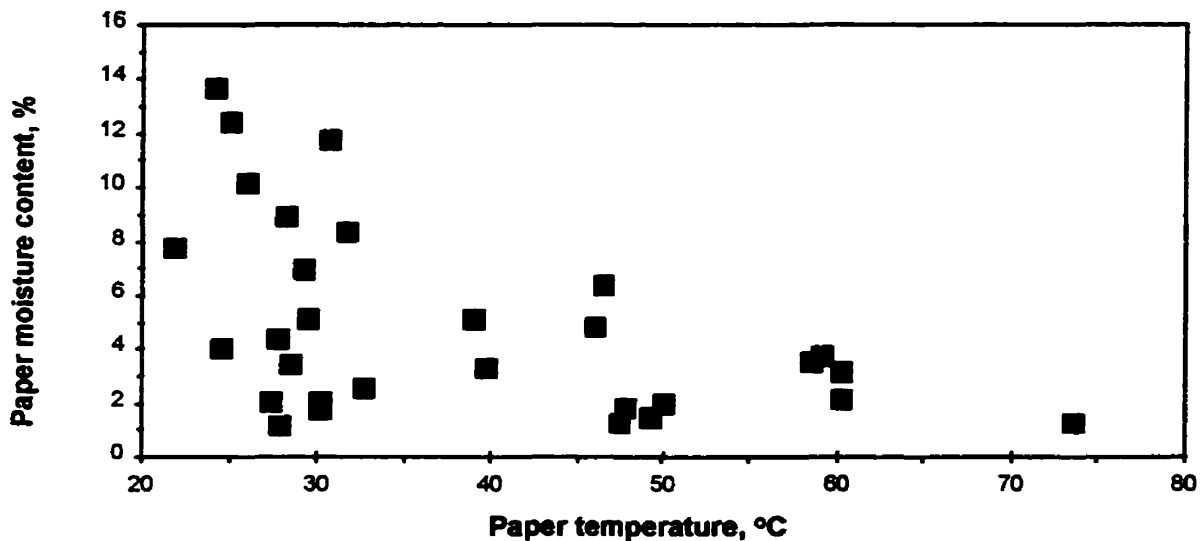


Figure 4.1: Experimental combinations of paper temperature and moisture content.

Data for most of these 30 sets were acquired for 29 combinations of calendering speed and nip load. For the latter, many replicates were taken as these are easily attainable with this calendering facility. However, such repetition involved only a few complete replicates with the same combination of all calendering variables: nip load, speed, paper temperature and moisture content. Two sets of calender rolls were used, 0.355 m and 0.202 m radius, with 23 experiments using the large roll, 7 with the small ones. The initial intention of using the third pair of rolls of intermediate size, 0.254 m radius, was abandoned in order to maintain an acceptable length of experimental program.

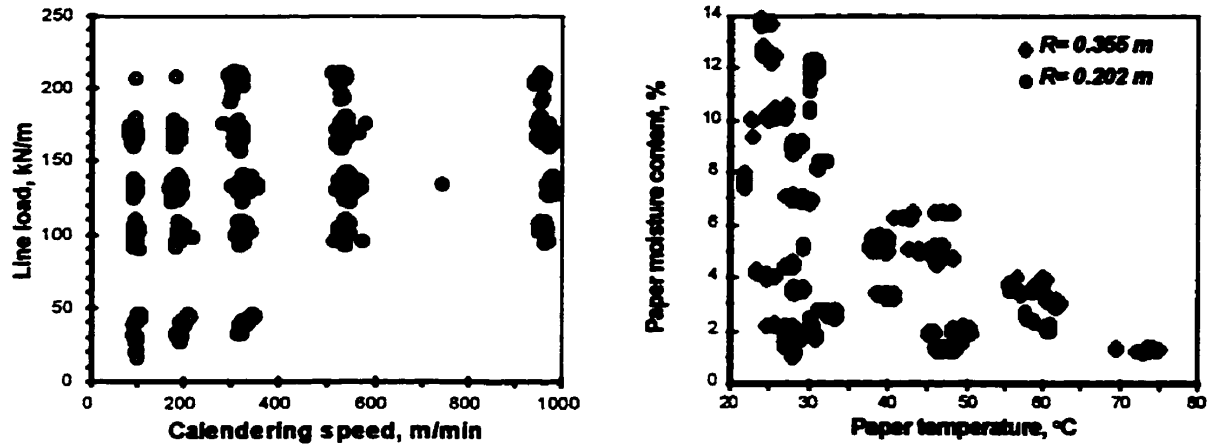


Figure 4.2: Combinations of calendering variables for 760 experiments

4.1 The calendering equations

The whole set of 760 data points was used to calculate the coefficients of both the permanent and the in-nip versions of the calendering equation. As all six calendering variables were investigated, the full version of the equation was used. With in-nip and permanent strains as ϵ_n and ϵ_p , initial bulk B_i , line load L , calendering speed S , roll radius R , and paper temperature and moisture content Θ and M , the calendering equations are:

$$\epsilon_n = A_n + \mu_n B_i,$$

and

$$\epsilon_p = A_p + \mu_p B_i$$

[Eq. 4.1]

where μ_n and μ_p are the in-nip and permanent nip intensities:

$$\mu_n = a_{0n} + a_{Ln} \log_{10} L + a_{Sn} \log_{10} S + a_{Rn} \log_{10} R + a_{Mn} M + a_{\Theta n} \Theta$$

and

[Eq. 4.2]

$$\mu_p = a_{0p} + a_{Lp} \log_{10} L + a_{Sp} \log_{10} S + a_{Rp} \log_{10} R + a_{Mp} M + a_{\Theta p} \Theta$$

The limits of validity of these equations relative to initial bulk B_i are:

$$-A_n / \mu_n \leq B_i \leq 0.5 (1 - A_n) / \mu_n$$

and

[Eq. 4.3]

$$-A_p / \mu_p \leq B_i \leq 0.5 (1 - A_p) / \mu_p$$

As the measured strains, in-nip and permanent, were always greater than zero, the lower limit is not relevant. The upper limit was involved for both in-nip and permanent paper strain. For in-nip and permanent bulk, and thus in-nip and permanent strain, the corresponding relationships are:

$$B_n = 0.25 (1 - A_n)^2 / \mu_n$$

$$\varepsilon_n = 1 - 0.25 (1 - A_n)^2 / (B_i \mu_n)$$

and

[Eq. 4.4]

$$B_p = 0.25 (1 - A_p)^2 / \mu_p$$

$$\varepsilon_p = 1 - 0.25 (1 - A_p)^2 / (B_i \mu_p)$$

The above equations are valid for:

$$B_i \geq 0.5 (1 - A_n) / \mu_n$$

and

[Eq. 4.5]

$$B_i \geq 0.5 (1 - A_p) / \mu_p$$

The calendering equations and these upper limits were elements of the data processing program. All experimental data were processed using the direct search procedure of the SYSTAT Simplex method for non-linear function minimisation [64]. This procedure searches for the global minimum to a function by calculating a value at one

point of the loss function, in this case the least squares, comparing this value with values elsewhere, and then stepping to a new point and repeating the procedure. When these steps become small, it stops. This procedure is slow compared with the Quasi-Newton method [24], an alternative SYSTAT method of non-linear regression, because the Simplex method does not use the information in the second derivatives to determine the size of step. However the Quasi-Newton method requires the existence of first and second derivatives at all points being computed. If these derivatives are undefined in the region of the true minimum value of the loss function this method is likely to find the closest local minimum rather than the global minimum, unless the initial estimate was exceptionally fortunate. In practice when using the Quasi-Newton method, first derivatives cannot be computed using finite differences because of truncation and cancellation errors. The more robust Simplex method is immune to such problems because it computes new estimates with each iteration.

The coefficients for the calendering equations, along with the asymptotic standard error (A.S.E.) and the 95% confidence limits, are presented in Tables 4.1 and 4.3. Estimates and residual errors are shown in Figures 4.3 to 4.6 for both permanent and in-nip strain. Figures 4.7 to 4.40 provide the data, regression curves, and conditions used.

Figures 4.7 to 4.35 show the data for permanent and in-nip strain obtained from 30 experiments for the unique combinations of roll radius, sheet temperature and moisture content of the present study. Variation in sheet speed is the main source of experimental variability, which is quite small. The calendering equation predictions are calculated for the mean value of sheet speed, except for experiment 13 (Fig. 4.18) where data were collected only for the sheet speed of 300 m/min. For experiment 30 (Fig. 4.35) only in-nip data are presented. In Figures 4.18 and 4.36 to 4.40, data for a single combination of all experimental variables are plotted along with the calendering equation predictions and the corresponding 95% confidence limits.

Browne et al. [6, 7] provided the first in-nip version of the calendering equation and measured in-nip coefficients for a TMP newsprint, Table 4.2. Their study was performed for ambient conditions only, which did not include variation in paper

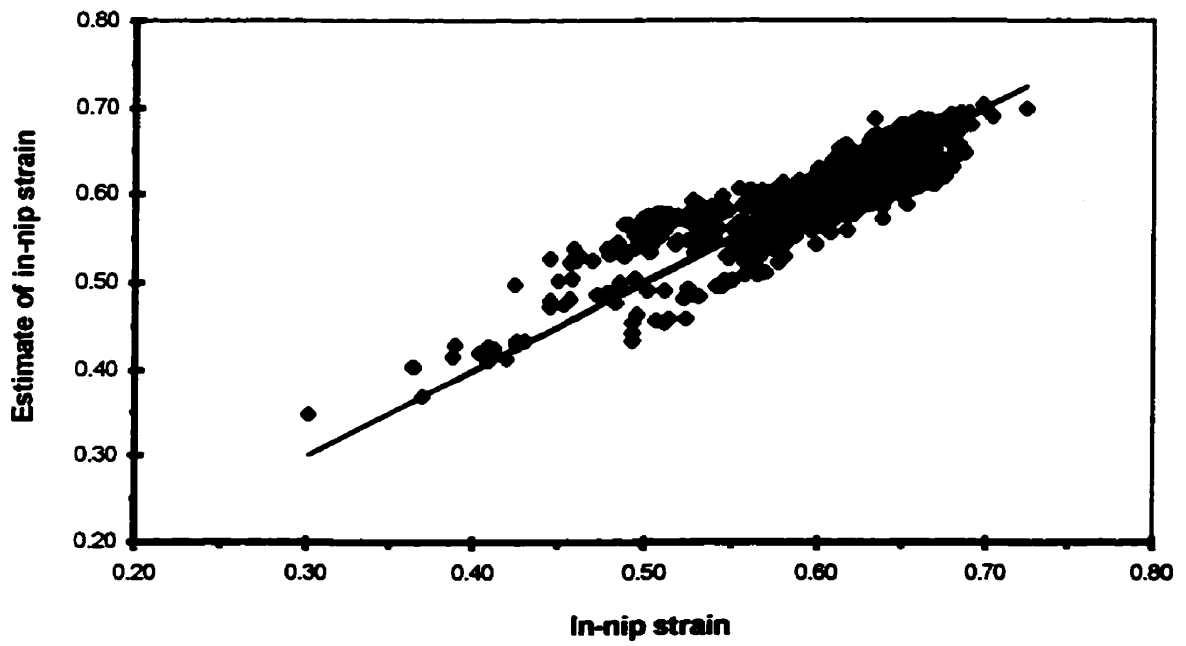
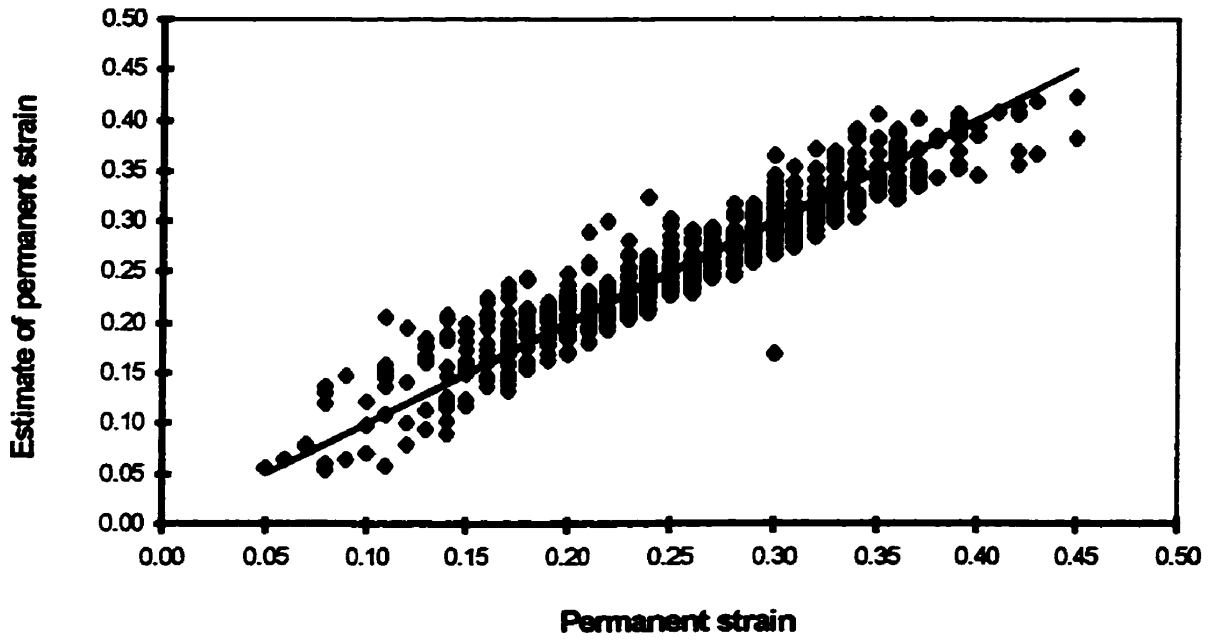


Figure 4.3: SYSTAT estimates of paper strain.

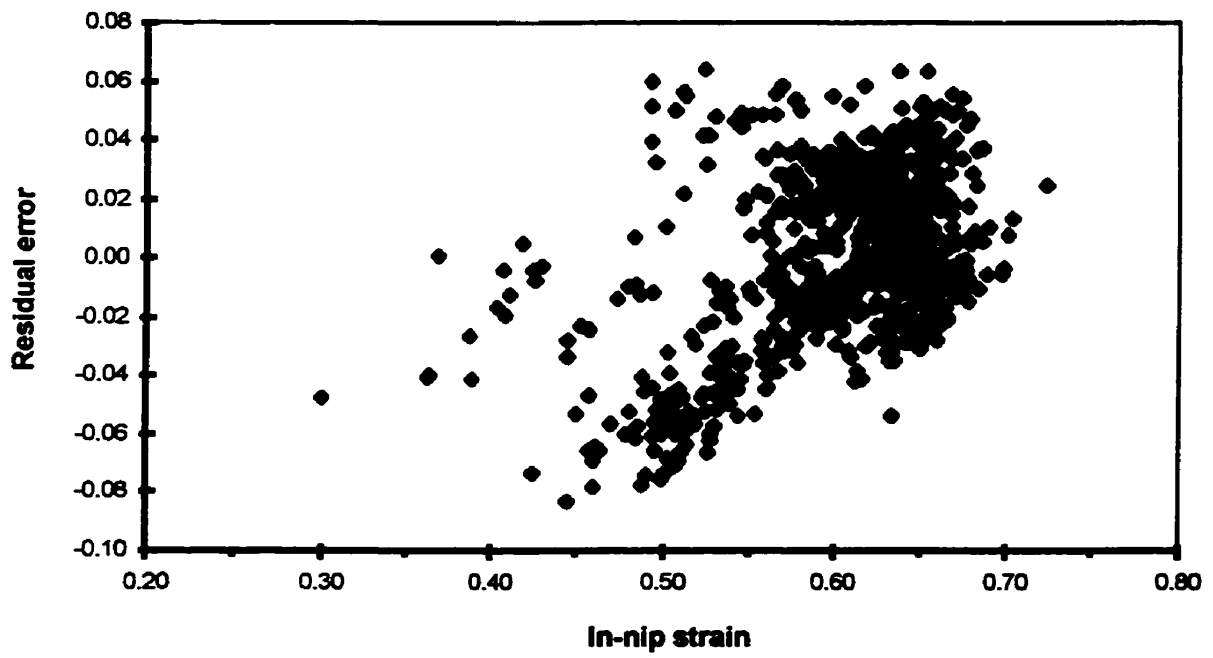
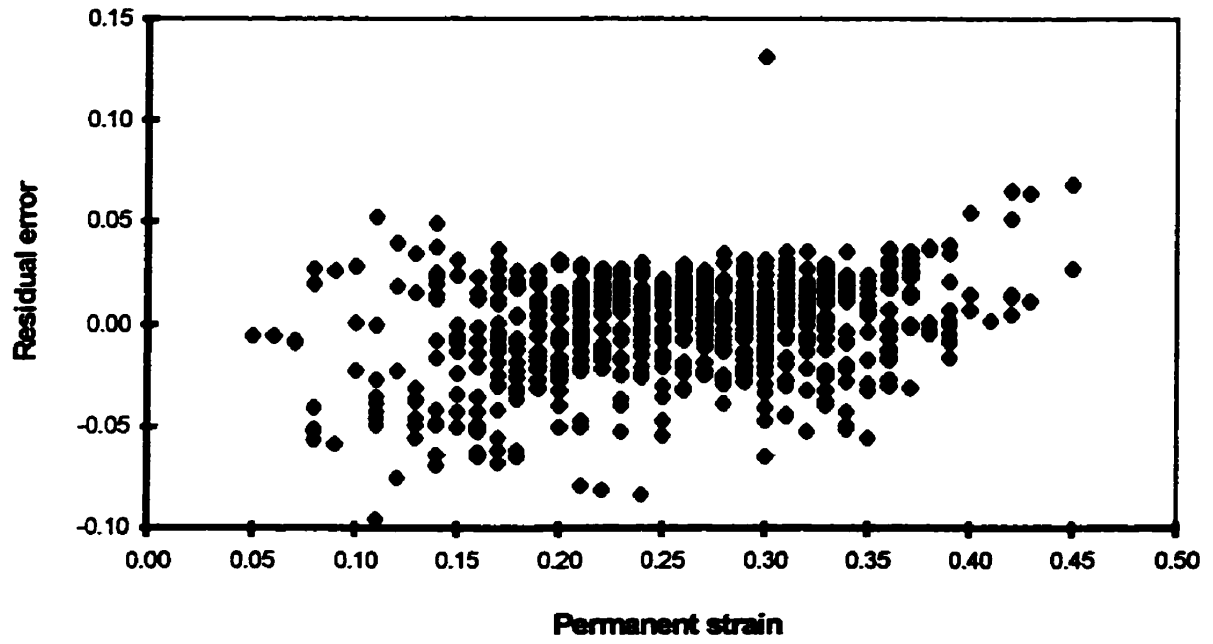


Figure 4.4: Residual error-paper strain relation.

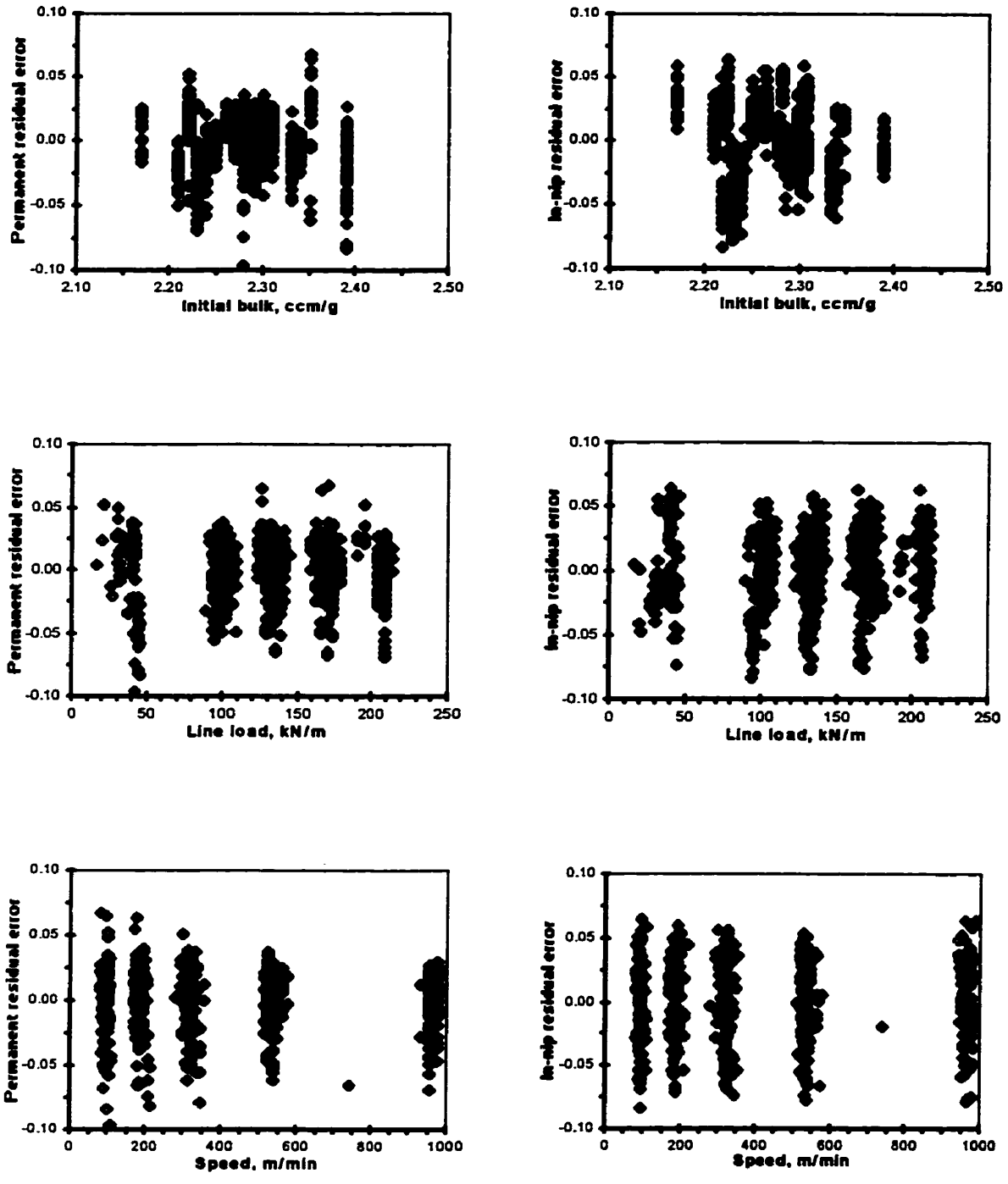


Figure 4.5: Residual error-calendering parameter relations for initial bulk, line load, and speed

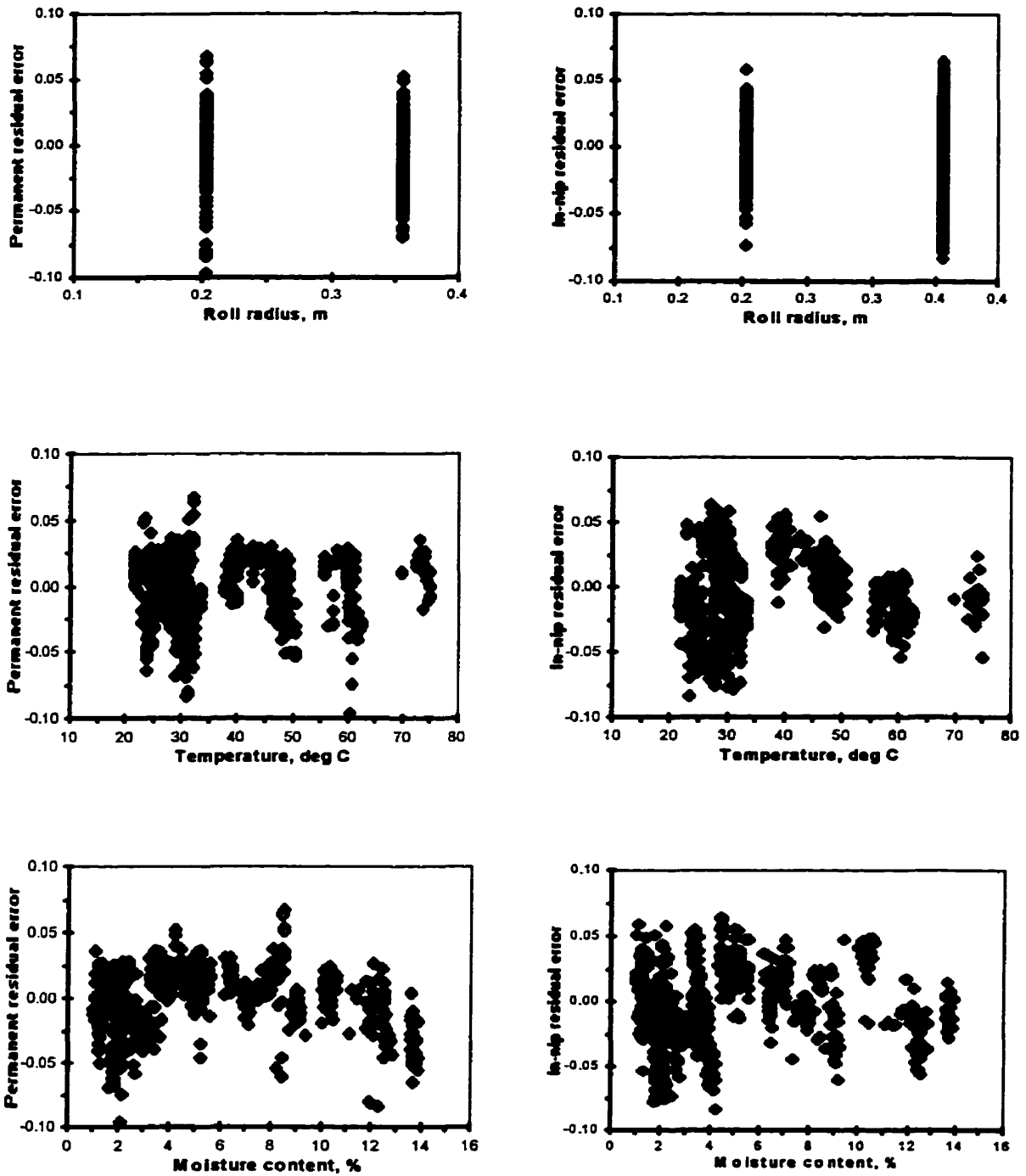


Figure 4.6: Residual error-calendering parameter relations for roll radius, sheet temperature and moisture content.

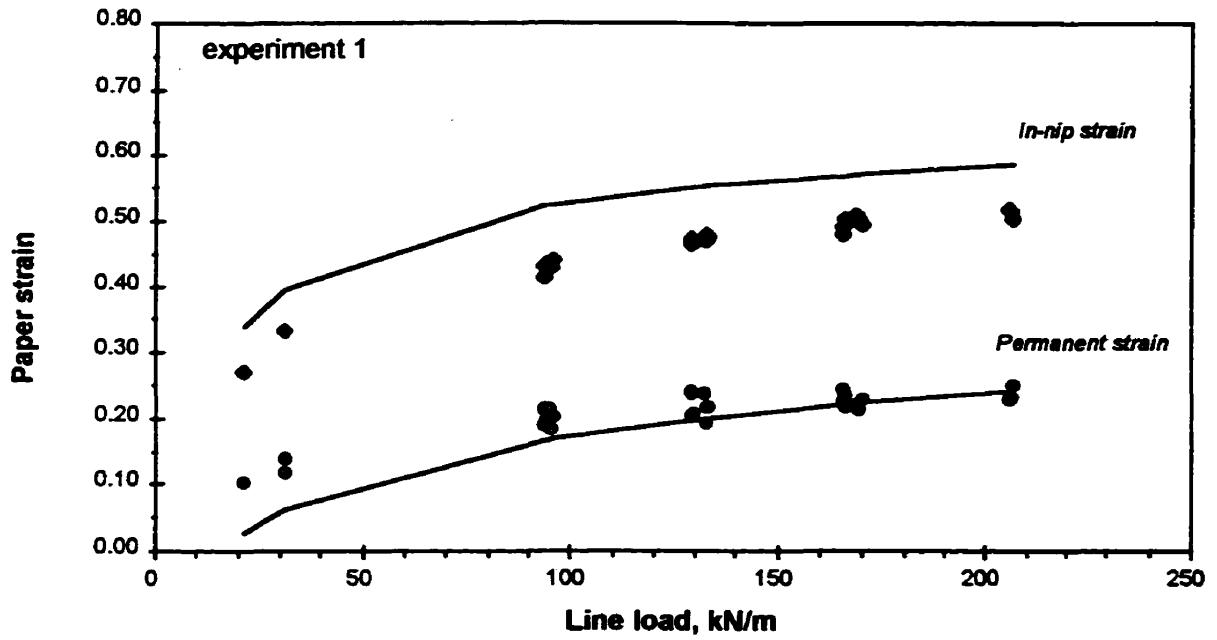


Figure 4.7: Effect of load on strain: $Bi = 2.22 \text{ cm}^3/\text{g}$, $R = 0.355 \text{ m}$, $M = 4.1\%$, $\Theta = 24.5 \text{ }^\circ\text{C}$, all speeds
Best fit lines are for $S = 400 \text{ m/min}$.

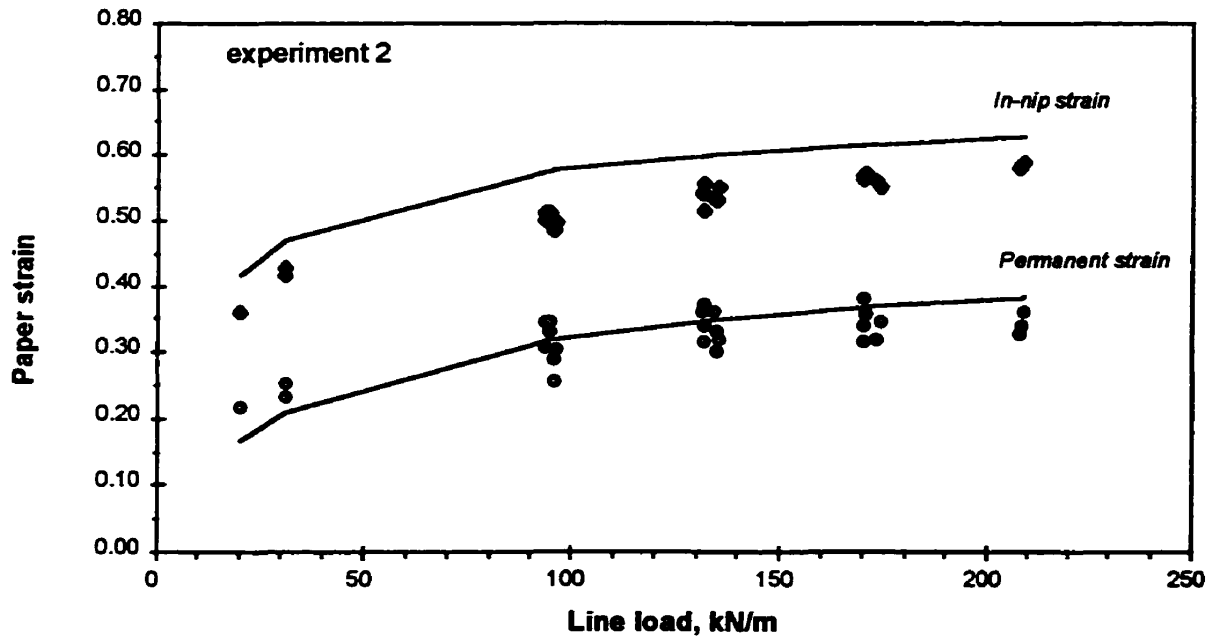


Figure 4.8: Effect of load on strain: $Bi = 2.33 \text{ cm}^3/\text{g}$, $R = 0.355 \text{ m}$, $M = 12.5\%$, $\Theta = 24.9 \text{ }^\circ\text{C}$, all speeds.
Best fit lines are for $S = 400 \text{ m/min}$.

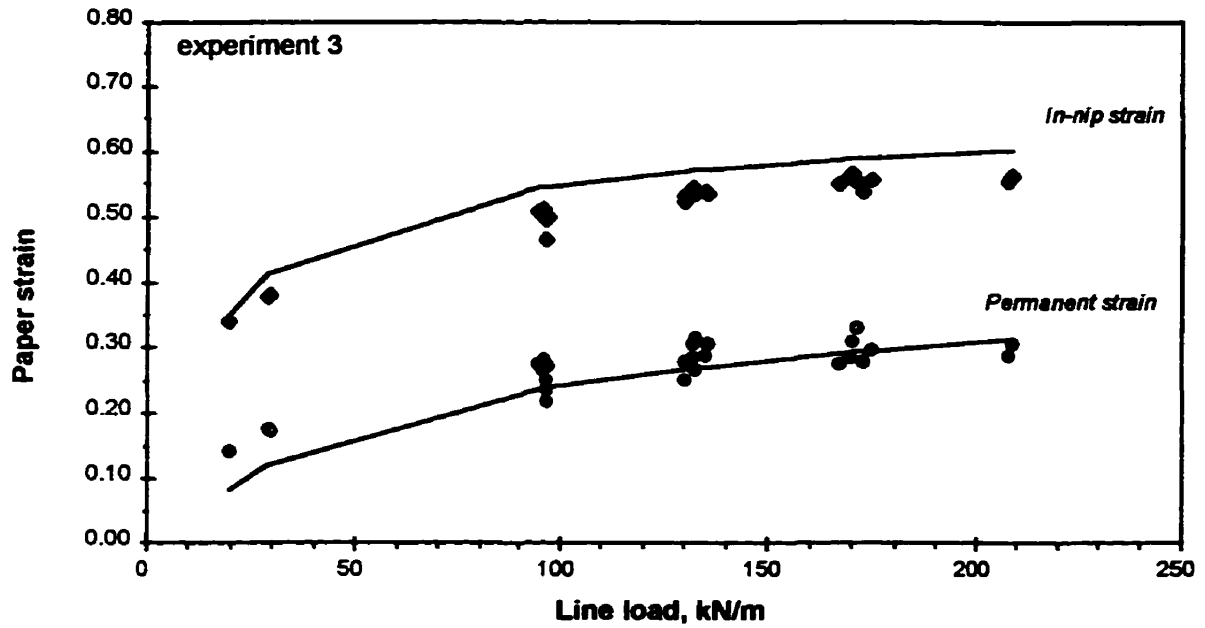


Figure 4.9: Effect of load on strain: $Bi= 2.31 \text{ cm}^3/\text{g}$, $R= 0.355 \text{ m}$, $M= 7.8\%$, $\Theta= 21.7 \text{ }^\circ\text{C}$, all speeds.
Best fit lines are for $S= 400 \text{ m/min}$.

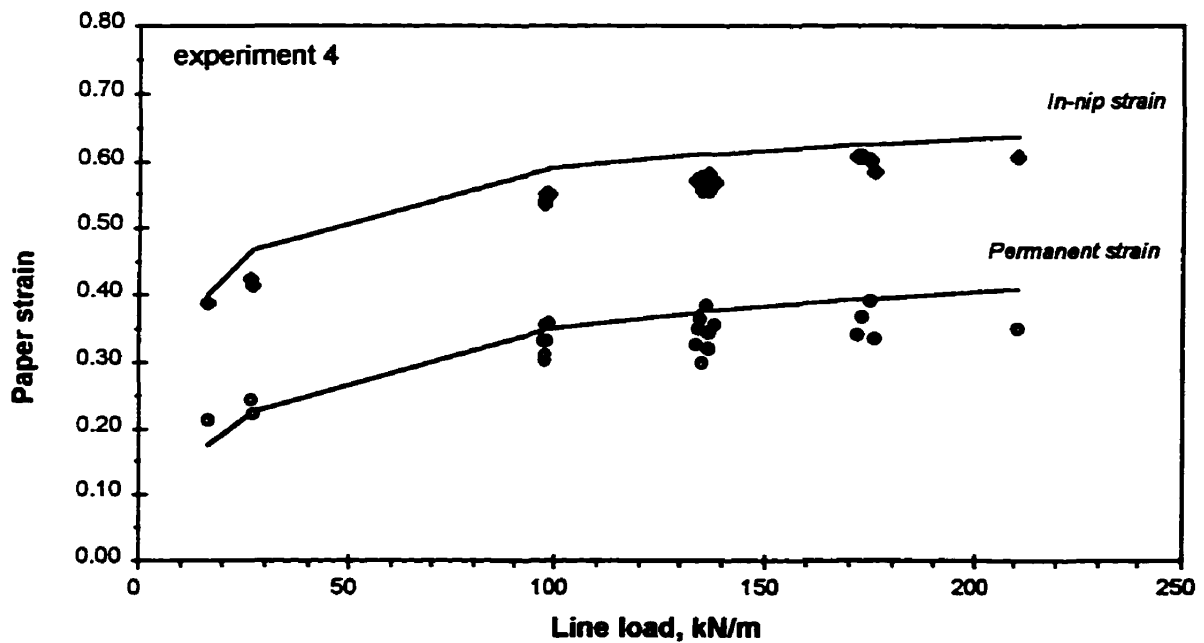


Figure 4.10: Effect of load on strain: $Bi= 2.39 \text{ cm}^3/\text{g}$, $R= 0.355 \text{ m}$, $M= 13.7\%$, $\Theta= 24.1 \text{ }^\circ\text{C}$, all speeds.
Best fit lines are for $S= 400 \text{ m/min}$.

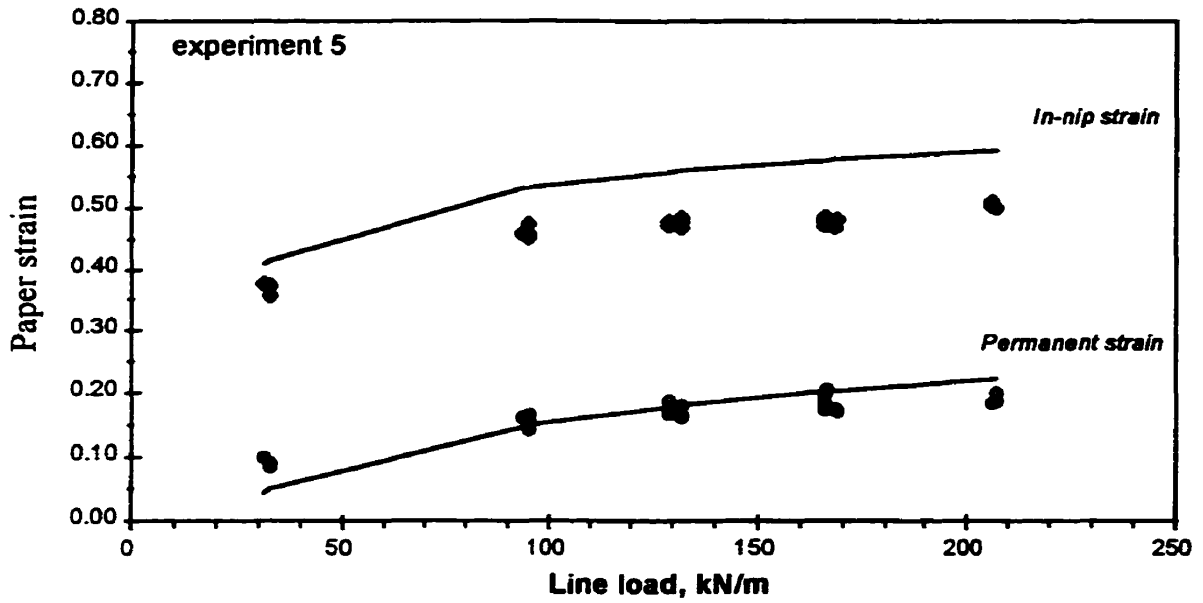


Figure 4.11: Effect of load on strain: $Bi = 2.23 \text{ cm}^3/\text{g}$, $R = 0.355 \text{ m}$, $M = 2.1\%$, $\Theta = 27.3 \text{ }^\circ\text{C}$, all speeds.

Best fit lines are for $S = 400 \text{ m/min}$.

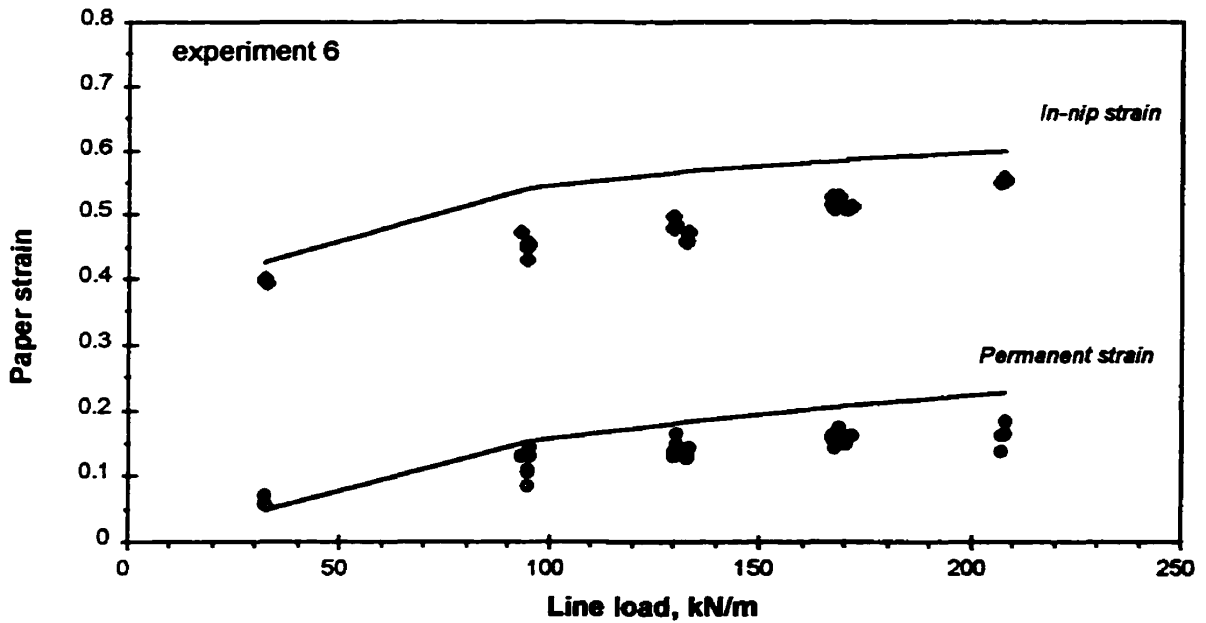


Figure 4.12: Effect of load on strain: $Bi = 2.23 \text{ cm}^3/\text{g}$, $R = 0.355 \text{ m}$, $M = 1.8\%$, $\Theta = 30.1 \text{ }^\circ\text{C}$, all speeds.

Best fit lines are for $S = 400 \text{ m/min}$.

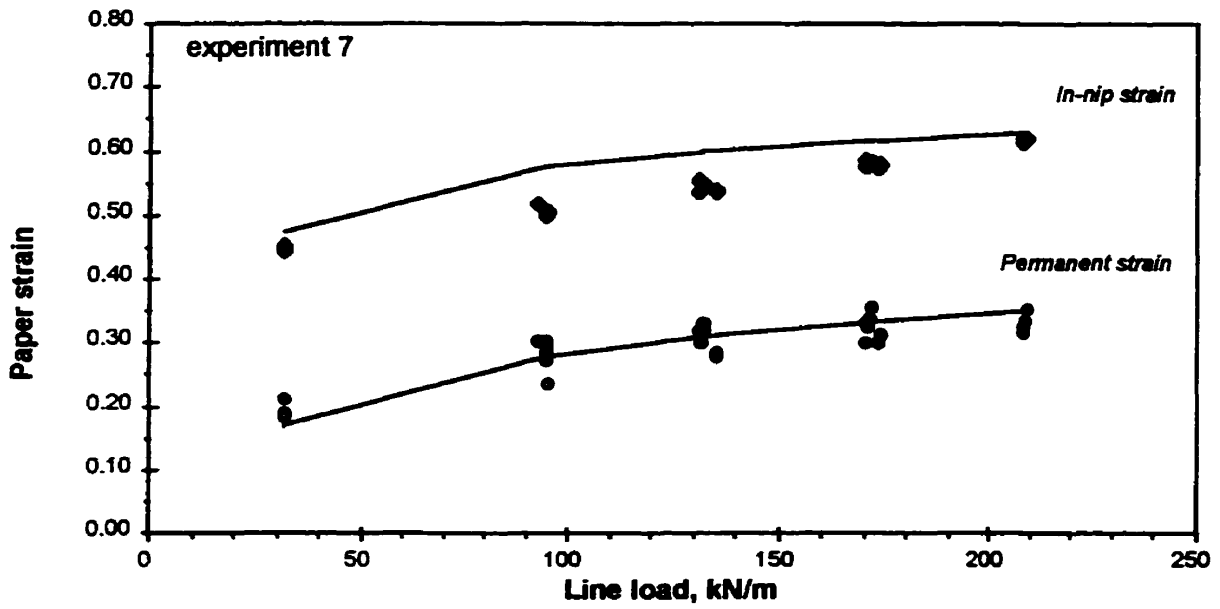


Figure 4.13: Effect of load on strain: $Bi = 2.34 \text{ cm}^3/\text{g}$, $R = 0.355 \text{ m}$, $M = 9.0\%$, $\Theta = 28.1 \text{ }^\circ\text{C}$, all speeds.
Best fit lines are for $S = 400 \text{ m/min}$.

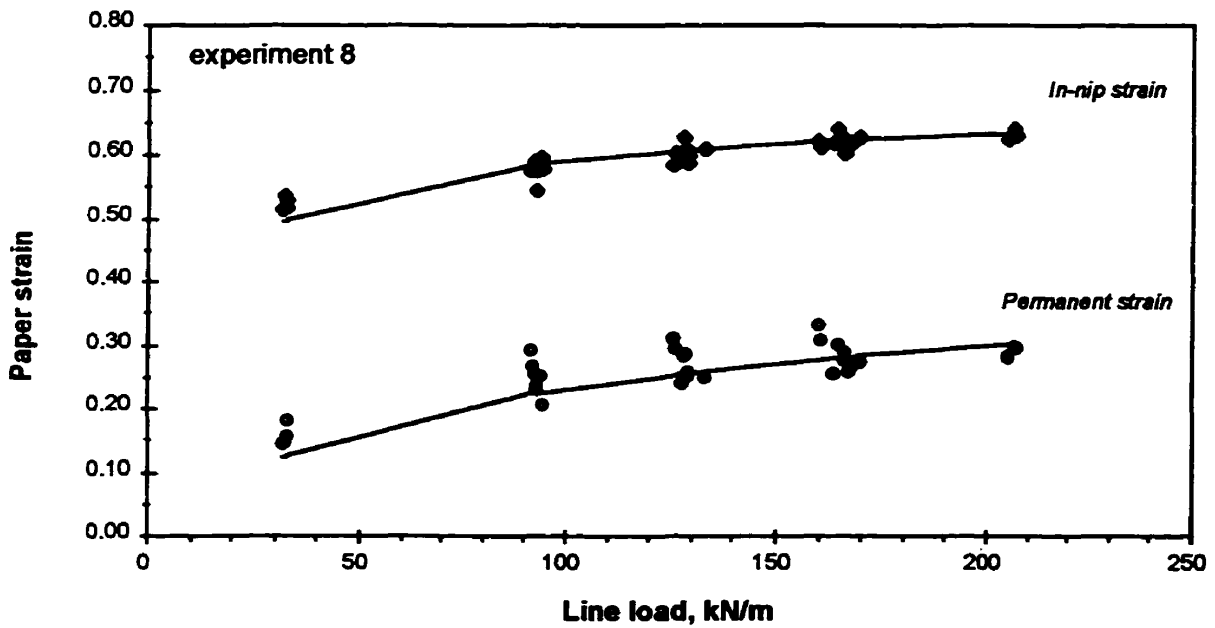


Figure 4.14: Effect of load on strain: $Bi = 2.27 \text{ cm}^3/\text{g}$, $R = 0.355 \text{ m}$, $M = 5.2\%$, $\Theta = 38.8 \text{ }^\circ\text{C}$, all speeds.
Best fit lines are for $S = 400 \text{ m/min}$.

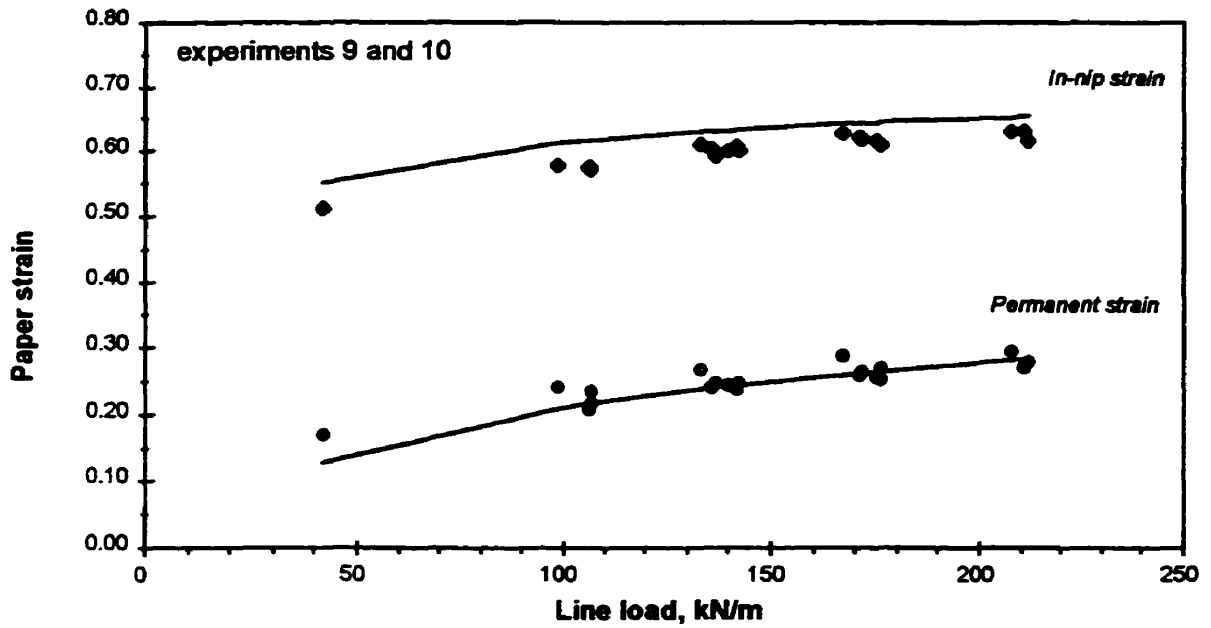


Figure 4.15: Effect of load on strain: $Bi= 2.28 \text{ cm}^3/\text{g}$, $R= 0.355 \text{ m}$, $M= 1.9\%$, $\Theta= 48.4 \text{ }^\circ\text{C}$, all speeds.
Best fit lines are for $S= 400 \text{ m/min}$.

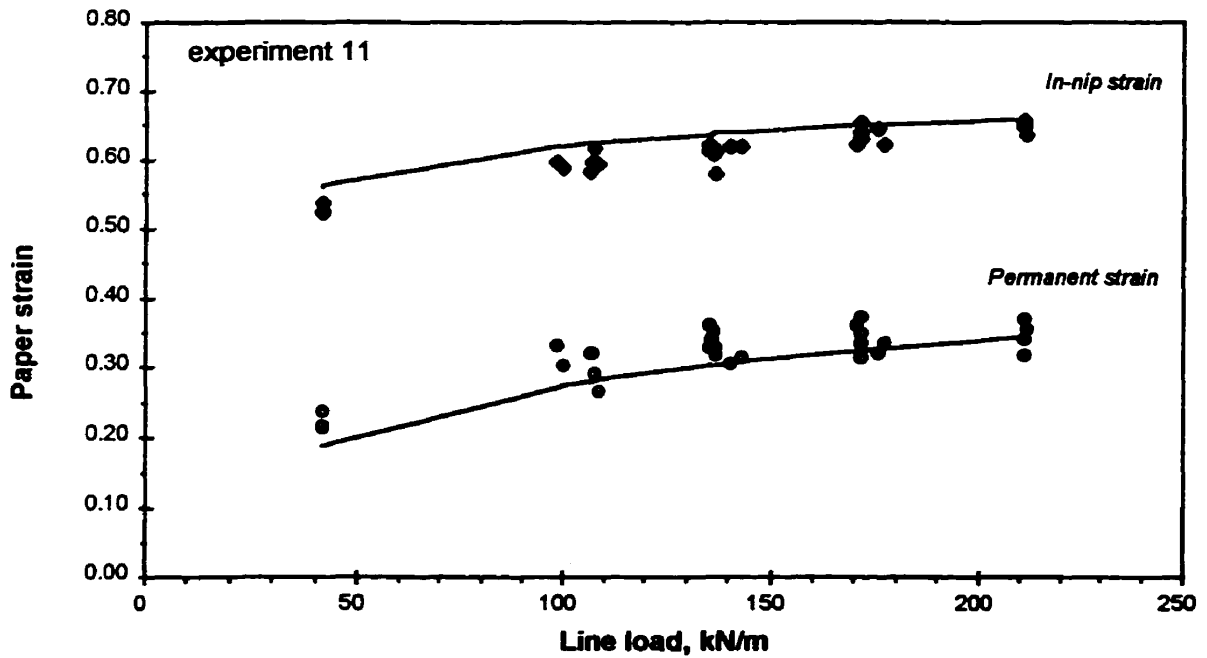


Figure 4.16: Effect of load on strain: $Bi= 2.30 \text{ cm}^3/\text{g}$, $R= 0.355 \text{ m}$, $M= 6.4\%$, $\Theta= 46.3 \text{ }^\circ\text{C}$, all speeds.
Best fit lines are for $S= 400 \text{ m/min}$.

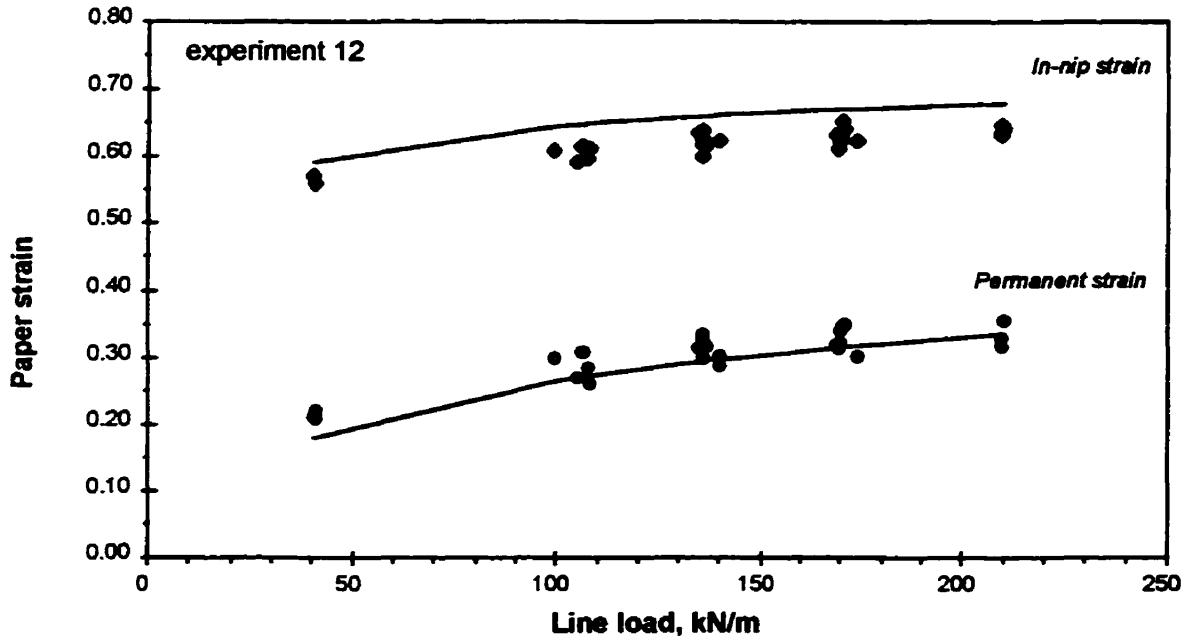


Figure 4.17: Effect of load on strain: $Bi = 2.29 \text{ cm}^3/\text{g}$, $R = 0.355 \text{ m}$, $M = 3.8\%$, $\Theta = 59.0 \text{ }^\circ\text{C}$, all speeds. Best fit lines are for $S = 400 \text{ m/min}$.

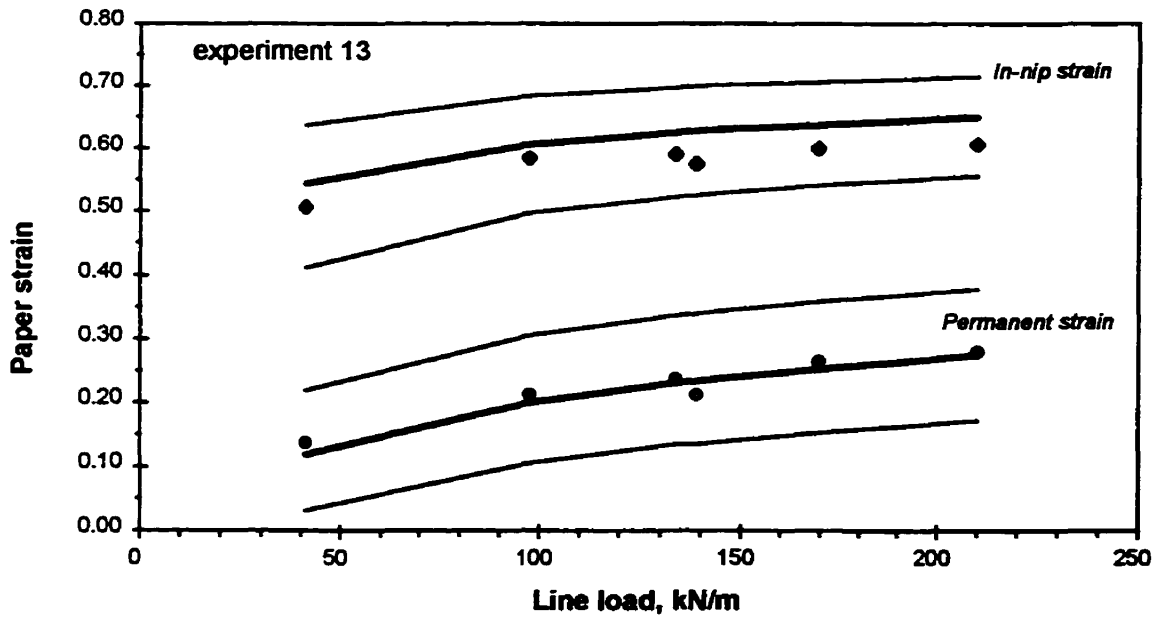


Figure 4.18: Effect of load on strain: $Bi = 2.24 \text{ cm}^3/\text{g}$, $R = 0.355 \text{ m}$, $M = 1.6\%$, $\Theta = 49.3 \text{ }^\circ\text{C}$, $S = 300 \text{ m/min}$.

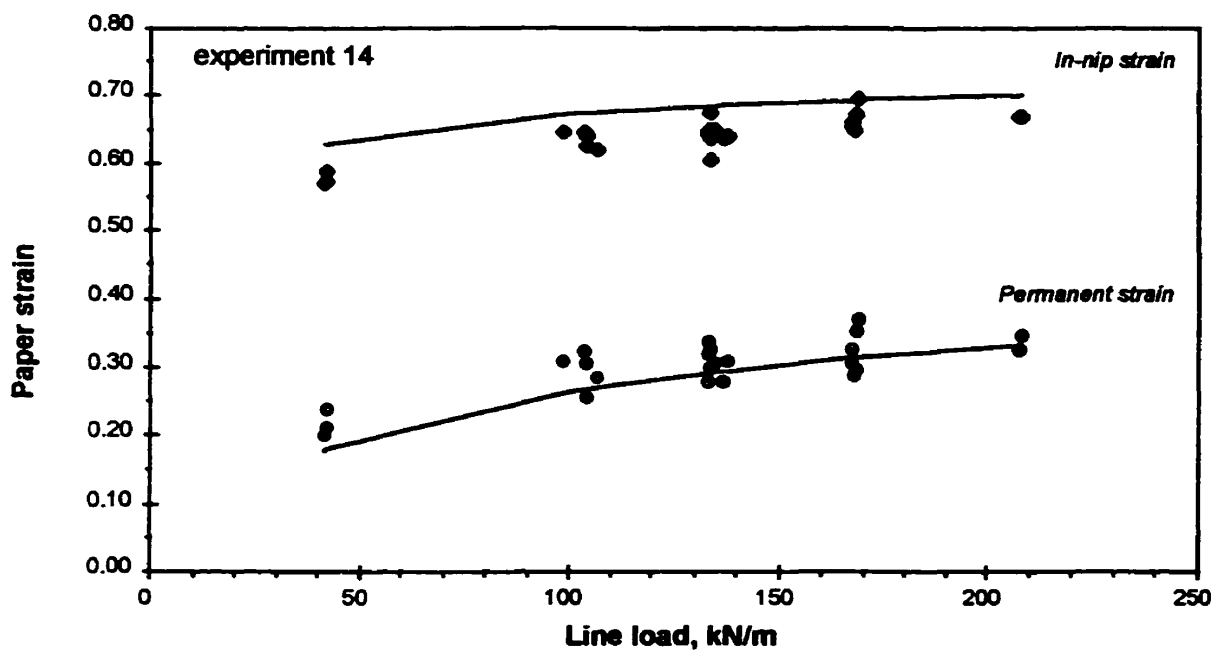


Figure 4.19: Effect of load on strain: $Bi = 2.30 \text{ cm}^3/\text{g}$, $R = 0.355 \text{ m}$, $M = 1.3\%$, $\Theta = 73.4 \text{ }^\circ\text{C}$, all speeds.
Best fit lines are for $S = 400 \text{ m/min}$.

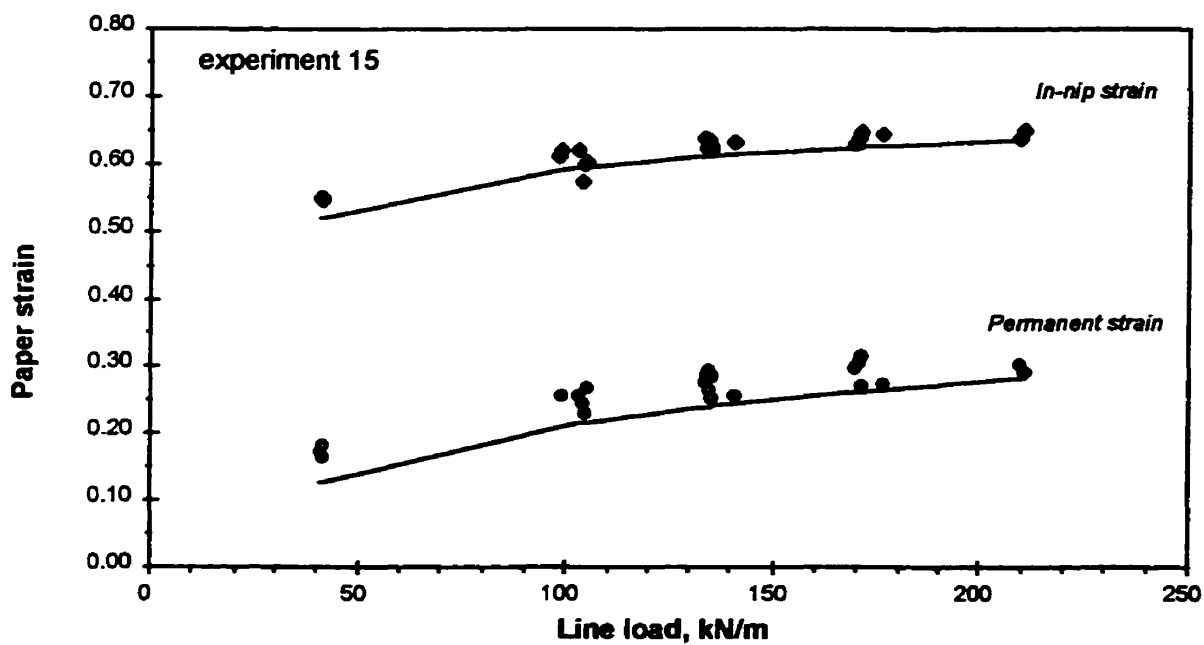


Figure 4.20: Effect of load on strain: $Bi = 2.28 \text{ cm}^3/\text{g}$, $R = 0.355 \text{ m}$, $M = 3.3\%$, $\Theta = 39.6 \text{ }^\circ\text{C}$, all speeds.
Best fit lines are for $S = 400 \text{ m/min}$.

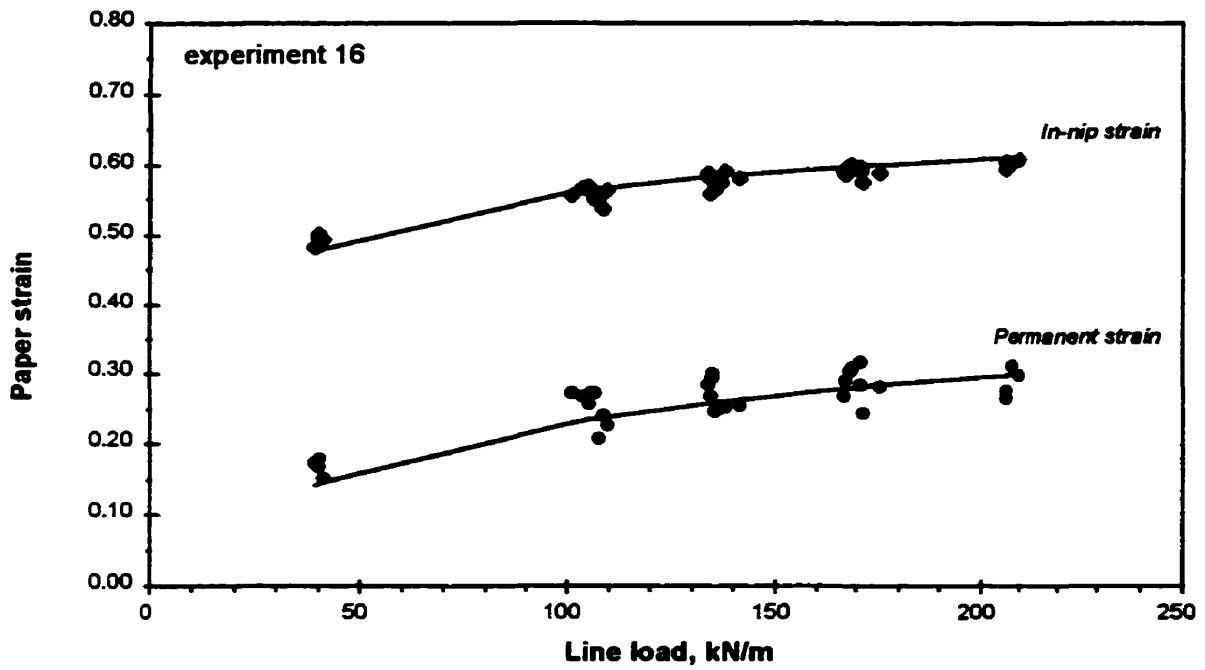


Figure 4.21: Effect of load on strain: $Bi = 2.25 \text{ cm}^3/\text{g}$, $R = 0.355 \text{ m}$, $M = 7.0\%$, $\Theta = 29.0 \text{ }^\circ\text{C}$, all speeds.
Best fit lines are for $S = 400 \text{ m/min}$.

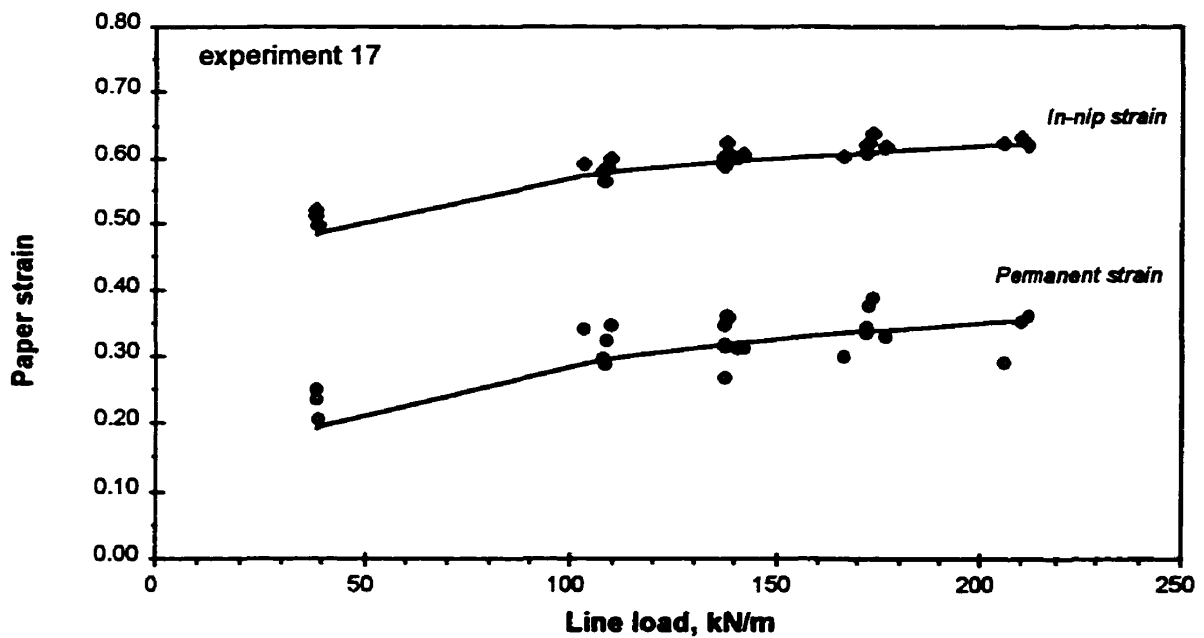


Figure 4.22: Effect of load on strain: $Bi = 2.3 \text{ cm}^3/\text{g}$, $R = 0.355 \text{ m}$, $M = 10.3\%$, $\Theta = 25.9 \text{ }^\circ\text{C}$, all speeds.
Best fit lines are for $S = 400 \text{ m/min}$.

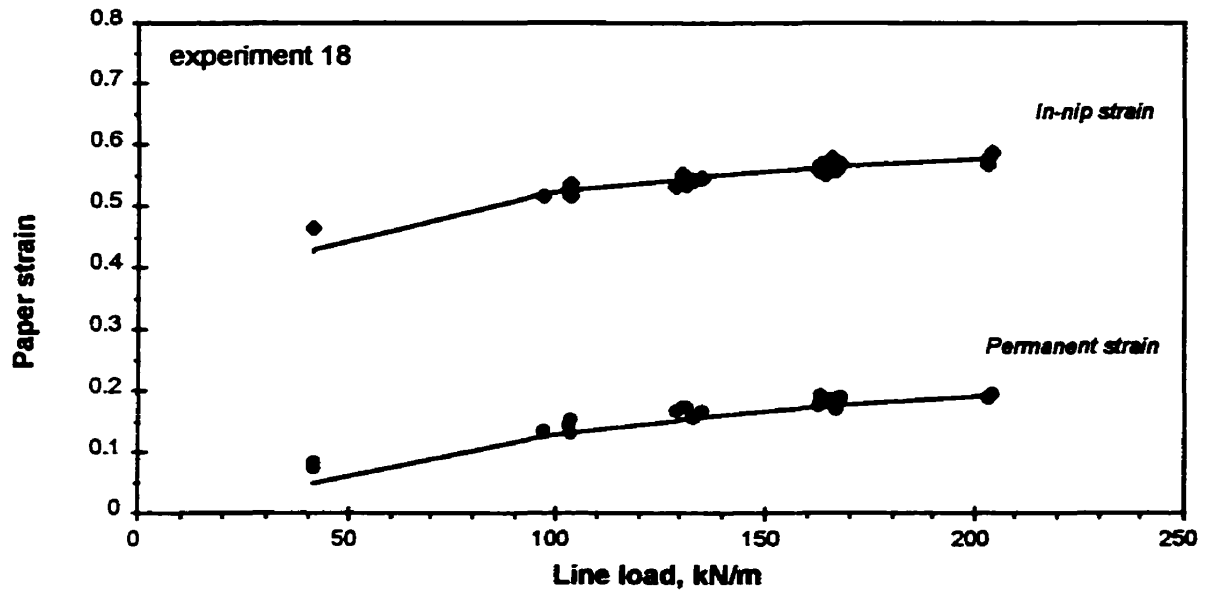


Figure 4.23: Effect of load on strain: $Bi = 2.17 \text{ cm}^3/\text{g}$, $R = 0.355 \text{ m}$, $M = 1.3\%$, $\Theta = 27.8 \text{ }^\circ\text{C}$, all speeds. Best fit lines are for $S = 400 \text{ m/min}$.

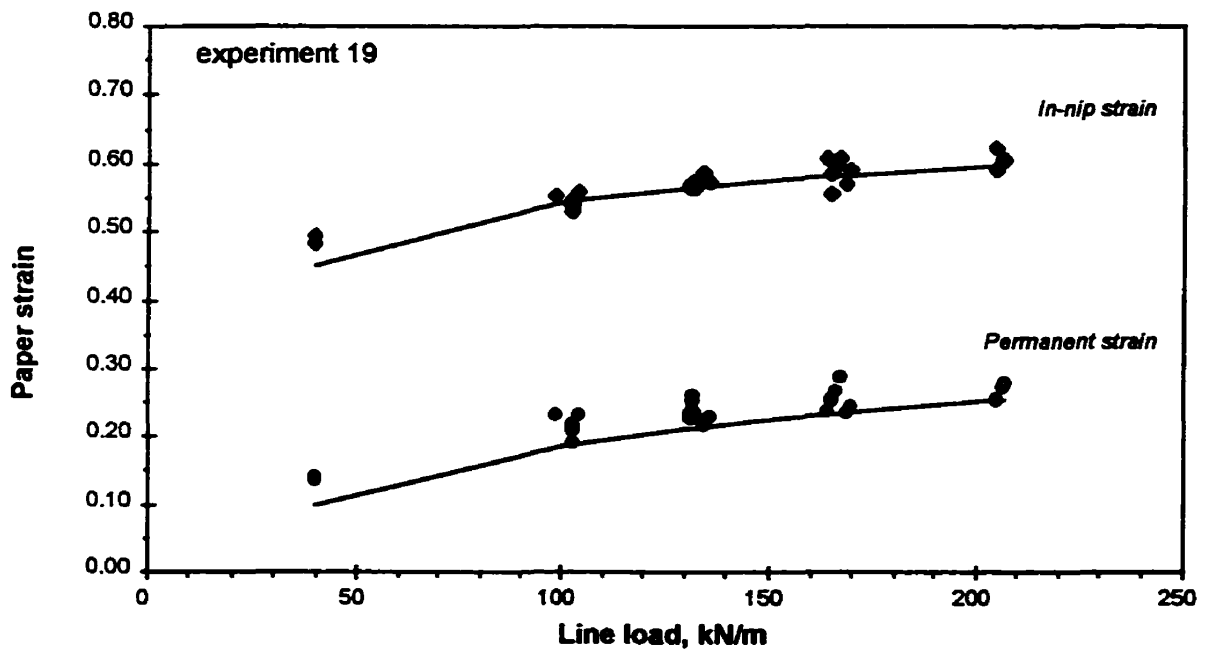


Figure 4.24: Effect of load on strain: $Bi = 2.22 \text{ cm}^3/\text{g}$, $R = 0.355 \text{ m}$, $M = 4.5\%$, $\Theta = 27.6 \text{ }^\circ\text{C}$, all speeds. Best fit lines are for $S = 400 \text{ m/min}$.

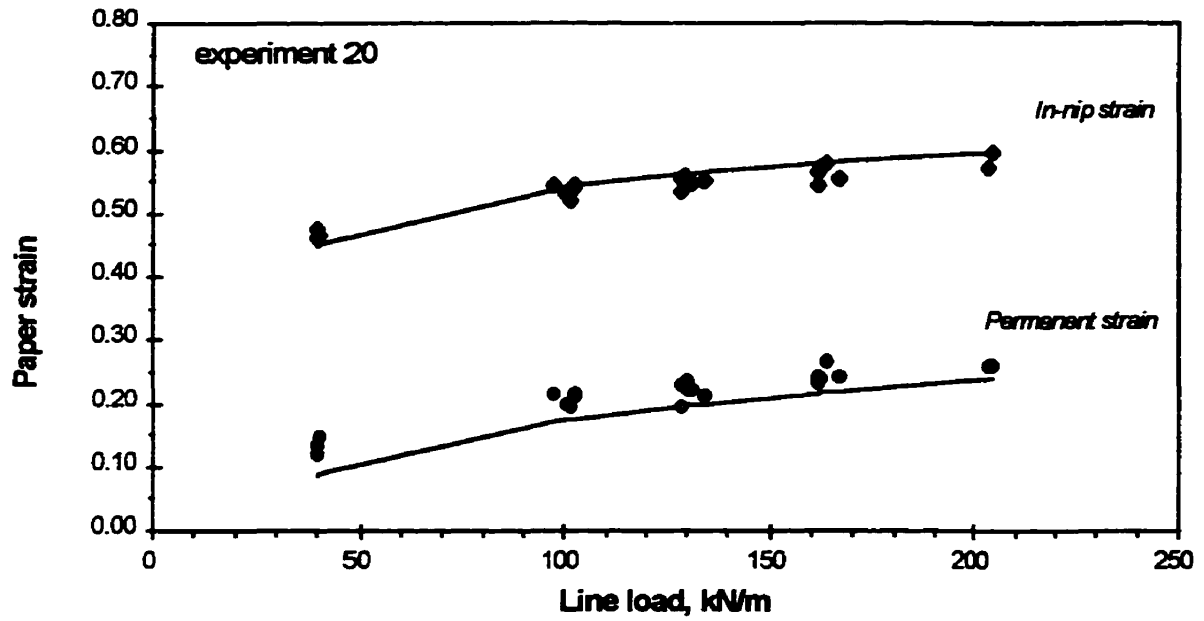


Figure 4.25: Effect of load on strain: $Bi = 2.22 \text{ cm}^3/\text{g}$, $R = 0.355 \text{ m}$, $M = 3.5\%$, $\Theta = 28.3 \text{ }^\circ\text{C}$, all speeds.
Best fit lines are for $S = 400 \text{ m/min}$.

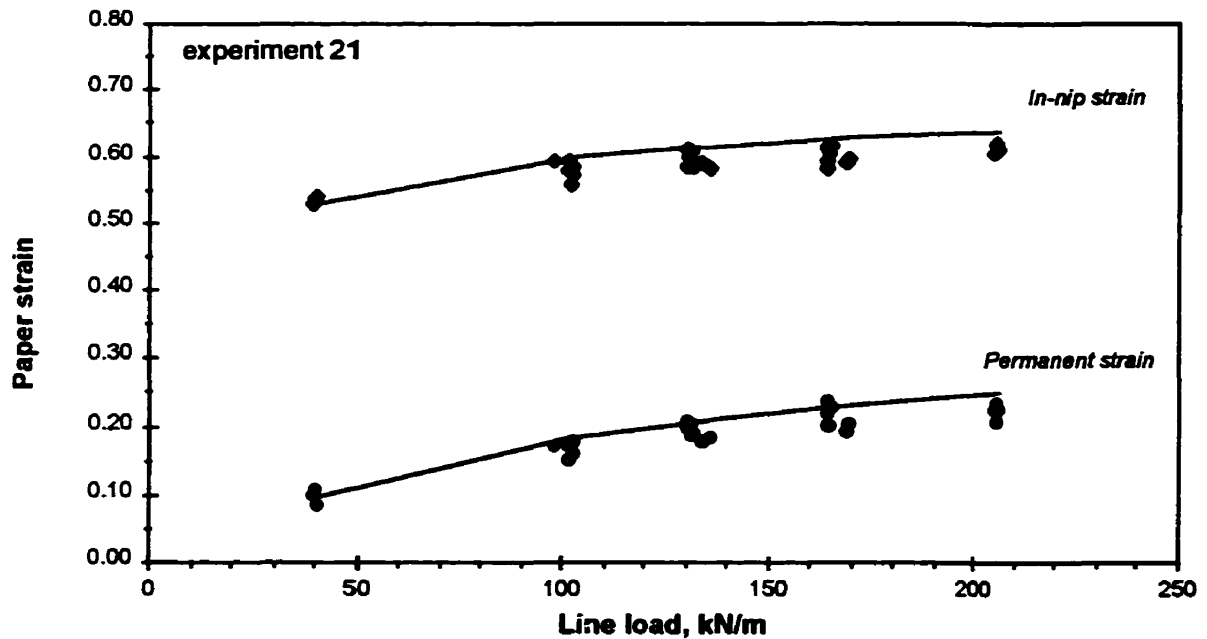


Figure 4.26: Effect of load on strain: $Bi = 2.21 \text{ cm}^3/\text{g}$, $R = 0.355 \text{ m}$, $M = 1.3\%$, $\Theta = 47.3 \text{ }^\circ\text{C}$, all speeds.
Best fit lines are for $S = 400 \text{ m/min}$.

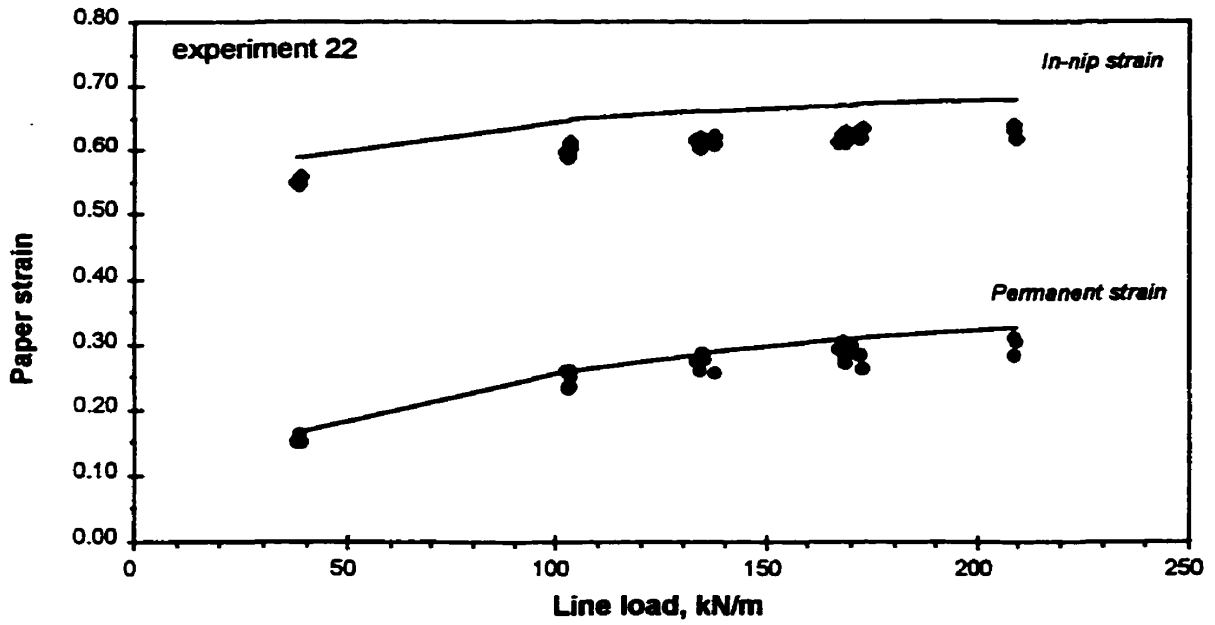


Figure 4.27: Effect of load on strain: $Bi = 2.29 \text{ cm}^3/\text{g}$, $R = 0.355 \text{ m}$, $M = 3.2\%$, $\Theta = 60.1 \text{ }^\circ\text{C}$, all speeds.
Best fit lines are for $S = 400 \text{ m/min}$.

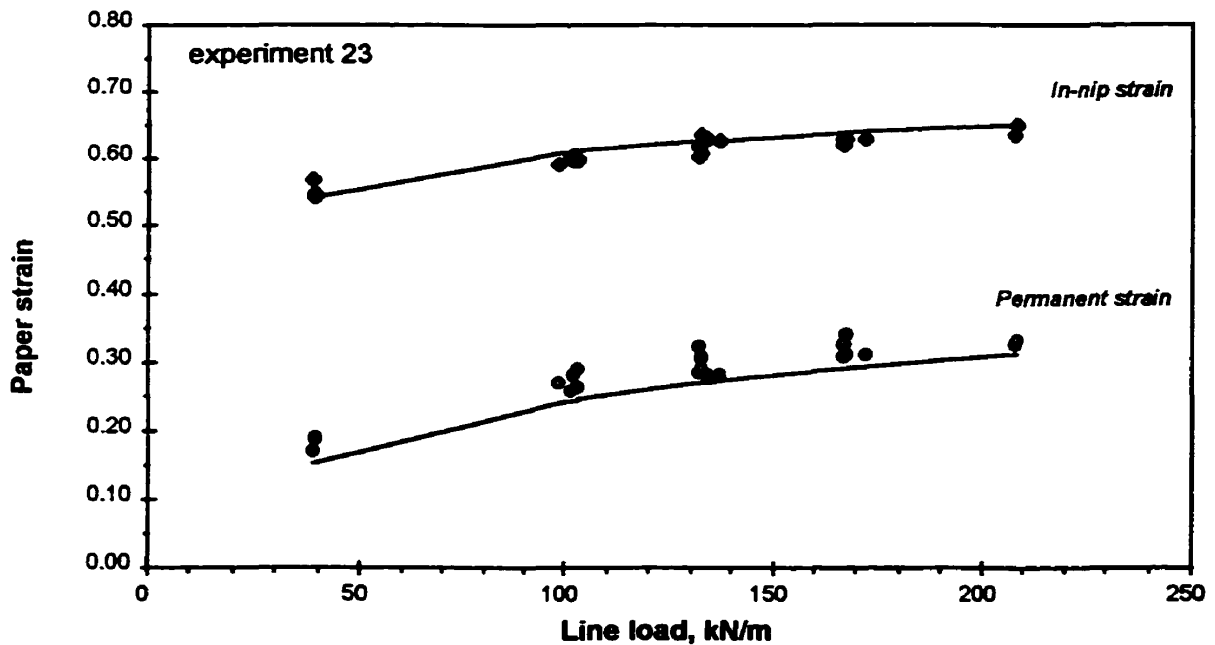


Figure 4.28: Effect of load on strain: $Bi = 2.26 \text{ cm}^3/\text{g}$, $R = 0.355 \text{ m}$, $M = 4.9\%$, $\Theta = 45.9 \text{ }^\circ\text{C}$, all speeds.
Best fit lines are for $S = 400 \text{ m/min}$.

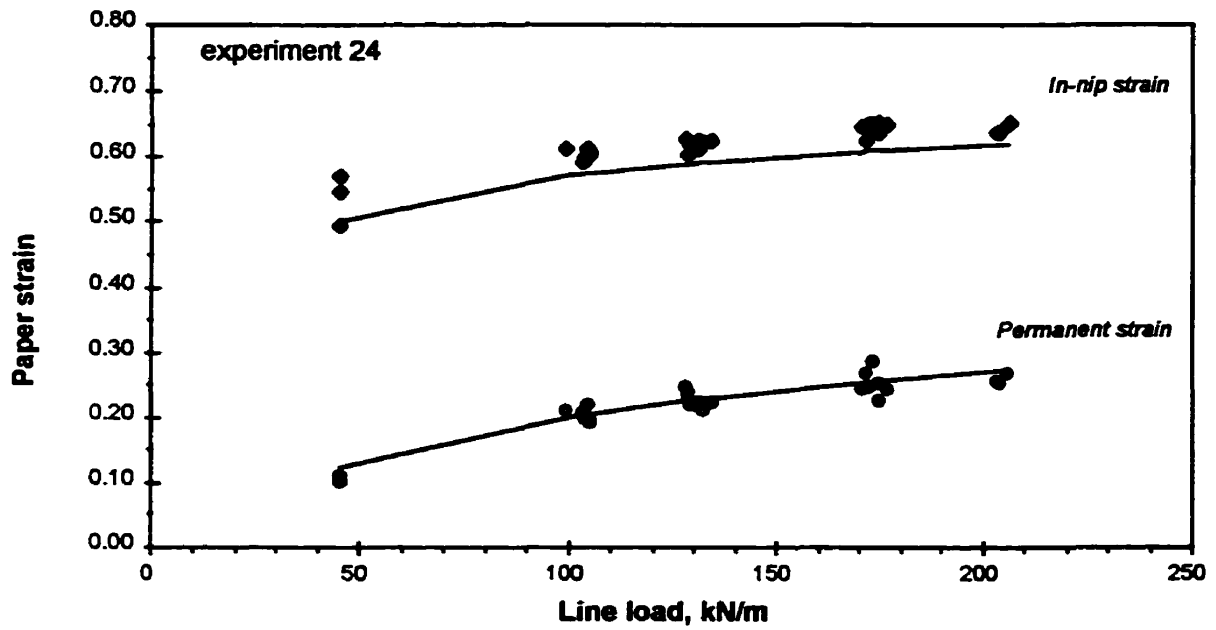


Figure 4.29: Effect of load on strain: $Bi = 2.30 \text{ cm}^3/\text{g}$, $R = 0.202 \text{ m}$, $M = 2.2\%$, $\Theta = 30.2 \text{ }^\circ\text{C}$, all speeds.
Best fit lines are for $S = 400 \text{ m/min}$.

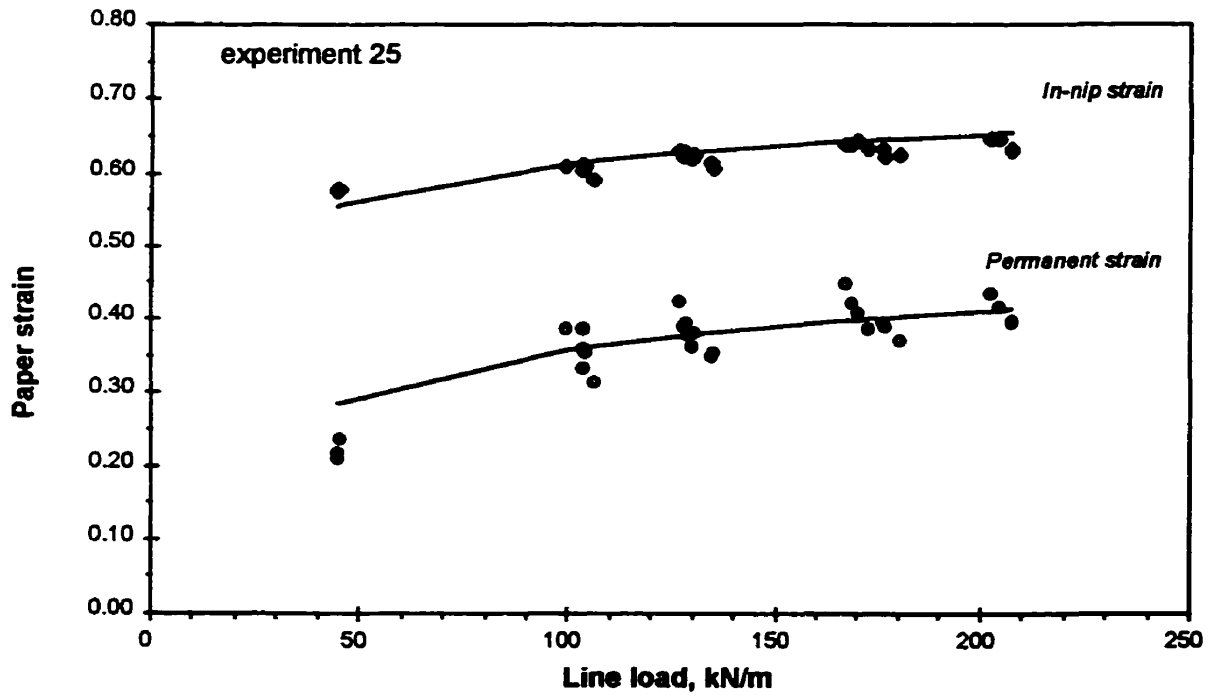


Figure 4.30: Effect of load on strain: $Bi = 2.4 \text{ cm}^3/\text{g}$, $R = 0.202 \text{ m}$, $M = 11.8\%$, $\Theta = 30.6 \text{ }^\circ\text{C}$, all speeds.
Best fit lines are for $S = 400 \text{ m/min}$.

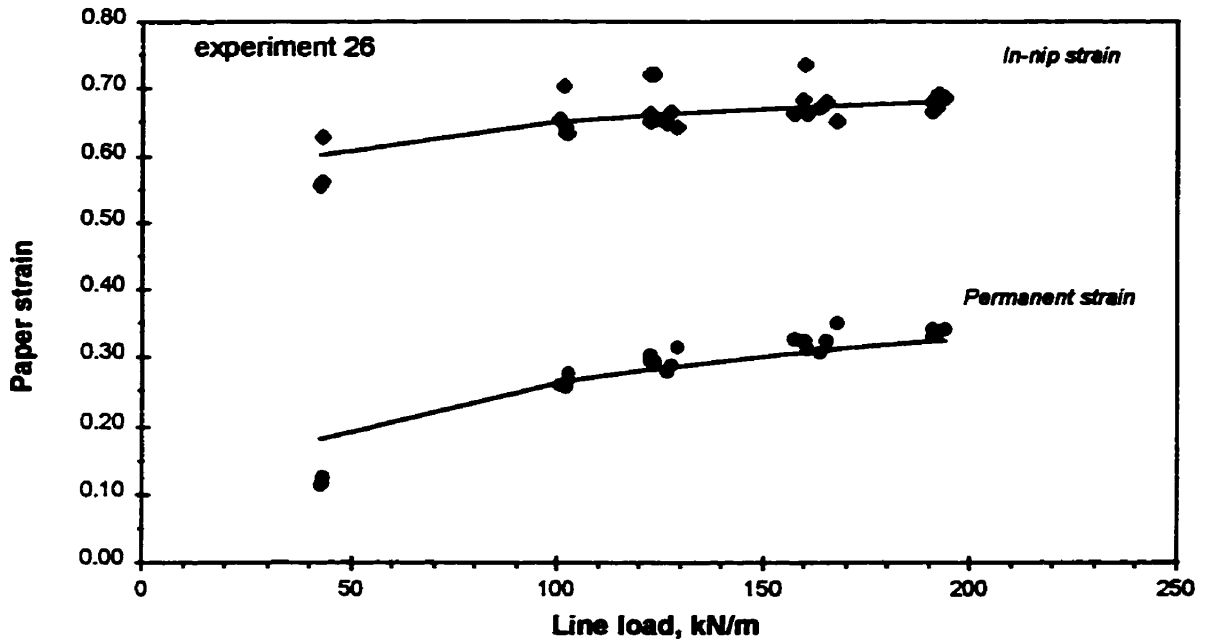


Figure 4.31: Effect of load on strain: $Bi = 2.28 \text{ cm}^3/\text{g}$, $R = 0.202 \text{ m}$, $M = 2.2\%$, $\Theta = 60.1 \text{ }^\circ\text{C}$, all speeds.
Best fit lines are for $S = 400 \text{ m/min}$.

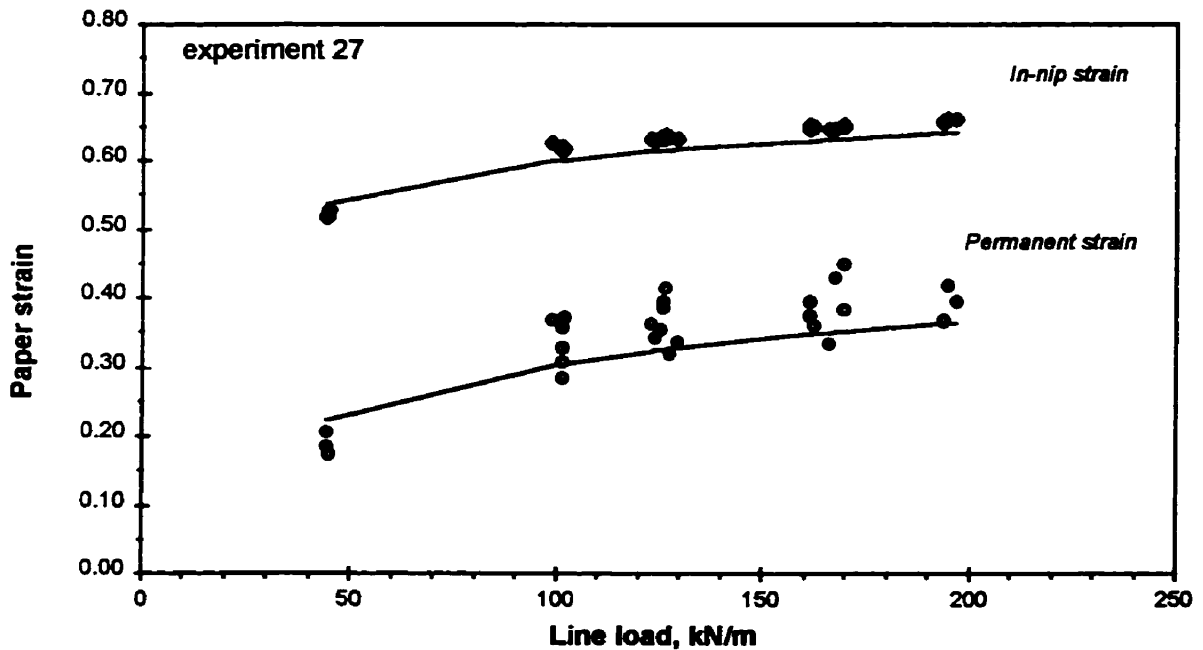


Figure 4.32: Effect of load on strain: $Bi = 2.35 \text{ cm}^3/\text{g}$, $R = 0.202 \text{ m}$, $M = 8.4\%$, $\Theta = 31.7 \text{ }^\circ\text{C}$, all speeds.
Best fit lines are for $S = 400 \text{ m/min}$.

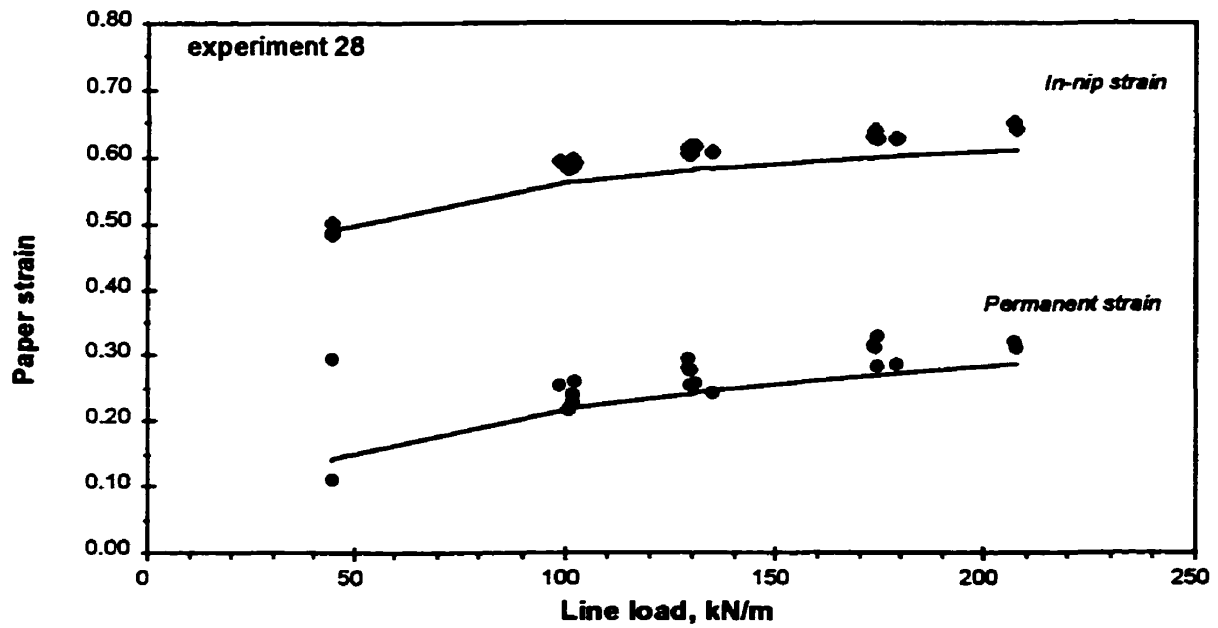


Figure 4.33: Effect of load on strain: $Bi = 2.22 \text{ cm}^3/\text{g}$, $R = 0.202 \text{ m}$, $M = 5.2\%$, $\Theta = 29.3 \text{ }^\circ\text{C}$, all speeds.
Best fit lines are for $S = 400 \text{ m/min}$.

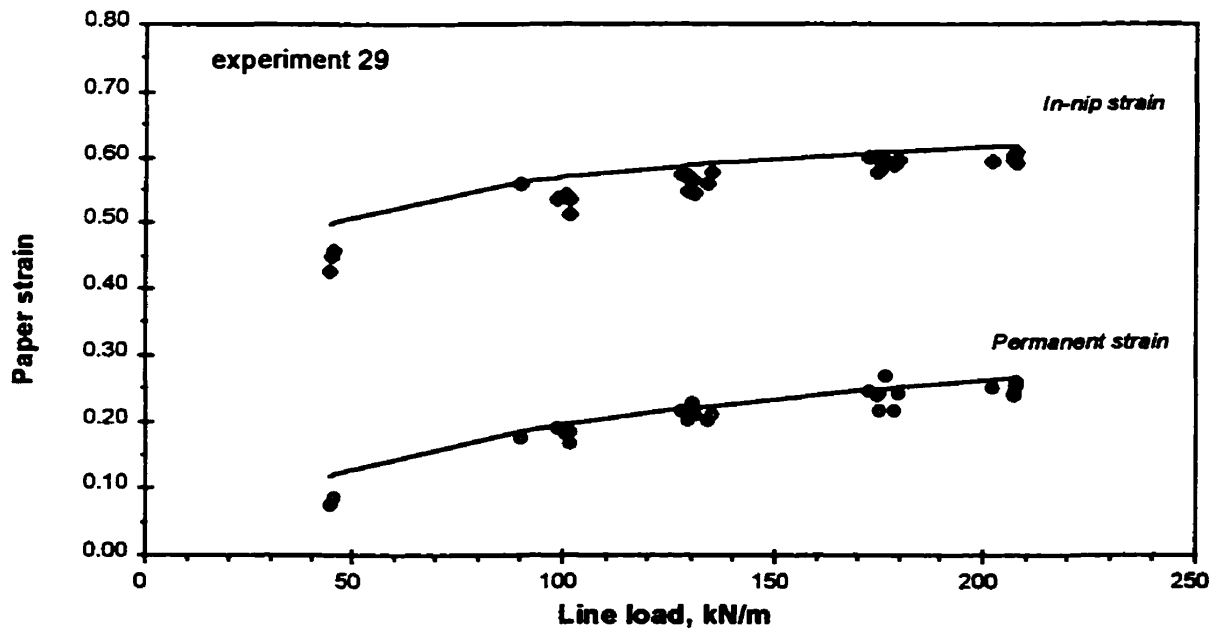


Figure 4.34: Effect of load on strain: $Bi = 2.24 \text{ cm}^3/\text{g}$, $R = 0.202 \text{ m}$, $M = 2.6\%$, $\Theta = 32.6 \text{ }^\circ\text{C}$, all speeds.
Best fit lines are for $S = 400 \text{ m/min}$.

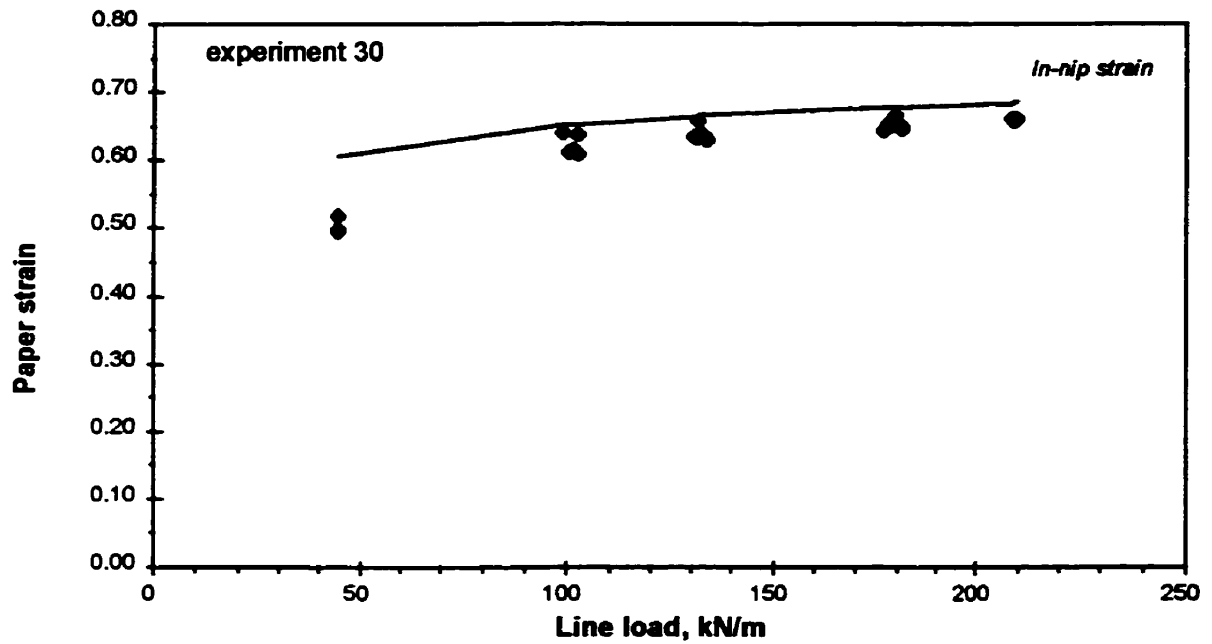


Figure 4.35: Effect of load on strain: $Bi = 2.30 \text{ cm}^3/\text{g}$, $R = 0.202 \text{ m}$, $M = 3.5\%$, $\Theta = 58.4^\circ\text{C}$, all speeds. Best fit lines are for $S = 400 \text{ m/min}$.

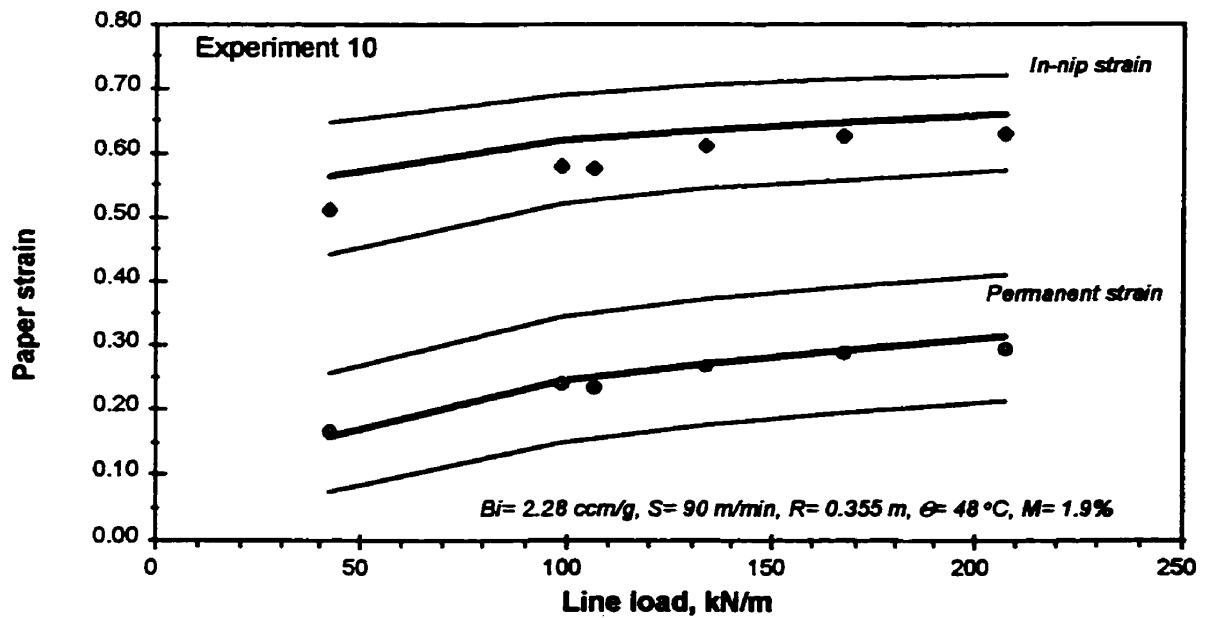


Figure 4.36: Effect of load on strain. Best fit lines with upper and lower 95% confidence limits.

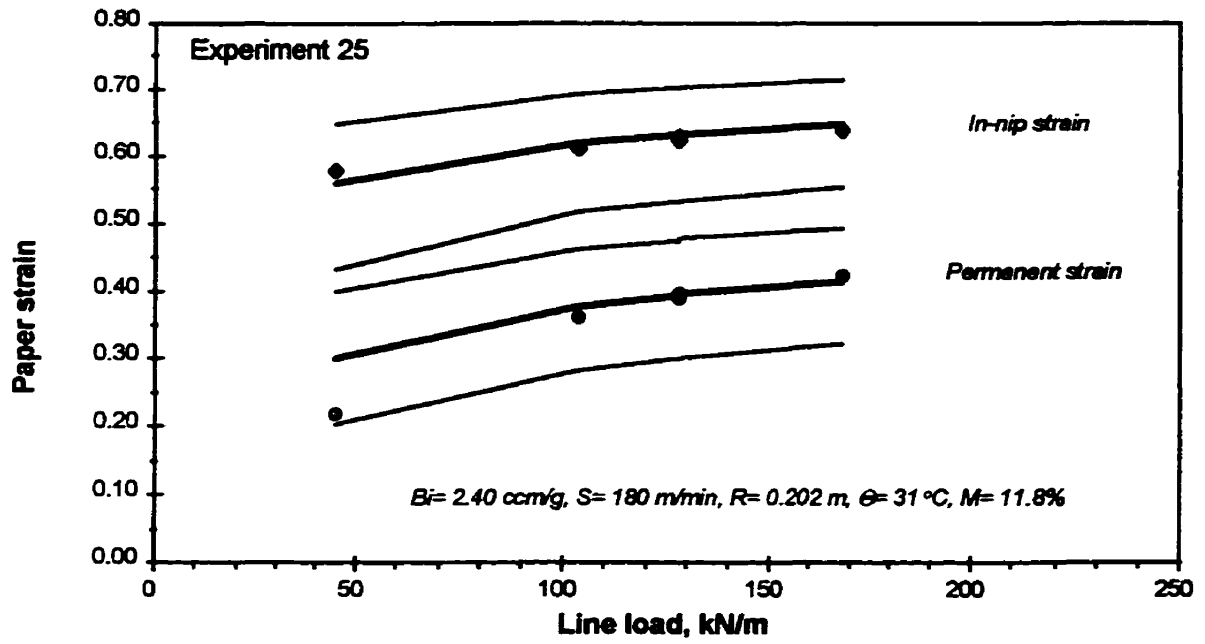


Figure 4.37: Effect of load on strain. Best fit lines with upper and lower 95% confidence limits.

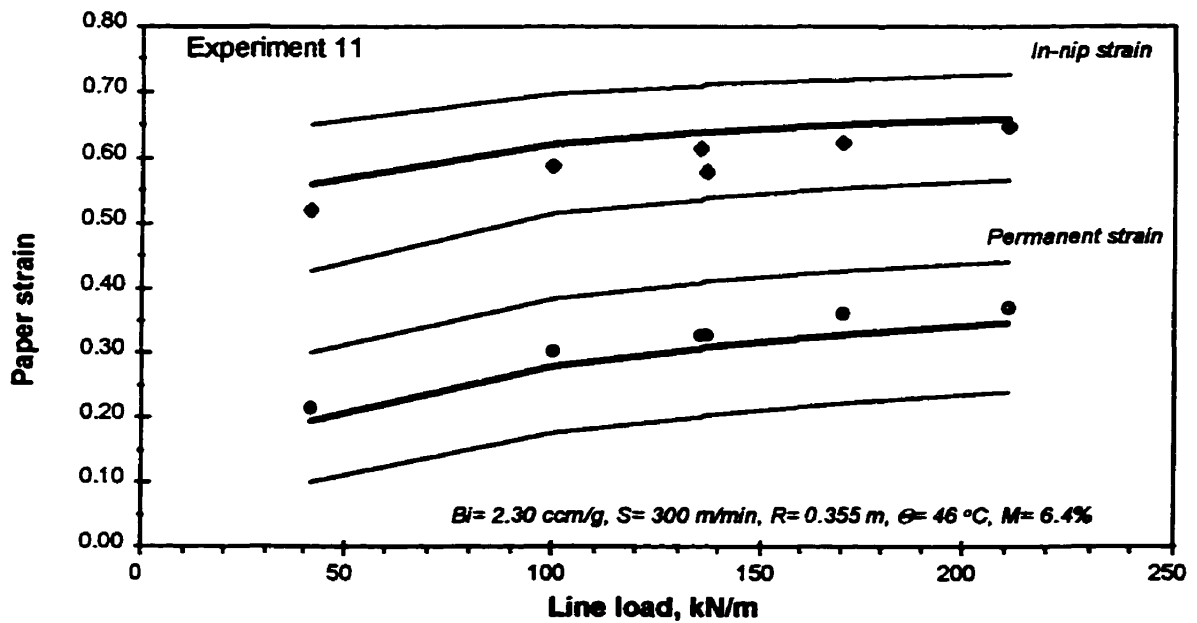


Figure 4.38: Effect of load on strain. Best fit lines with upper and lower 95% confidence limits.

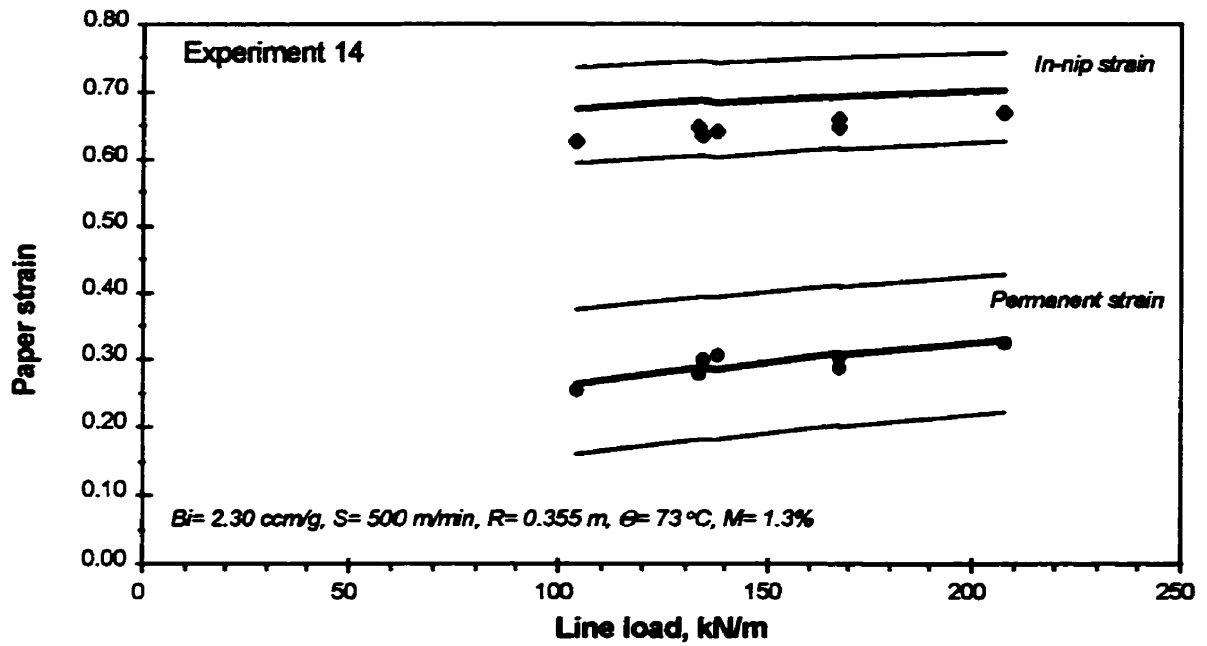


Figure 4.39: Effect of load on strain. Best fit lines with upper and lower 95% confidence limits.

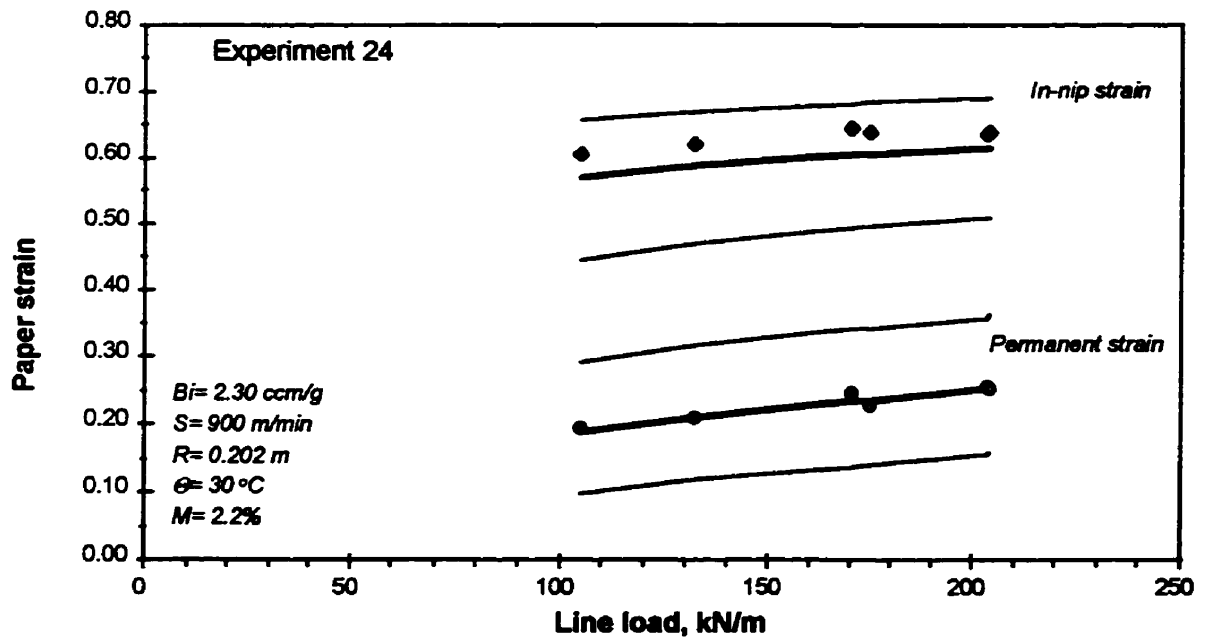


Figure 4.40: Effect of load on strain. Best fit lines with upper and lower 95% confidence limits.

Table 4.1: In-nip coefficients for the calendering equation, present study.

PARAMETER	ESTIMATE	A.S.E. (%)	LOWER 95%	UPPER 95%
A_n	-0.3172	0.02388 (7.5)	-0.3641	-0.2704
a_{0n} (g/cm ³)	-0.0239	0.01275 (53)	-0.0490	-0.0011
a_{Ln} (g/cm ³)	0.1781	0.00853 (5)	0.1614	0.1949
a_{Sn} (g/cm ³)	-0.0128	0.00412 (32)	-0.0209	-0.0047
a_{Rn} (g/cm ³)	-0.0413	0.01265 (31)	-0.0662	-0.0165
a_{Cn} (g/cm ³ °C)	0.00347	0.000112 (3)	0.00325	0.00369
a_{Mn} (g/cm ³)	0.00299	0.000383 (13)	0.00224	0.00375
R-squared	0.76			

Table 4.2: In-nip coefficients for the calendering equation, Browne et al. [6, 7].

PARAMETER	TMP
A_n	-0.3647
a_{0n} (g/cm ³)	0.0247
a_{Ln} (g/cm ³)	0.1920
a_{Sn} (g/cm ³)	-0.0216
a_{Rn} (g/cm ³)	-0.1068
R-squared	0.86

temperature and moisture content while the present study is the first to determine the effect of the sheet temperature and moisture content on the in-nip behaviour of paper. The coefficients of the in-nip calendering equation as found by Browne et al. [6, 7] and from the present study are shown in Tables 4.1 and 4.2.

The in-nip intercept coefficient A_n measured by Browne et al. for a TMP newsprint is seen to be just within the 95% confidence limits of the value found in the present study. This coefficient is the paper property which shows the ease with which in-nip strain is achieved. As the paper used in the two studies was in both cases made from a TMP pulp, those coefficients should to be similar.

As the in-nip coefficient a_{0n} of Browne et al. includes the temperature and moisture content terms, $a_{\Theta}\Theta + a_M M$, which they did not determine, the a_{0n} coefficients of the two studies cannot be compared. As the Browne et al. version of this coefficient allows for all effects not included in their version of the calendering equation their a_{0n} would depend strongly on the pulp processing and papermaking conditions used, i.e. type of spruce and the refining, forming, pressing and drying conditions. Thus even for grades of paper made from the same type of pulp, the coefficient a_{0n} can vary. However, if the ambient conditions of Browne et al. were approximated as paper temperature $\Theta = 20^\circ\text{C}$ and paper moisture content $M = 5\%$, the value of this coefficient can be corrected for these two effects. Using the permanent temperature and moisture content coefficients of the present study, $a_{\Theta n} = 0.00347$ and $a_{Mn} = 0.00299$, the new value for the present study becomes $a_{0n} = 0.0605$, a value within the 95% confidence limits of the a_{0n} value, 0.0247 (S.E. = 0.0194), of the Browne et al. data.

The in-nip load coefficient a_{Ln} reported in this study is slightly lower than as determined by Browne et al. The permanent load coefficients reported by Crotofino et al. [14, 17] and Browne et al. [6, 7] appear to be effectively a paper property. By similarity to the permanent strain case, the in-nip load coefficient could be expected to be a paper property as well. However, the in-nip load coefficient is strongly dependent on nip load. In the present work the nip load was varied from 15 to 210 kN/m, with most experiments using loads above 40 kN/m, whereas Browne et al. used the range 8 to 210 kN/m. Their measurements showed in-nip paper compression to be extremely sensitive to nip load, especially in their lower range of load. A detailed discussion of this subject appears subsequently in Section 4.1.1.

The in-nip speed coefficient a_{sn} measured in the present study is considerably lower than that reported by Browne et al. but, again by similarity to the case for permanent strain, this coefficient is expected to be a paper property. However, extensive use here of high temperatures and moisture contents, along with mostly heavy line loads, resulted in a high proportion of results with very high in-nip paper compression, in the range 60 to 73%. When the in-nip paper thickness is in the order of only 1/3 of the initial thickness, the effect of sheet speed for such extreme calendering conditions could be expected to be considerably lower than with in-nip paper strain of 30 to 60%.

This hypothesis was tested by determining the in-nip speed coefficient for two subsets of the data; 307 data with normal in-nip strains (30 to 60%) and 442 data with high in-nip strains (60 to 73%). The in-nip speed coefficient values were -0.0175 for the 30 to 60% strain data, but a much lower value -0.0116, for the 60 to 73% strain data. These two values for a_{sn} naturally bracket the value -0.0128 applicable for the complete set of data. As the standard error calculated for the data set at the lower strains was 0.00274, the a_{sn} value of Browne et al. -0.0216 is now seen to be within the 95% confidence limits for the lower strain value of -0.0175 from the present study. In the Browne et al. study the range of in-nip strain varied from 13% to 65%, with most values below 60%.

The radius coefficient a_{rn} is also lower in the present study than in that of Browne et al. This difference may be attributed to the unequal number of experiments performed for different size rolls used here (23 experiments for the larger rolls, 7 experiments for the smaller rolls) and to the associated effect of loads from 15 to 210 kN/m with the larger rolls, but 40 to 210 kN/m for the smaller rolls. This aspect is discussed further in Section 4.1.1.

The in-nip temperature and moisture content coefficients, $a_{\Theta n}$ and a_{Tn} , presented in Table 4.1 have never previously been determined. Although Colley and Peel [12] measured the effect of temperature and moisture content on in-nip paper thickness, they used a fundamentally different form of equation to fit those data, the master creep equation, and thus their in-nip temperature and moisture content coefficients cannot be

compared directly with the corresponding coefficients obtained for the calendering equation. A complete study of the master creep equation is given in Section 4.5. For both in-nip and permanent behaviour it is notable that temperature and moisture content have an effect on paper compression second only to that from nip load, thus confirming the need for the present study.

All calculated in-nip coefficients are statistically different from zero, and all the asymptotic standard errors are relatively small except for the in-nip intercept coefficient a_{0n} for which the coefficient of variation is about 50%, and thus the 95% confidence limits for a_{0n} just barely exclude the $a_{0n} = 0$ possibility.

The permanent calendering coefficients as determined in the Crotogino et al. [14, 17] and Browne et al. [6, 7] studies are shown in Table 4.4. Since all the above measurements were performed for a variety of newsprints, the permanent coefficients reported in present study, Table 4.3, are compared with their results.

The permanent intercept coefficient A_p reported here is significantly different from that of Browne et al. but is exactly the average of the three determinations of the A_p coefficient reported by Crotogino et al. The variation between the three A_p determinations of Crotogino et al. is large compared to the standard error of A_p in the present study.

For the permanent coefficient a_{0p} , the three values reported by Crotogino et al. vary greatly, from -0.001 to 0.057, with their highest value close to the present value of 0.0642. As the effects of all variables not included in the calendering equation, including particularly the conditions of pulping and papermaking processes prior to calendering, appear as variability in a_{0p} , the observed wide fluctuations in a_{0p} between studies are not unexpected.

The a_{0p} coefficient obtained by Browne et al. is much higher yet but, as for the in-nip case, cannot be compared directly with the a_{0p} value of the present study. Their a_{0p} coefficient includes the temperature and moisture content terms, as they did not have the $a_{\Theta p} \Theta + a_{Mp} M$ terms of the present study. As for the in-nip case, by approximating the ambient conditions of Browne et al. as paper temperature $\Theta = 20$ °C and paper moisture content $M = 5\%$ the value of this coefficient can be corrected for these two effects. Using

Table 4.3: Permanent coefficients for the calendering equation, present study.

PARAMETER	ESTIMATE	A.S.E.	LOWER 95%	UPPER 95%
A_p	-0.4186	0.01678	-0.4508	-0.3860
a_{Op} (g/cm ³)	0.0642	0.00179	0.0608	0.0673
a_{Lp} (g/cm ³)	0.0973	0.00451	0.0882	0.1065
a_{Sp} (g/cm ³)	-0.0218	0.00124	-0.0237	-0.0188
a_{Rp} (g/cm ³)	-0.0351	0.00406	-0.0438	-0.0279
a_{Tp} (g/cm ³ °C)	0.00097	0.000053	0.000869	0.00107
a_{Mp} (g/cm ³)	0.00607	0.000363	0.00534	0.00680
R-squared	0.90			

Table 4.4: Permanent coefficients for the calendering equation, from Crotogino et al. (1, 2, 3) and Browne et al. (4).

PARAMETER	1	2	3	4
A_p	-0.3340	-0.5000	-0.4170	-0.6095
a_{Op} (g/cm ³)	-0.0010	0.0498	0.0568	0.1256
a_{Lp} (g/cm ³)	0.0922	0.0988	0.0912	0.1085
a_{Sp} (g/cm ³)	-0.0175	-0.0208	-0.0204	-0.0170
a_{Rp} (g/cm ³)	-0.0374	-0.0390	-0.0354	-0.0530
a_{Tp} (g/cm ³ °C)	0.00088	0.00094	0.00086	—
a_{Mp} (g/cm ³)	0.00462	0.00545	0.00520	—
R-squared	0.94	0.93	0.89	0.90

the permanent temperature and moisture content coefficients of the present study, $a_{\Theta p} = 0.00097$ and $a_{Mp} = 0.00607$, the new value becomes $a_{op} = 0.1140$, a value within the 95% confidence limits of the a_{op} value, 0.1256 (S.E. = 0.0101), of the Browne et al. data.

The value of permanent load coefficient a_{Lp} reported here is similar to those of Crotagino et al. and Browne et al. and thus seems independent of nip load, contrary to the case of the in-nip load coefficient.

The permanent speed coefficient a_{Sp} measured in the present study is slightly higher than those reported previously. However, the variation in values of the speed coefficients reported by Crotagino et al. and Browne et al. suggests that it is a paper property which varies with the type of paper.

The permanent radius coefficient a_{Rp} here is considerably lower than that reported by Browne et al. but is similar to the three determinations of the radius coefficient reported by Crotagino et al. It was suggested by Kerekes [49] that the radius coefficient be calculated from the average of the load and speed coefficients:

$$a_{Rp} = -0.5 (a_{Lp} + a_{Sp}) \quad [\text{Eq. 4.6}]$$

The above equation predicts that for the present study, with $a_{Lp} = 0.0973$ and $a_{Sp} = -0.0218$, the permanent radius coefficient a_{Rp} should be -0.0377 , which is not statistically different from the measured value of -0.0351 , Table 4.3.

The permanent temperature coefficient $a_{\Theta p}$ found in this investigation is slightly higher than those of Crotagino et al., which in turn are within 95% confidence limits of the $a_{\Theta p}$ value obtained here. The small variations in value of this coefficient suggest that it can also be paper dependent.

The permanent moisture content coefficient a_{Mp} measured during present study is higher than those of Crotagino et al., but again is probably a paper property as well. In previous studies the a_{Mp} coefficient varied between 0.00462 to 0.00545, with the present value of 0.00607 not differing greatly from this range. Browne et al. did not measure the effect of either paper temperature or moisture content on permanent paper deformation.

For the permanent case, all coefficients are non-zero at the 95% confidence limits since all standard errors are at least one order of magnitude smaller than the corresponding estimates. The residual error computed from the full set of data are plotted in terms of strain in Figure 4.4 for both the permanent and in-nip cases. For the in-nip case, Figure 4.4b, there is a tendency for the residuals to be negative at low values of in-nip strain, 0.30 to 0.55, and positive at higher values of that strain, over 0.60. These trends imply that the form of the calendering equation used to describe behaviour of the paper in the nip tends to predict higher values of in-nip strain for the lower range of strain, and lower values for the higher range of strain. This tendency can be seen in the estimate of in-nip strain vs. measured in-nip strain on Figure 4.3b. In the permanent case, Figures 4.3a and 4.4a, no such trend is observable, with the residuals distributed more uniformly over the full range of strain. There is a slight tendency for these residuals to be more scattered at lower and higher values of strain than at intermediate values.

The plots of residual error as a function of all independent calendering variables used here, Figures 4.5 and 4.6, show that the forms of the calendering equation proposed in this section, Equations 4.1 and 4.2, do not adequately predicted the moisture and temperature effects for in-nip strain, the moisture effect for permanent strain.

4.1.1 Effect of nip load on radius and load coefficients

The in-nip radius coefficient a_{Rn} calculated here, Table 4.1, is less than half the corresponding coefficient reported by Browne et al., Table 4.2. Kerekes [49] suggestion that the radius coefficient be calculated from the average of the load and speed coefficients was verified by Browne et al. [6, 7] to apply to both the permanent and in-nip calendering coefficients:

$$a_{Rp,n} = -0.5 (a_{Lp,n} + a_{Sp,n}) \quad [\text{Eq. 4.7}]$$

When results obtained during the present study are used, Table 4.1, the above equation predicts an in-nip radius coefficient a_{Rn} of -0.0827, which is similar to the value obtained by Browne et al. but twice the value of this coefficient, -0.0413, as determined during the present study. This disagreement between measured and predicted values of the in-nip radius coefficient derives from the unequal number of experiments performed for the two sets of calender rolls, 23 experiments for the largest rolls, 7 for the smallest rolls. Those two sets of experiments were also performed for a slightly different range of nip load; 15 to 210 kN/m for the largest rolls, 40 to 210 kN/m for the smallest ones. Although the experimental line loads differ only at the lower part of the range, this is where in-nip paper deformation is most sensitive to nip load.

To correct for the above differences, the calendaring coefficients were re-estimated for the common range of line load by excluding the data for line load of 15 to 40 kN/m with the largest rolls. This more restricted data set contained 385 data points. To ensure equal weight to all data points, single average values of independent and dependent variables were used when two or more data points were obtained at a similar combination of experimental conditions. This process reduced the data set to 312 points.

Estimates of the resultant in-nip and permanent calendaring coefficients are presented in Table 4.5 along with the asymptotic standard errors of in-nip estimates. In-nip data and prediction curves generated with the in-nip version of the calendaring equation and the conditions used to generate those curves are given in Figures 4.41 to 4.46 using both sets of in-nip coefficients, Table 4.1 and 4.5b.

The permanent coefficients obtained for the narrower set of strain data, Table 4.5a, were found to be statistically indifferent from those of Table 4.3, thus there is no major effect of nip load.

The in-nip calendaring coefficients reported in Table 4.1 are significantly different from those of Table 4.5b. However for loads higher than 40 kN/m the in-nip version of the calendaring equation is seen (Figures 4.41 to 4.45) to generate similar prediction curves for both sets of calendaring coefficients. For loads lower than 40 kN/m, Figure 4.46, the in-nip strain curves start to respond differently. Curves generated using

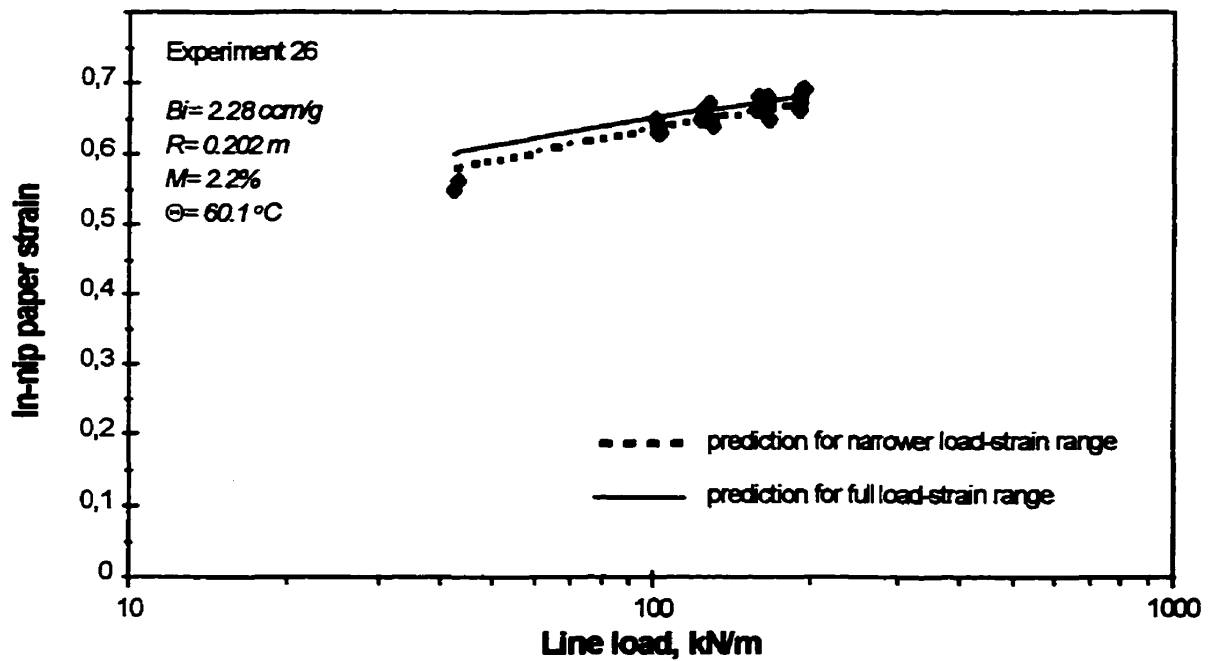
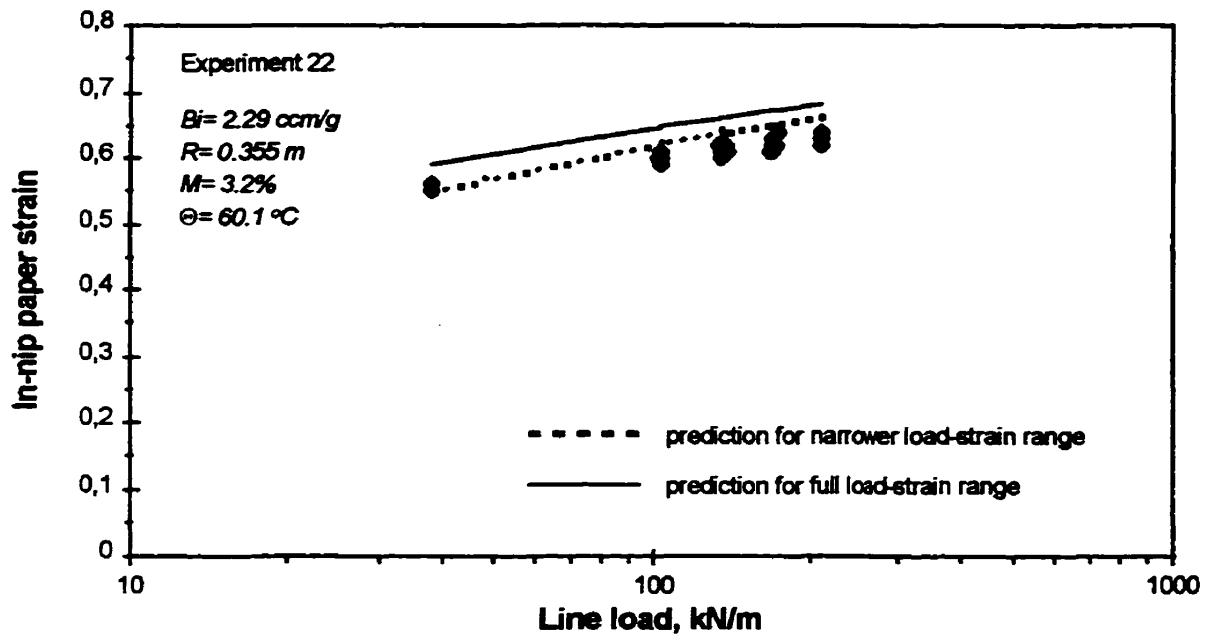


Figure 4.41: Effect of load on in-nip strain.

Best fit lines are for $S = 400 \text{ m/min}$.

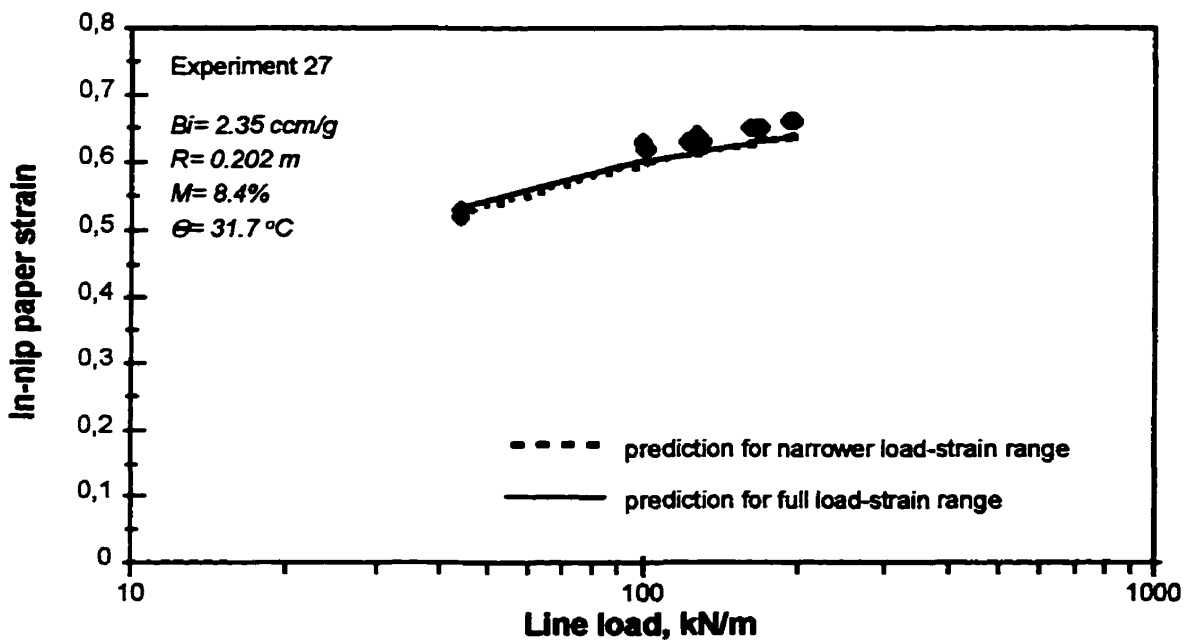
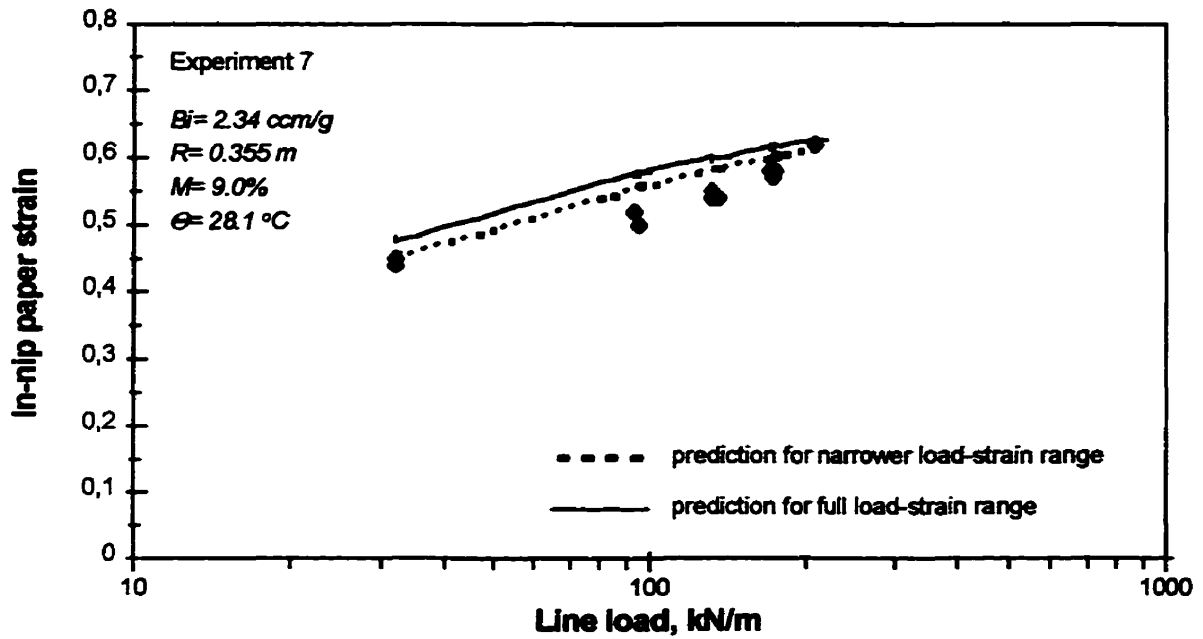


Figure 4.42: Effect of load on in-nip strain.

Best fit lines are for $S = 400 \text{ m/min}$.

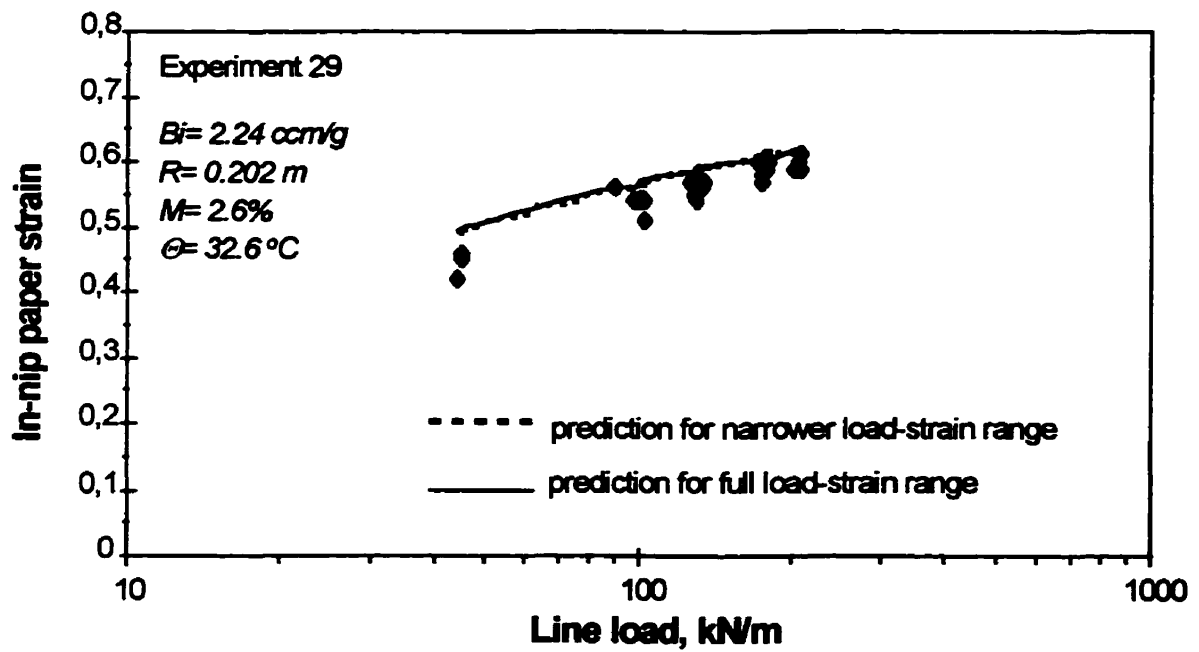
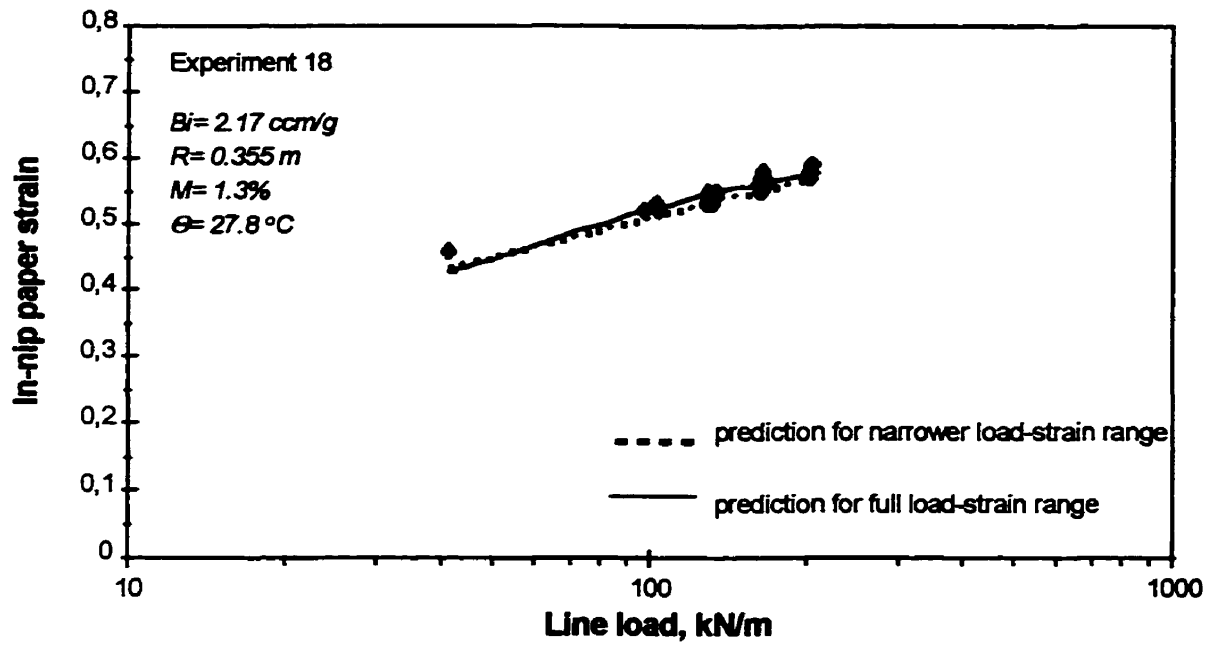


Figure 4.43: Effect of load on in-nip strain.

Best fit lines are for $S = 400 \text{ m/min}$.

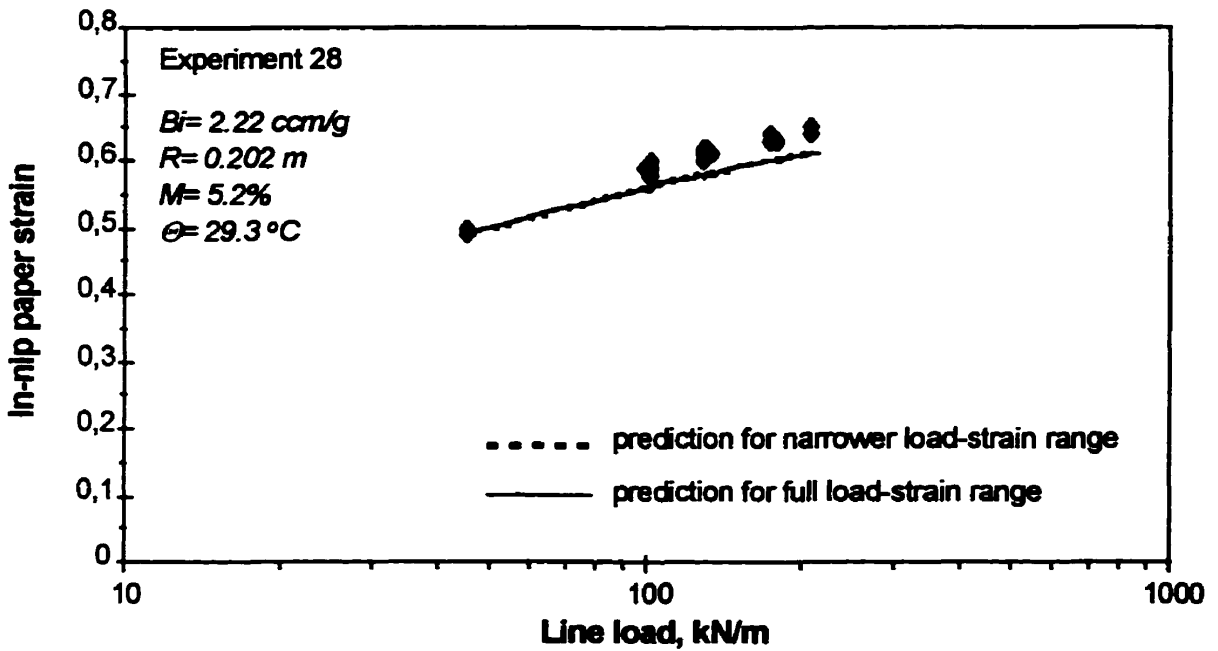
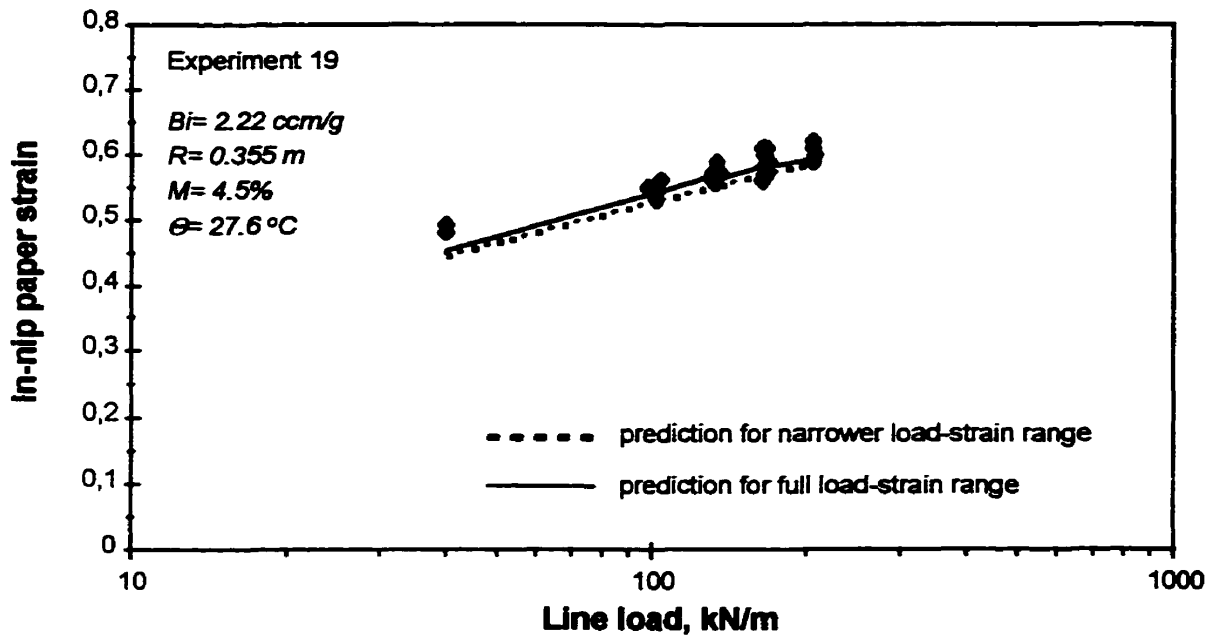


Figure 4.44: Effect of load on in-nip strain.

Best fit lines are for $S = 400 \text{ m/min}$.

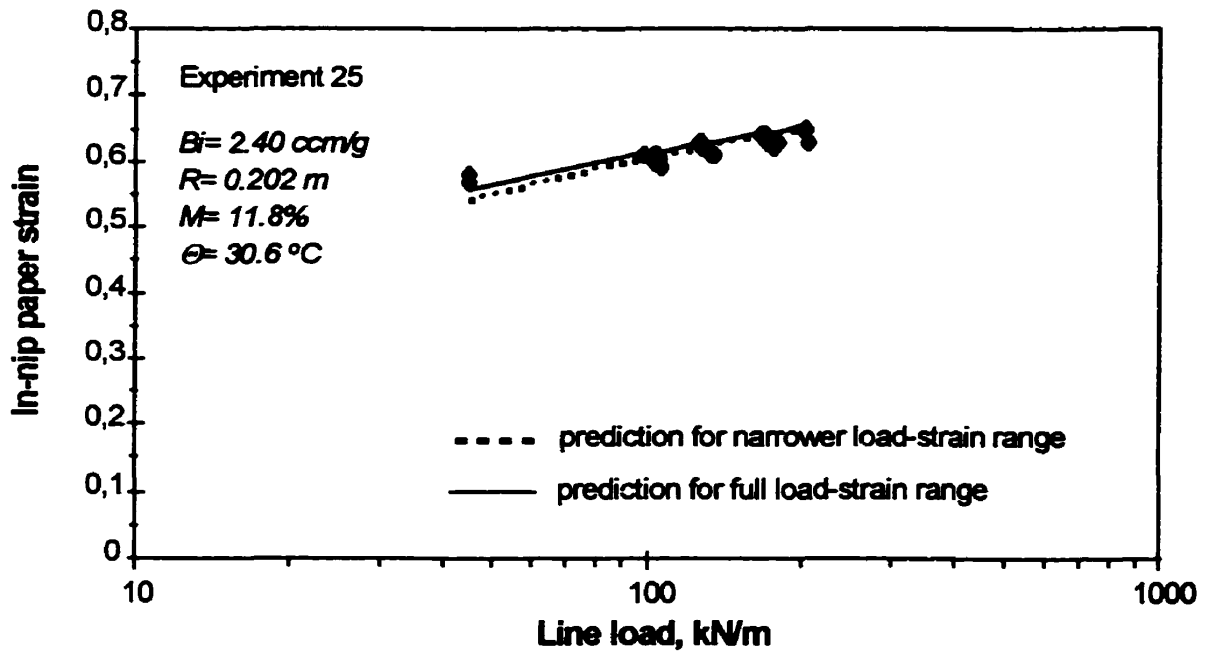
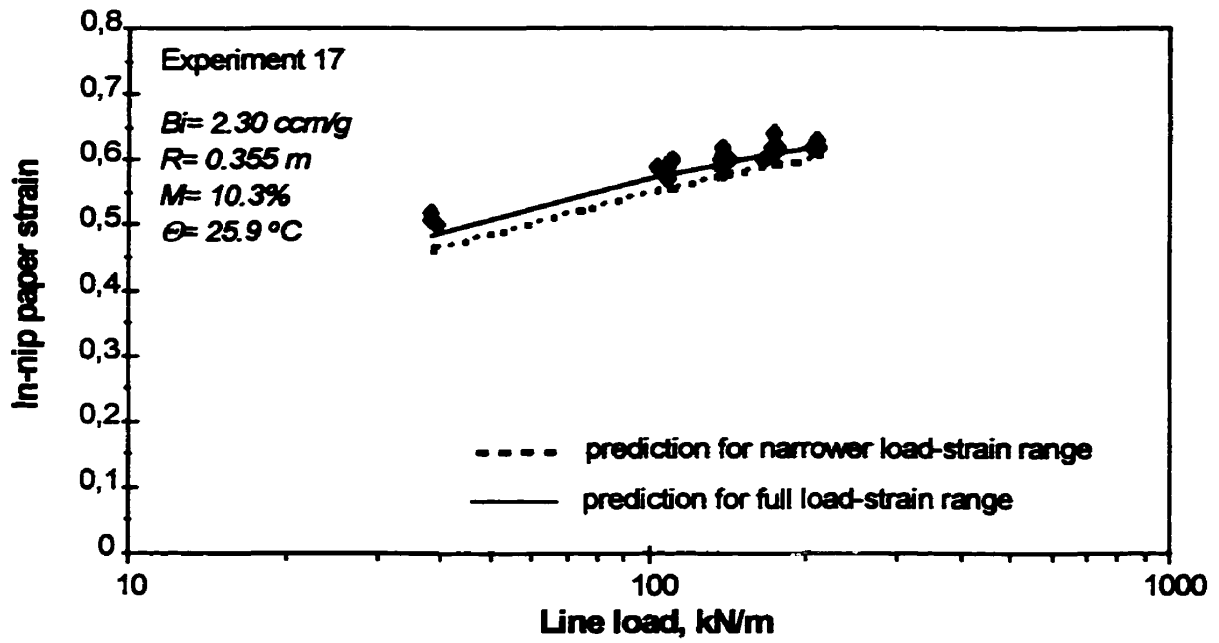


Figure 4.45: Effect of load on in-nip strain.

Best fit lines are for $S = 400 \text{ m/min}$.

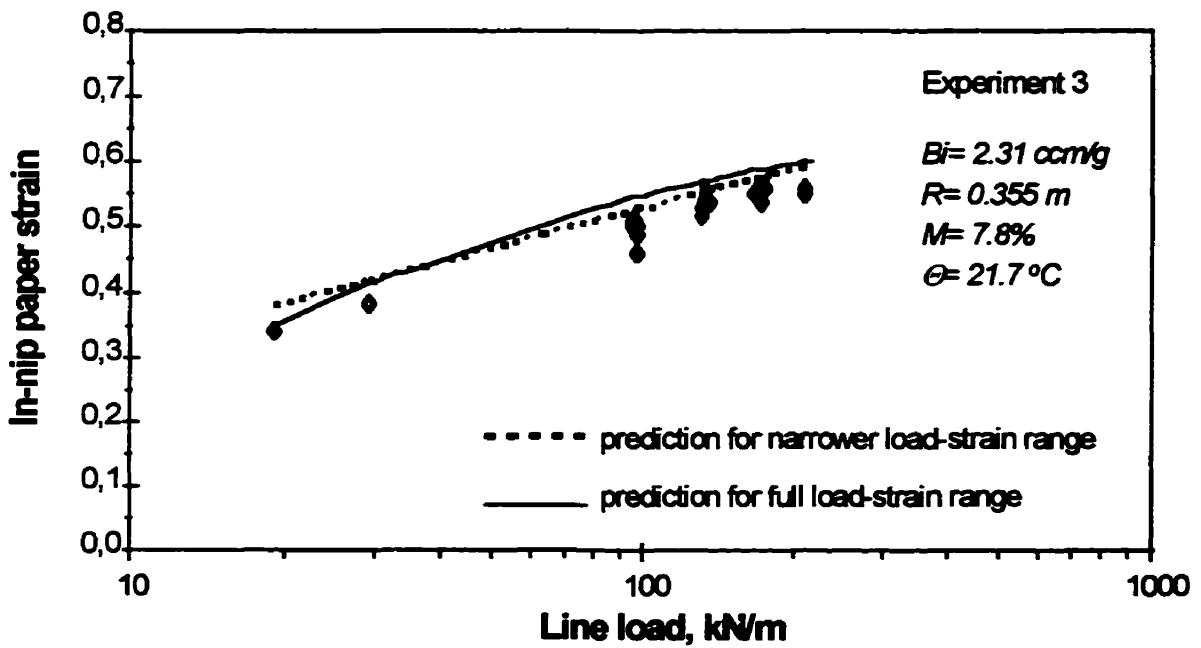
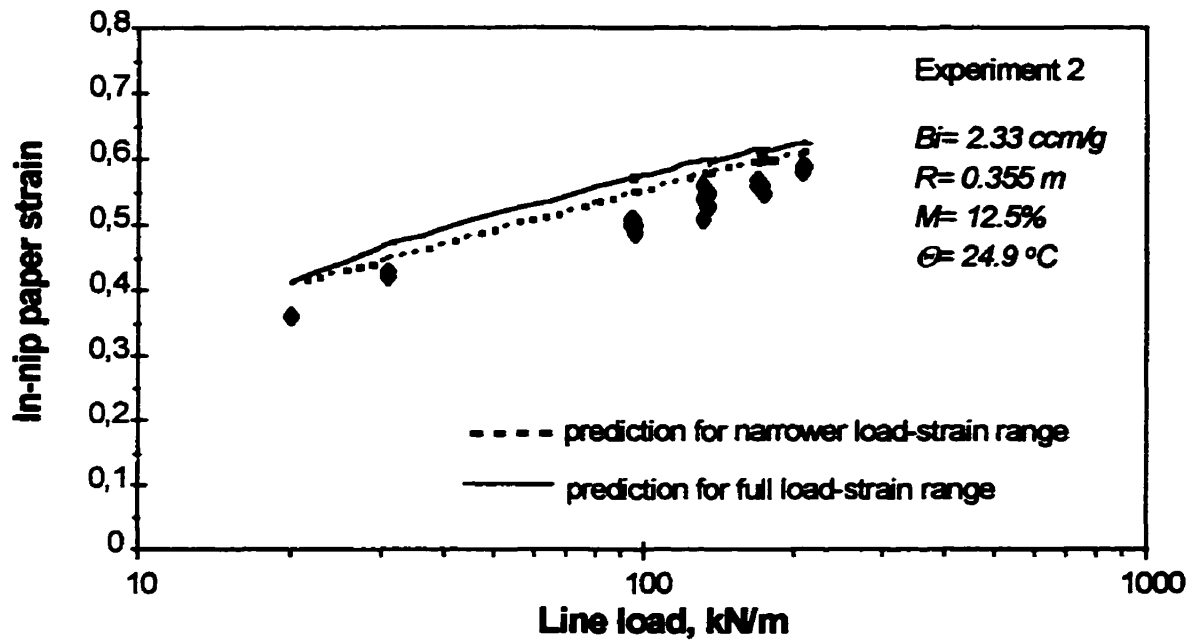


Figure 4.46: Effect of load on in-nip strain.

Best fit lines are for $S = 400 \text{ m/min}$.

Table 4.5: Calendering coefficients for narrower range of nip loads, present study.

a.) permanent coefficients

PARAMETER	ESTIMATE
A_p	-0.3233
$a_{Op} (g/cm^3)$	0.0070
$a_{Lp} (g/cm^3)$	0.1011
$a_{Sp} (g/cm^3)$	-0.0222
$a_{Rp} (g/cm^3)$	-0.0375
$a_{Tp} (g/cm^3 \text{ } ^\circ C)$	0.00109
$a_{Mp} (g/cm^3)$	0.00647
R-squared	0.91

b.) in-nip coefficients

PARAMETER	ESTIMATE	A.S.E.
A_n	0.1018	0.0306
$a_{On} (g/cm^3)$	-0.0416	0.0110
$a_{Ln} (g/cm^3)$	0.0907	0.0053
$a_{Sn} (g/cm^3)$	-0.0045	0.0025
$a_{Rn} (g/cm^3)$	-0.0534	0.0087
$a_{Tn} (g/cm^3 \text{ } ^\circ C)$	0.0009	0.0001
$a_{Mn} (g/cm^3)$	0.00131	0.0003
R-squared	0.78	

calendering coefficients obtained for the full range of the nip loads follow the strongly nonlinear behaviour of the experimental data, while those for the Table 4.5b coefficients do not.

The finding of Browne et al. [6, 7] that the logarithmic relation between in-nip paper deformation and line load is strongly nonlinear, especially at lower loads, was confirmed in the present study.

The regression analysis of Figures 4.41 to 4.46, Tables 4.1 and 4.5b attempts to fit a linear part of the calendering equation through data at the lowest loads. The result of this procedure is that for different ranges of line loads, the linear part of the calendering equation is applied to different sets of in-nip strain data, Figure 4.47, and thus different calendering coefficients are estimated, as given in Table 4.1 and 4.5b.

Table 4.6 shows the results of splitting both the narrower (386 points) and full (760 points) in-nip data sets into subsets based on which part of the calendering equation is applied to fit those data. Since no in-nip strain data fall below the lower limit of the calendering equation, only the upper limit of the calendering equation is used to classify

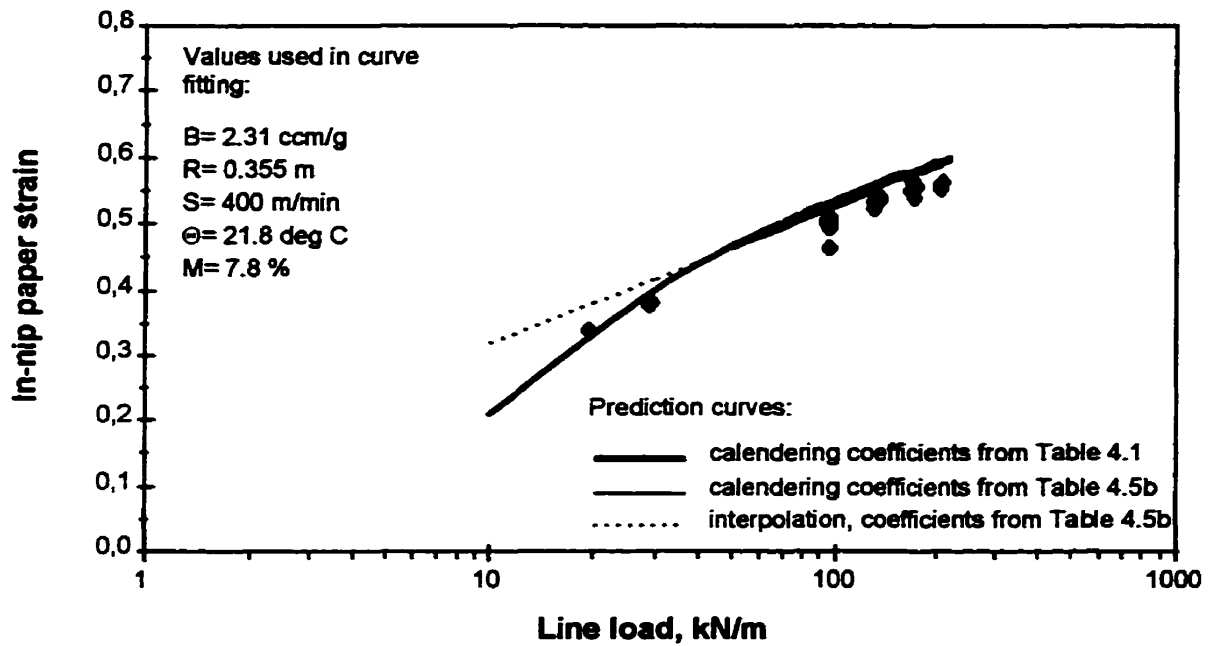


Figure 4.47: Effect of load on in-nip strain:

$\Theta = \sim 21.8 \text{ }^\circ\text{C}$, $M = \sim 7.8\%$, $R = 0.355 \text{ m}$, all speeds.

data points into the linear or nonlinear part:

Linear part: $B_i < 0.5 (1 - A_n) / \mu_n$

$$\varepsilon_n = A_n + \mu_n B_i$$

Nonlinear part: $B_i \geq 0.5 (1 - A_n) / \mu_n$

$$\varepsilon_n = 1 - 0.25 (1 - A_n)^2 / (\mu_n B_i)$$

For the data set with the narrower range of load-strain, 82% of the in-nip strain data fall in the nonlinear range of the calendering equation. However, when the data set including the full range of load-strain is used, the calendering equation predicts that virtually all of the in-nip strain data fall above their upper limits. The calendering equation is seen to fit these two sets of data differently, which in turn suggests that the standard

Table 4.6: Distribution of data according to calendering equation upper limit, narrow and full data sets.

IN-NIP STRAINS	LINEAR PART	NONLINEAR PART
NARROW LOAD-STRAIN RANGE (TABLE 4.5B)	75 (18%)	310 (82%)
FULL LOAD-STRAIN RANGE (TABLE 4.1)	1 (0%)	759 (100%)

form of the calendering equation is, for the in-nip case, extremely sensitive to the line load-strain range.

Results obtained for the full range of line load, 15 to 210 kN/m, are consistent with the Browne et al. [7] report that 95% of the in-nip data, measured for a similar range of line load, also fall above the upper limit. For the industrially relevant range of line load therefore, virtually all in-nip data are fitted only with the nonlinear part of the calendering equation.

Since the in-nip strain data used for the radius effect correction are just a subset of the whole in-nip data set, a nonlinear portion of the calendering equation could be used to fit these results as well. Such results for the above set of 386 in-nip data points are given in Table 4.7. All coefficients, except those for radius and temperature, are similar to those of Table 4.1.

The in-nip radius coefficient reported above differs from that reported in Table 4.1 but is similar to the coefficient reported by Browne et al., Table 4.2. Using the load and speed coefficients reported in Table 4.6, Kerekes' prediction (Equation 4.7) gives $a_{Rn} = -0.0958$, which statistically is not different from the in-nip radius coefficient reported here. For the calendering coefficients of Table 4.5b, Equation 4.7 predicts a radius coefficient of -0.0431 , which is statistically similar to the calculated radius coefficient of -0.0534 at the 95% confidence limits. Thus Kerekes' prediction for the radius effect works for both sets of in-nip calendering coefficients obtained for the narrower set of in-nip data.

Table 4.7: In-nip coefficients for the nonlinear portion of the calendering equation, 386 data points.

PARAMETER	ESTIMATE	A.S.E.
A_n	<i>-0.3565</i>	<i>0.0372</i>
$a_{0n} (g/cm^3)$	<i>-0.0307</i>	<i>0.0157</i>
$a_{Ln} (g/cm^3)$	<i>0.1820</i>	<i>0.0126</i>
$a_{Sn} (g/cm^3)$	<i>-0.0095</i>	<i>0.0055</i>
$a_{Rn} (g/cm^3)$	<i>-0.1087</i>	<i>0.0168</i>
$a_{Tn} (g/cm^3 \text{ } ^\circ C)$	<i>0.0018</i>	<i>0.0005</i>
$a_{Mn} (g/cm^3)$	<i>0.0029</i>	<i>0.0001</i>
R-squared	<i>0.78</i>	

The in-nip temperature coefficient reported here is approximately half the value determined using the whole set of in-nip data, Table 4.1. This difference can be attributed to an unequal distribution of data over the range of paper temperature; 90% of data were obtained at the paper temperature of $\sim 28^\circ C$, the remaining 10% at $\sim 60^\circ C$.

4.2 Effect of moisture content and temperature on uncalendered paper thickness

As the thickness of uncalendered paper varied with paper temperature and moisture content, thickness was measured at the exact conditions with an electronic micrometer. Each measurement was taken at 60 points, as three rows of 20, along the machine direction of the paper, over a length of about 2 meters, one row along the centreline of the 70 mm wide sheet, the other two rows about 15 mm from each edge. Uncalendered paper thickness was measured using paper located in the roll just before and just after that which was calendered, before and after each experiment, thus 120 data were

collected for each experimental combination of paper temperature and moisture content. Since no significant difference in thickness, before and after each experiment, was found, the single average value of uncalendered thickness, shown in Figures 4.48 to 4.51, was used in data processing.

The increase in uncalendered paper thickness caused by swelling of the wood pulp fibers is seen to be linear throughout the experimental range for both moisture content, Figures 4.48 and 4.49, and temperature, Figures 4.50 and 4.51. Thus at constant paper moisture content the pulp fibers expand linearly with temperature for these levels of moisture contents. The Forseth and Helle [25] investigation of the effect of moisture content on thickness of calendered paper showed that an increase in thickness with moisture content is caused of two factors: the cross-sectional expansion of compressed mechanical pulp fibers, and the development of interfibre voids and pores in the paper structure. The two factors are interrelated, as cross-sectional expansion of fibers pushes surrounding fibers up, and thus creates voids between them.

For paper temperature of approximately 30 °C, Figure 4.48a, uncalendered paper thickness increases from approximately 107 to 114 μm when moisture content is increased from 2 to 12%, an increase of 0.7 μm per percentage point increase of moisture content. Figure 4.50 shows that by increasing paper temperature from 30 to 75 °C at a relatively constant moisture content of 1.8%, uncalendered paper thickness increases from approximately 106 to 110 μm, a change of 0.9 μm per 10 °C. Over the industrially relevant ranges there is thus a comparable sensitivity of paper thickness to its temperature and moisture content.

The data show that uncalendered paper thickness can be approximated as a linear function of both temperature and moisture content,

$$t_i = t_0 + t_M M + t_\theta \Theta \quad [\text{Eq. 4.9}]$$

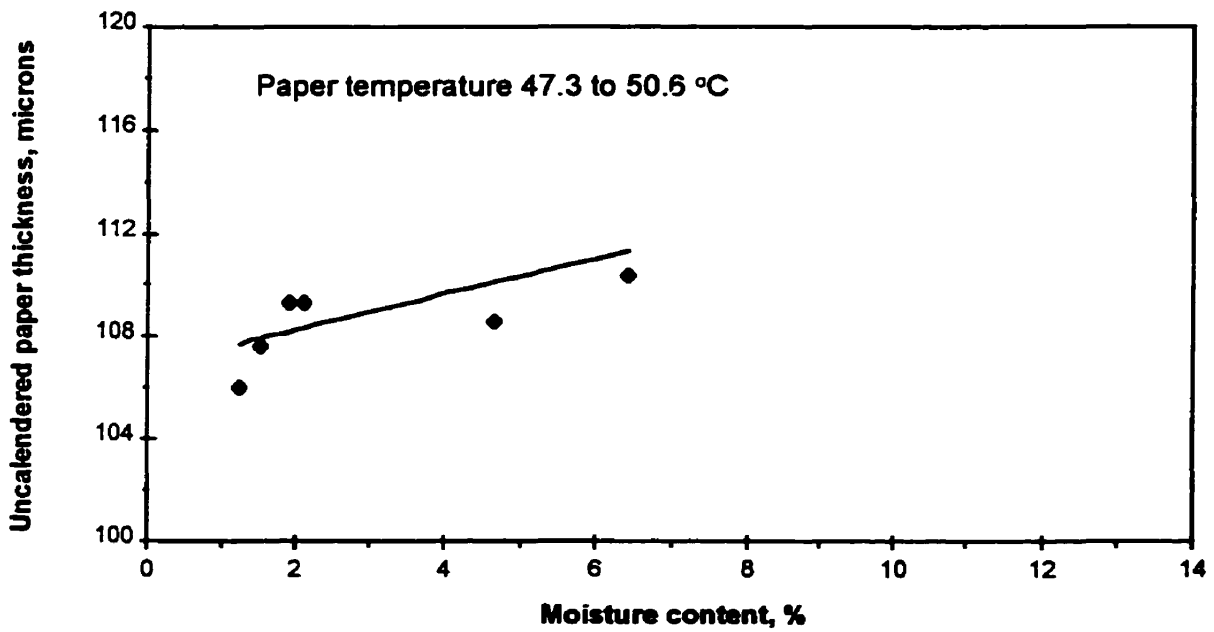
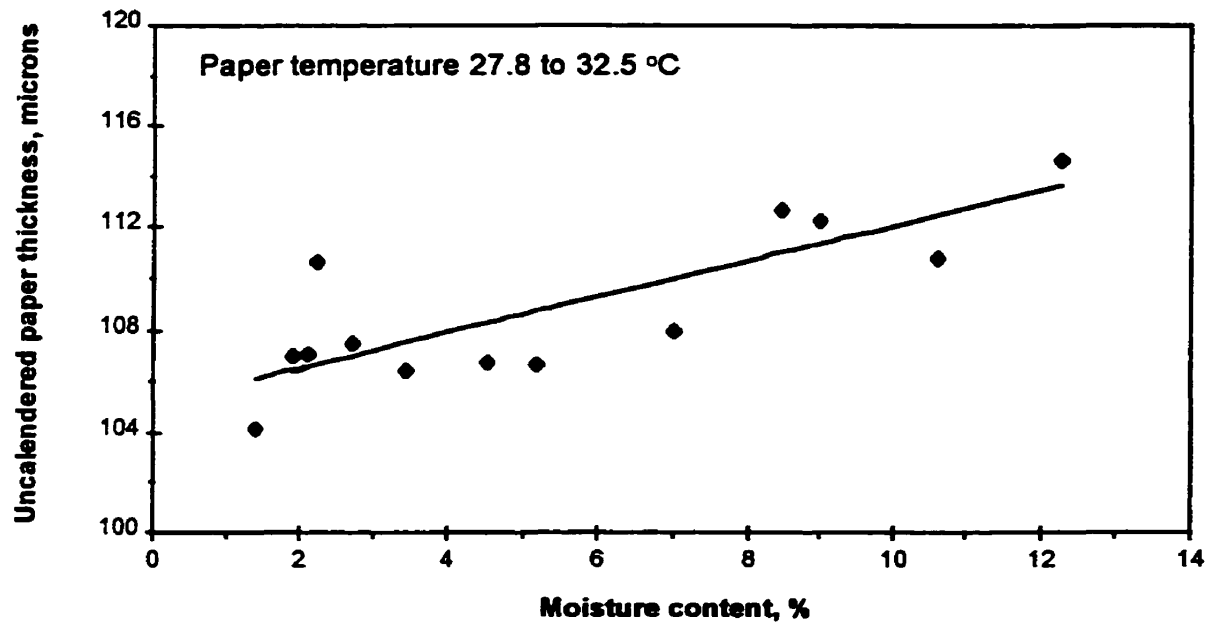


Figure 4.48: Effect of moisture content on thickness of uncalendered paper

a) $\Theta = \sim 30\text{ }^{\circ}\text{C}$

b) $\Theta = \sim 40\text{ }^{\circ}\text{C}$

Lines from Equation 4.9

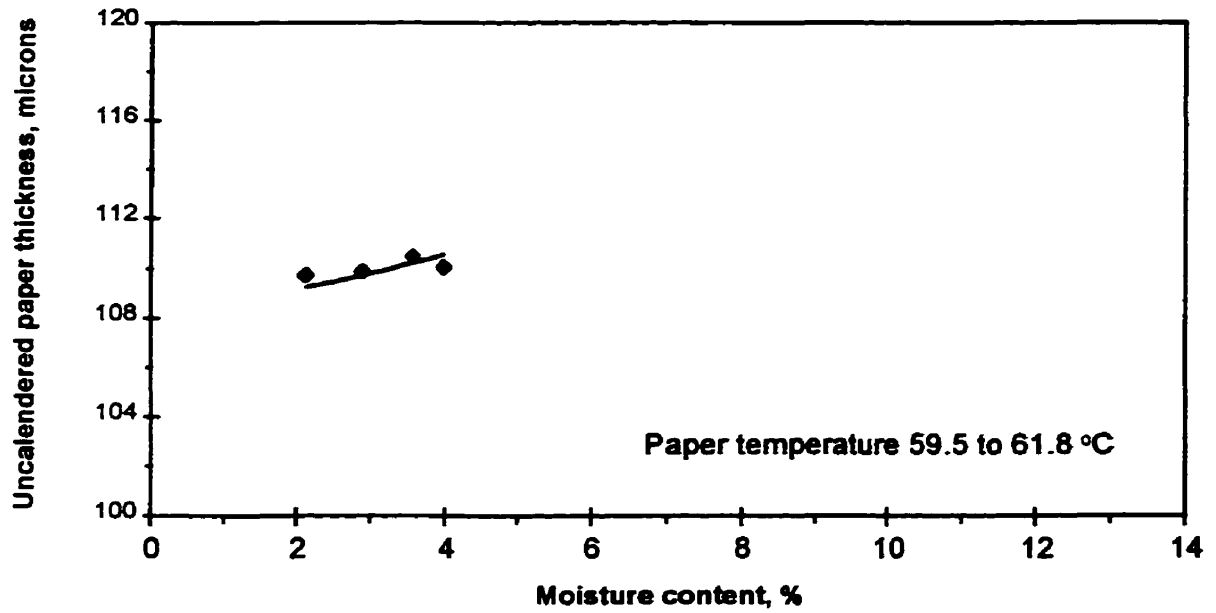


Figure 4.49: Effect of moisture content on thickness of uncalendered paper: $\Theta = \sim 60^\circ\text{C}$
 Line from Equation 4.9

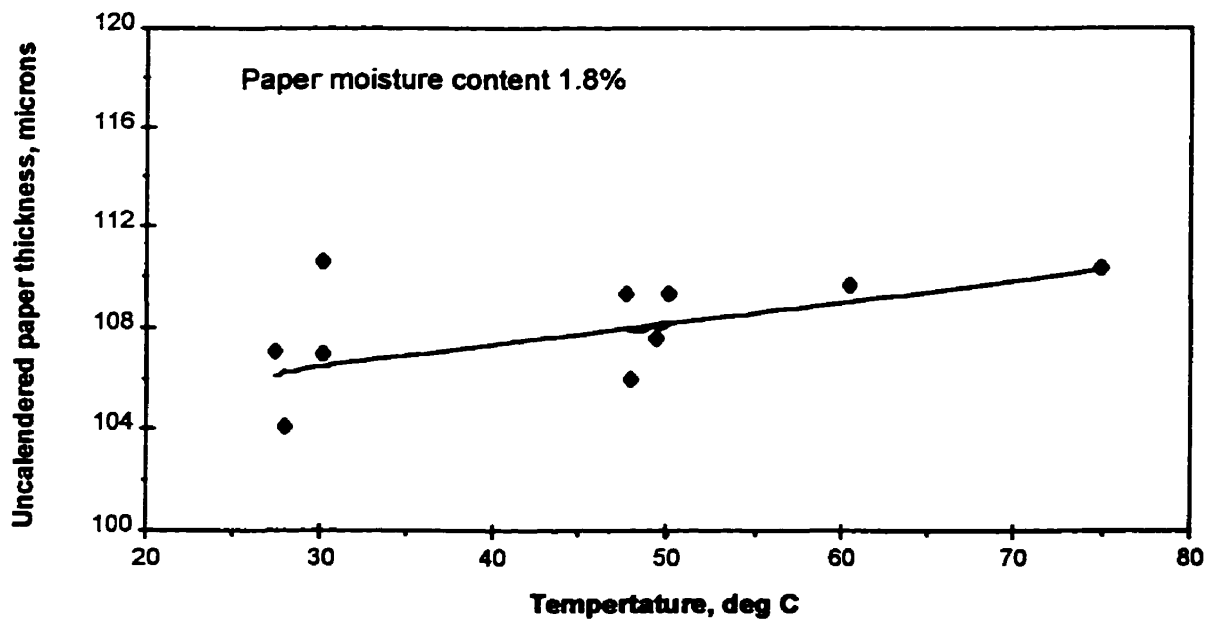


Figure 4.50: Effect of temperature on thickness of uncalendered paper: $M = 1.8\%$
 Line from Equation 4.9

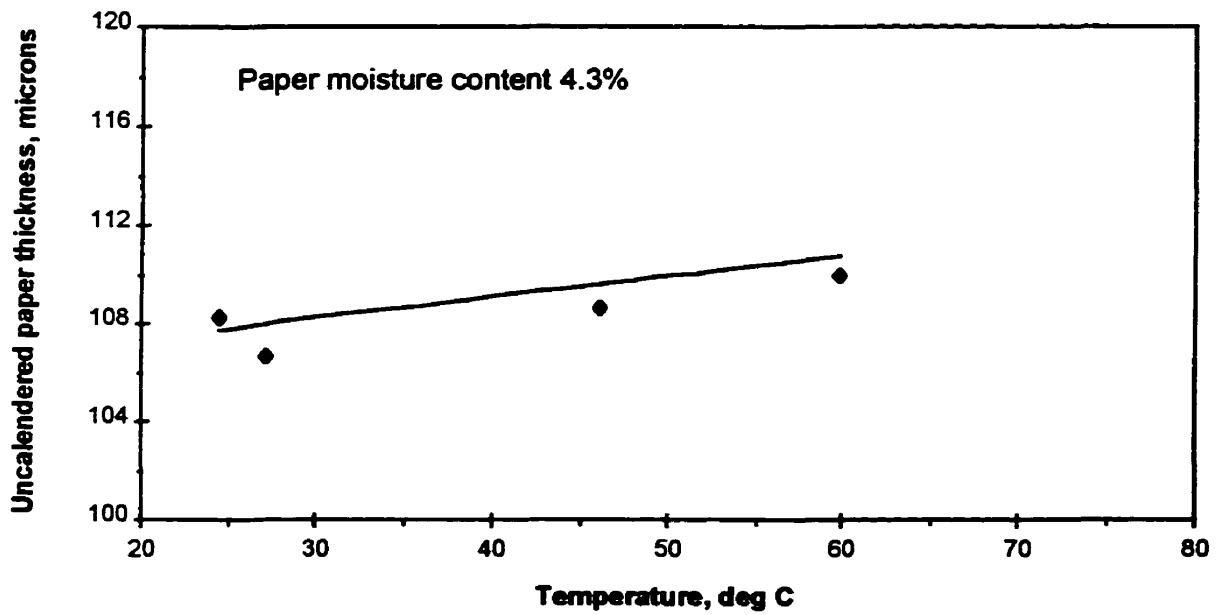
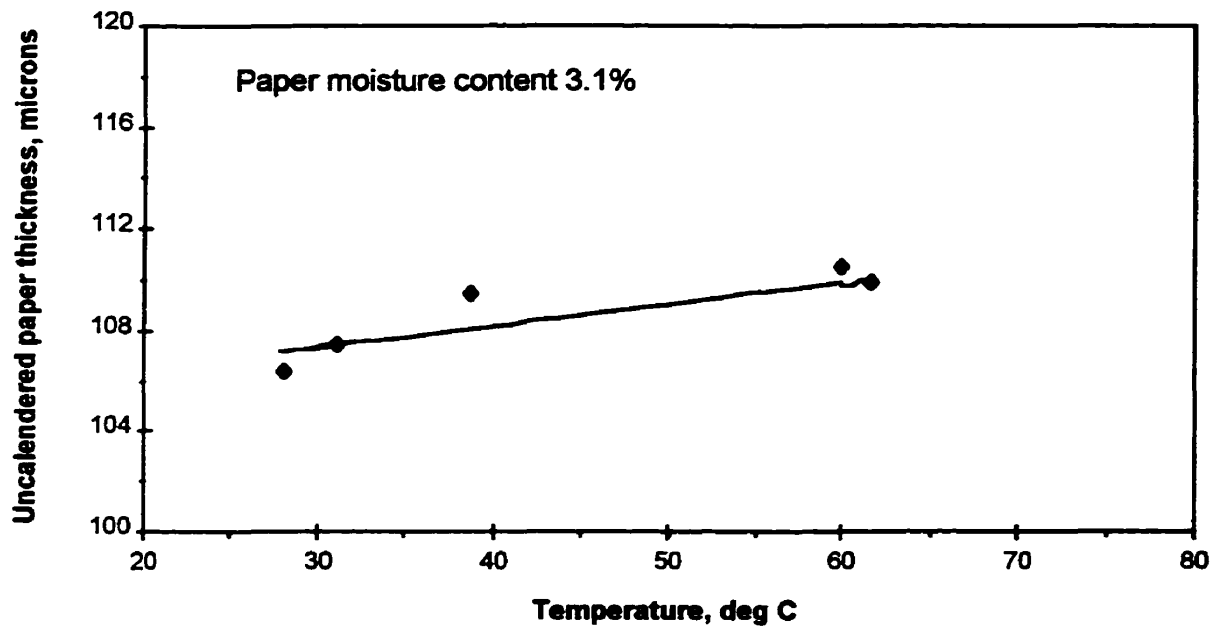


Figure 4.51: Effect of temperature on thickness of uncalendered paper

- a) $M \approx 3.1\%$
- b) $M \approx 4.3\%$

Lines from Equation 4.9

Table 4.8: Parameters of correlation for uncalendered paper thickness, Equation 4.8.

PARAMETER	ESTIMATE	STD ERROR	C.V.
t_0 (μm)	102.69	1.056	1 %
t_M (μm)	0.70	0.079	11 %
t_θ ($\mu\text{m} / ^\circ\text{C}$)	0.08	0.020	25 %
$R_{\text{-squared}}$	0.74		

The results for the entire set of initial thickness data from all 30 experiments is presented in Table 4.8. All the coefficients are statistically non-zero, and the predicted lines appear in Figures 4.48 to 4.51.

4.3 Effect of moisture content and temperature on paper strain.

Both moisture content and temperature are important parameters for calendering; their importance lies in the corresponding effect of the fibers becoming more pliable and plastically deformable, making the paper more easily deformable. The increased paper compressibility allows the desired final deformation to be obtained at a lower nip load, thus reducing the stress to which the paper is subjected during calendering. This effect is very important in minimizing the loss in paper strength from heavy calendering.

The effect of paper moisture content on both permanent and in-nip strain was determined here for several paper temperatures. However the most intensive measurements were performed at the low temperatures, 21 to 33 °C, with the paper moisture content varied from 1.5 to 13.5%, Figures 4.52 to 4.57. The effect of paper temperature was determined for both permanent and in-nip strain. Figures 4.58 and 4.59 give the permanent and in-nip strain data as a function of paper temperature at two levels of moisture content of ~1.8 and 4.1%. In the case of moisture content of ~1.8%, the paper

temperature is varied from 20 to 75 °C, while for the higher moisture content the paper temperature range is slightly narrower, 20 to 60 °C. Line load and paper speed were varied from 20 to 210 kN/m, 90 to 900 m/min. For the case of moisture effect, data obtained with both sets of the calender rolls are used while only data for the largest rolls are used to show the temperature effect.

The effect of moisture content and temperature on permanent paper strain has been well documented in earlier studies, the results reproduced in Figure 4.60 showing the trends for calendering a western Canadian newsprint, made from a furnish containing 24% semi-bleached kraft and 76% groundwood, at 3 m/min under a load of 30 kN/m. The permanent deformation-moisture content relation displays a maximum in the range of 15 to 20% moisture content. As the temperature increases and the permanent paper strain shifts to higher values, this maximum in permanent deformation shifts to lower values of moisture content.

The data for paper at 23 to 30 °C displayed on Figures 4.52 to 4.57 show consistent trends. With other calendering conditions fixed, the slope of the permanent deformation-moisture content relation decreases with increasing paper moisture content. This sensitivity decreases at first slowly then, at moisture contents above about 8%, decreases substantially, in some cases vanishing. Such behaviour is caused by a conflict between two phenomena encountered when paper moisture content is increased: with the sorption of water, wood pulp fibers both swell and become more pliable.

If the only effect was the fibers becoming more pliable, paper strain would increase continuously with paper moisture content. If fiber pliability did not change and the only effect was the increasing amount of incompressible water in the fibers, then paper strain would decrease steadily with increasing moisture content. With in fact both effects present and the fiber pliability increase being greater at lower moisture contents, the actual behaviour is of a decreasing sensitivity of deformation to moisture content with increasing moisture content.

For paper at 23 to 30 °C at lower moisture contents, the sensitive increase in

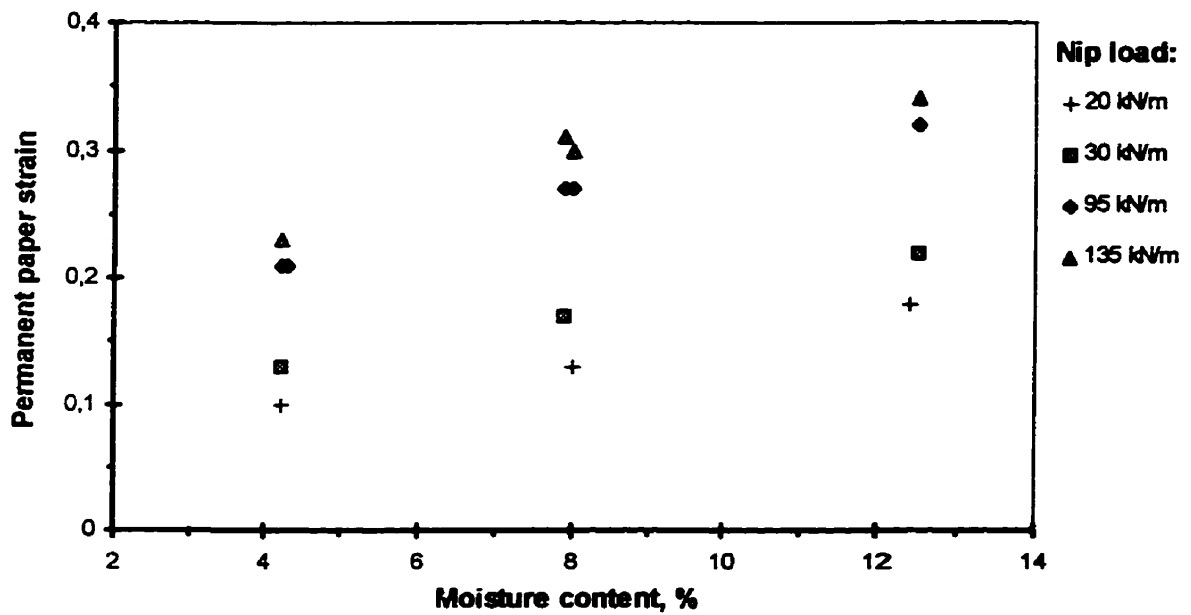
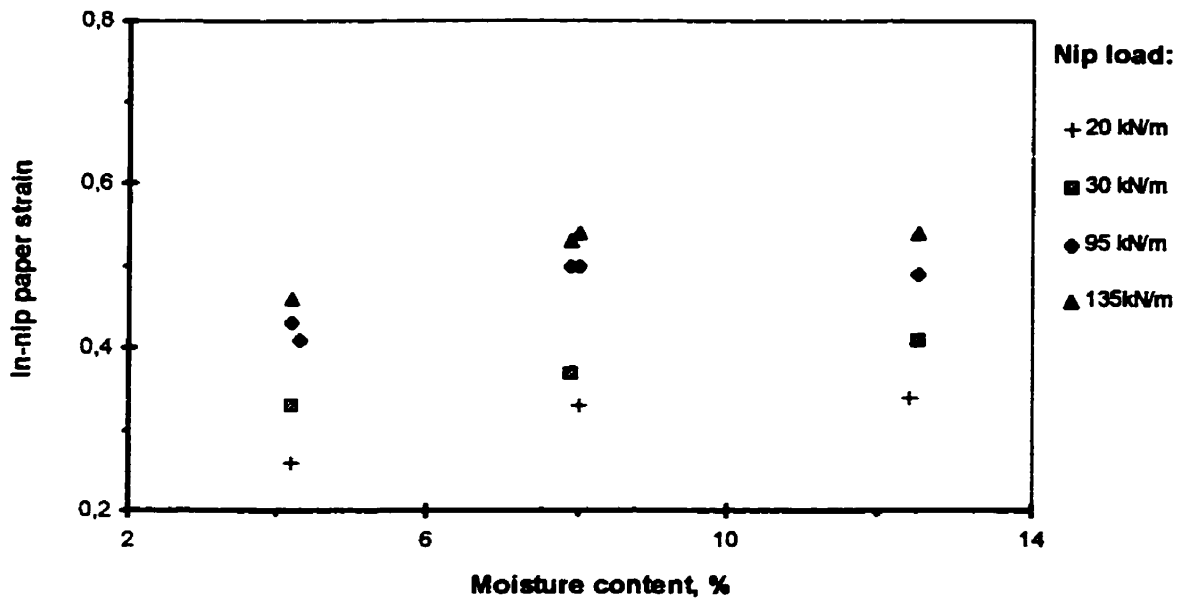


Figure 4.52: Effect of moisture content and line load on paper strain

$R = 0.355 \text{ m}$, $\Theta = \sim 23.5 \text{ }^\circ\text{C}$, $S = 90 \text{ m/min}$

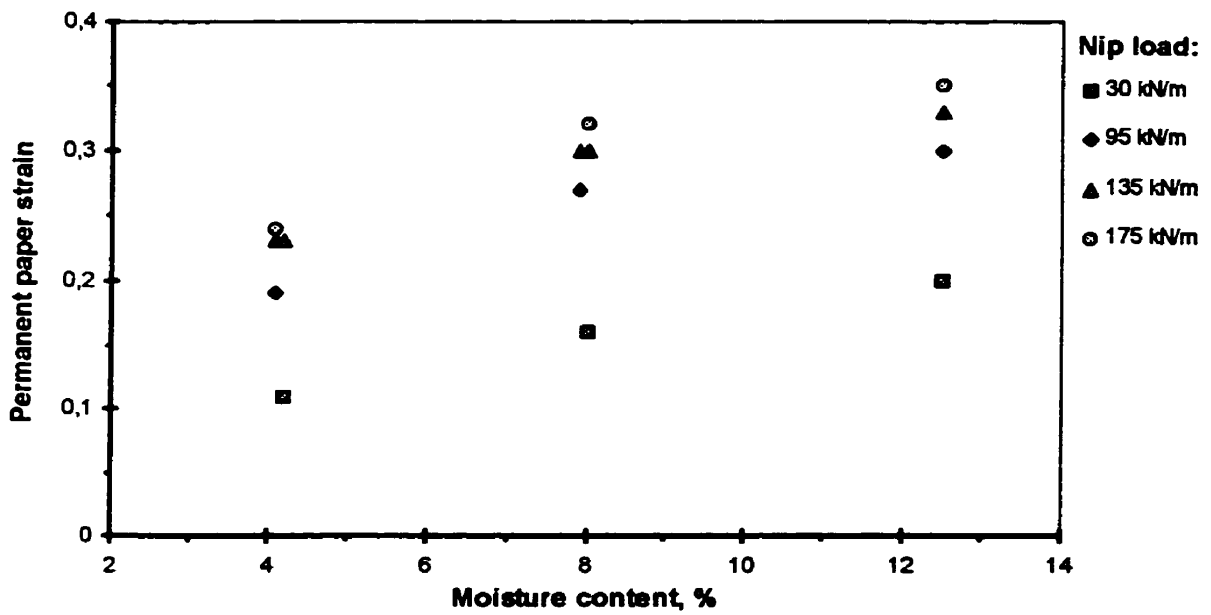
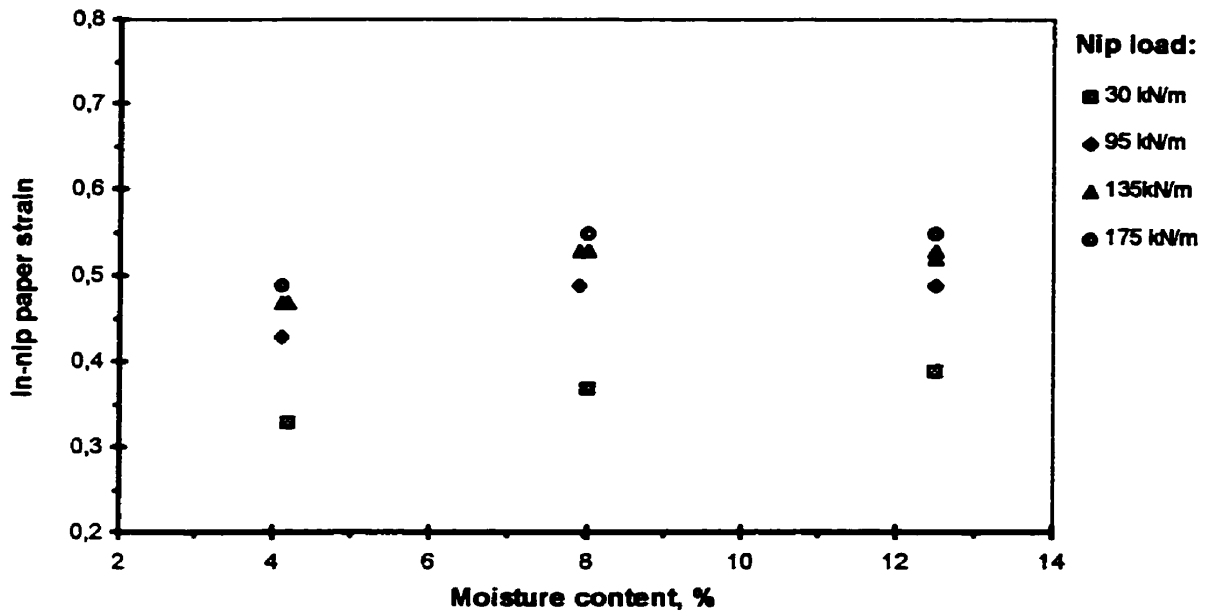


Figure 4.53: Effect of moisture content and line load on paper strain

$R = 0.355 \text{ m}$, $\Theta = \sim 23.5 \text{ }^\circ\text{C}$, $S = 180 \text{ m/min}$

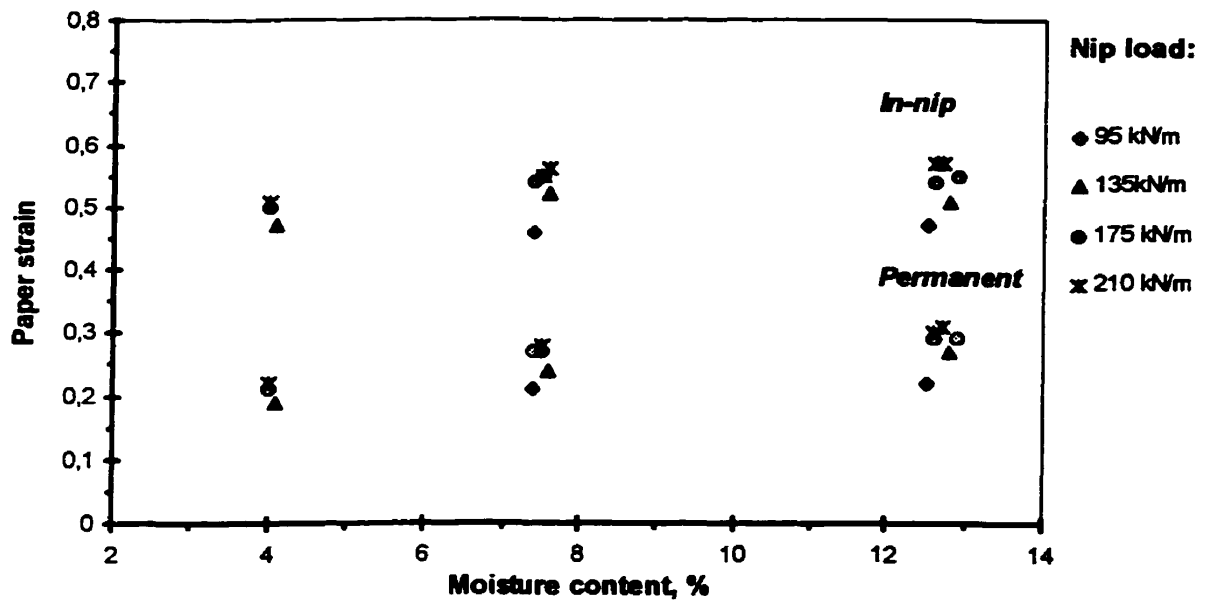
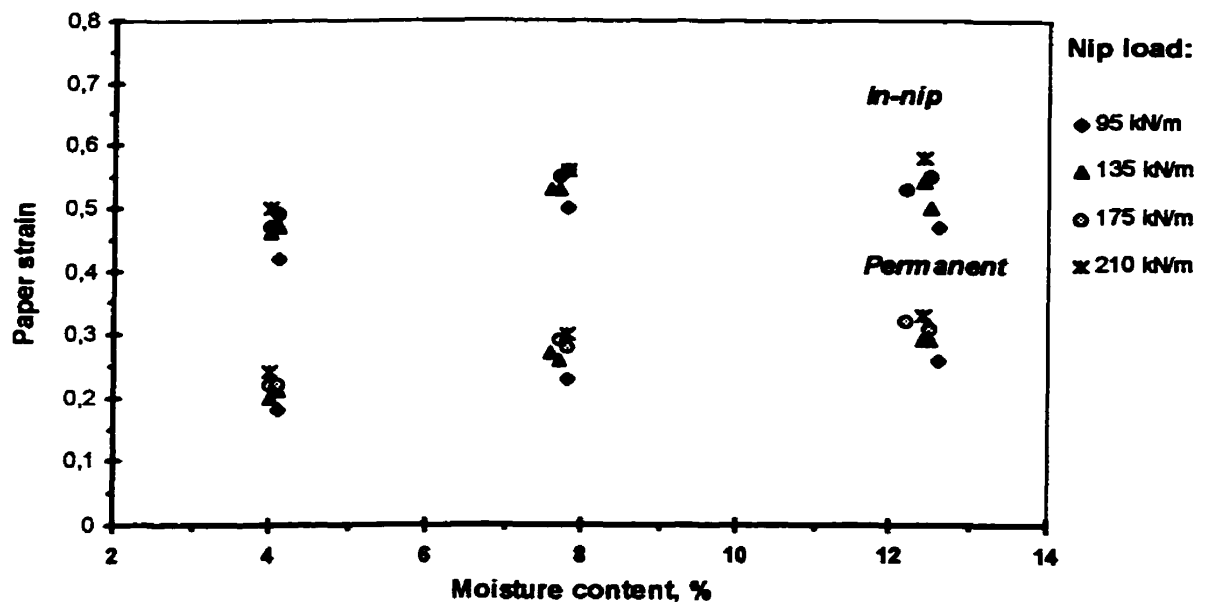


Figure 4.54: Effect of moisture content and line load on paper strain,
 $R = 0.355 \text{ m}$, $\Theta = \sim 23.5 \text{ }^\circ\text{C}$

- a) $S = 500 \text{ m/min}$
- b) $S = 900 \text{ m/min}$

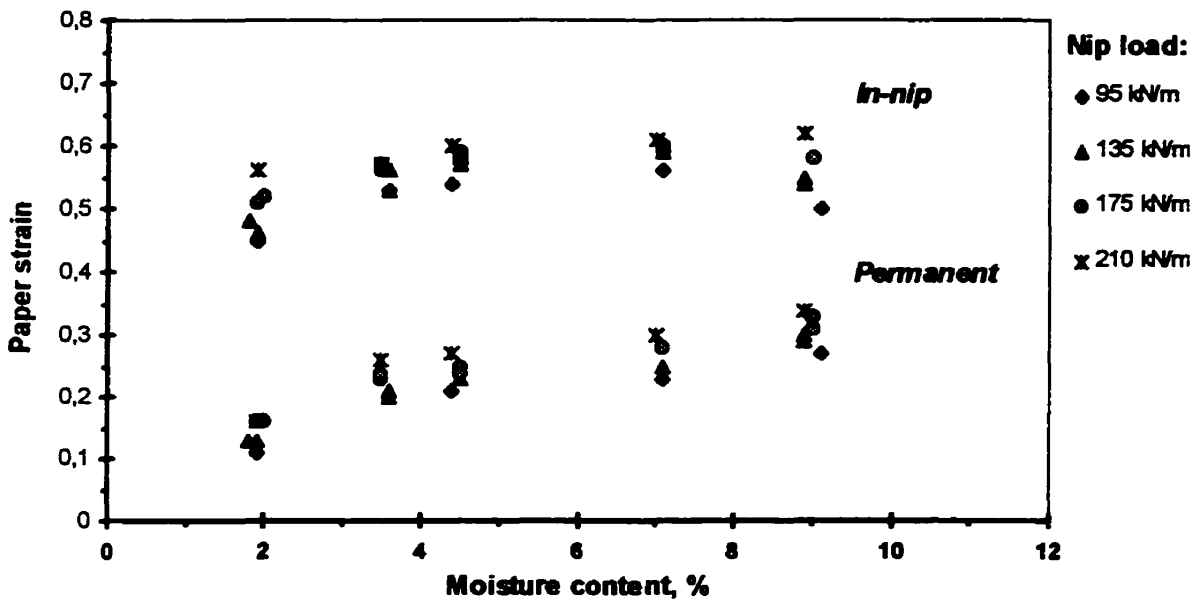
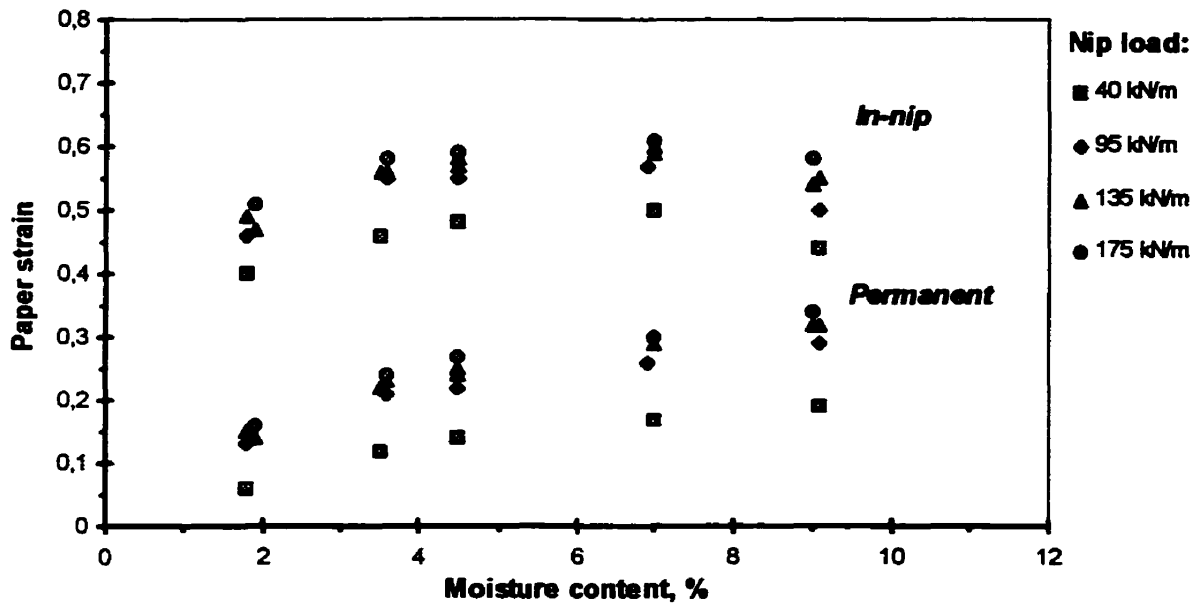


Figure 4.55: Effect of moisture content and line load on paper strain, $R=0.355\text{ m}$, $\Theta = \sim 30^\circ\text{C}$

- a) $S=180\text{ m/min}$
- b) $S=500\text{ m/min}$

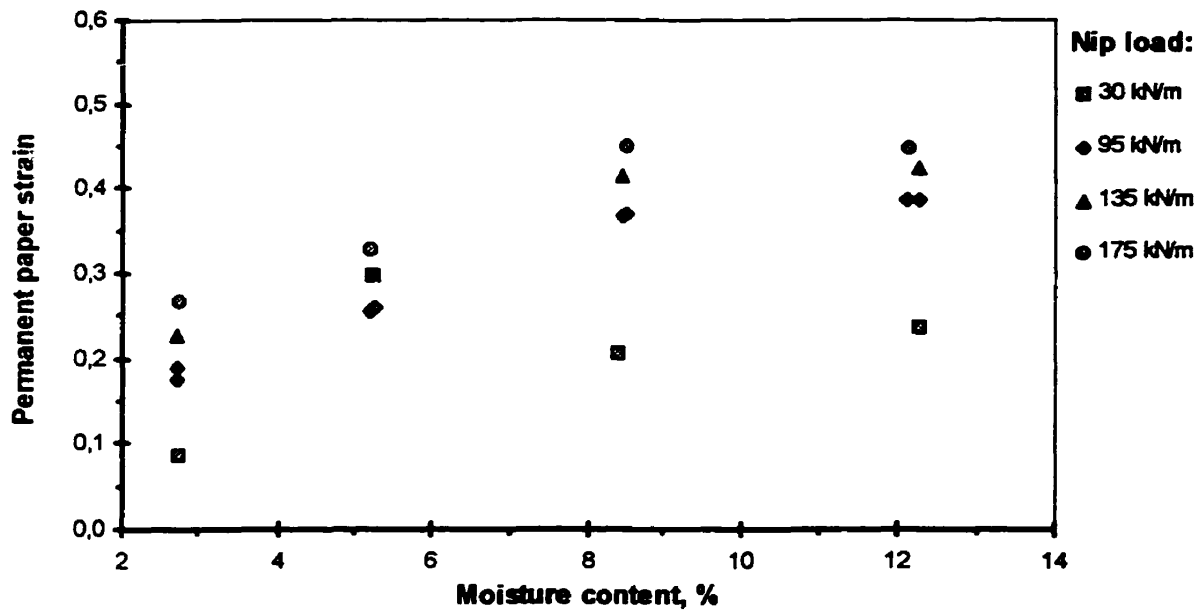
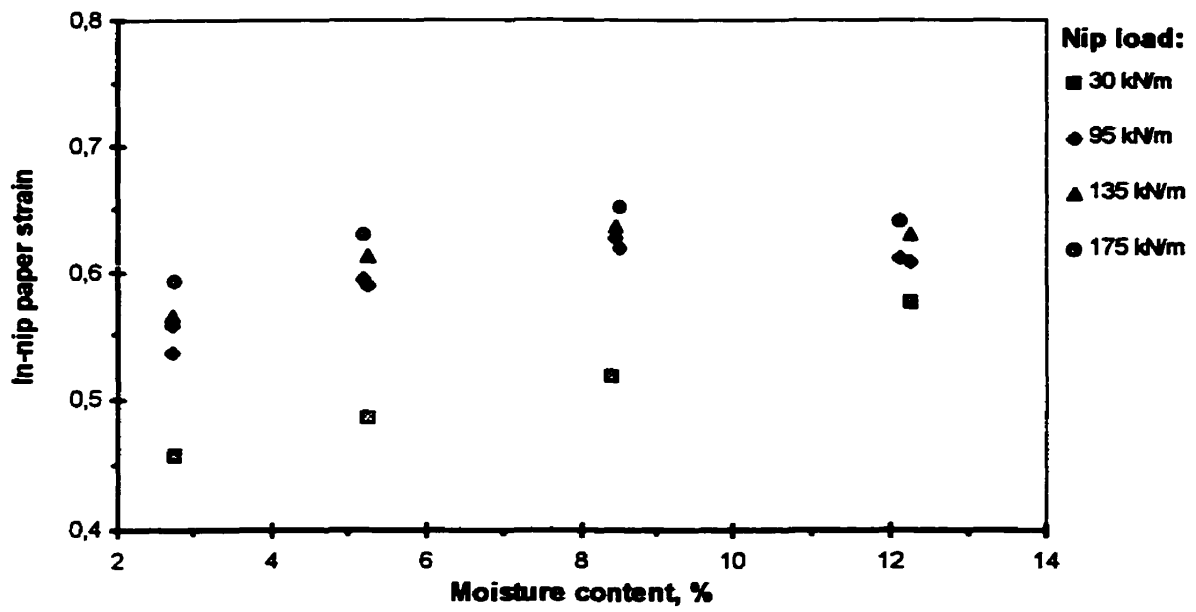


Figure 4.56: Effect of moisture content and line load on paper strain,
 $R=0.202\text{ m}$, $\Theta \sim 30\text{ }^\circ\text{C}$, $S=90\text{ m/min}$

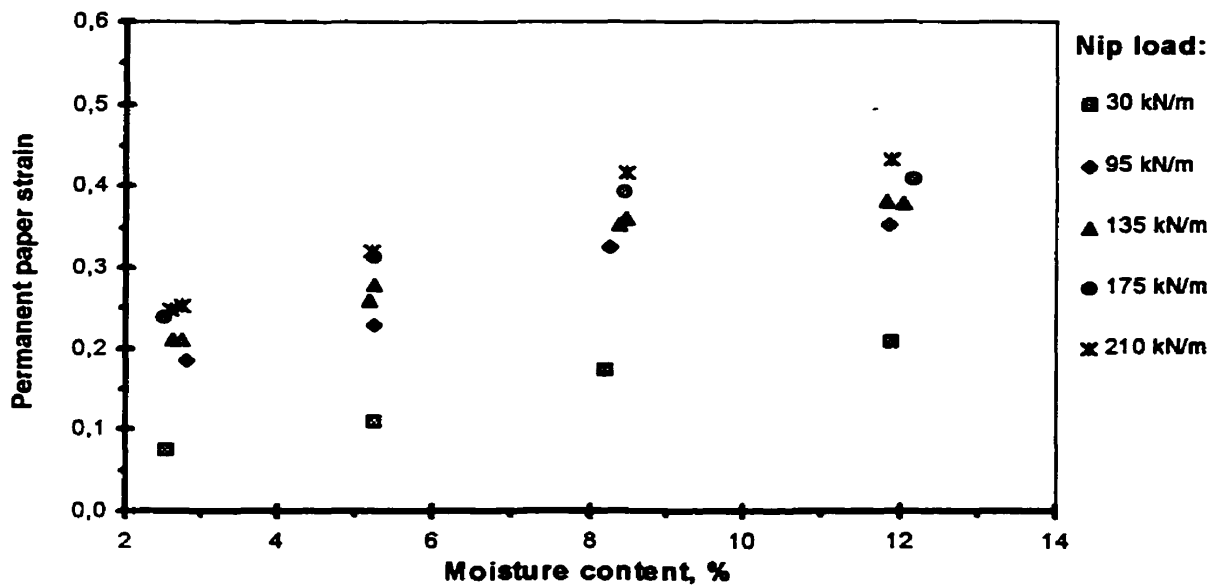
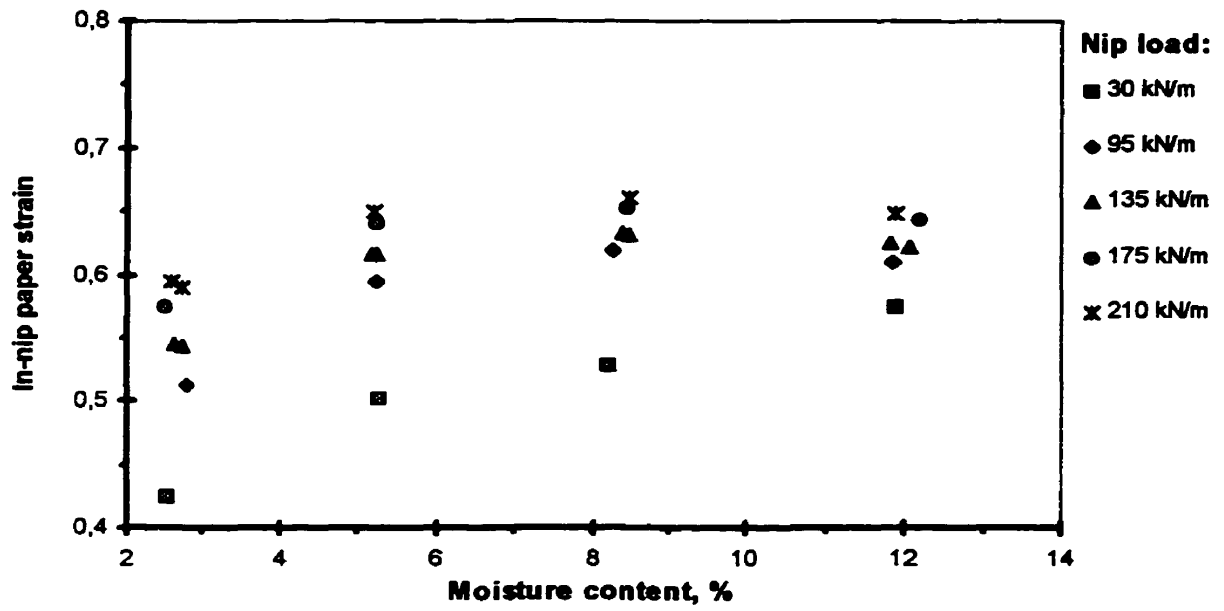


Figure 4.57: Effect of moisture content and line load on paper strain,
 $R = 0.202 \text{ m}$, $\Theta = \sim 30 \text{ }^\circ\text{C}$, $S = 300 \text{ m/min}$

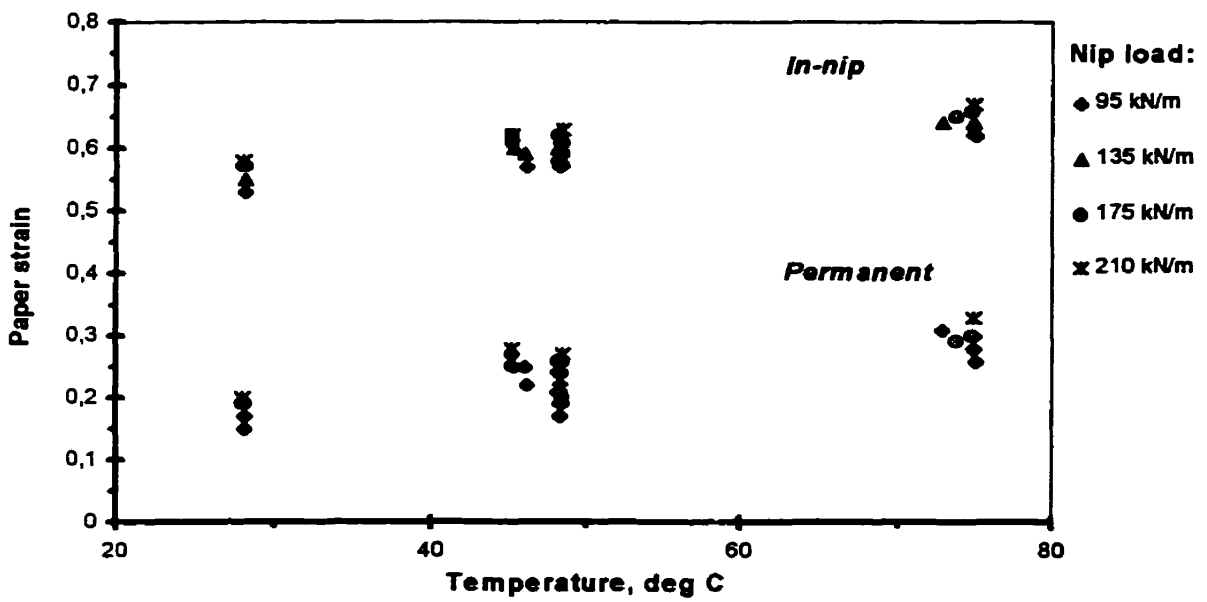
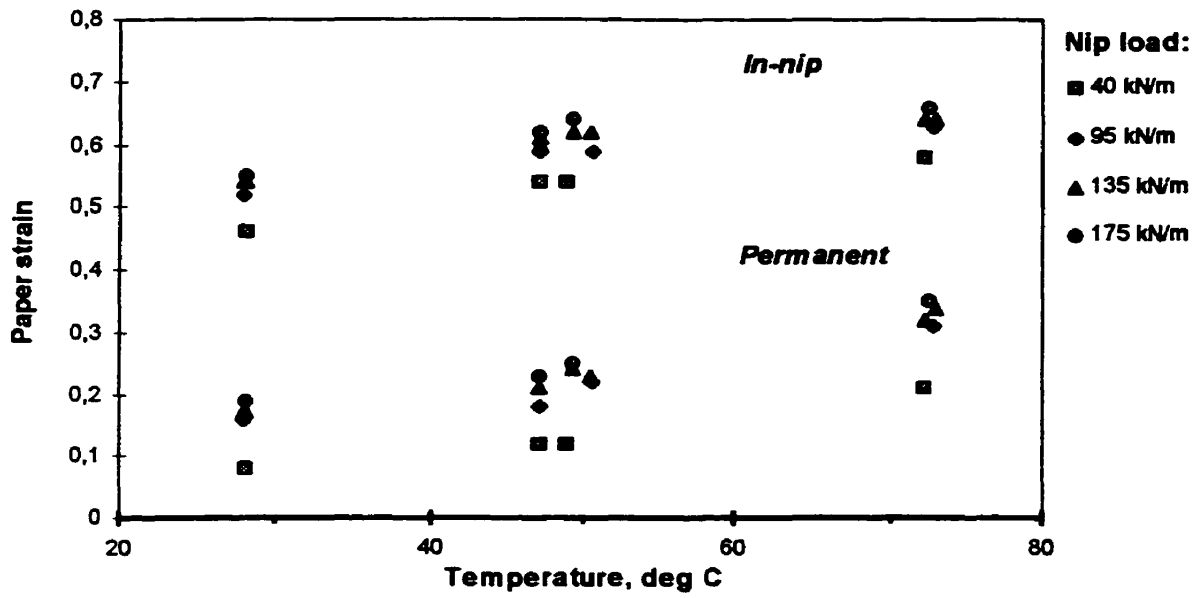


Figure 4.58: Effect of temperature and line load on paper strain,
 $R = 0.355$ m, $M = \sim 1.8\%$

- a) $S = 90$ m/min
- b) $S = 500$ m/min

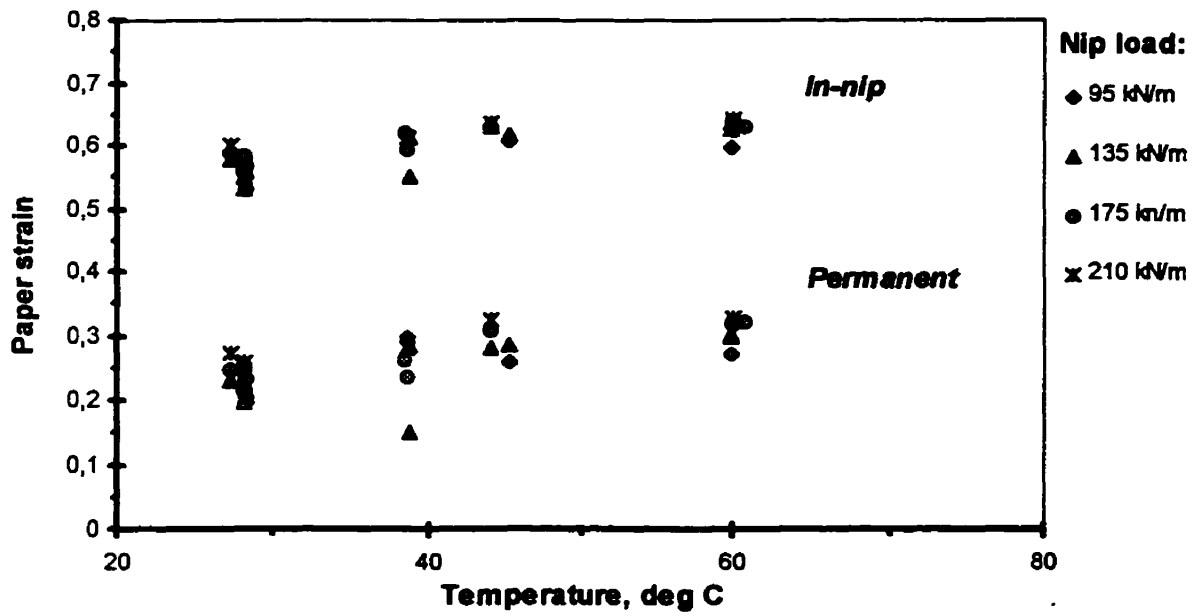
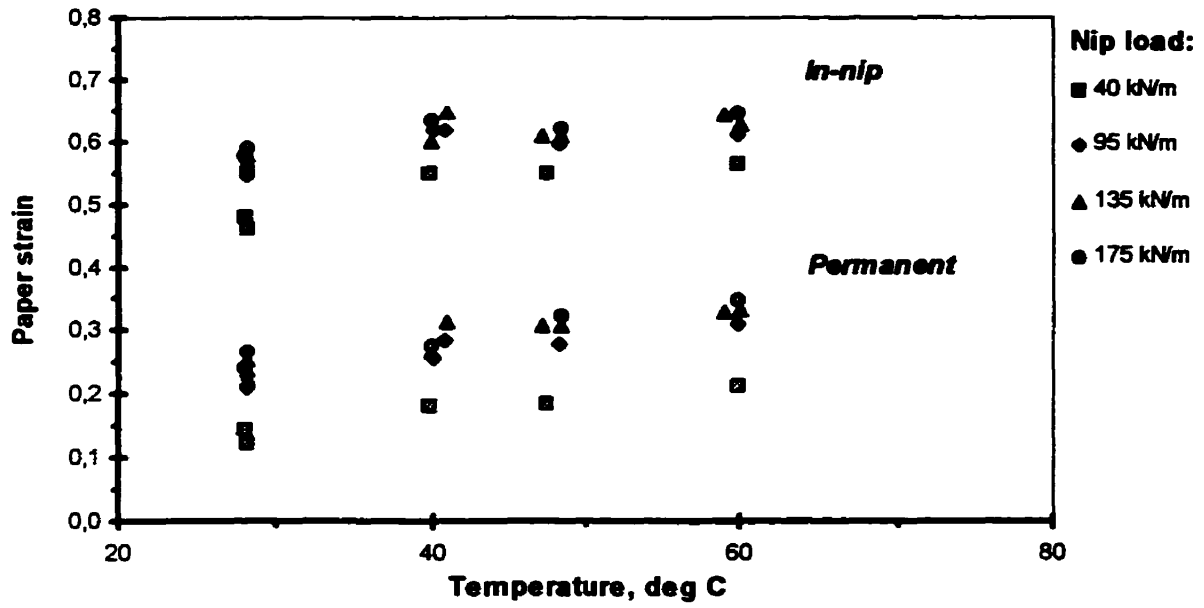


Figure 4.59: Effect of temperature and line load on paper strain,
 $R=0.355$ m, $M\sim 4.1\%$

- a) $S=180$ m/min
- b) $S=500$ m/min

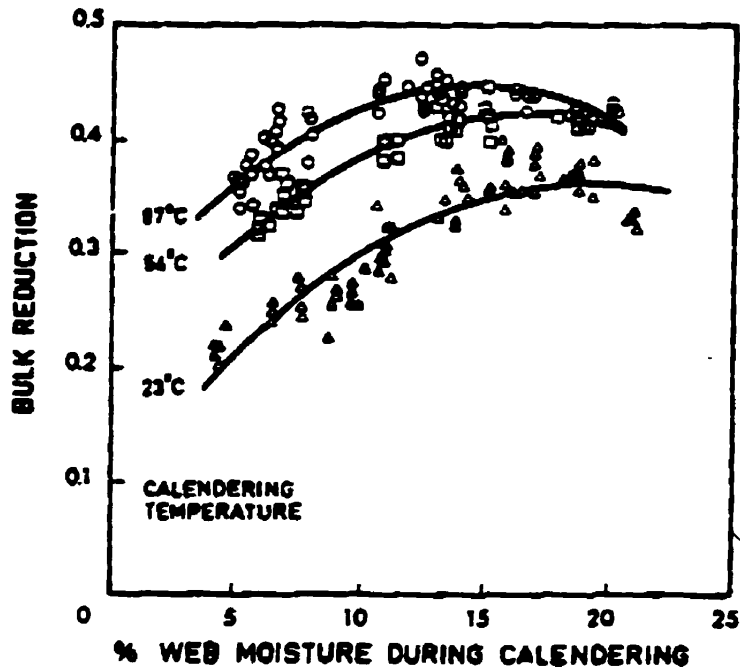


Figure 4.60: Effect of paper moisture content on permanent strain at three levels of paper temperature, Crotagino and Pye data, Pulp and Paper Research Institute of Canada.

permanent strain with increasing moisture content indicates that the effect from the fibers becoming more pliable is so strong that it more than compensates for the additional resistance to deformation coming from the increased amount of water in the fibers. However at higher moisture content the situation is reversed, with a now smaller increase in fiber pliability being insufficient to compensate for the restriction on paper deformation coming from the larger amount of water in the fibers. In numerous cases displayed on Figures 4.52 to 4.59, there is little or no increase in permanent strain for paper at 12% moisture content relative to that for 8% moisture. In Figure 4.56 at the heaviest line load, 175 kN/m, the permanent strain is actually less at 12% than at 8% moisture content.

The increase in uncalendered paper thickness with moisture content was seen in Section 4.2 to be about linear over the range of moisture content investigated. The observed permanent deformation-moisture content behaviour thus provides evidence that the extent to which pulp fibers become more pliable with increasing moisture content

declines at higher moisture content, probably becoming quite small above about 12% moisture content.

The effect of moisture content for paper at 23 to 30 °C is smaller on in-nip than permanent strain, which is reasonable considering the high compression of paper in the nip shown on Figures 4.52 to 4.57. With the much higher levels of in-nip strain it would be expected that, of the two counteracting effects noted above, that of the restraint on deformation from the increased amount of water in the fibers would be more important than increased fiber pliability. This is the behaviour observed, with the relation between in-nip strain and paper moisture content either reaching a plateau or, most often, passing through a maximum. When the in-nip strain does not exceed about 0.4 to 0.5, i.e. at the lowest calendering loads of 20 and 30 kN/m, the in-nip strain dependence on moisture content is, as would be suspected, similar to that for permanent strain. However at heavier calendering loads, when paper thickness in the nip is as little as 1/3 the entering thickness, the in-nip strains pass through a maximum which occurs at approximately 7 to 9% moisture content. In such cases the in-nip paper thickness is as little as 30 to 40 μm and thus a change in initial thickness of 8 μm , caused by the additional water in the fibers at a moisture content of 10% compared to 2%, has naturally a stronger effect on in-nip than permanent strain.

At any paper moisture content, pulp fibers are more pliable at higher temperature. Thus at higher paper temperature the fibers are already more pliable at low moisture content, hence there is less scope for increase of fiber pliability with increasing moisture content. Consequently it would be expected that, of the two counteracting effects at increasing moisture content i.e. increased fiber pliability and increased amount of incompressible water in the fibers, the latter effect would more quickly become the dominant effect. Thus all the effects described above are more pronounced at 30 °C (Figures 4.55 to 4.57) than at 23 °C (Figures 4.52 to 4.54). Results obtained at higher temperature, Figure 4.61, indicate that as paper temperature is increased from 30 °C to 48 °C the maximum in the deformation-moisture content relation shifts from approximately 7 to 9% to between 2 and 5% of moisture content. Moreover Figure 4.61 clearly shows that

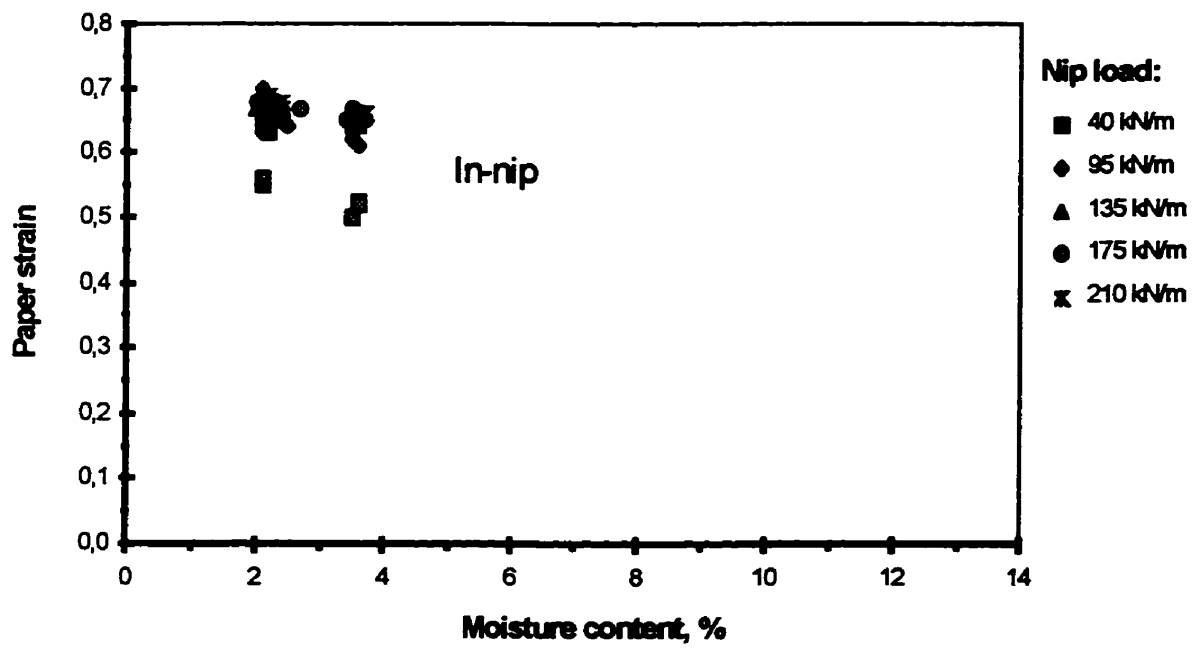
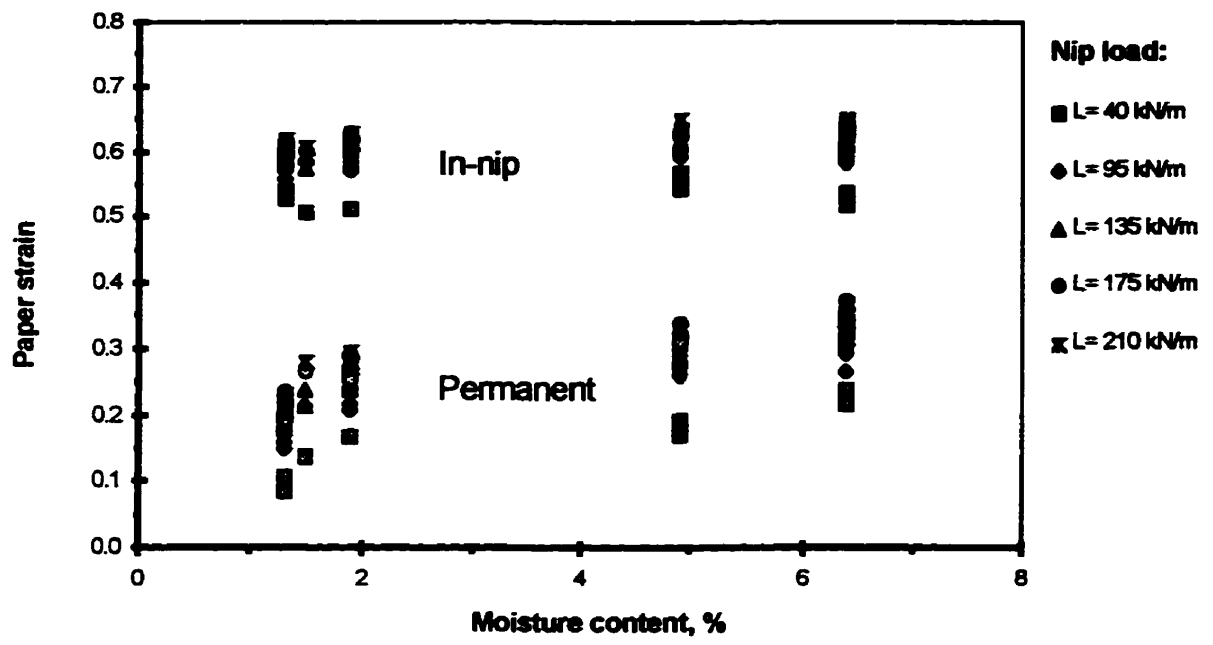


Figure 4.61: Effect of moisture content and load on paper in-nip strain, all speeds

a) $R= 0.355 \text{ m}$, $\Theta= \sim 48 \text{ }^\circ\text{C}$

b) $R= 0.202 \text{ m}$, $\Theta= \sim 60 \text{ }^\circ\text{C}$

at 60 °C, all data are now above the maximum in the deformation-moisture content curve, with in-nip strain in all cases decreasing with increasing moisture content, even at the lowest nip load of 40 kN/m where in-nip strain is in the range 0.50 to 0.55. Thus at 60 °C the maximum in the deformation-moisture content relationship occurs at some very low value of moisture content, less than 2%. At 60 °C the pulp fibers are so pliable at these very low levels of moisture content that the in-nip strain-moisture content relation is completely dominated by the restraint on paper deformation coming from the varying amount of incompressible water in the fibers.

Data displayed on Figures 4.52 to 4.57 is cross-plotted on Figures 4.58 to 4.59 as a function of paper temperature at two levels of moisture content which are limited to about 4% in order to show results up to about 60 °C. The sensitivity of paper strain, both in-nip and permanent, is naturally less at the higher level of moisture content for which the levels of strain are higher. As was already seen in connection with Figures 4.52 to 4.57, the higher the level of deformation, the less increase there is in paper strain. At the high levels of in-nip deformation existing for temperatures above 50 °C, especially at the higher moisture content, there is little increase in in-nip strain with further increase in paper temperature. The present work supports the findings of Colley and Peel [12] that at high moisture content the effect of increase of temperature is very small above 50 °C for groundwood furnish paper and above 70 °C for cotton paper.

4.4 Modified calendering equation

The results of Section 4.3 suggest that the present form of the calendering equation, which is linear with paper temperature and moisture content, could be improved. Although the moisture effect has been shown to be nonlinear for both permanent and in-nip paper strain, for permanent strain the linear approximation appears satisfactory. The range of paper moisture content for calendering in industrial practice is 4 to 10%, which is below the strongly nonlinear range. However, the nonlinear effect of the paper moisture

content must be allowed for when operating at a high level of moisture content, for example 14% moisture for 30 °C paper.

For in-nip strain, however, the strong nonlinear effect of moisture content is seen to occur within the operating range of a standard calender stack. This suggests that one possibility for providing a better fit to the in-nip data is addition to the standard calendering equation of a second order term for paper moisture content:

$$\begin{aligned} \varepsilon_n &= A_n + \mu_n B_i, & \text{when: } & B_i < 0.5 (I - A) / \mu_n \\ \varepsilon_n &= I - 0.25 (I - A_n)^2 / (\mu_n B_i) & \text{when: } & B_i \geq 0.5 (I - A) / \mu_n \end{aligned}$$

where:

[Eq. 4.10]

$$\mu_n = a_{0n} + a_{Ln} \log_{10} L + a_{Sn} \log_{10} S + a_{Rn} \log_{10} R + a_{Mn} M + a_{M2n} M^2 + a_{\Theta n} \Theta$$

This equation is valid within the limits defined for the standard calendering equation. Because the condition of zero in-nip strain was never experienced, the lower limit is irrelevant. Thereby Equation 4.10 along with the upper limit was used as input to the data processing program to fit the full set of in-nip strain data.

Estimates of the coefficients for Equation 4.10, along with their asymptotic standard errors (A.S.E.) are presented in Table 4.9. Figures 4.62 to 4.65 show the experimental data and the regression curves which include that for the standard calendering equation.

Compared with results obtained for the standard calendering equation, Table 4.1, the coefficients which are changed the most when Equation 4.10 is used are those for the intercept and moisture content, a_{0n} and a_{Mn} , changed by 45 and 76%. The other coefficients change by less than 8%, except 14% change for the intercept coefficient A_n . The R -squared value using Equation 4.10 of is higher, but only slightly i.e. 0.77 vs. 0.76. Inspection of Figures 4.62 to 4.65 indicates that the curves generated with Equation 4.10 better predict the nonlinear behaviour of in-nip strain with moisture content.

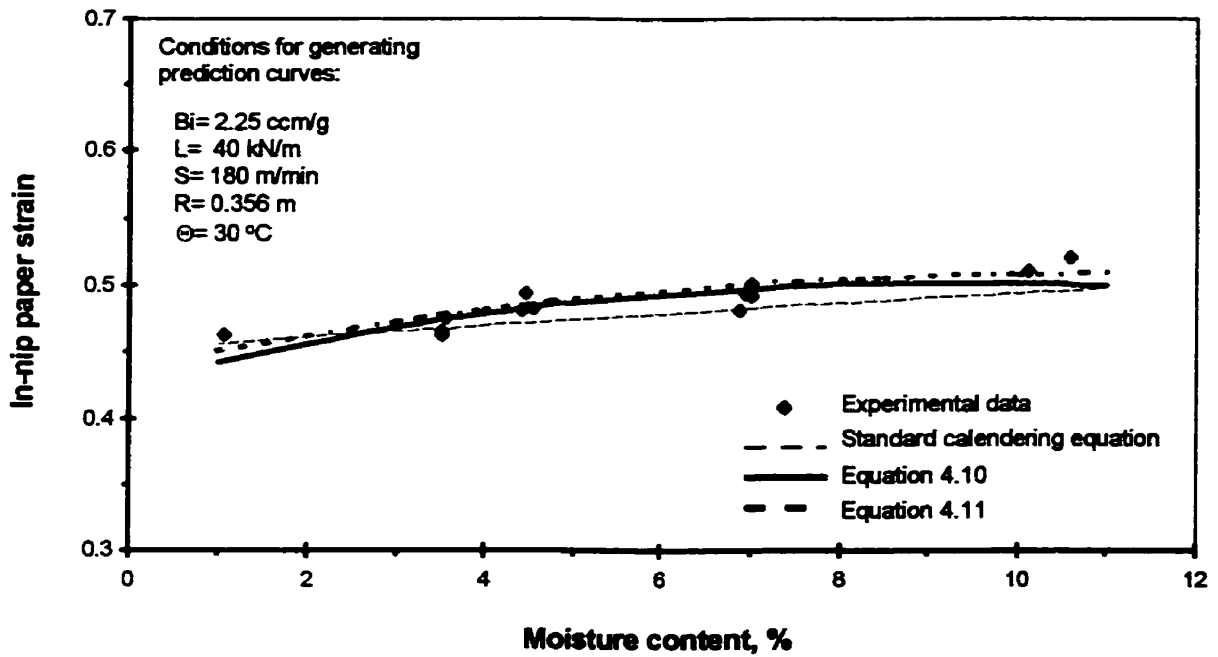
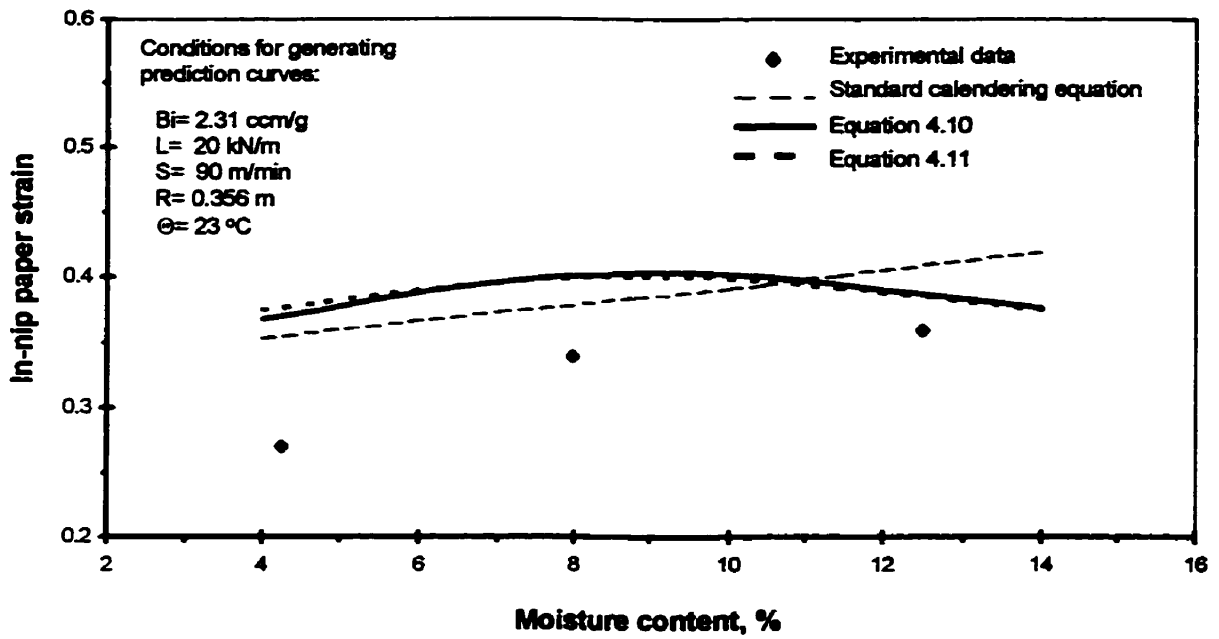


Figure 4.62 Effect of moisture content on in-nip strain, $R = 0.356 \text{ m}$, $\Theta = 27 \text{ to } 30 \text{ }^\circ\text{C}$,

a) $L = 20 \text{ kN/m}$, $S = 90 \text{ m/min}$

b) $L = 40 \text{ kN/m}$, all speeds

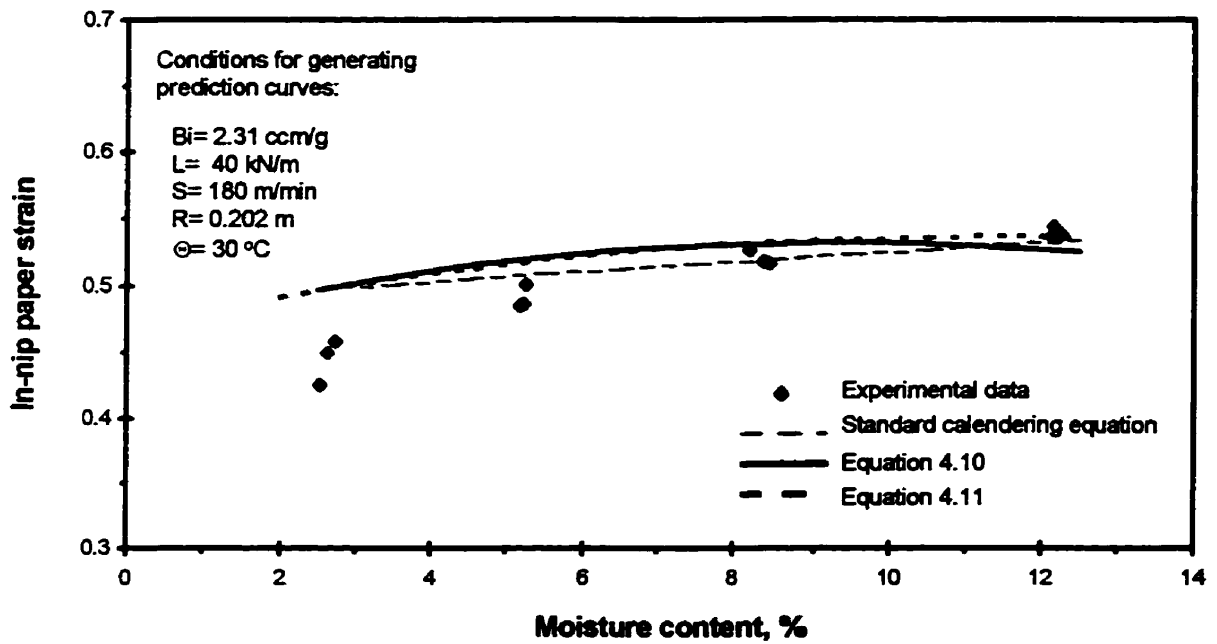
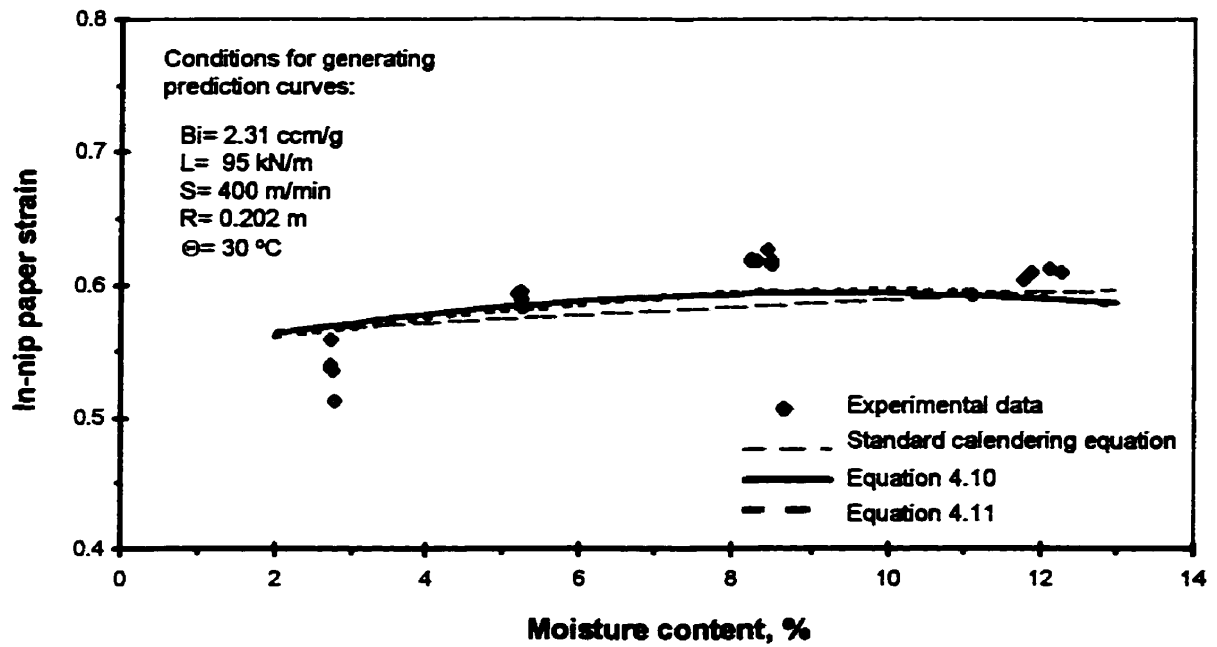


Figure 4.63: Effect of moisture content on in-nip strain, $R = 0.202 \text{ m}$, $\Theta = 29 \text{ to } 32 \text{ }^\circ\text{C}$, all speeds.

- a) $L = 40 \text{ kN/m}$
- b) $L = 95 \text{ kN/m}$

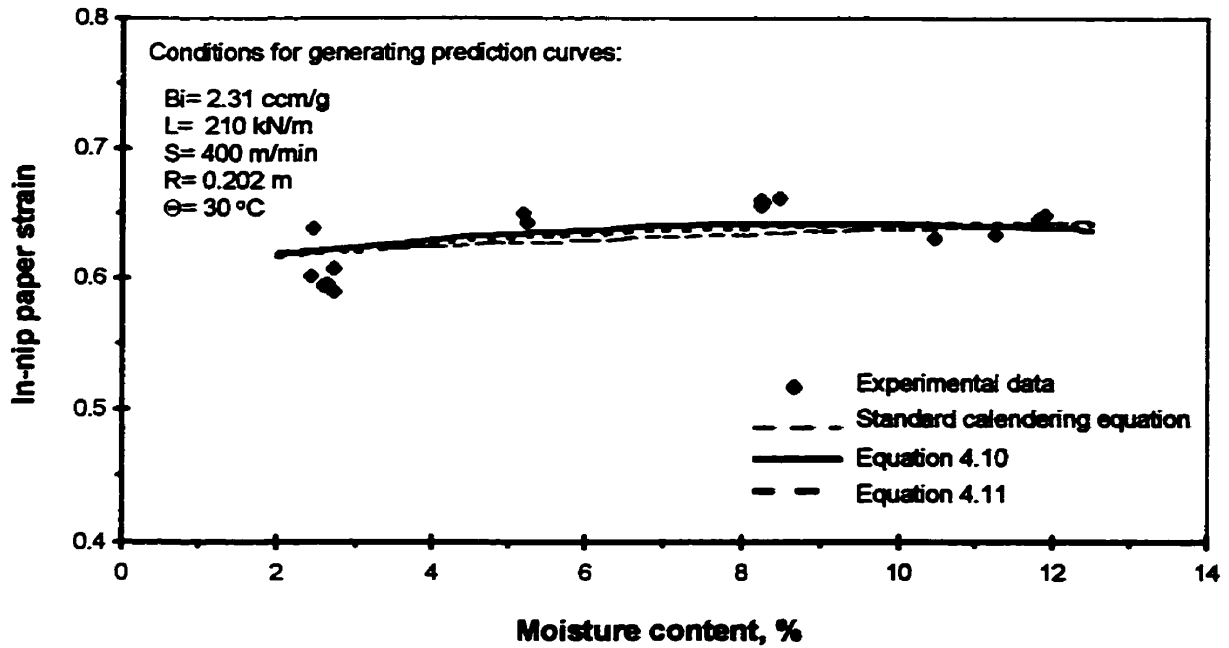


Figure 4.64: Effect of moisture content on in-nip strain, $R = 0.202 \text{ m}$, $L = 210 \text{ kN/m}$, $\Theta = 29 \text{ to } 32 \text{ }^\circ\text{C}$, all speeds.

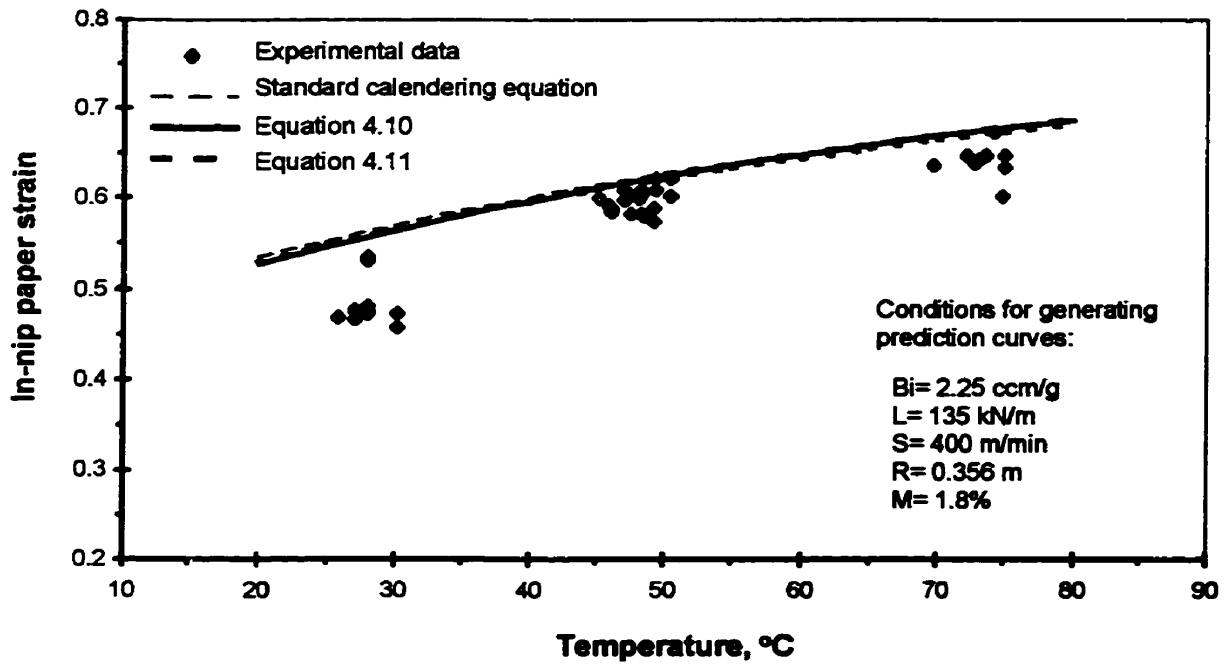


Figure 4.65: Effect of temperature on in-nip strain, $R = 0.356 \text{ m}$, $L = 135 \text{ kN/m}$, $M = 1.1 \text{ to } 2.2 \%$, all speeds.

Table 4.9: In-nip coefficients for Equation 4.10.

PARAMETER	ESTIMATE	A.S.E.	C.V.
A_n	-0.3727	0.02681	7 %
$a_{0n} \text{ (g/cm}^3\text{)}$	-0.0438	0.01344	31 %
$a_{Ln} \text{ (g/cm}^3\text{)}$	0.1926	0.00966	5 %
$a_{Sn} \text{ (g/cm}^3\text{)}$	-0.0141	0.00440	31 %
$a_{Rn} \text{ (g/cm}^3\text{)}$	-0.0440	0.01348	31 %
$a_{Tn} \text{ (g/cm}^3\text{ }^\circ\text{C)}$	0.00381	0.000125	3 %
$a_{Mn} \text{ (g/cm}^3\text{)}$	0.01230	0.000403	3 %
$a_{M2n} \text{ (g/cm}^3\text{)}$	-0.00066	0.000005	1 %
R-squared	0.77		

The in-nip moisture effect has been seen to be a function of line load and paper temperature, which suggests the alternative of including those two calendering parameters with the moisture coefficient a_{M2n} :

$$a_{M2n} = a_{M2o} + a_{ML} \log_{10}L + a_{Me} \Theta \quad [\text{Eq. 4.11}]$$

However, there is insufficient data available at low line load and high paper temperature to be able to extract a statistically meaningful relationship involving those variables. Thereby fitting Equations 4.10 and 4.11 to the set of in-nip strain data provided only a small improvement over that of Equation 4.10 alone, as seen on Figures 4.65 to 4.68.

Although the overall fit and thus value of R-squared is slightly improved with each modification (Tables 4.1, 4.9, and 4.10), none of these versions of a calendering equation adequately predicts the nonlinear effect of increased moisture content that is particular

Table 4.11: In-nip coefficients for Equation 4.10 modified with Equation 4.11

PARAMETER	ESTIMATE	A.S.E.
A_n	-0.3241	0.02681
$a_{0n} \text{ (g/cm}^3\text{)}$	-0.0252	0.00721
$a_{Ln} \text{ (g/cm}^3\text{)}$	0.1774	0.00875
$a_{Sn} \text{ (g/cm}^3\text{)}$	-0.0126	0.00341
$a_{Rn} \text{ (g/cm}^3\text{)}$	-0.0323	0.01183
$a_{Tn} \text{ (g/cm}^3\text{ }^\circ\text{C)}$	0.00333	0.000112
$a_{Mn} \text{ (g/cm}^3\text{)}$	0.00946	0.000384
$a_{Mo} \text{ (g/cm}^3\text{)}$	-0.00092	0.000005
$a_{MT} \text{ (g/cm}^3\text{ }^\circ\text{C)}$	0.000016	0.000004
$a_{ML} \text{ (g/cm}^3\text{)}$	0.0000075	0.00000035
R-squared	0.78	

evident for in-nip strain at high level of strain, Figures 4.52 to 4.59. This inadequacy results in a lower value of the in-nip moisture coefficient than could be expected. On the other hand, the value of the in-nip temperature coefficient is much higher than the permanent temperature coefficient despite the fact that the experimental data shown on Figure 4.61 indicate otherwise. It seems that the inadequate prediction of the in-nip moisture effect is compensated by the value of the in-nip temperature coefficient being too high.

The relatively low values of $R_{\text{-squared}}$ can also be attributed to the use of experimental data collected during the first 7 experiments. As explained in Section 3.3, a change in an experimental procedure was necessary to provide more accurate measurement of the in-nip paper strain at higher temperature. However, experiments 1 to 7 were performed using earlier, slightly less accurate procedure, as seen on Figures 4.9 to

Table 4.11: In-nip calendering coefficients, Experiments 8 to 30

a.) the calendering equation

PARAMETER	ESTIMATE
A_n	-0.3534
$a_{0n} (g/cm^3)$	0.0188
$a_{Ln} (g/cm^3)$	0.1289
$a_{Sn} (g/cm^3)$	-0.0072
$a_{Rn} (g/cm^3)$	-0.0592
$a_{Tn} (g/cm^3 \text{ } ^\circ\text{C})$	0.00141
$a_{Mn} (g/cm^3)$	0.00181
R-squared	0.80

b.) Equation 4.10

PARAMETER	ESTIMATE
A_n	-0.3733
$a_{0n} (g/cm^3)$	0.0202
$a_{Ln} (g/cm^3)$	0.1829
$a_{Sn} (g/cm^3)$	-0.0103
$a_{Rn} (g/cm^3)$	-0.0866
$a_{Tn} (g/cm^3 \text{ } ^\circ\text{C})$	0.00201
$a_{Mn} (g/cm^3)$	0.00481
$a_{M2n} (g/cm^3)$	-0.00019
R-squared	0.81

4.15. Table 4.11 lists the in-nip calendering coefficients computed for both the standard calendering equation and Equation 4.10 using only data from experiments 8 to 30. The exclusion of the less accurate data from experiments 1 to 7 is clearly beneficial, the R-squared values increasing to 0.80 and 0.81.

The coefficients in Table 4.11 differ slightly from those computed for the full set of data, Table 4.1. These differences can be attributed not only to the elimination of the data from less accurate procedure but also to a resulting change in range of line load, 30 to 210 kN/m for Experiments 8 to 30, 15 to 210 kN/m for the full set of data. As explained in Section 4.1.1, the regression analysis attempts to fit a linear part of the calendering equation through data at the lowest loads. Consequently for different ranges of line load, the linear part of the calendering equation is applied to a different set of in-nip strain data, leading to different calendering coefficients.

The in-nip temperature coefficient is still higher than that for permanent strain but now their difference is much smaller. The in-nip load coefficient is smaller than that

Table 4.12: In-nip coefficients for Equation 4.12.

PARAMETER	ESTIMATE	S.E.	C.V.
A_2	<i>1.4525</i>	<i>0.56795</i>	<i>39 %</i>
$a_{o2} (g/cm^3)$	<i>-0.7109</i>	<i>0.27333</i>	<i>38 %</i>
$a_{L2} (g/cm^3)$	<i>0.4297</i>	<i>0.01450</i>	<i>3 %</i>
$a_{S2} (g/cm^3)$	<i>-0.0328</i>	<i>0.00887</i>	<i>27 %</i>
$a_{R2} (g/cm^3)$	<i>-0.0914</i>	<i>0.02882</i>	<i>32 %</i>
$a_{T2} (g/cm^3 \text{ } ^\circ\text{C})$	<i>0.00745</i>	<i>0.000307</i>	<i>4 %</i>
$a_{M2} (g/cm^3)$	<i>0.00940</i>	<i>0.001758</i>	<i>19 %</i>
R-squared	<i>0.75</i>		

reported in Table 4.1 for a wider range of line load, 15 to 210 kN/m, but is higher than the Table 4.5 value for a narrower range of line load, 40 to 210 kN/m.

Another alternative to the standard calendering equation was proposed by Browne et al. [7]. As 90% of their in-nip data fell above the upper limit of the calendering equation, they suggested that in-nip paper deformation be described in terms of the density ratio ρ / ρ_i .

$$1 / (1 - \epsilon_n) = \rho / \rho_i = A_2 + \mu_2 / \rho_i$$

where:

[Eq. 4.12]

$$\mu_2 = a_{o2} + a_{L2} \log_{10}L + a_{S2} \log_{10}S + a_{R2} \log_{10}R + a_{M2} M + a_{e2} \Theta$$

In the present study as well, all in-nip strain, except for one data point, fell above the upper limit of the calendering equation, Table 4.6 in Section 4.1.1. For the industrially relevant range of line loads, 15 to 210 kN/m, virtually all in-nip data can then be fitted with the nonlinear part of the calendering equation only, and thus with Equation 4.12

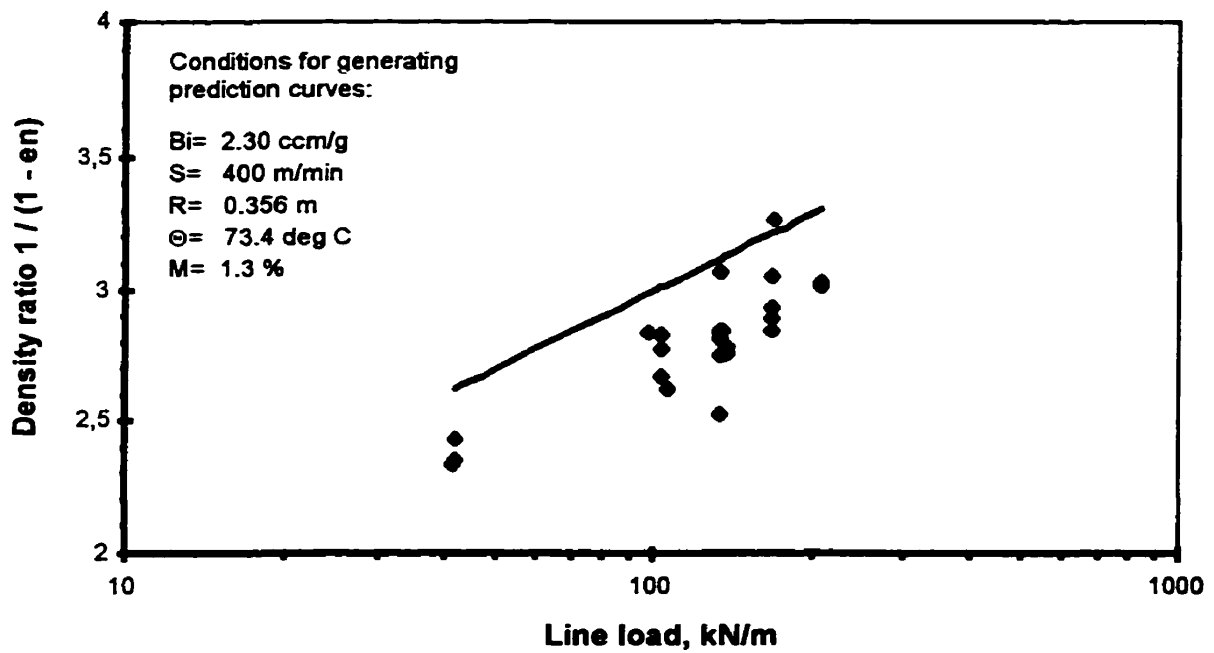
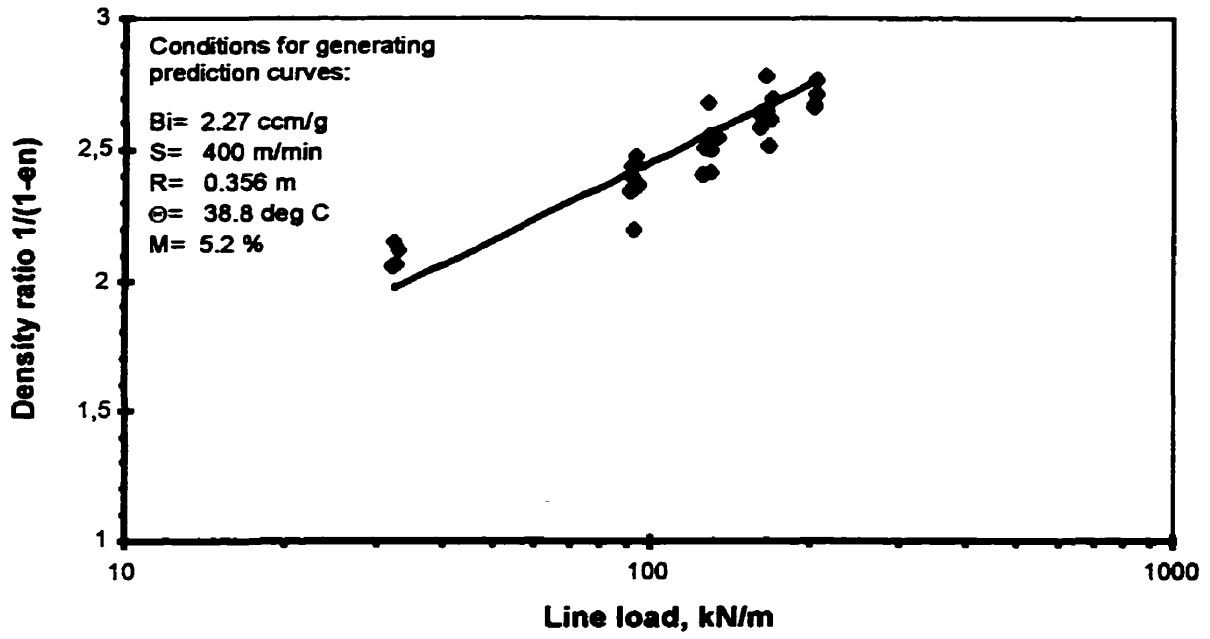


Figure 4.69: Effect of line load on density ratio, $R= 0.356$ m, all speeds

- a.) $\Theta= 38.8$ °C, $M= 5.2\%$
- b.) $\Theta= 73.4$ °C, $M= 1.3\%$

Lines from Equation 4.12

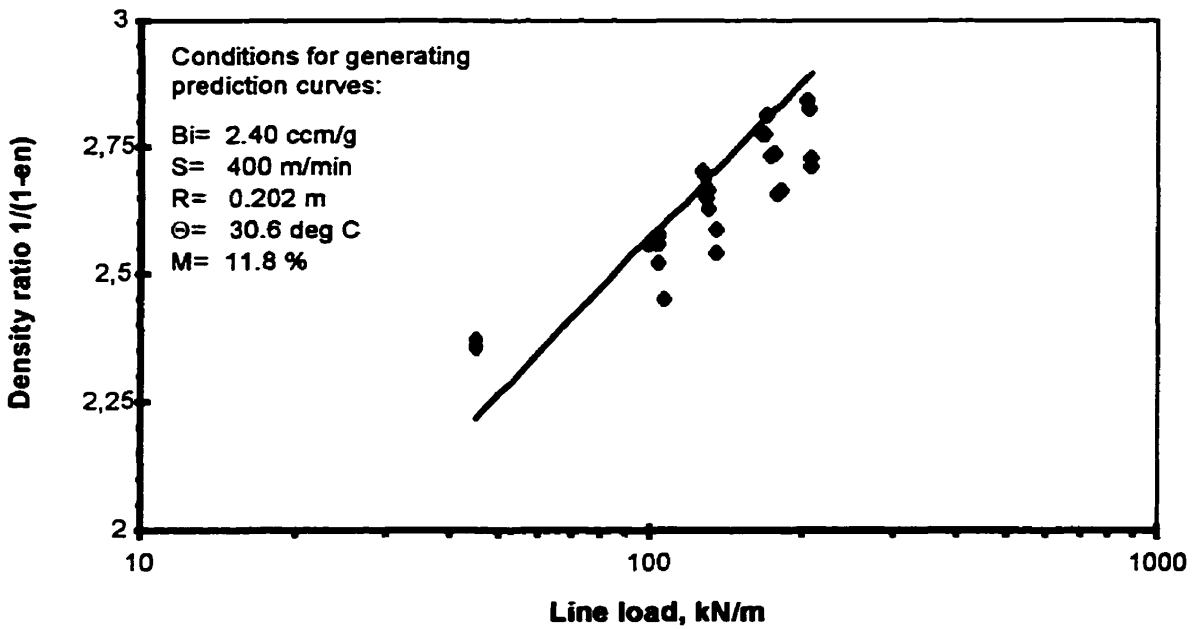
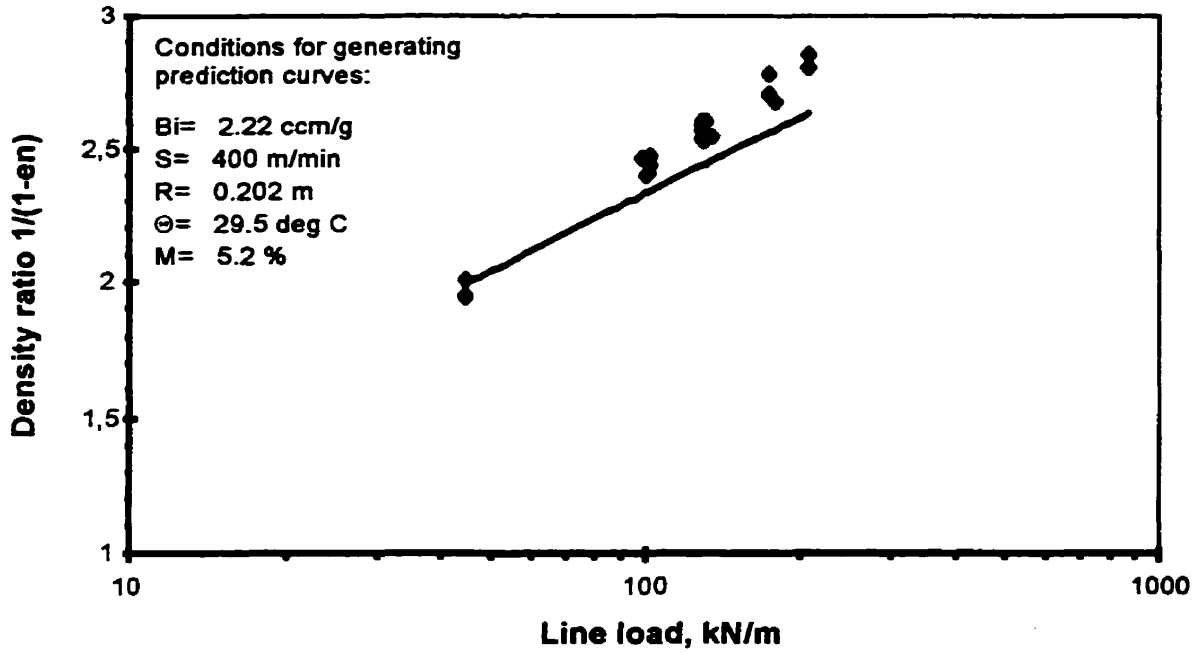


Figure 4.70: Effect of line load on density ratio, $R = 0.202 \text{ m}$, all speeds

- a.) $\Theta = 29.5 \text{ }^\circ\text{C}$, $M = 5.2\%$
- b.) $\Theta = 30.6 \text{ }^\circ\text{C}$, $M = 11.8\%$

Lines from Equation 4.12

which is its algebraic equivalent. This was done, with results shown in Table 4.12 and Figures 4.69 to 4.70.

The overall fit is similar to that from the standard calendering equation, with its lower and upper limits, Table 4.1. However, the importance of this approach lies mainly in the fact that Equation 4.12 is less likely to be sensitive to the range of in-nip strain investigated, as was shown in Section 4.1.1. Another advantage of this method is its linear form, which eliminates the need for complex and time consuming non-linear regression analysis.

4.5 Master creep equation

An equation of a quite different form, the master creep equation, can also be used to relate permanent and in-nip paper strain to the same variables as the calendering equation. The original form of the master creep equation, as proposed by Peel and co-workers [11, 12] to fit data obtained in the platen press, was modified by Kerekes [49] and Haglund and Robertson [30] in order to fit data from a more realistic calendering process. The final version of the master creep equation, suitable for the present study, was proposed by Browne et al. [6, 7]:

$$\epsilon_{n,p} = 0.5 (1 - \rho_i / \rho_{n,p,max}) [1 + \tanh(\mu_{n,p})] \quad [\text{Eq. 4.13}]$$

The permanent and in-nip calendering intensities $\mu_{n,p}$ are both defined as for the calendering equation:

$$\mu_{n,p} = a_{0n,p} + a_{Ln,p} \log_{10}L + a_{Sn,p} \log_{10}S + a_{Rn,p} \log_{10}R + a_{Mn,p}M + a_{\Theta n,p}\Theta$$

where: $\rho_{n,p,max}$ is the maximum density obtainable either in or after the nip, q/cm^3 ; ρ_i is initial paper density, g/cm^3 , the inverse of initial paper bulk B_i ; L is line load, kN/m ; S is

paper speed, m/min; R is a relative roll radius, m; Θ is paper temperature, °C; M is paper moisture content, %.

The SYSTAT statistical software was used to fit the modified version of the master creep equation, Equation 4.13, to the set of 760 strain data, exactly as with the calendering equation. As SYSTAT does not have a built-in hyperbolic tangent function the exponential definition of this function was used.

The permanent and in-nip calendering coefficients, along with the asymptotic standard error (A.S.E.) and 95% confidence limits, are presented in Tables 4.13 and 4.15. Estimates and residual errors are shown in Figures 4.71 to 4.74 for both in-nip and permanent strain. The experimental data and regression curves with the master creep equation are plotted in Figures 4.75 to 4.79 with, for comparison, prediction curves from the calendering equation.

Tables 4.14 and 4.16 list the permanent and in-nip coefficients reported previously by Colley and Peel [12], Kerekes [49] and Browne et al. [6, 7]. Since Colley and Peel measured strain data in a platen press, the original version of the master creep equation, Equation 4.14, used the maximum applied pressure P [MPa] and dwell time t [sec] as the calendering variables instead of nip load L and paper speed S .

$$\epsilon_{n,p} = A_{n,p} [1 + \tanh(\mu_{n,p})] \quad [\text{Eq. 4.14}]$$

the permanent and in-nip calendering intensities $\mu_{n,p}$ are

$$\mu_{n,p} = a_{0n,p} + a_{Pn,p} \log_{10} P + a_{tn,p} \log_{10} t + a_{Mn,p} M + a_{\Theta n,p} \Theta$$

The following relationships between the coefficients of those variables, as proposed by Kerekes [49], are used:

$$\begin{aligned} a_L &= a_P \\ a_S &= -a_t \end{aligned} \quad [\text{Eq. 4.15}]$$

Table 4.13: Permanent coefficients for the master creep equation, present study.

PARAMETER	ESTIMATE	A.S.E.	LOWER 95%	UPPER 95%
ρ_{p_max} (g/cm ³)	0.7983	0.02461	0.7499	0.8466
a_{Op}	-2.5126	0.09150	-2.6922	-2.3330
a_{Lp}	1.0510	0.05364	0.9456	1.1563
a_{Sp}	-0.2289	0.01736	-0.2629	-0.1948
a_{Rp}	-0.4397	0.04304	-0.5242	-0.3551
a_{Tp}	0.01180	0.000643	0.01054	0.01206
a_{Mp}	0.07597	0.004382	0.06736	0.08457
R-squared	0.90			

Table 4.14: Permanent coefficients for the master creep equation

a) Colley and Peel (1) and Kerekes (2)

PARAMETER	1	2
A_p	0.33	0.39 <i>(fixed value)</i>
a_{Op}	-6.71	—
a_{Lp}	0.900	0.890
a_{Sp}	-0.130	-0.165
a_{Rp} (predicted)	-0.39	-0.363
a_{Tp}	0.0069	—
a_{Mp}	0.022	—

b) Browne et al.

PARAMETER	ESTIMATE
ρ_{p_max} (g/cm ³)	0.5930
a_{Op}	-3.1502
a_{Lp}	1.8863
a_{Sp}	-0.2729
a_{Rp}	-0.8294
R-squared	0.88

Table 4.15: In-nip coefficients for the master creep equation, present study.

PARAMETER	ESTIMATE	A.S.E.	LOWER 95%	UPPER 95%
ρ_{n_max} (g/cm ³)	<i>1.4071</i>	<i>0.02821</i>	<i>1.3518</i>	<i>1.4625</i>
a_{0n}	<i>-1.8394</i>	<i>0.11629</i>	<i>-2.0677</i>	<i>-1.6111</i>
a_{Ln}	<i>0.8394</i>	<i>0.04154</i>	<i>0.8150</i>	<i>0.9780</i>
a_{Sn}	<i>-0.0604</i>	<i>0.02207</i>	<i>-0.1037</i>	<i>-0.0171</i>
a_{Rn}	<i>-0.3106</i>	<i>0.07065</i>	<i>-0.4493</i>	<i>-0.1719</i>
a_{Tn}	<i>0.02341</i>	<i>0.001940</i>	<i>0.01960</i>	<i>0.02722</i>
a_{Mn}	<i>0.02305</i>	<i>0.002256</i>	<i>0.01862</i>	<i>0.02748</i>
R-squared	<i>0.77</i>			

Table 4.16: In-nip coefficients for the master creep equation

a) Colley and Peel

PARAMETER	ESTIMATE
A_n	<i>0.33</i>
a_{0n}	<i>-7.32</i>
a_{Ln}	<i>1.090</i>
a_{Sn}	<i>-0.063</i>
a_{Rn} (predicted)	<i>-0.514</i>
a_{Tn}	<i>0.00305</i>
a_{Mn}	<i>0.0185</i>

b) Browne et al.

PARAMETER	ESTIMATE
ρ_{n_max} (g/cm ³)	<i>1.2807</i>
a_{0n}	<i>-1.4197</i>
a_{Ln}	<i>1.0076</i>
a_{Sn}	<i>-0.0976</i>
a_{Rn}	<i>-0.4340</i>
R-squared	<i>0.87</i>

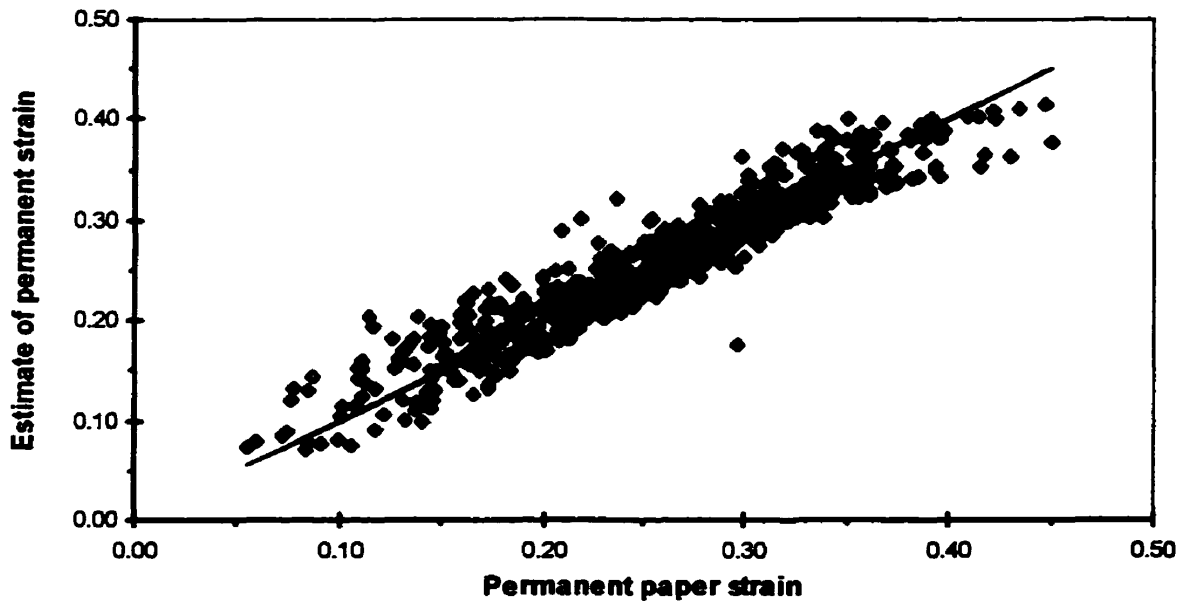


Figure 4.71: SYSTAT estimates of the permanent paper strain: Master creep equation

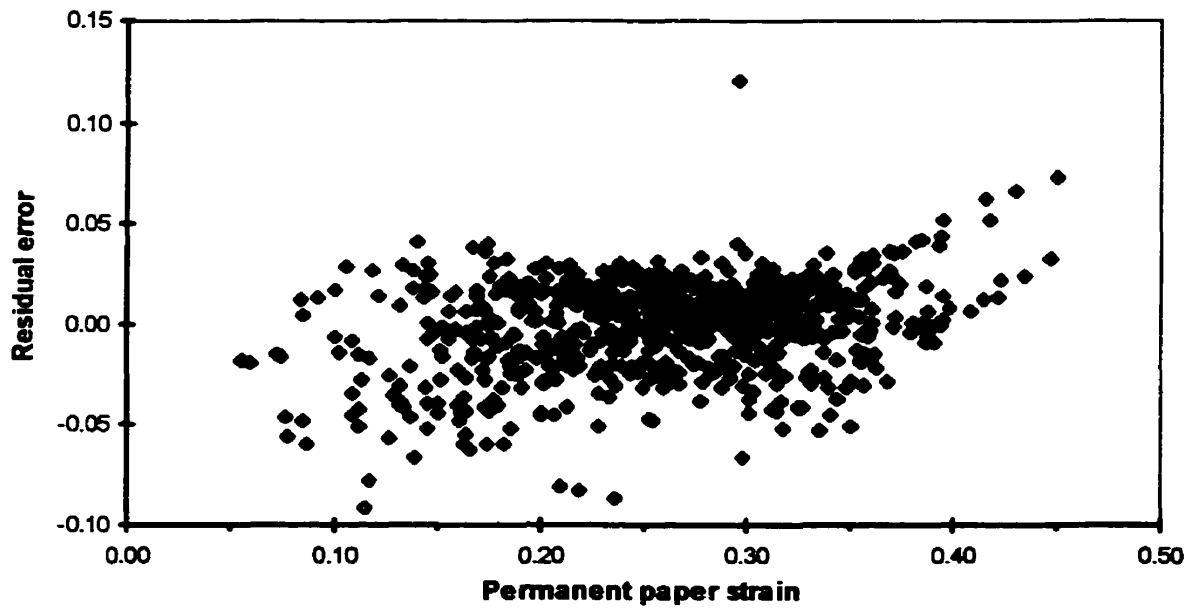


Figure 4.72: Residual error vs. permanent strain: Master creep equation

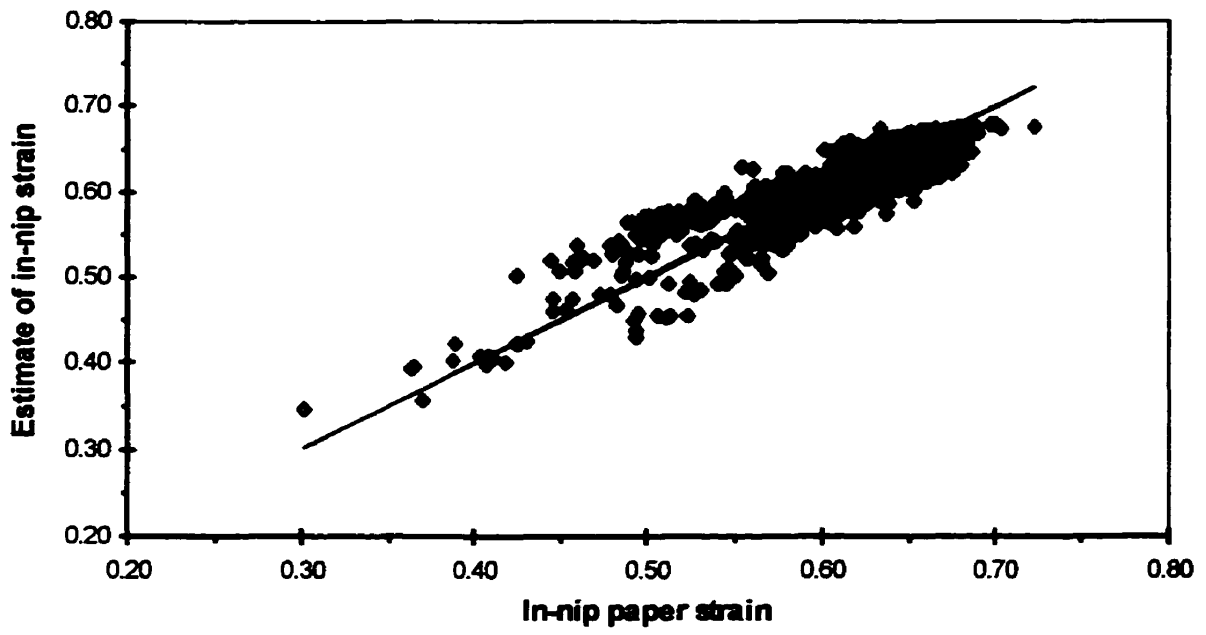


Figure 4.73: SYSTAT estimates of the in-nip paper strain: Master creep equation

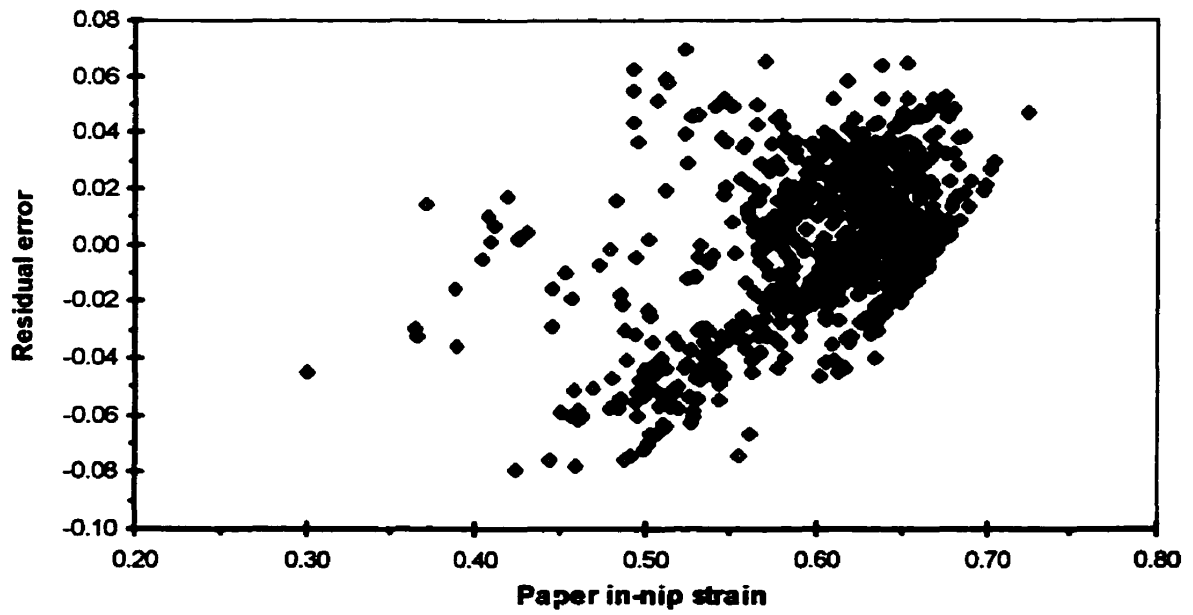


Figure 4.74: Residual error vs. in-nip strain: Master creep equation

The radius effect was measured experimentally only by Browne et al. [6, 7]; in the case of the data of Kerekes and Colley and Peel the radius effect was predicted using the suggestion of Kerekes that the radius coefficient be calculated as an average of the load and speed coefficients:

$$a_R = - (a_L + a_S) / 2 = (a_t - a_p) / 2 \quad [\text{Eq. 4.16}]$$

The limiting density obtainable after the nip is higher in the present study, $\rho_{p_max} = 0.80 \text{ g/cm}^3$, than that reported by Browne et al., $\rho_{p_max} = 0.59 \text{ g/cm}^3$. This difference is attributed to the higher paper temperatures and moisture contents used in the present study. As paper temperature or moisture content increases, the wood fibers become more pliable and plastically deformable. Application of the extreme calendering conditions, high load plus high temperature or moisture content, resulted after just one heavily loaded nip in the final bulk as low as 1.39 to 1.43 cm^3/g , or paper density of 0.70 to 0.72 g/cm^3 . When nips more heavily loaded yet are used, final paper density can approach the limiting value of 0.80 g/cm^3 .

The limiting in-nip density is 1.41 g/cm^3 , which is higher than that reported by Browne et al. This high density is attributed mostly to the use of high paper temperatures. In the previous Section 4.3 it was shown that the strongest moisture effect on the in-nip strain is achieved around 8% moisture, so the use of higher levels is counterproductive. The in-nip data obtained here showed that a combination of high nip load with high paper temperature produces in-nip paper compression approaching 70%, even at the low level of moisture content, i.e. in-nip paper thickness only 30% of its initial value. At this point the actual in-nip paper density was 1.40 g/cm^3 , very close to the reported limiting density obtainable in the nip. This implies that in-nip strain of 0.72 to 0.75 is the highest possible compression the paper can experience in the nip after heavy calendering, a reasonable conclusion as such a paper density would be only slightly lower than the accepted value for the density of the component fibers, 1.50 g/cm^3 .

Values of the permanent and in-nip limiting densities for data reported by Colley and Peel were computed using a relationship between the coefficient $A_{p,n}$, Equation 4.14, and the limiting density obtainable either in the nip or after, as proposed by Haglund and Robertson [30]:

$$A_{p,n} = 0.5 (1 - \rho_i / \rho_{p,n,max}) \quad [\text{Eq. 4.17}]$$

Using results given in Tables 4.12a and 4.13a and a typical initial density of 0.45 g/cm³, which corresponds to the initial bulk of 2.20 cm³/g, Equation 4.17 estimates the limiting density to be 1.32 g/cm³, for both the permanent and in-nip data. This implies that paper in the nip could be deformed so strongly that it would not recover at all. The above value of the limiting density is slightly smaller the corresponding value reported in the present study but it is higher than the in-nip limiting density given by Browne et al. However there is a large difference in values of limiting density for the permanent data. The present results and those of Browne et al. show that the limiting density for permanent compression is substantially lower than the corresponding limiting density given by Colley and Peel, and thus that it is lower than the limiting density for in-nip compression.

The in-nip load, speed and radius coefficients reported in the present study, Table 4.15, are statistically not different from the previous data, given in Table 4.16. As Kerekes and Browne et al. did not measure the effect of temperature and moisture content on paper behaviour in the nip, only Colley and Peel data can be used for comparison with the effect reported here of paper temperature and moisture content.

The in-nip moisture effect is slightly higher than the corresponding moisture coefficient of Colley and Peel, but are within the 95% confidence limits. On the other hand the in-nip temperature coefficient found here is one order of magnitude higher in the present work than that reported previously. This difference can be attributed to the different combinations of paper temperature and moisture content used in the two studies.

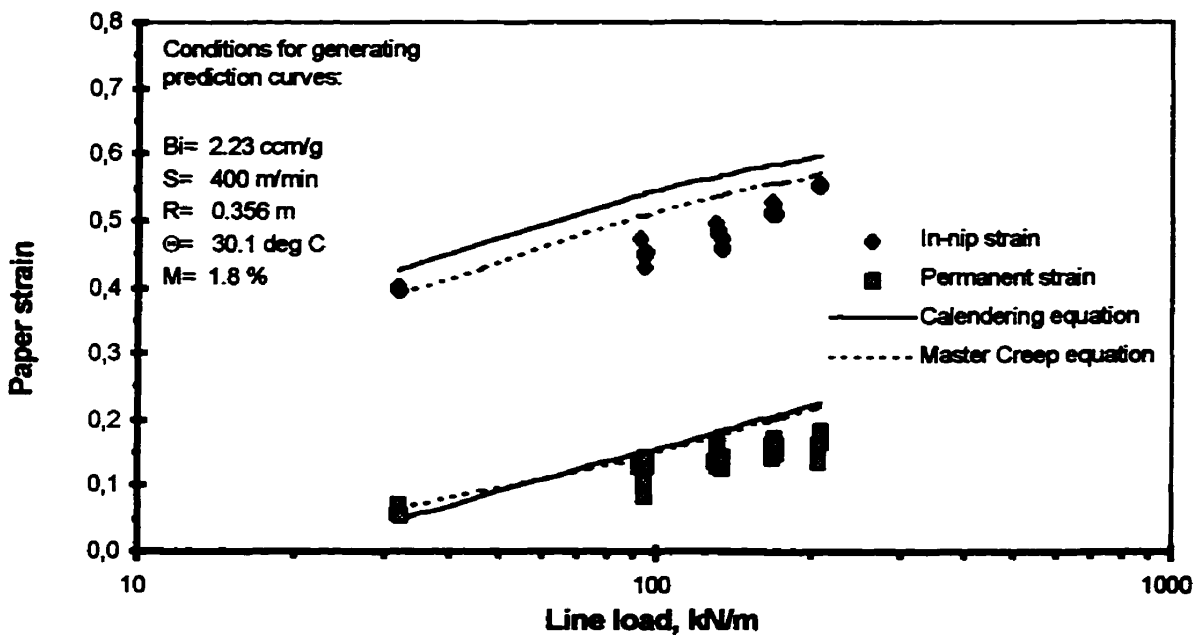
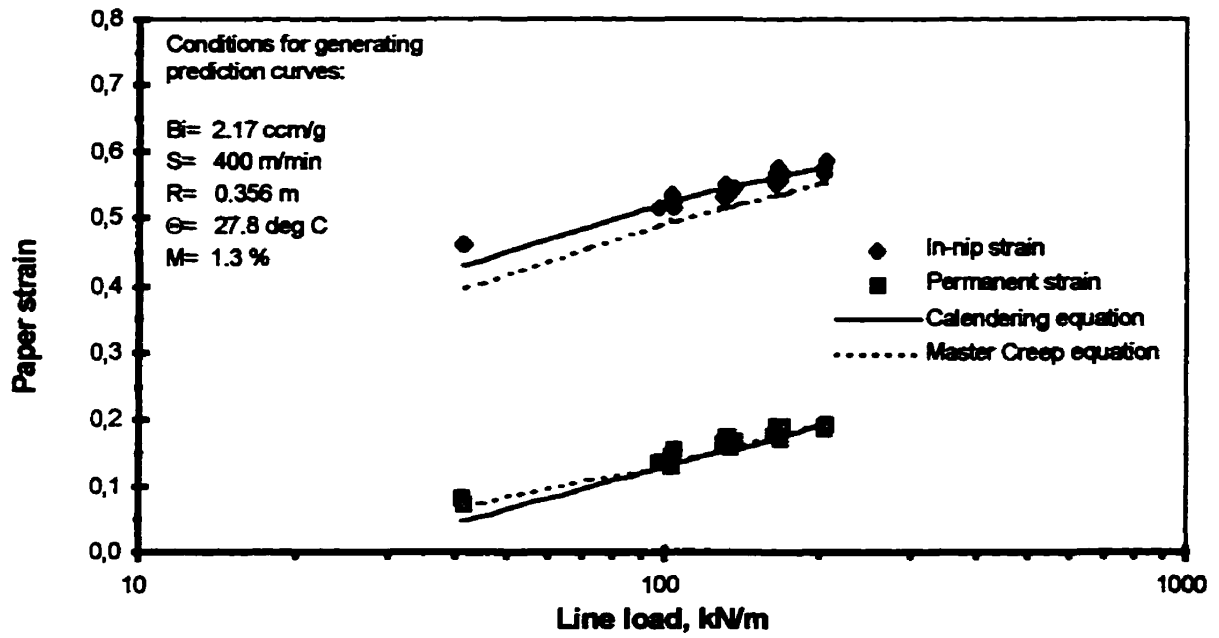


Figure 4.75: Effect of line load on strain, all speeds.
 Lines from the master creep and calendering equations

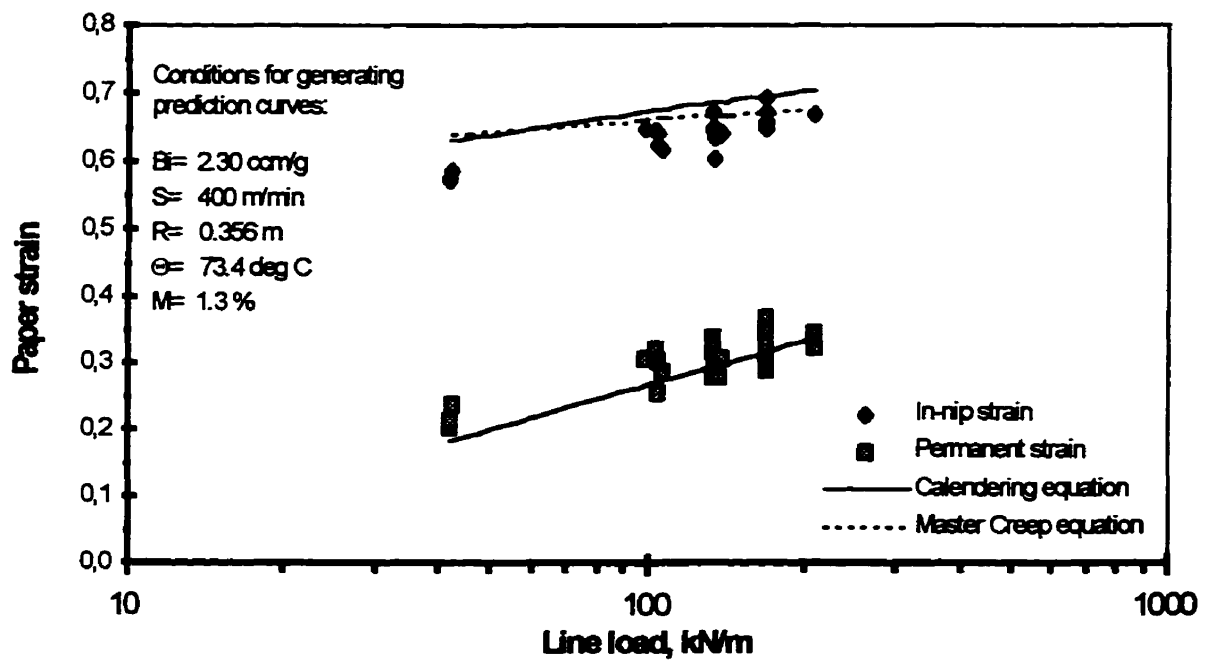
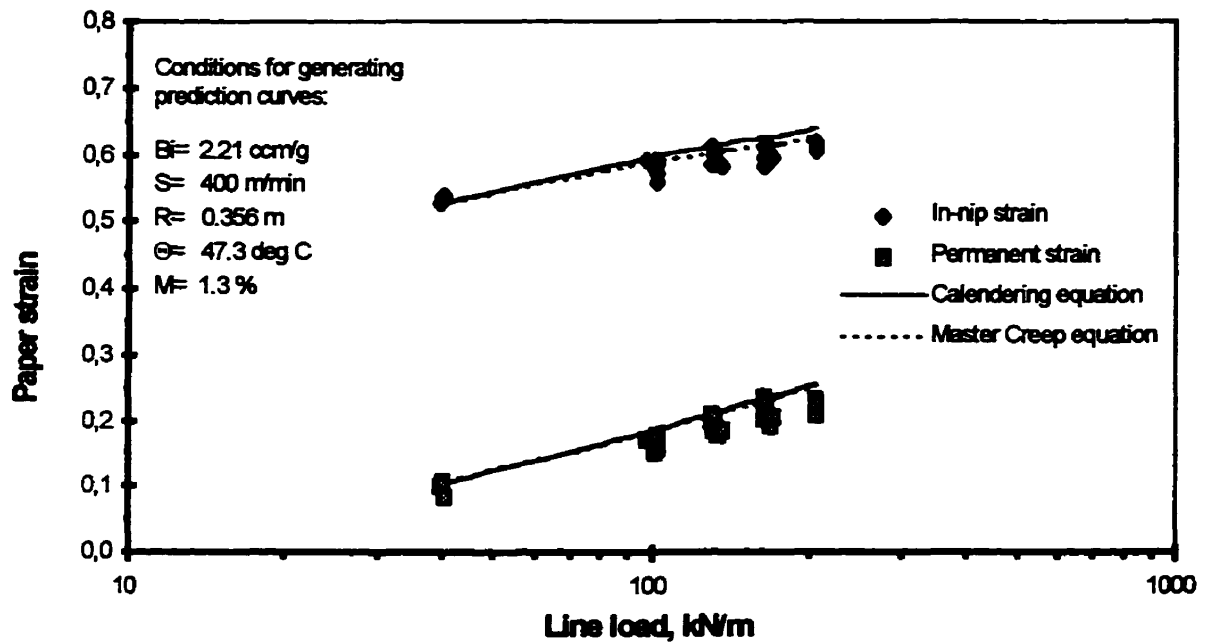


Figure 4.76: Effect of line load on strain, all speeds.
 Lines from the master creep and calendering equations

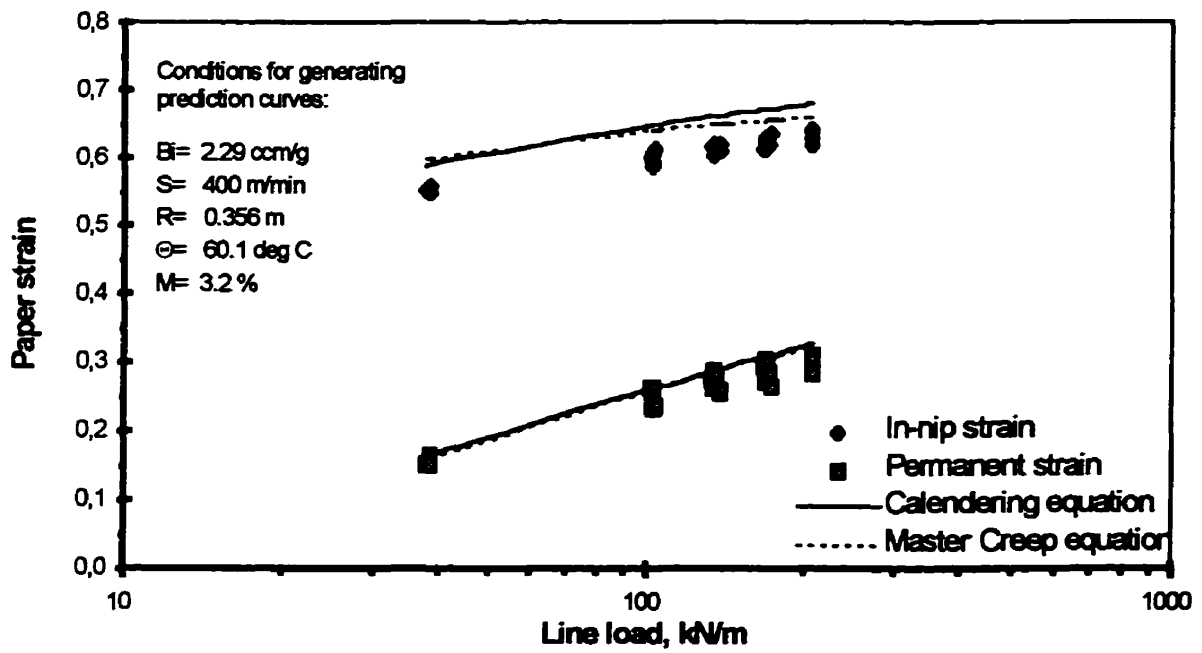
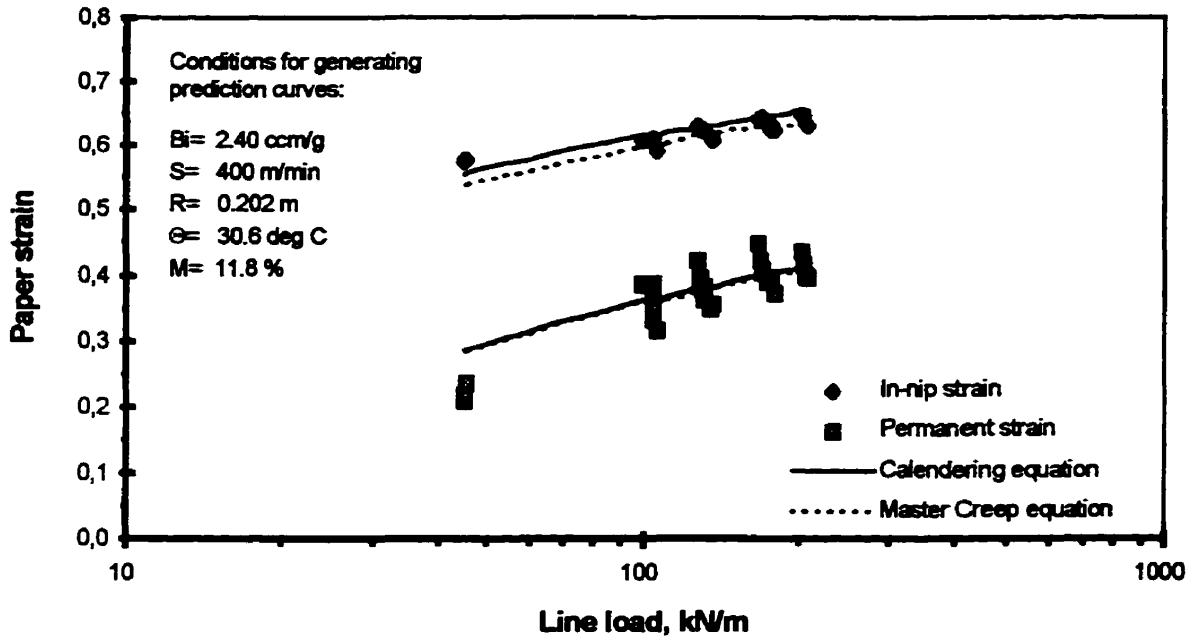


Figure 4.77: Effect of line load on strain, all speeds.

Lines from the master creep and calendering equations

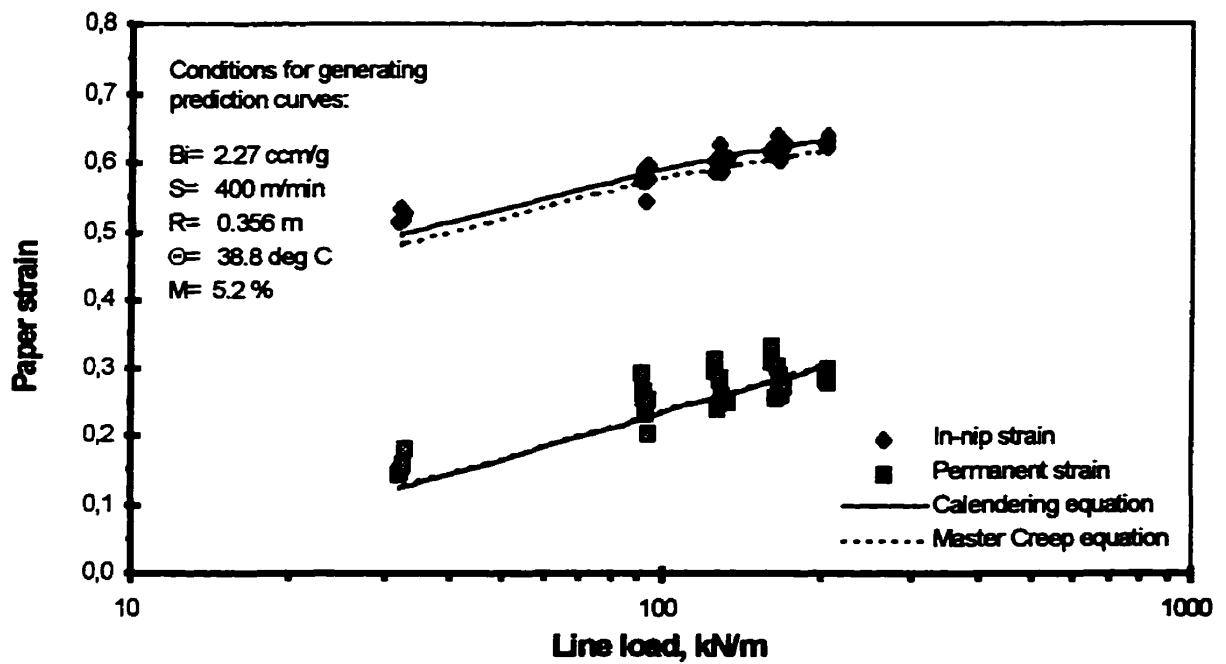
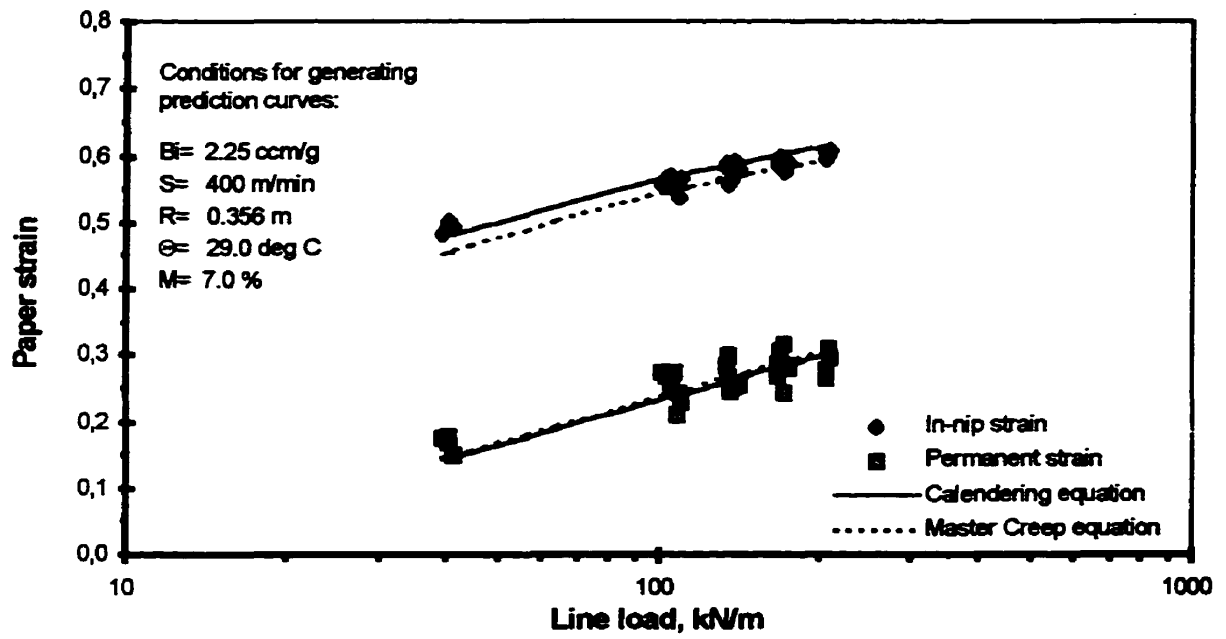


Figure 4.78: Effect of line load on strain, all speeds.

Lines from the master creep and calendering equations

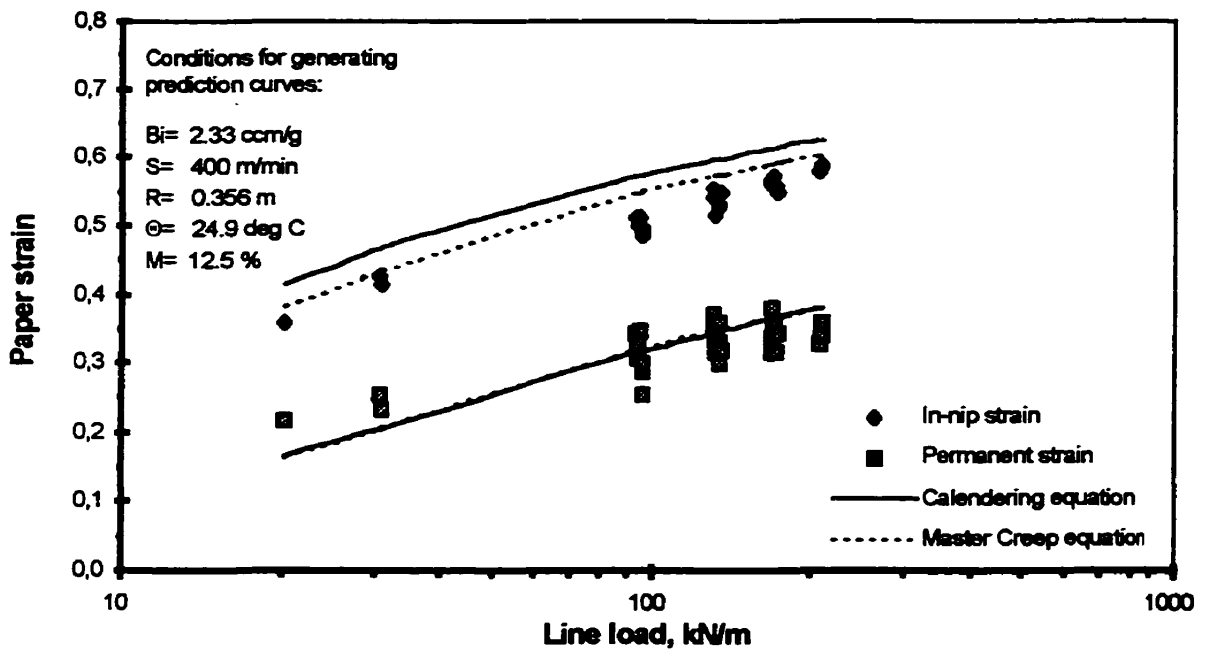
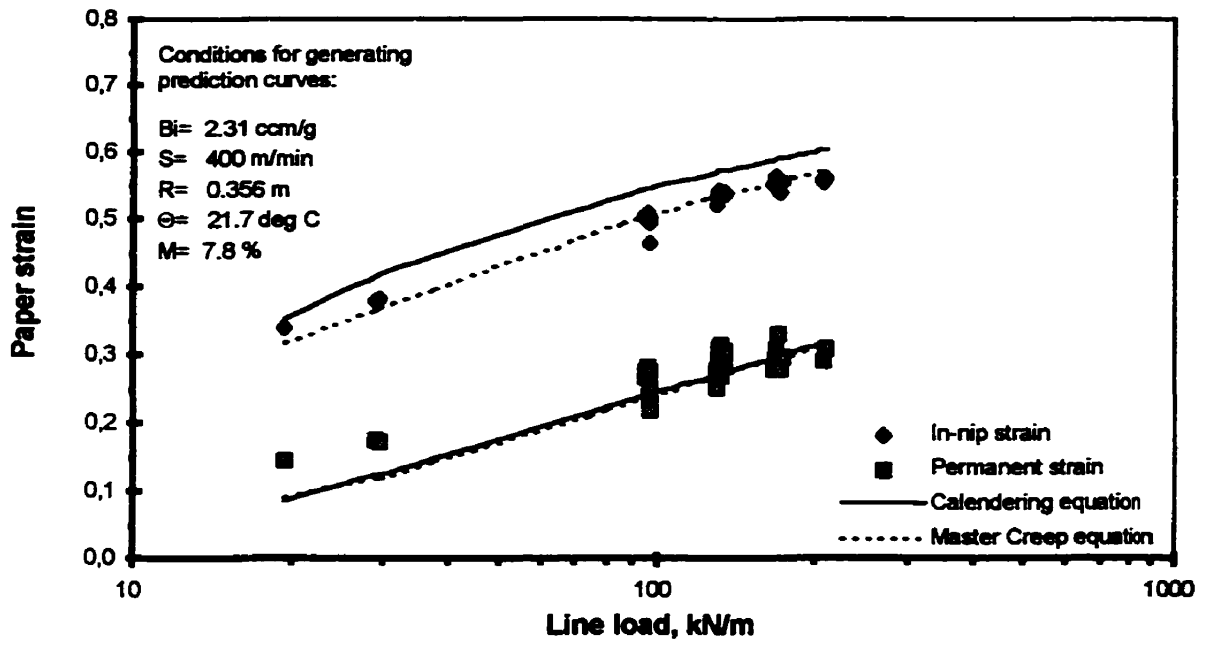


Figure 4.79: Effect of line load on strain, all speeds.

Lines from the master creep and calendering equations

Colley and Peel [12] investigated extensively the effect of temperature on the in-nip paper compression for high levels of moisture content ranging from 9 to 13%, where the effect of increased temperature was reported to be very small above 50 °C for groundwood. But their data also showed that, for the temperature range 20 to 80 °C, the temperature effect is approximately 3 to 4 times bigger for a moisture content of 2.3% than for 9.3 and 12.6% moisture.

The temperature effect was investigated here over nearly the same range of paper temperature, 20 to 74 °C, but only for a moisture content of 2%. The temperature effect for higher levels of moisture content was investigated for a range of temperature: 20 to 60 °C for moisture content of 3 to 4%, 20 to 50 °C for moisture content of 6 to 7%. On the other hand, this difference can be also attributed to the compensation effect for the inadequate prediction of the nonlinear moisture effect, as in the case of the calendering equation.

For permanent strain, the load and radius coefficients are substantially lower than those given by Browne et al. but are not statistically different from the load and radius coefficients of Colley and Peels and Kerekes, Table 4.14a. The permanent speed coefficient is the same as found by Browne et al. but is higher than those reported by Kerekes and Colley and Peel. The temperature and moisture content coefficients obtained in the present study are significantly different from those reported in Table 4.14a.

This difference can be attributed to the different value of the limiting density or A_p between those studies. Colley and Peel assumed that the limiting densities are the same for both permanent and in-nip strain, and thus their value of the coefficient A_p corresponding to the value of the permanent limiting density of 1.32 g/cm^3 is much higher than that obtained here. To correct for this difference, the present permanent data were fitted with the master creep equation again, but this time with the limiting density fixed at 1.32 g/cm^3 . For those results, given in Table 4.17, all coefficients but those for temperature and moisture content are statistically not different from the corresponding coefficients given in Table 4.13, but the new coefficients are generally slightly lower. The moisture and temperature coefficients are changed but in this case are comparable with the coefficients

Table 4.17: Permanent coefficients for the master creep equation, $\rho_{p_max} = 1.32 \text{ g/cm}^3$.

PARAMETER	ESTIMATE	A.S.E.
$\rho_{p_max} \text{ (g/cm}^3\text{)}$	<i>1.32</i>	<i>(0.0000)</i>
a_{0p}	<i>-2.168</i>	<i>0.10150</i>
a_{Lp}	<i>0.8810</i>	<i>0.06621</i>
a_{Sp}	<i>-0.1190</i>	<i>0.01376</i>
a_{Rp}	<i>-0.3781</i>	<i>0.04134</i>
a_{Tp}	<i>0.0064</i>	<i>0.000352</i>
a_{Mp}	<i>0.0374</i>	<i>0.003271</i>
R-squared	<i>0.88</i>	

obtained by Colley and Peel. Apparently the lower value of the limiting density used here was balanced mostly by the higher values of those two coefficients.

Overall the fit of the master creep equation is similar to the calendering equation, as shown on Figure 4.75 to 4.79, especially for permanent strain. The only visible distinction is at strains lower than 0.10 where the master creep equation predicts the permanent strain better than the calendering equation, Figure 4.75. For the in-nip case, the master creep and calendering equations fit the data somehow differently but with about the same precision. Since for the industrially relevant range of calendering conditions both the calendering and master creep equations require non-linear regression to obtain the coefficients, the computational effort is the same for both of them.

Thus the continuous form of the master creep equation is an attractive alternative to the calendering equation with its lower and upper limits, especially for the in-nip case where the pieced-together form of the calendering equation was shown to depend on the range of nip intensities investigated.

4.6 Relationship between permanent and in-nip strain

Browne et al. [6, 7] showed that a convenient relationship exists between permanent and in-nip strain, thus verifying the suggestion made by Ionides et al. [40] from theoretical considerations. Using a theoretical analysis of fiber distribution inside the sheet Ionides et al. argued that a simple linear function can be used to relate permanent strain to an unknown in-nip strain:

$$\epsilon_n = a + c_e \epsilon_p \quad [\text{Eq. 4.18}]$$

Browne et al. showed that Equation 4.18 fits the experimental data relatively well when permanent strains higher than 0.20 are used. They showed that a nonlinear function is required with strain data covering the range of strains 0 to 0.45. Accordingly, they proposed a logarithmic relationship:

$$\epsilon_n = a + c_e \log_{10} \epsilon_p \quad [\text{Eq. 4.19}]$$

Since in the present study the permanent strains cover the range 0.05 to 0.45, a logarithmic relationship was used to fit the full set of strain data. The coefficients for Equation 4.19 and their standard errors (S.E.) are listed in Table 4.18a. The present results are comparable with the coefficients given in Table 4.18b but R -squared is much lower, which suggests that the simple form of relationship proposed by Browne et al. provides a poor fit of the present data.

This problem can be attributed to the different experimental conditions used. Browne et al. measured the permanent and in-nip strains at ambient conditions, whereas a wide range of paper temperature and moisture content was investigated in the present study. As paper temperature and/or moisture content increases, the pulp fibers become more plastically deformable which allows obtaining the final deformation at a lower nip load. Since paper has been shown to have a visco-elastic behaviour, the application of

Table 4.18: Coefficients for Equation 4.19.

a.) present study

PARAMETER	ESTIMATE	STD ERROR
a	0.7587	0.00787
c _ε	0.3029	0.01243
R ²	0.45	

b.) Browne et al. data.

PARAMETER	ESTIMATE	STD ERROR
a	0.778	0.049
c _ε	0.354	0.007
R ²	0.74	

different combinations of nip load, temperature and moisture content makes it possible to obtain the same permanent strain through compressing the paper in the nip to different levels. On the other hand, Section 4.4 has shown that for paper at 23 to 30 °C increasing the moisture content from 2 to 12% with other calendering variables fixed causes the in-nip strain to pass through a maximum at approximately 8% of moisture content. Therefore by changing its moisture content, paper can be compressed to the same or even a lower in-nip strain, while its permanent strain would be higher.

This analysis suggests that the relationship between in-nip and permanent strain is a function of the calendering variables. Since nip load, temperature and moisture content are three calendering variables which affect both permanent and in-nip paper deformation the most, a modified version of Equation 4.19 is proposed:

$$\epsilon_n = a + c_\epsilon \log_{10} \epsilon_p \quad [\text{Eq. 4.20a}]$$

Table 4.19 Coefficients for Equation 4.20.

PARAMETER	ESTIMATE	STD ERROR
a	0.7602	0.01432
c ₀	0.4956	0.02326
c _L	-0.0636	0.01474
c _Θ (1/°C)	-0.0028	0.00025
c _M	0.0089	0.00142
R ²	0.76	

where the slope coefficient c_z is a function of line load L , paper temperature Θ , and paper moisture content:

$$c_z = c_0 + c_L \log_{10}L + c_M M + c_\Theta \Theta \quad [\text{Eq. 4.20b}]$$

The coefficients defined in Equation 4.20 are listed in Table 4.19 and the prediction curves are plotted in Figure 4.80. All coefficients are statistically significant and the new R -squared, 0.76, is much better than the 0.45 value in Table 4.18a. The value of the intercept coefficient, α , is the same as for Equation 4.19, but the other coefficients cannot be compared directly with the previous results. The overall fit of Equation 4.20 and the R -squared = 0.76 value are comparable with the in-nip versions of the calendering and master creep equations. Taking into account the form of this equation, continuous and linear with respect to the calendering variables, it is a very attractive alternative for estimating in-nip strain from permanent strain, and thus for implementing in a model for a cross-direction control of calendering.

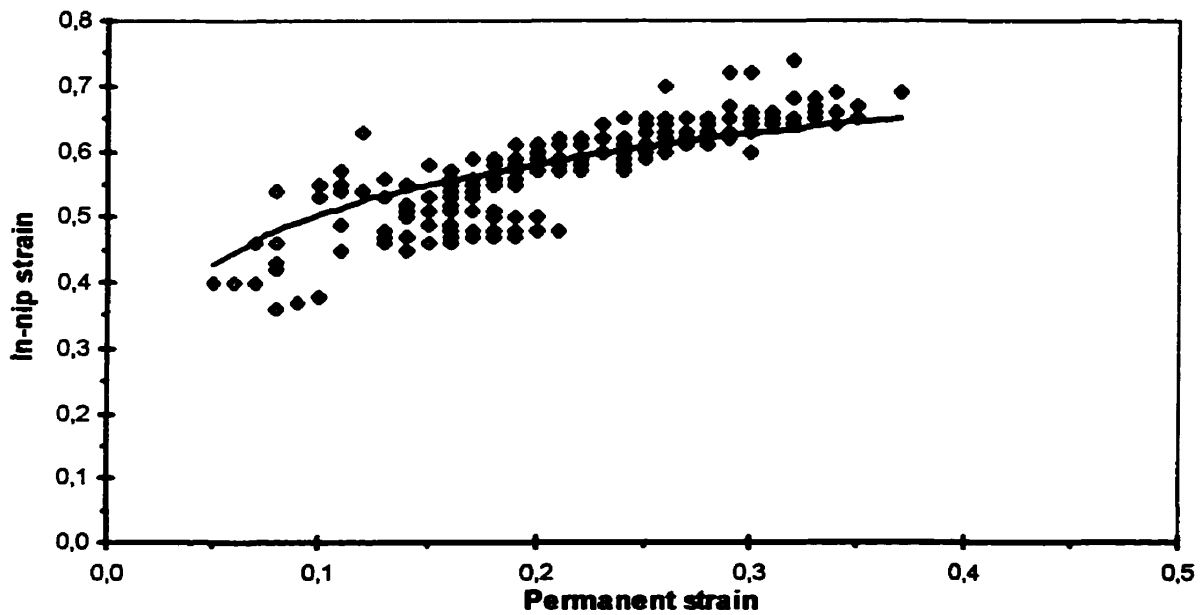
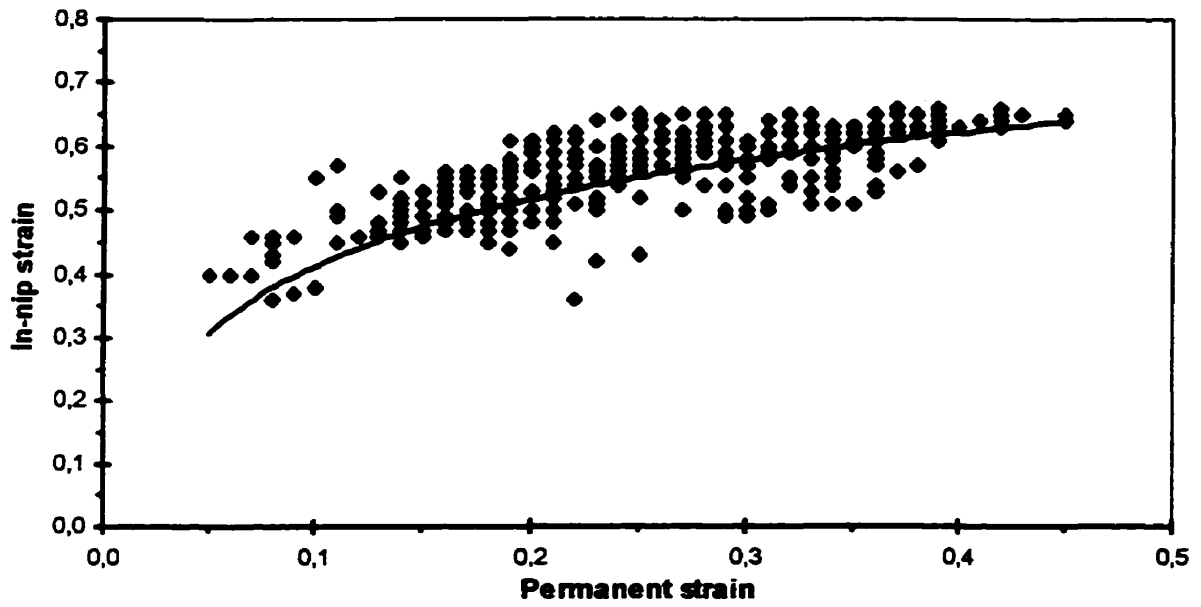


Figure 4.80: Relationship between permanent and in-nip strain

a.) $\Theta = 25$ to 33 °C, all loads and moisture contents

b.) $M = 1.3$ to 2.3% , all loads and temperatures

Lines from Equation 4.20

4.7 Conclusions

In-nip and permanent paper strain was determined in a controlled environment calender for 30 sets of combinations of calendering load, speed and roll radius, and for paper temperature and moisture content covering the range 22 to 75 °C and 1 to 14 % moisture.

The calendering and master creep equations are shown to provide almost identical descriptions of permanent paper deformation after a calender nip for industrially relevant line loads. However for a very low loads, the master creep equation provides better predictions.

The in-nip version of the calendering equation, proposed by Browne et al., is now verified to give a satisfactory description of paper deformation in the calender nip over the wide range of paper temperature and moisture content. This equation can be used to relate local in-nip strain to local values of the calendering variables.

The calendering equation is found to be sensitive to the range of in-nip strain obtained experimentally. Because the regression analysis attempts to fit a linear part of the calendering equation through the data with the lowest values, and thus for different sets of in-nip data, different in-nip coefficients are found. Caution must be used when comparing in-nip calendering coefficients obtained at different experimental conditions.

Because essentially all the in-nip strain data falls above the upper limit of the calendering equation, only the nonlinear part of the calendering equation can be used to fit this in-nip data obtained for industrially relevant calendering variables. This relationship is less likely to be sensitive to the range of in-nip strain investigated. To eliminate the consuming non-linear regression analysis, in-nip paper deformation can be described in terms of the density ratio ρ / ρ_t .

The in-nip master creep equation, another alternative for the standard calendering equation, provides a similar description of paper deformation in a calender nip and, at the same time, its continuous form makes it less likely to be sensitive to the range of in-nip strain investigated.

Initial paper thickness is found to be a linear function of both paper temperature and moisture content.

Increased moisture content is seen to have a strong nonlinear effect on in-nip paper strain. Permanent strain is also affected but, for industrially relevant moisture contents, a linear relationship can be used. Increased temperature has a similar effect on paper deformation both after and in a calender nip.

The relationship between permanent and in-nip strain is a function of paper temperature and moisture content as well as line load. This relationship is advantageous for estimating local in-nip strain for a given local permanent strain, but another calendering equation must be used to estimate the local value of line load.

5 Thermal deformation of a calender roll

5.1 Transient and steady state local heat transfer and roll deformation

5.1.1 Introduction

An essential element of any CD calender control system is the ability to predict the roll radius deformation, and thus the calender nip profile, due to a specific heating/cooling CD profile from a control actuator. Subsequent to the measurement by Pelletier et al. [67, 68] of local heat transfer for a calender roll with heating or cooling impinging air jets as the control actuator, Journeaux [42] obtained the transient and steady state aspects the CD profile of local radius of a calender roll. The latter study used finite volume and finite element numerical methods to calculate, for a variety of roll designs, the CD local roll deformation profile due to a CD local heat flux profile. Although this determination of the dynamic local roll deformation was obtained with the heat flux from air showers, their analysis applies with any type of control device for which CD local heat transfer rates to the roll can be specified, provided the heat is applied sufficiently close to the roll surface to be a boundary condition not a volumetric term. Induction heaters (Calcoils), now the industry standard, generate the heat in the body of the roll but very close to the surface, thus for all practical purposes they can be treated as a boundary condition. The Journeaux steady state and unsteady state analysis, detailed in Chapter 2, Section 2.5, used a finite element solution for the steady state deformation of a shell $u_r(z)$, combined with a finite volume solution for the temperature distribution $\Theta(r_p, z, t)$ in order to calculate the roll deformation profile u_r , a function of z and t . Steady and unsteady state solutions were satisfactorily validated against published results of experimental measurements.

The results of the steady state solutions were represented by the maximum height of the deformation, Δr_{peak} , and the characteristic width of this peak, $W_{\Delta r}$, taken as the width in the axial direction over which $\Delta r \geq \Delta r_{\text{peak}} / 3$ (Chapter 2, Figure 2.2). The results of the unsteady state solution may be simplified to the maximum value of the deformation profile as a function of time, denoted $\Delta r(t)$. However, due to the substantial time required for numerical solution of the unsteady state roll response to a calender control action, this method is currently practical only for off-line analysis. Journeaux [42] expressed these unsteady state results for the

maximum local deformation of roll radius, $\Delta r(t)$, in terms of a simple two-parameter exponential relation:

$$\Delta r(t) = \Delta r_{peak} (1 - e^{-t/\tau}) \quad [\text{Eq. 5.1}]$$

The specific configuration of control device used by Journeaux consisted of a row of 10 identical jets with a repeating sequence of either 1 cooling jet and 9 heating jets, or 1 heating jet and 9 cooling jets. For the jets, of $Re = 60,000$, the nozzle exit temperature was 20°C for cooling or 150°C for heating. A jet-to-jet spacing of $S_j / d = 4$ was used throughout, corresponding to a separation, S_j , of 100 mm between the centerlines of impinging jets from nozzles of diameter $d = 25$ mm. For heated rolls the temperature of the internal heating fluid was 150°C . Journeaux obtained the numerical solution results for unheated and internally heated rolls of a range of roll radius and shell thickness covering industrial practice and including solid rolls, the case which connects the results for unheated and heated shell rolls.

According to Equation 5.1 the dynamic response of a calender roll is represented as a function of two parameters, the limiting steady state value of the maximum local roll deformation, i.e. the peak deformation Δr_{peak} , and a roll deformation time constant, τ . Journeaux [42] showed that Equation 5.1 gives a satisfactory approximation of the complete finite element and finite volume simulation. They used their numerical solution to determine, for a variety of roll designs and thermal boundary conditions, values of the the peak roll deformation Δr_{peak} , the characteristic width of deformation $W_{\Delta r}$, and the transient roll response to local heating/cooling $\Delta r(t)$. The transient state roll deformation results were used with Equation 5.1 to compute the deformation time constant τ .

With respect to the two parameters of Equation 5.1, Δr_{peak} and τ , Journeaux did not relate these to the system operating conditions. In the present study the numerical methods results of Journeaux were used to obtain relations between the system parameters and the three deformation characteristics, Δr_{peak} , $W_{\Delta r}$ and τ , thereby obtaining practical control model equations for predicting the transient response of a calender roll.

5.1.2 Factors governing roll thermal deformation

Before the detailed results of calender thermal deformation are presented some general characteristics are outlined which underlay all the specific cases to be discussed subsequently. As the difference in characteristics between exercising control on internally heated or unheated shell rolls is a central feature of the results, this aspect is considered first.

The shell-type unheated roll is the base case, with its effectively adiabatic boundary condition at the interior surface. As a result of the control actuator there is within such a shell a radial heat flux which at steady state is equalled by axial heat flows to or from the region beyond the influence of the actuator. For an unheated roll at steady state the height of the deformation, the Δr_{peak} of Equation 5.1, and the axial width of the deformation $W_{\Delta r}$ are determined by the interaction between these radial and axial heat flows and the associated radial and axial temperature distribution. For a specific roll radius, the thicker the shell, the larger the cross-sectional area for axial heat conduction and hence the smaller the expected steady state peak deformation Δr_{peak} . For a specific shell thickness, the larger the roll radius, likewise the larger the cross-sectional area for axial heat conduction, and again the smaller the expected Δr_{peak} value. In both cases just cited the decreased resistance to axial heat conduction associated with the increased ratio, cross-section area/external shell area, would also produce a relatively flatter axial profile of the roll deformation. The latter feature is represented by the ratio $W_{\Delta r}/\Delta r_{\text{peak}}$, the roll deformation index I_D . For fine resolution of CD control it is advantageous to have more peaked profiles, not flatter profiles i.e. a low value of the I_D index. While the sensitivity to roll geometry of height and width of steady state roll deformation is clear, as noted above, there is no comparable reason for the deformation time constant τ for unheated rolls to be sensitive to roll geometry.

By contrast to an unheated shell, an internally heated roll has an additional radial heat flux at the interior surface of the roll and an additional parameter, i.e. the temperature of the heated core which controls that heat flux. Results from Journeaux [42] show that

with the roll heating fluid at 150 °C, the switch between all heating jets at 150 °C and all cooling jets at 20 °C never moved the roll surface temperature beyond the range 121 to 138 °C. This indicates that with shell thickness not greater than about half the radius, the behaviour of the shell, including its temperature distribution, is dominated by radial conduction from the heated core. This dominance is a consequence of the much higher value of heat transfer coefficient for the heating fluid (water) than for the air from the control jet, as $h_{\text{air}} \ll h_{\text{core liquid}}$, plus the fact that heat transfer from the control actuator is applied to just half the roll circumference.

The fact that the temperature distribution in the shell of an internally heated roll is dominated by the heated core boundary condition means that the effect of the control actuator would be less than for an unheated roll, i.e. the steady state peak deformation Δr_{peak} must be less than for an unheated roll. With the temperature distribution within a heated shell dominated by the large radial heat flux from the heated core it also follows that the characteristic time constant of the heated shell would be significantly less than for the unheated shell. As shell thickness of a heated roll increases, the effect that the heat flux from the heated core has on thermal deformation at the roll surface would decrease for two reasons: the area available for heat transfer from the heated core decreases, and the resistance to radial conduction of this flux increases with the increased shell thickness. Thus as the shell thickness of a heated roll increases, the Δr_{peak} must increase. A solid roll represents the limiting common case where, for unheated and heated rolls, values of control characteristics - height and width of the deformation and its response time - will converge.

With the heat flux from the heated core depending on the heating fluid-roll temperature difference, then as the temperature of the heating fluid is decreased the internal heat flux decreases and the behaviour of a heated roll will become more similar to the base case of an unheated roll. Thus for a fixed roll geometry, as the temperature of the internal heating fluid approaches that of the adiabatic core of an unheated roll, the values of all roll deformation characteristics for heated and unheated rolls would converge.

5.2 Peak roll deformation at steady state

The numerical solution results of Journeaux [42] for a 250 mm radius roll of shell thickness 100 mm, Figure 5.1, show that the peak deformation at steady state for an unheated roll is somewhat over 3 times that for a heated roll. This enormous effect is a consequence of the difference for heated and unheated rolls in the radial boundary condition at the interior surface of the roll as described in Section 5.1.2. Local roll deformation at steady state is a function of the thermal boundary condition and of roll design - the roll radius and shell thickness, as illustrated by Figure 5.1.

The effect of roll radius on peak roll deformation is essentially the same for unheated and heated rolls. In both cases, as roll radius increases at constant shell thickness, the peak roll deformation decreases. The peak deformation is created by the radial heat flux from the control actuator, but this deformation is moderated by the axial heat conduction between the region under the control actuator and that beyond. Thus as detailed in Section 5.1.2, peak deformation is a function of the ratio of the roll perimeter acted upon by the control actuator, to the cross-sectional area for axial heat transfer. With the results for four roll sizes available for heated rolls, Figure 5.1, this effect is seen to be nonlinear, with the sensitivity to roll radius decreasing with larger rolls. Although only data for two roll sizes are available for unheated rolls, similar trends would be expected.

Figure 5.1 shows that, between internally heated and unheated rolls, the effect of shell thickness on peak roll deformation is just the opposite, with an increase in shell thickness increasing the Δr_{peak} of heated rolls but decreasing it for unheated rolls. With the adiabatic boundary condition at the inside surface of an unheated roll, as the shell becomes thicker, the larger cross-sectional area leads to increased axial heat conduction to the regions of the roll beyond the control actuator which in turn reduces the thermal deformation. As outlined in Section 5.1.2, with heated rolls the large heat flux from the internal core reduces Δr_{peak} . With a thicker shell this attenuation of Δr_{peak} becomes less strong as the heat flux from the heated core decreases with decreasing heat transfer area and increasing distance of the core from the external surface.

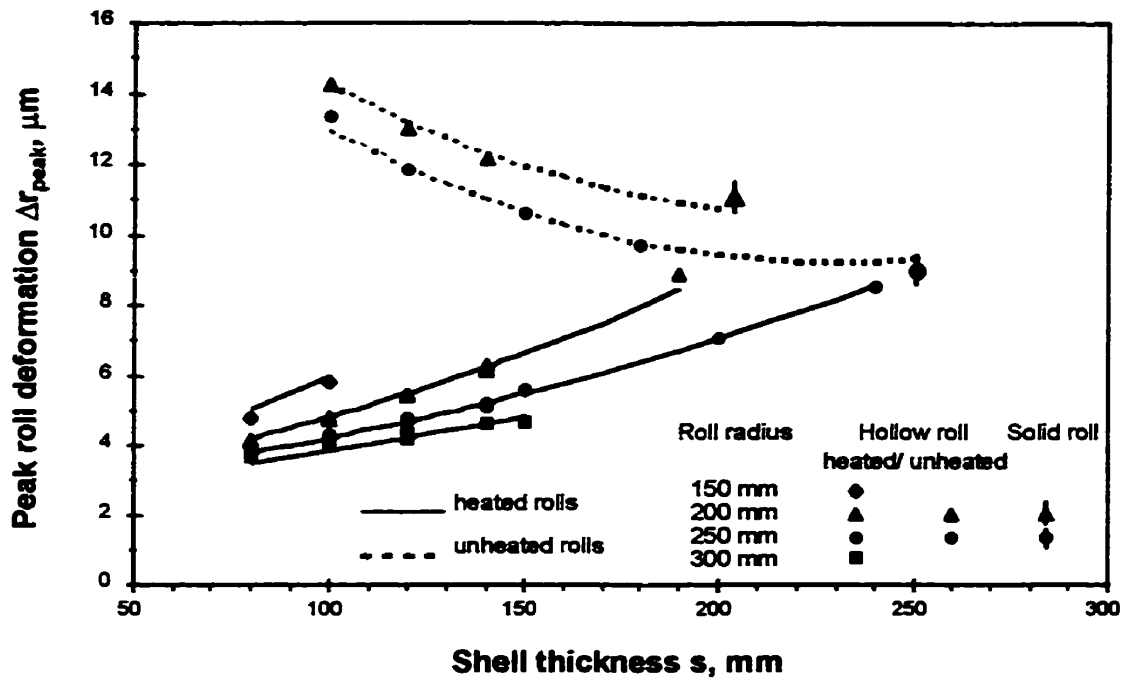


Figure 5.1: Effect of roll geometry on peak roll deformation

Data: numerical simulation of Journeaux [42]

Lines: Equations 5.2 and 5.3

For unheated rolls, the effects of shell thickness and roll radius on peak roll deformation are in the same direction, with Δr_{peak} decreasing as either r or s increases. The effect of shell thickness is clearly nonlinear, Figure 5.1, but with data available for only two values of r , this effect was assumed linear. For unheated rolls, Δr_{peak} becomes increasingly insensitive to shell thickness as s approaches the limit of a solid roll.

As noted in Section 5.1.1 the numerical solution results of Journeaux were used in the present study as input data for a regression analysis to relate the deformation characteristics Δr_{peak} , $W_{\Delta r}$, I_D and τ to the system parameters, thereby determining the equations constituting a roll deformation model appropriate for use in real-time CD control of calendering. As reported in Chapter 2, Journeaux [42] showed that for conditions of industrial relevance the magnitude of thermal roll deformation for heating and cooling jets is generally indistinguishable. Thus their numerical analysis results with both types of

control actuator were combined here for this regression analysis. For unheated rolls the local peak deformation is described as:

$$\Delta r_{\text{peak}} = a_0 + a_{s1} s + a_{s2} s^2 + a_r r \quad [\text{Eq. 5.2}]$$

where r is roll radius [mm], and s is shell thickness [mm].

For internally heated rolls, because peak roll deformation increases nonlinearly with shell thickness and decreases nonlinearly with roll radius, an exponential relation describes well these roll geometry effects:

$$\Delta r_{\text{peak}} = a_0 + a_r e^{(s/r)} \quad [\text{Eq. 5.3}]$$

Coefficients of these correlations for unheated and heated rolls are given in Tables 5.1 and 5.2, with the resulting prediction curves plotted on Figure 5.1. The favorable coefficient of variation values in Tables 5.1 and 5.2 for these experimentally determined parameters are reflected in the good predictive ability apparent on Figure 5.1, thus supporting the acceptability of the approach taken here. Figure 5.1 shows the effect of shell thickness, with peak roll deformation for heated and unheated rolls proceeding in the opposite direction from the common case of a solid roll.

Table 5.1: Coefficients for Equation 5.2, unheated rolls.

PARAMETER	ESTIMATE	STD. ERROR	C.V.
a_0 [μm]	27.4661	1.71539	6 %
a_{s1}	-0.1010	0.01677	17 %
a_{s2} [mm^{-1}]	0.00022	0.000049	22 %
a_r	-0.0263	0.00435	17%
R_{required}	0.98		

Table 5.2: Coefficients for Equation 5.3, internally heated rolls.

PARAMETER	ESTIMATE	STD. ERROR	C.V.
a_0 [μm]	-1.5793	0.10685	7 %
a_{SR} [μm]	3.8825	0.06215	2 %
R_{required}	0.99		

For heated rolls the Δr_{peak} values for solid rolls, the common case for heated and unheated rolls, were not included in the regression analysis and thus the Figure 5.1 curves do not extend to these limits. For such rolls the industrially relevant range of shell thickness is 80 to 160 mm. To include solid rolls in the regression, which would require adding higher order terms, would increase the complexity of Equation 5.3 in order to make it applicable over a region for which it would not be used.

5.3 Width of roll deformation at steady state

The width of deformation, like peak roll deformation, depends on roll design and thermal boundary conditions as discussed in Section 5.1.2. Because $W_{\Delta r}$ and Δr_{peak} are the two dimensions of roll deformation, a considerable similarity in their behaviour should be expected. As for Δr_{peak} , the values of $W_{\Delta r}$, Figure 5.2, depend strongly on whether the roll is internally heated. For hollow rolls that are heated internally the presence of a strong radial heat flux which is uniform in the axial direction is the effect which decreases both of these axially local effects, $W_{\Delta r}$ and Δr_{peak} . The thinner the shell, the stronger this effect. As for Δr_{peak} , the difference in $W_{\Delta r}$ for heated and unheated rolls vanishes as shell thickness approaches roll radius.

For the base case, an unheated roll with its adiabatic boundary condition at the inside surface, Figure 5.2 shows that $W_{\Delta r}$ is essentially invariant with respect to both

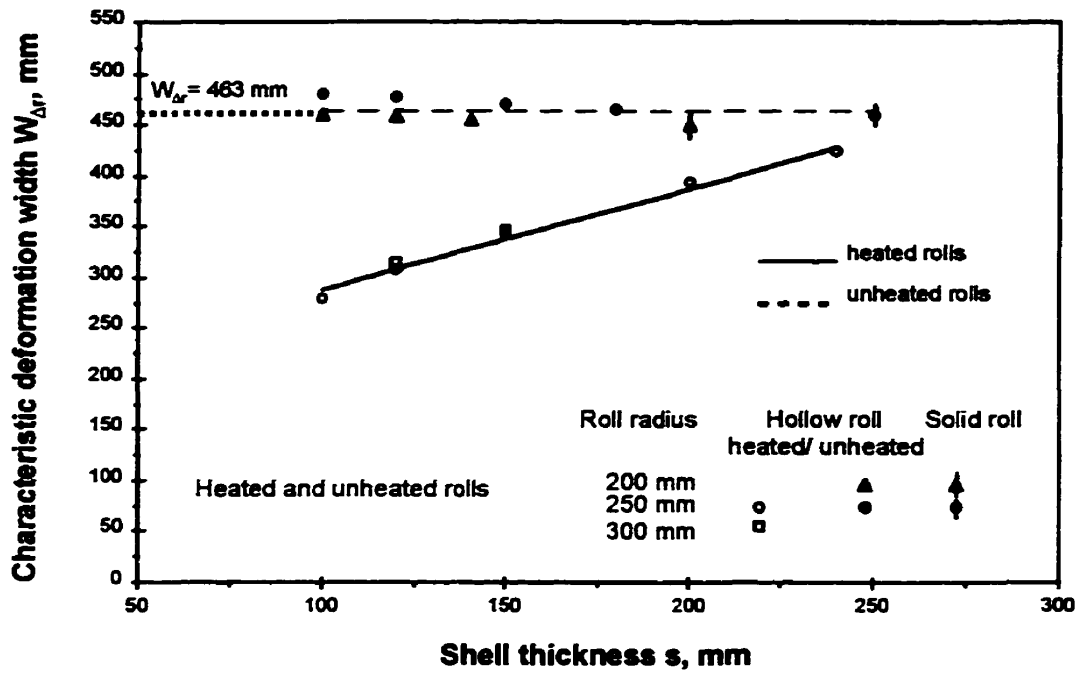


Figure 5.2: Effect of roll geometry on characteristic deformation width

Data: numerical simulation of Journeaux [42]

Lines: Equations 5.4 and 5.5

geometric parameters. For use in a calendering control model, an average of this set of data serves as the characteristic dimension $W_{\Delta r}$ for unheated rolls, independent of roll geometry i.e.:

$$W_{\Delta r} = 463 \text{ mm} \quad [\text{Eq. 5.4}]$$

The characteristic deformation width of heated rolls can be represented as:

$$W_{\Delta r} = c_0 + c_s s \quad [\text{Eq. 5.5}]$$

Table 5.3: Coefficients for Equation 5.5, internally heated rolls.

PARAMETER	ESTIMATE	STD. ERROR	C.V.
c_0 [mm]	188.369	8.8868	5 %
c_s	1.0133	0.0552	5 %
R_{squared}	0.98		

The coefficients for Equation 5.5, Table 5.3, provide the prediction line plotted on Figure 5.2. For reasons given in connection with Figure 5.1, values of $W_{\Delta r}$ for solid rolls were not included in this regression analysis, so the Figure 5.2 lines do not include this limit. Discussion of the interrelation between effects of roll geometry and internal thermal conditions on height and width of roll deformation is deferred to Section 5.4.

5.4 Roll deformation index

The most effective steady state limit for calender control would combine a high Δr_{peak} with a low $W_{\Delta r}$. Accordingly Journeaux defined a calender control deformation index, I_D , as the characteristic width of deformation, millimeters, per micrometer of peak roll deformation:

$$I_D = W_{\Delta r} / \Delta r_{\text{peak}} \quad [\text{Eq. 5.6}]$$

As the steady state limit for CD control of calendaring a low value of this I_D index is desirable. Based on his numerical solution results Journeaux reported values ranging from a high of $I_D = 86 \text{ mm}/\mu\text{m}$ for a large radius, thick-walled internally heated roll, to a low of $I_D = 35 \text{ mm}/\mu\text{m}$ for a small radius, thin-walled unheated roll. Thus for a given roll deformation, use of a conditions giving a low value of the I_D index provides a control action that is felt over a

narrower width of roll, thereby permitting at steady state a finer resolution of CD control over the width of the paper machine.

Using correlations 5.2 to 5.5 for Δr_{peak} and $W_{\Delta r}$, the deformation index I_D can now be evaluated for a variety of roll designs for unheated rolls as:

$$I_D = 463 / (a_0 + a_{11} s + a_{12} s^2 + a_{13} r) \quad [\text{Eq. 5.7}]$$

and for heated rolls:

$$I_D = (c_0 + c_1 s) / (a_0 + a_{11} e^{s/r}) \quad [\text{Eq. 5.8}]$$

The Figure 5.3 results for the deformation index I_D from Equations 5.7 and 5.8 show that, for the base case of unheated rolls, the improvement of a lower I_D index is achieved by reducing both roll radius and shell thickness. As Figure 5.1 showed that reducing r and s gives a larger Δr_{peak} , such changes are doubly good in giving a roll deformation profile that is both larger and more peaked. For internally heated rolls, the desired lower I_D is still achieved by decreasing roll radius but the effect of shell thickness is just the opposite. At steady state a finer resolution of cross-machine direction control is achieved by increasing shell thickness, a change which is again doubly good as Figure 5.1 shows that Δr_{peak} would also be increased. Unheated rolls are seen to be strongly advantageous over heated rolls, combining finer resolution of CD control, Figure 5.3, with larger deformation, Figure 5.1. Current industrial practice is for calender rolls in the range of shell thickness 80 to 160 mm, with 120 mm being a commonly used thickness. For shell thickness in the 80 to 160 mm range, the I_D deformation index values for unheated rolls are in the range 30 to 40 mm/ μm while heated rolls have considerably less advantageous values of I_D in the range 50 to 70 mm/ μm .

As the definition of the I_D index provides the ratio of the width to the height of the deformation profile, Figure 5.3 shows that roll deformation profiles are flatter on heated rolls, are more peaked on unheated rolls. Furthermore, to obtain the more peaked deformation profiles that are advantageous for fine

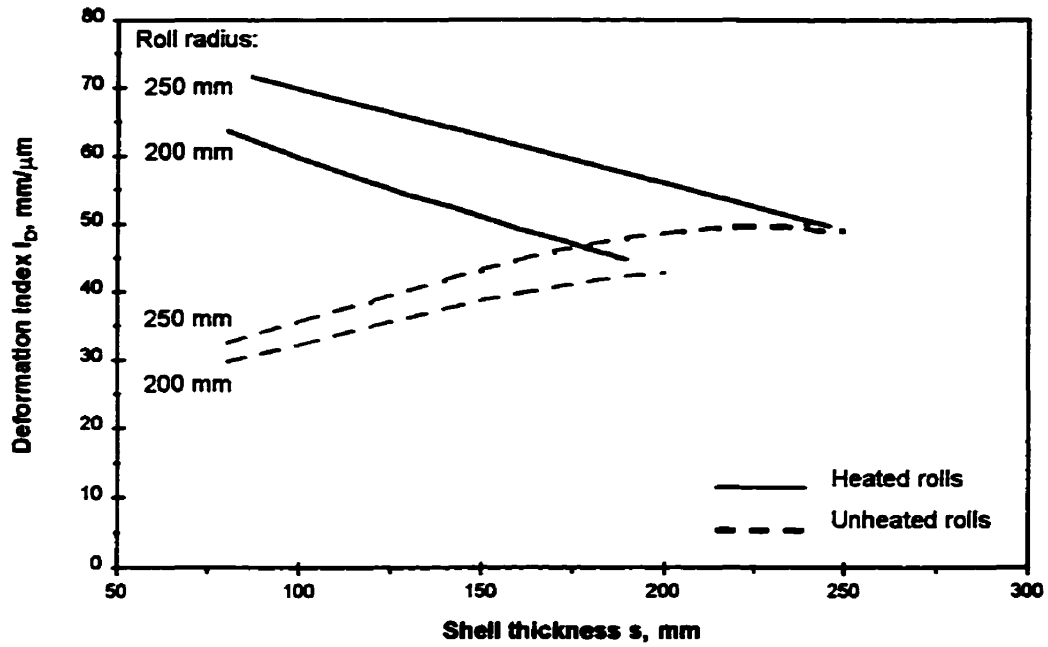


Figure 5.3: Effect of roll geometry on deformation index

Lines: Equations 5.7 and 5.8

resolution of CD control, the shell thickness of heated rolls should be increased while that for unheated rolls should be decreased.

The above results show that the greatest potential for fine resolution of CD control at steady state is provided by unheated rolls of small radius and thin shells. Although the deformation index I_D constitutes a useful combination of two characteristics, the definition of I_D gives equal weight to the variables Δr_{peak} and $W_{\Delta r}$. Thus if the optimum control strategy gives more importance to one of these variables, the deformation index I_D could not be used as a precise guide to the best control system. Also, as the I_D index relates to the potential for CD control at steady state it provides no guidance as to the other desirable control characteristic, i.e. fast response, the aspect considered next.

5.5 Roll deformation time constant

With characterization of the steady state values of roll deformation dimensions as functions of roll design and control action parameters, it remains only to characterize the time constant of this deformation. With the symmetry of thermal conditions for unheated rolls, the deformation time constant is independent of the choice of heating or cooling control actuator, hence this aspect of control conditions need not be considered. For unheated rolls the numerical solution data on Figure 5.4 shows that τ is only very weakly affected by either r or s . With the time constant for unheated rolls effectively independent of roll geometry, for control model use an average value yields:

$$\tau = 21.8 \text{ min} \quad [\text{Eq. 5.9}]$$

Figure 5.4 shows that the deformation time constant can be very much lower for heated than for unheated rolls, again due to the dynamic behaviour of the shell being dominated by the large radial heat flux from the heated core which, for the internal core and external actuator conditions used here, is much greater than the heat flux from the actuator. For the internal heating and external actuator conditions tested, and over the 80 to 160 mm shell thickness range common to industry, the 22 minute time constant τ for unheated rolls is very much longer than the 2.5 to 8 minutes applicable for heated rolls. As $s \rightarrow r$, for internally heated rolls τ increases exponentially toward that for a solid roll, the limiting case common to heated and unheated rolls.

The deformation time constant of internally heated rolls varies somewhat with roll radius but greatly with shell thickness. The results for a 200 mm radius roll, Figure 5.4, show that the $\tau = f(s)$ effect is distinctly nonlinear. For internally heated rolls the time constant should then be taken as linear with roll radius, nonlinear with shell thickness:

$$\tau = b_0 + b_{s1} s + b_{s2} s^2 + b_r r \quad [\text{Eq. 5.10}]$$

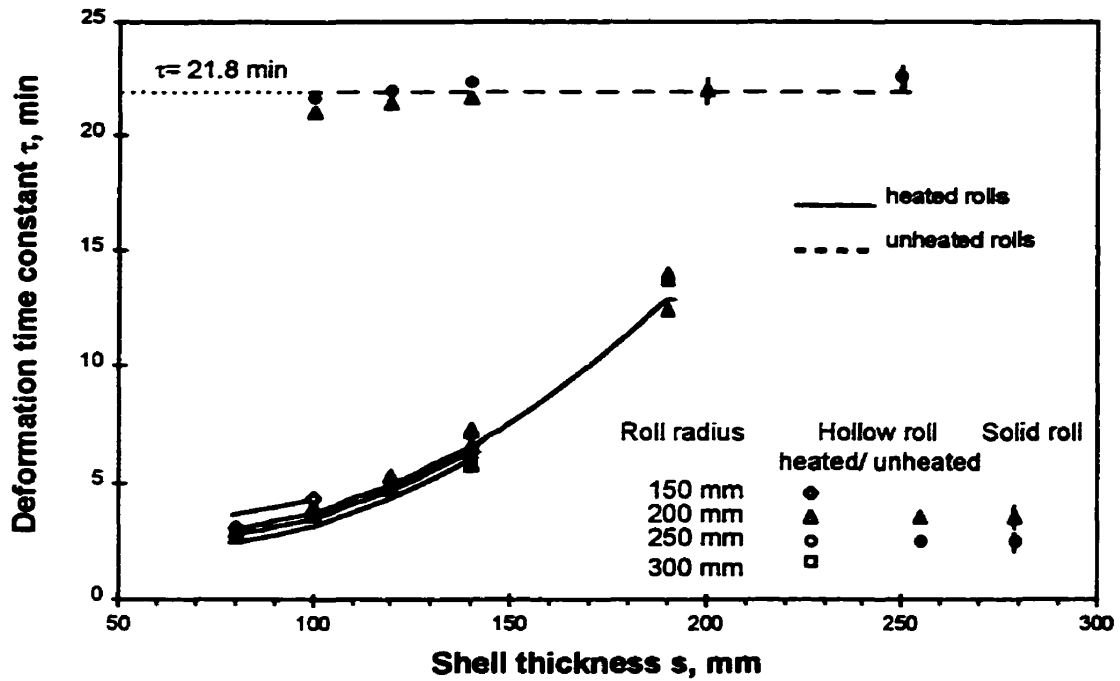


Figure 5.4: Effect of roll geometry on deformation time constant

Data: numerical simulation of Journeaux [42]

Lines: Equations 5.9 and 5.10

Table 5.4: Coefficients for Equation 5.10, internally heated rolls.

PARAMETER	ESTIMATE	STD. ERROR	C.V.
b_0 [min]	6.0865	0.85483	14 %
b_{s1} [min/mm]	-0.0726	0.01364	19 %
b_{s2} [min/mm ²]	0.0006	0.00005	8 %
b_r [min/mm]	-0.00553	0.00162	29 %
R_{required}	0.99		

Coefficients for Equation 5.10 and the corresponding coefficient of variation values are given in Table 5.4, and the resulting prediction curves for a variety of roll designs appear on Figure 5.4. Values of τ for solid rolls were not included in the regression analysis, as noted for Figures 5.1 and 5.2.

5.6 Comparison of unheated and heated calender rolls

The preceding sections demonstrate the very large differences between the characteristics with control exercised on unheated and heated rolls. To integrate this aspect we now examine the ratio of each parameter, peak deformation Δr_{peak} , deformation index I_D , and deformation time constant τ , for the case of internally heated rolls relative to that for unheated rolls. Of the three characteristics, Δr_{peak} , $W_{\Delta r}$ and I_D , only two are independent. For this comparison I_D is used rather than $W_{\Delta r}$ because I_D gives a direct measure of the axial dimension shape of the profile, $W_{\Delta r} / \Delta r_{\text{peak}}$, and therefore provides a direct measure of the fineness of resolution of control in the CD dimension. As $W_{\Delta r}$ is defined relative to Δr_{peak} as the deformation width where $\Delta r_{\text{peak}} \geq \Delta r/3$, $W_{\Delta r}$ cannot be interpreted independently of Δr_{peak} . For these parameters the data can be further condensed by presenting these ratios as a function of relative shell thickness, s/r . The results in this condensed form appear on Figure 5.5. The ratio plots must converge to the value of one for the $s/r=1$ limit. As it is apparent that use of the nondimensional variable s/r does not account entirely for the separate effects of roll geometry, thus separate lines are shown for roll radius.

These three figures show clearly the conflict between conditions which are advantageous for the various desirable aspects for CD control. To have at steady state high values of peak roll deformation and low values of the deformation index, Figures 5.5a and 5.5b show the superiority of unheated over heated rolls. This advantage of unheated rolls is counterbalanced by heated rolls of conventional wall thickness having a response time constant τ only 1/5 to 1/6 as long. Even for quite thick walled rolls, of s/r in the range

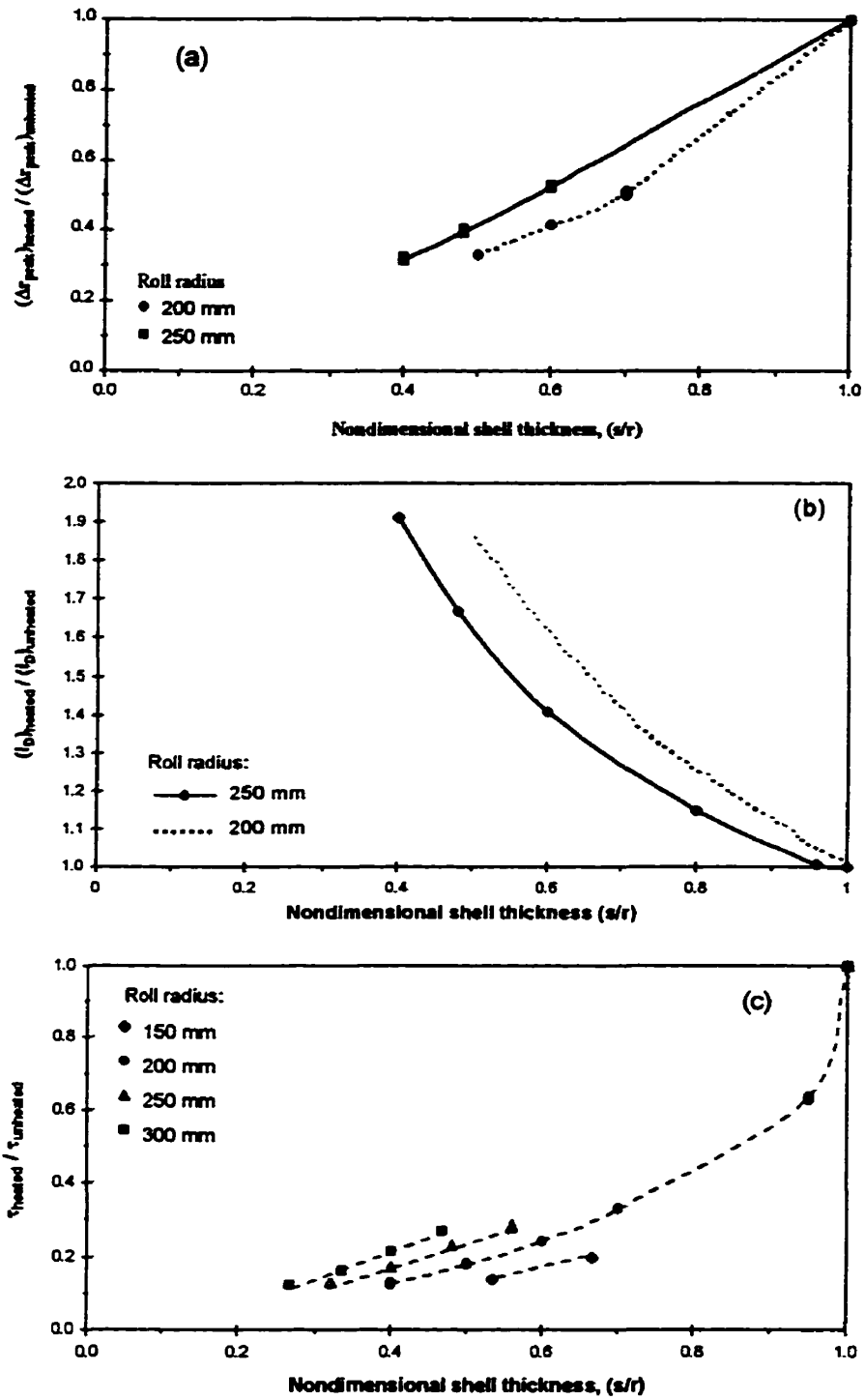


Figure 5.5: Effect of roll geometry on
 a) $(\Delta r_{\text{peak}})_{\text{heated}} / (\Delta r_{\text{peak}})_{\text{unheated}}$
 b) $(I_D)_{\text{heated}} / (I_D)_{\text{unheated}}$
 c) $\tau_{\text{heated}} / \tau_{\text{unheated}}$

0.6 to 0.7, τ for such heated rolls is still only 1/4 to 1/3 that for unheated rolls. Thus Figure 5.5 is effective in demonstrating the impossibility of identifying any single combination of conditions which would give the ideal control system: high Δr_{peak} , low I_D and small τ . For a specific calender CD control system it is therefore necessary to seek a satisfactory compromise between the conflicting objectives of the potential for large roll deformation, fine CD resolution and fast control response time.

5.7 Simulation of dynamic roll deformation

The analysis in the preceding sections of the effect of various geometric and thermal parameters on calender roll response to a control action in terms of its steady state characteristics Δr_{peak} , I_D , and $W_{\Delta r}$ and the response time constant τ provides an integrated perspective and shows that changes which are favorable to one or more of these are unfavorable to the other characteristics. Thus the analysis in terms of these characteristics, while necessary, is insufficient to identify optimal CD control strategy. Therefore the dynamic response of calender rolls to a specific control action, Figures 5.6 and 5.7, was determined as the roll surface deformation, $\Delta r(t)$, evaluated at the axial centreline of the control actuator. These simulations for 200 mm radius rolls with a local cooling control jet in an array of heating jets are generated with Equation 5.1, combined with correlations 5.2 and 5.9 for unheated rolls, with correlations 5.3 and 5.10 for internally heated rolls. As already noted, results with heating and cooling control jets are equivalent. This choice of conditions permits comparing the simulation results for $\Delta r(t)$ with the results that Journeaux [42] computed numerically for the same conditions.

The dynamic roll deformations on Figures 5.6 and 5.7 compare well with those obtained by finite volume and finite element numerical methods. As this agreement supports the correctness of the approximation of transient roll deformation presented as Equations 5.1 to 5.5, the approach taken here can be considered a satisfactory

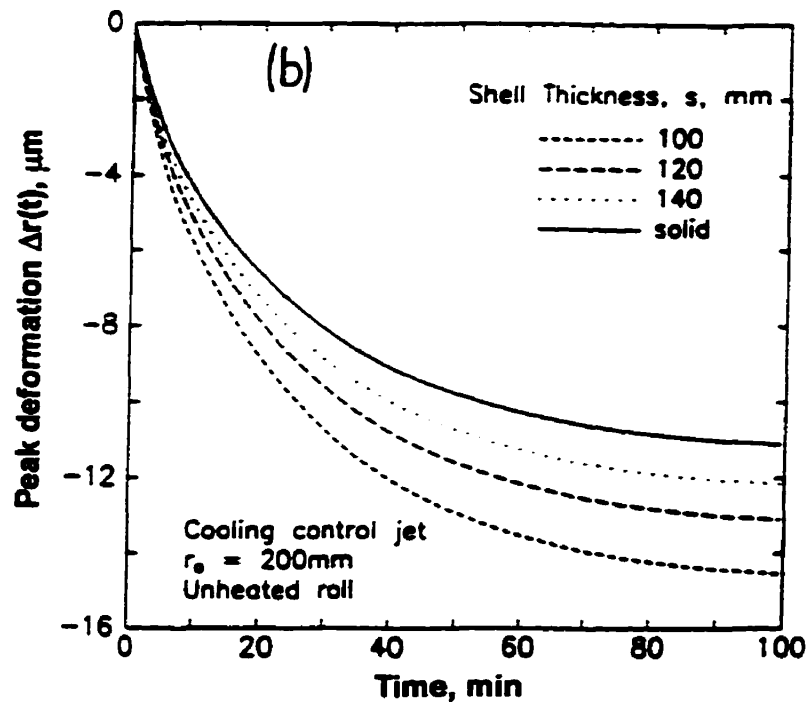
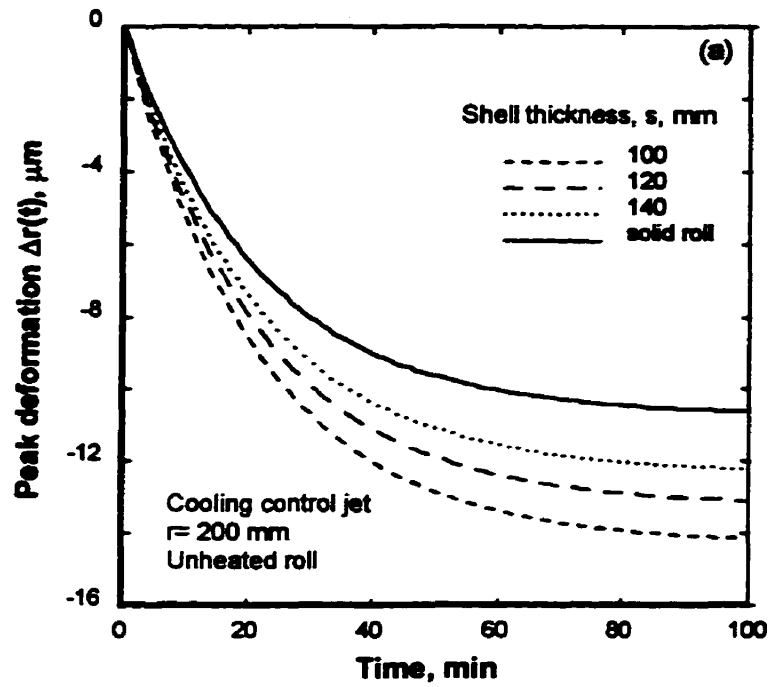


Figure 5.6: Local roll deformation for unheated rolls

- a) simulation results, present study
- b) numerical results, Journeaux [42]

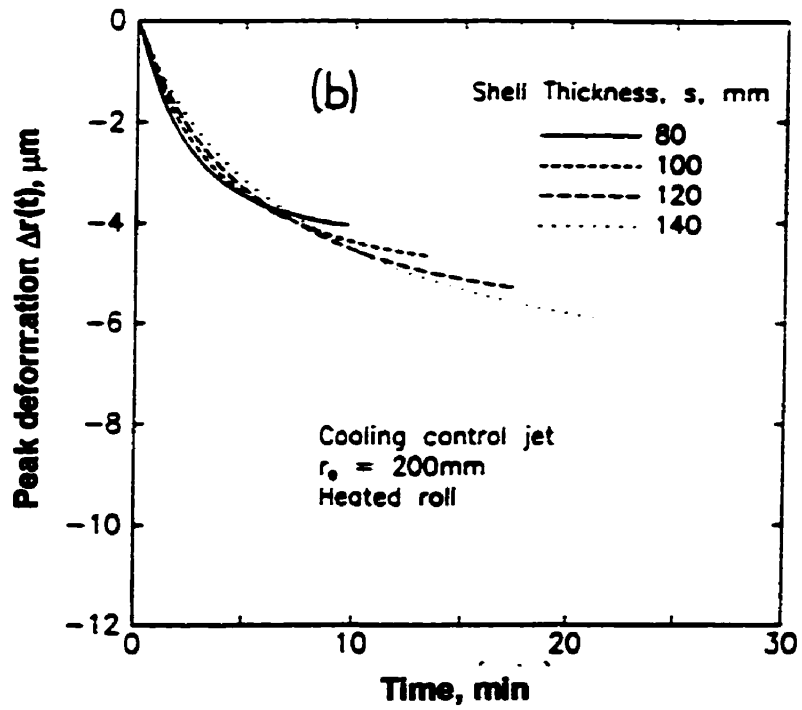
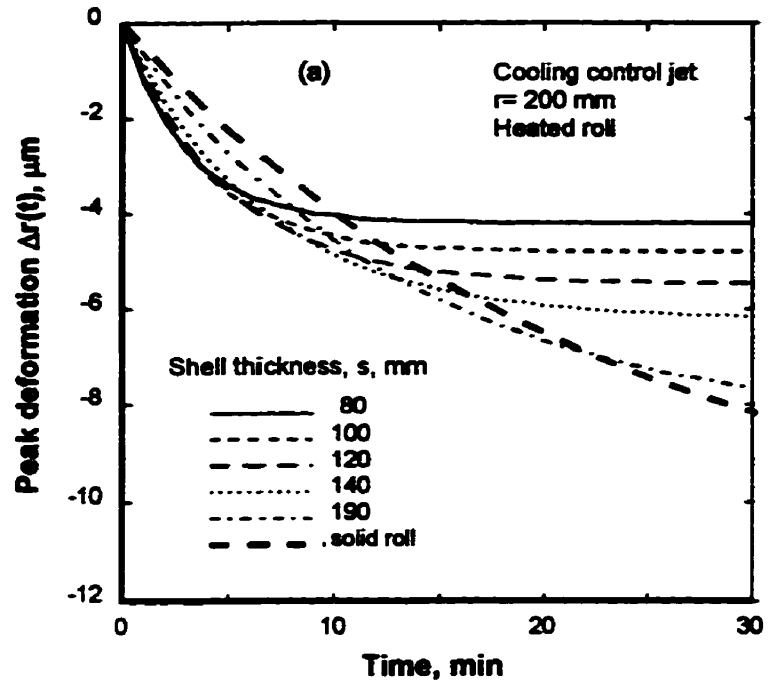


Figure 5.7: Local roll deformation for heated rolls

- a) simulation results, present study
- b) numerical results, Journeaux [42]

representation of the dynamic behaviour of the system. A major advantage of the present method is that, using similar computing power, the time required to compute the local deformation of the calender roll is seconds where the numerical simulation takes hours.

For an unheated roll the thermal deformation, which was seen on Figure 5.1 to increase with a decrease in shell thickness for the steady state limit, is seen on Figure 5.6 to do so starting immediately after the control action. As Figure 5.4 showed the time constant is effectively independent of roll geometry, for unheated rolls there is no conflict between the role of Δr_{peak} and τ , so in practice one would choose calender roll parameters giving the most favorable steady state peak deformation. In Figure 5.6 this criterion is seen to correspond to use of the thinnest practical shell thickness. Because Figure 5.3 showed that for unheated rolls the use of the thinnest practical shell thickness also provides the lowest deformation index I_D , i.e. the most peaked deformation profile and thereby the smallest resolution control in the CD dimension.

For heated rolls the relationship between dynamic roll deformation and shell thickness is more complicated, Figure 5.7. At longer times $\Delta r(t)$ increases as s increases towards the solid roll limit, as applies also for the Δr_{peak} steady state limit on Figure 5.1. However between 4 and 10 minutes all the Figure 5.9 curves cross, so that at times shorter than 4 minutes the thermal deformation of a 200 mm radius heated roll is just the opposite, i.e. decreases with increasing shell thickness. This behaviour at short times was qualitatively predictable from Figure 5.4 where the time constant τ of heated rolls is shown to improve strongly as shell thickness is decreased. For heated rolls the opposing trends of Δr_{peak} and τ with changes in shell thickness are reflected on Figure 5.7 by the crossing of lines at some intermediate value of time, which is now seen to start at 4 minutes after the control action.

Thus the control characteristics for heated rolls constitute a particularly interesting case of conflict between the effects of various parameters on Δr_{peak} and τ . Figure 5.1 shows that the desirably large steady state Δr_{peak} is obtained by the use of thick walled shells, while Figure 5.4 shows that a favorable small time constant τ is obtained by the use of thin shells. Thus at large values of time it is clear that the response of thick walled shells

will be superior, but the results in terms of Δr_{peak} and τ do not establish directly the time at which this behaviour becomes dominant. At short times after the control action the results expressed as Δr_{peak} and τ leave even more uncertainty because it would be possible that a shell thickness giving a high value of Δr_{peak} at steady state could produce the better performance at short times of practical interest in spite of the disadvantage of a larger time constant τ .

It is the transient deformation results on Figure 5.7 that resolve this question. Here we see the important finding that thin shells, giving a smaller time constant τ , do indeed give a better roll deformation for a significant period initially. However for the period up to 5 minutes after the control action the response for rolls of 100, 120 and 140 mm shell thickness is essentially indistinguishable (within 0.3 μm) from that for a roll with $s = 80$ mm. This insignificant difference in short time dynamic roll deformation occurs in spite of the fact that Figure 5.4 shows the time constant τ for 100 to 140 mm thick shells being up to double that for $s = 80$ mm. Thus for s of 100 to 140 mm, during the period up to 5 minutes their disadvantage of a longer time constant τ is nearly fully compensated by their correspondingly larger values of Δr_{peak} at steady state. For the thinnest shell roll, $s = 80$ mm, the disadvantage of the lowest Δr_{peak} at steady state becomes dominant by 5 minutes following the control action, after which its deformation is exceeded by that of rolls with thicker wall shells. For the $s = 100$ mm roll, by 7 minutes after the control action its disadvantage of low Δr_{peak} becomes dominant over its low τ , hence its deformation is exceeded by that of thicker shelled rolls.

From the results of the present simulation for control on heated rolls of 200 mm radius, Figure 5.7a, the shell thickness which gives the best CD control, i.e. the largest peak deformation is seen to be as follows:

<u>time, min</u>	<u>s, mm</u>	<u>s/r</u>
5	120 or less	0.6 or less
5 to 10	120	0.6
10 to 13	140	0.7
13 to 22	190	0.95
22 to 30	solid	1

At 11 minutes after the control action with 200 mm radius rolls an interesting cross-over at roll deformation of $\Delta r(11) = 4 \mu\text{m}$ occurs between the $s= 80$ mm and the solid roll. This cross-over constitutes an equivalence between the opposing effects on roll deformation from the steady state and dynamic control characteristics which, from Figures 5.1 and 5.4, are as follows:

<u>shell thickness</u>	<u>Δr_{peak} μm</u>	<u>τ, min</u>
$s= 80$ mm	4.2	3.3
solid roll	10.8	21.8

Thus for 200 mm radius rolls at 11 minutes, the advantage of the solid roll having a steady state Δr_{peak} value 2.6 times that of the thin ($s= 80$ mm) walled heated shell exactly counterbalances the disadvantage of having a time constant τ that is 7 times that of the 80 mm shell thickness roll.

At 5 minutes after the control action the deformation for 200 mm radius rolls of shell thickness $80 < s < 140$ mm is about $1 \mu\text{m}$ greater than for the poorest case, a solid roll. At 11 minutes, which is the time of the solid roll - 80 mm shell roll cross-over noted above, the deformation of the best case (s of 120 to 140 mm) is about $1 \mu\text{m}$ greater than for the poorest choice, either a very thin ($s= 80$ mm) walled shell or a solid roll. At 17 minutes the deformation of the best case ($s= 190$ mm) is about $2 \mu\text{m}$ greater than the worst case ($s= 80$ mm). At 23 minutes, when the highest deformation is given by the solid roll, its deformation is $3 \mu\text{m}$ greater than the worst case ($s= 80$ mm).

Since transient roll deformation is affected by both peak roll deformation at steady state and deformation time constant, which in Sections 5.1 to 5.5 showed quite different characteristics for internally heated and unheated rolls, it is of interest to make this comparison for the transient deformation. Although unheated rolls have an unattractively large time constant their steady state deformation is, advantageously, very much larger. For this comparison of transient control characteristics Journeaux [42] used the values of local roll deformation at 10 minutes after the control action. Their numerical analysis

results are shown in Figure 5.8b for 200 and 250 mm radius rolls with a range of shell thickness. Corresponding simulations were performed in the present study, Figure 5.8a. Again the results based on the approximation of Equations 5.1 to 5.3, 5.9 and 5.10 compare well with those based on the full numerical simulation, thus further supporting the reliability of the approach developed here.

The Figure 5.8 results from both studies show that for rolls of the same diameter and with shells thinner than 140 mm, the thermal deformation obtained after 10 minutes is greater for unheated rolls. With increasing shell thickness the present simulation, Figure 5.8a, shows that the peak thermal deformation of a 200 mm radius unheated roll after 10 minutes decreases from 5.3 μm for 100 mm shell to 4 μm for a solid roll. For a heated, 200 mm radius roll, the deformation initially increases from 4 to 4.5 μm with shell thickness increasing from 80 to 190 mm, then with a further increase in shell thickness deformation decreases to the value for a solid roll, 4 μm . The results for heated and unheated rolls of course converge as shell thickness approaches that of the common case, a solid roll.

For the heated roll results on Figure 5.8a it is not surprising to see the deformation at 10 minutes pass through a maximum as shell thickness is changed. For heated rolls, the opposing effects of shell thickness on Δr_{peak} and τ lead to the cross-over of lines on Figure 5.7a and to the occurrence of the maximum on Figure 5.8a.

The roll with the combination of the advantage of the lowest time constant τ but the disadvantage of the lowest Δr_{peak} at steady state is shown by Figure 5.7a to have the highest deformation for only about the first 5 minutes after the control action. Figure 5.8 shows that unheated rolls generally give a higher deformation at 10 minutes after the control action. Figures 5.1 and 5.4 show that, relative to heated rolls, unheated rolls have a longer response time τ but larger values of Δr_{peak} . Therefore in the Figure 5.8a comparison of unheated and heated rolls at 10 minutes after the control action the dominant effect is from Δr_{peak} , not τ . Had Journeaux made this comparison of unheated

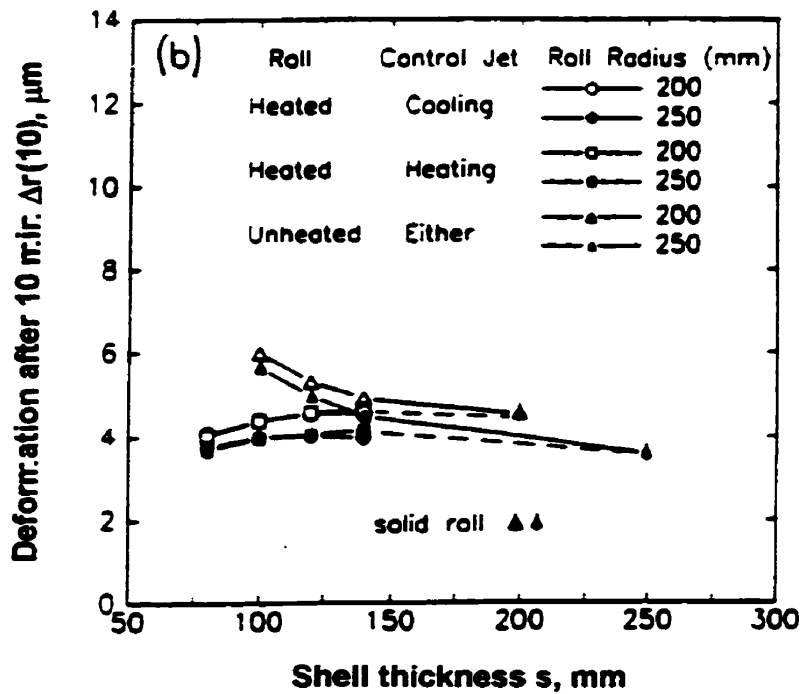
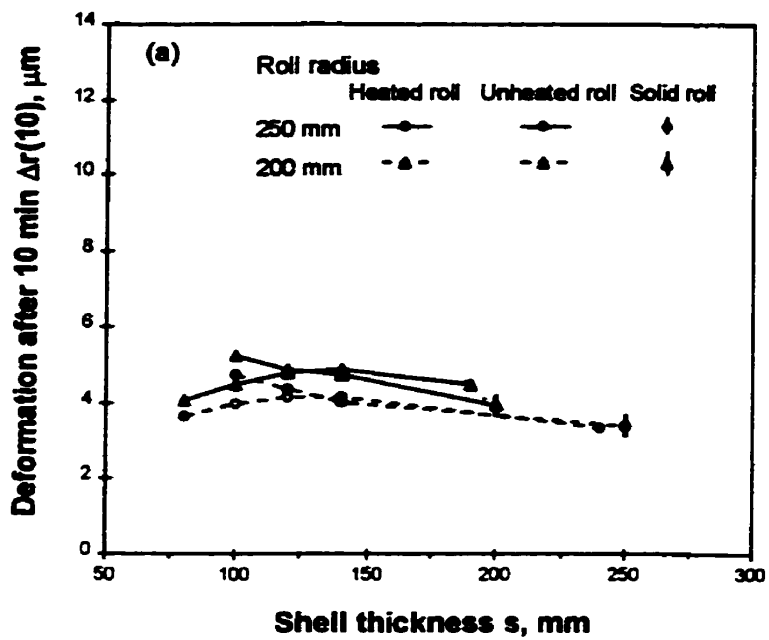


Figure 5.8: Local roll deformation for unheated and heated rolls after 10 minutes

- a) simulation results, present study
- b) numerical results, Journeaux [42]

and heated rolls at shorter time, say 3 minutes after the control action, the results would have been the opposite of those they reported after 10 minutes. After only 3 minutes the combination having the faster response time τ , not the larger steady state Δr_{peak} , i.e. thin walled heated rolls, would give the largest deformation.

From the large number of cross-overs apparent on Figure 5.7a at 10 minutes after the control action, due to the transition from the early advantage of rolls with a low τ to the later advantage of rolls with a high Δr_{peak} , it is not surprising that at 10 minutes the differences in deformation on Figure 5.8 are rather small, in the order of $0.5 \mu\text{m}$. If this type of comparison of unheated and heated rolls had been made at a longer time, say 20 minutes after the control action, inspection of Figures 5.6 and 5.7 shows that the Figure 5.8 differences of less than about a micron at 10 minutes after the control action would have been substantially greater at 20 minutes. Figure 5.7a shows that for heated rolls at 20 minutes after the control action the advantage of larger deformation is now more strongly with solid or near-solid cylinders with their much higher steady state peak deformation, Figure 5.1. Figure 5.7 indicates that at 20 minutes the peak deformation of heated rolls is in the range 4 to $6 \mu\text{m}$ for shells of 80 to 140 mm thickness. For shell thickness in the range 100 to 140 mm and after 20 minutes, Figure 5.6 shows that the peak deformation for unheated rolls, 7.3 to $8.4 \mu\text{m}$, considerably surpasses the 5 to $6 \mu\text{m}$ indicated by Figure 5.7a for heated rolls. Thus at 20 minutes after the control action for a shell thickness of 100 to 140 mm, unheated rolls give 2 to $2.5 \mu\text{m}$ greater deformation than heated rolls. Moreover, not only is the roll deformation of unheated rolls higher at 20 minutes but Figure 5.3 shows that the deformation index $I_D = W_{\Delta r} / \Delta r_{\text{peak}}$ at steady state for unheated rolls is only about $2/3$ of that for heated rolls, so the roll deformation for the unheated rolls is both substantially larger and more peaked, thus giving a higher resolution CD control.

As the industrial objective is to maintain the time the paper is off specification to well under 20 minutes, the availability of the model of dynamic roll deformation developed here provides the capability of choosing roll design parameters consistent with practical needs.

5.8 Conclusions

The thermal deformation of calender rolls in response to a local CD control action for a variety of roll designs and thermal conditions, as determined previously by a full numerical solution, can be satisfactorily approximated as an exponential decay depending on two parameters, a local peak deformation of the roll at steady-state and a roll deformation time constant. The characteristics which describe the thermal deformation of calender rolls, the height and width of the deformation at steady state, Δr_{peak} and either $W_{\Delta r}$ or I_D and the deformation time constant τ were obtained as a function of roll geometry and whether the roll is internally heated or unheated. These relations constitute a model of dynamic roll deformation appropriate as an element in a model of calendaring for use in CD control.

For unheated rolls, with an effectively adiabatic boundary condition at the interior surface, the steady state and dynamic characteristics of local roll deformation are determined by the balance between a radial heat flux from the control actuator and the axial heat conduction between the region of the roll under the control actuator and that beyond the influence of the actuator. For internally heated rolls, local deformation is dominated by the large radial heat flux at the interior surface of the roll. This heat flux, substantially larger than that from the control actuator, gives heated rolls the advantage of a much lower time constant τ but the disadvantages of much smaller peak deformation Δr_{peak} and much flatter deformation profiles at steady state as shown by the deformation index I_D . Flatter deformation profiles mean a less fine resolution of deformation in the CD dimension.

Increasing the shell thickness is disadvantageous for both Δr_{peak} and I_D of unheated rolls but is advantageous for heated rolls, with a solid roll being the limiting case common to unheated and heated shells. The deformation time constant of unheated rolls is independent of roll radius and shell thickness. With the dynamic response of internally heated shells being dominated by the large heat flux from the core, the deformation time

constant for such rolls decreases sensitively with decreasing shell thickness because this change increases the importance of the heat flux from the central core.

For a specific calender CD control system it is therefore necessary to seek a compromise between conflicting objectives - a large roll deformation and fine CD resolution (unheated rolls), and fast control response time (with heated rolls). Thus the dynamic response of calender rolls to a control action was determined, using the dynamic model of roll deformation developed here, in order to identify optimal CD control strategy. For unheated rolls, with the deformation time constant effectively independent of roll geometry, the response time is not a factor. For such rolls, both the peak deformation Δr_{peak} and the deformation index I_D improve with decreasing shell thickness and roll radius. Therefore with unheated rolls, the smallest diameter and thinnest shell thickness that is practical would be the best choice. For heated rolls the relationship between dynamic roll deformation and geometric parameters is complex. Thin shells, with a small time constant τ , give a better roll deformation initially. However at longer times after the control action it is thick walled heated shells, giving at steady state both better peak roll deformation Δr_{peak} and better deformation index I_D , which produce both a larger deformation and a finer resolution in the CD dimension.

The additional results available for deformation 10 minutes after the control action lead to the following observations. These simulation results show that for rolls of the same diameter and with shells thinner than 120 mm, the 10 minute thermal deformation is greater for unheated rolls. With increasing shell thickness, the 10 minute deformation for unheated rolls decreases to the value for a solid roll. For a heated roll, as shell thickness is increased the 10 minute deformation initially increases, passes through a maximum then decreases to the common value for a solid roll.

As the industrial objective is to minimize the time the paper is off-specification, the model of dynamic roll deformation developed here enables determining combinations of roll geometry and thermal conditions which are consistent with achieving this objective.

6 Simulation of calendering

6.1 Introduction

Systems using feedback methods to minimize nonuniformity of thickness of paper in the CD dimension require excessive time to settle if a strong control action is used to minimize the time that the local caliper is off specification, or else produce extended times off specification if a restrained control action is used to avoid overshooting. The response time to corrective action of current systems may be as long as 10 to 20 minutes. As a 9 meter wide newsprint machine running at 1100 m/min produces about 30 tonnes/hour, if the control system requires even 10 minutes to arrive at 95% of the target variation, about 5 tonnes of substandard paper will have been made. The objective of the present work is to provide a dynamic model of the calendering process, thereby enabling application to CD calender control of the most effective strategy for processes difficult to control, i.e. model-based predictive control.

An explicit CD profile control law involves four steps to determine the control action:

1. From an existing CD thickness profile, calculate the load profile required to obtain a uniform thickness profile;
2. Calculate the in-nip paper strain profile to produce the required load profile;
3. Calculate the roll radius profile equivalent to the desired in-nip strain profile;
4. Calculate the roll temperature profile which will generate the required roll radius profile, and select the actuator settings to reach that profile quickly.

Methods for accomplishing each of these steps are given next.

The calendering equation, described in Chapters 2 and 4, gives permanent bulk reduction in terms of web speed S , roll radius R , nip load L and the paper properties: initial bulk B_i , sheet temperature Θ , and sheet moisture content M :

$$\varepsilon_p = A_p + \mu_p B_i \quad [\text{Eq. 6.1}]$$

where μ_p is the permanent calendering intensity:

$$\mu_p = a_{0p} + a_{Lp} \log_{10} L + a_{Sp} \log_{10} S + a_{Rp} \log_{10} R + a_{Mp} M + a_{\Theta p} \Theta \quad [\text{Eq. 6.2}]$$

The in-nip calendering equation complementing the above equation, described in Chapter 4, provides an empirical relationship relating in-nip paper deformation to the same calendering variables, and is expressed as:

$$\varepsilon_n = A_n + \mu_n B_i, \quad [\text{Eq. 6.3}]$$

where μ_n is the in-nip calendering intensity:

$$\mu_n = a_{0n} + a_{Ln} \log_{10} L + a_{Sn} \log_{10} S + a_{Rn} \log_{10} R + a_{Mn} M + a_{\Theta n} \Theta \quad [\text{Eq. 6.4}]$$

Equations 6.1 and 6.3 are valid between the limits:

$$-A_{p,n} / \mu_{p,n} \leq B_i \leq (1 - A_{p,n}) / 2\mu_{p,n}$$

Outside these limits a new set of equations must be used:

$$\begin{aligned} \varepsilon_{p,n} &= 0 & \text{if } B_i < -A_{p,n} / \mu_{p,n} \\ \varepsilon_{p,n} &= (1 - A_{p,n})^2 / 4B_i \mu_{p,n} & \text{if } B_i > (1 - A_{p,n}) / 2\mu_{p,n} \end{aligned}$$

Those limits are particularly important for the in-nip calendering equation because in-nip strains were shown in Section 4.1.2 to be generally above the upper limit of the calendering equation.

Both the permanent and in-nip versions of the calendering equation express strain relative to initial bulk, thus the calendering equation treatment may be applied successively for multiple nips, with the final bulk from the previous nip serving as the new initial bulk, Figure 6.1.

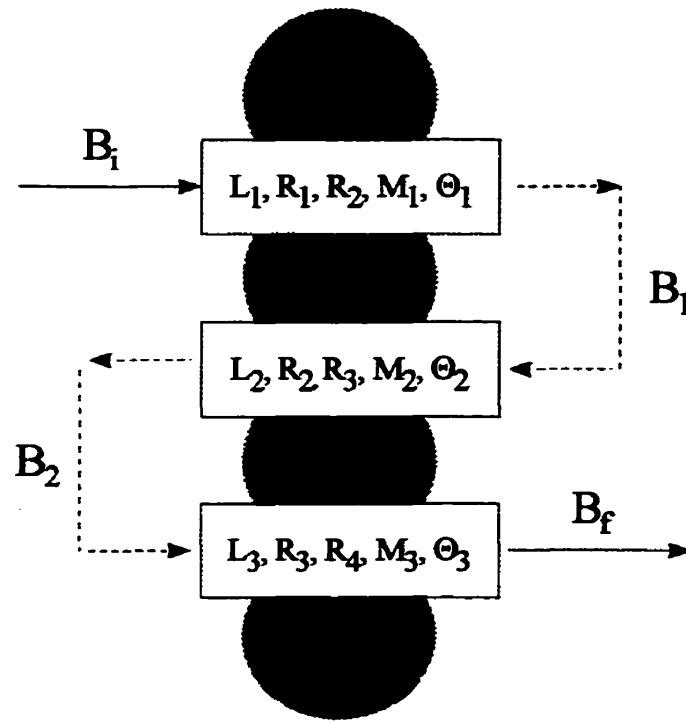


Figure 6.1: Simulation of multi-nip calendering

An equation of quite different form, referred to as the master creep equation (Section 4.5), provides an alternate mathematical form for relating both permanent and in-nip paper deformation to the same calendering variables:

$$\varepsilon_{n,p} = 0.5 (1 - \rho_i / \rho_{n,p_max}) [1 + \tanh(\mu_{n,p})] \quad [\text{Eq. 6.5}]$$

for which the permanent and in-nip calendering intensities, μ_p and μ_n , are defined as with the calendering equation:

$$\mu_{n,p} = a_{0n,p} + a_{Ln,p} \log_{10} L + a_{Sn,p} \log_{10} S + a_{Rn,p} \log_{10} R + a_{Mn,p} M + a_{\Theta n,p} \Theta \quad [\text{Eq. 6.6}]$$

with ρ_{n_max} and ρ_{p_max} the maximum density obtainable either in or after the nip, g/cm^3 , ρ_i is the initial paper density bulk, g/cm^3 , and thus the inverse of initial paper bulk (specific

volume) B_i . As in the calendaring equation, the permanent and in-nip versions of the master creep equation provide strain relative to initial bulk, thereby enabling both versions of Equation 6.3 to be used successively for multiple nips.

Dynamic deformation of a calender roll, $\Delta r(t)$, can be calculated from the maximum local deformation of the roll at steady state, Δr_{peak} , through using an exponential decay involving a roll deformation time constant τ :

$$\Delta r(t) = \Delta r_{peak} (1 - e^{-t/\tau}) \quad [\text{Eq. 6.7}]$$

Both the peak roll deformation and deformation time constant are functions of roll design and whether the roll is internally heated. Methods for computing those two parameters are shown in Chapter 5.

6.2 Calculation procedure for simulation of calendaring

The calculation procedure for calendaring simulation is shown as a block diagram in Figure 6.2. Both the calendaring equation and master creep equation have been shown in Section 4.5 to provide comparable results, thus either one can be used to estimate the in-nip strain at a specific CD position, given the permanent strain measured at that position. The in-nip and permanent versions of the calendaring equation, Equations 6.1 to 6.4, were chosen for present demonstration. The dynamic roll thermal deformation is given by Equation 6.7.

The required input data are:

- details of the calender stack configuration:

n : number of rolls in the stack

r_i : radius of each roll [mm], $i = 1, 2, \dots, n$

s_i : shell thickness of each roll [mm], $i = 1, 2, \dots, n$

whether each calender roll is internally heated.

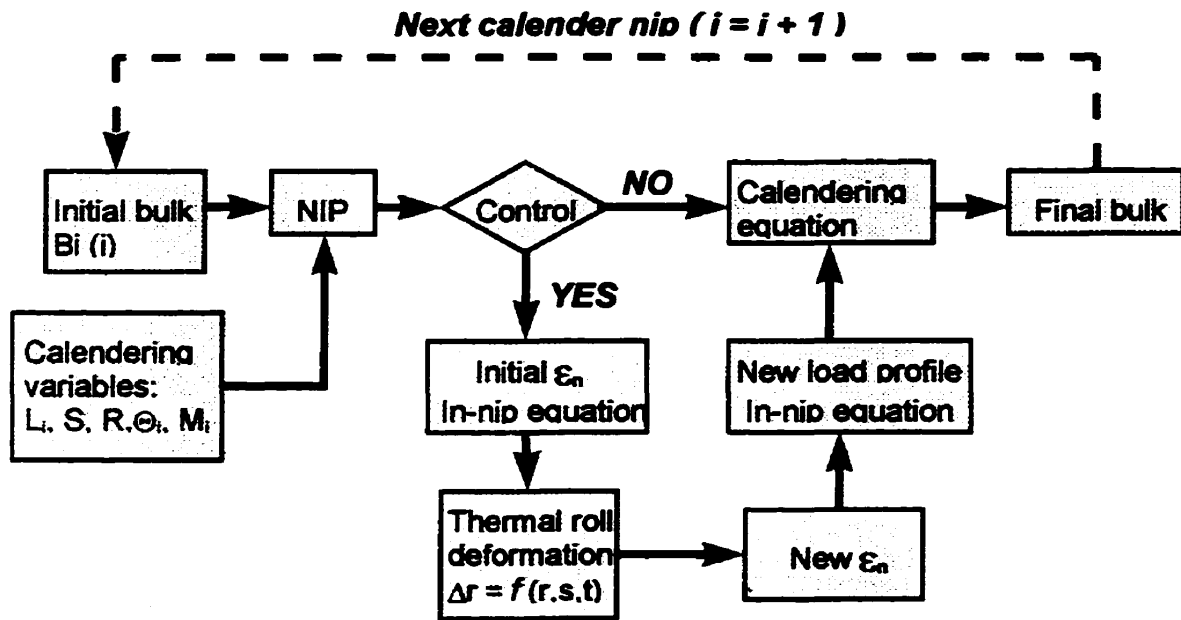


Figure 6.2: Procedure for simulation of multi-nip calendering

- calendering parameters:

S : machine speed [m/min]

L_i : initial local load for each nip [kN/m], $i = 1, 2, \dots, n-1$

W : sheet width [m]

- paper properties:

B_i : initial local paper bulk [cm^3/g]

Θ_i : local paper temperature entering each nip [$^\circ\text{C}$], $i = 1, 2, \dots, n-1$

M_i : local paper moisture content entering each nip [%], $i = 1, 2, \dots, n-1$

permanent and in-nip coefficients for the calendering equation.

The sheet width for this illustration was set at 6 m for the reasons explained in Section 6.3. The required input data also include the cross-direction profiles of local paper properties entering each nip - bulk, temperature and moisture content. The initial bulk entering each nip is that leaving the previous nip.

Although paper temperature can be measured accurately before each nip, such data may not be available. Alternately, the paper temperature leaving a nip can be estimated satisfactorily from the temperatures of the entering paper and the roll surface, as outlined by Hamel and Dostie [32] and Kerekes [50, 51].

Likewise, moisture content of the paper may be measured before each nip, but this is not practical. The paper moisture content in a nip may be estimated based on the measured value of moisture content either entering or leaving the calender stack, adjusted by 0.2 to 0.4 percentage points moisture loss per nip, depending on calender roll temperature [42].

To simplify the present illustration of the method for simulation of calendering, paper temperature and moisture content were assumed constant in the machine direction throughout the calender stack, i.e.

$$\begin{aligned} \Theta(i) &= \Theta_{\text{initial}} \\ M(i) &= M_{\text{initial}} \end{aligned} \quad [\text{Eq. 6.8}]$$

where i indicates the specific nip, $i = 1, 2, \dots, n-1$, for n rolls in the calender stack.

Average nip load can generally be determined from roll weight and applied force. Local nip load cannot be measured but must be calculated using the calendering equation applied for the measured CD thickness profile of the paper leaving the calender. The procedure for such calculations was proposed by Hamel et al. []. In the present illustration the initial profiles of local nip load were assumed uniform over the CD width of each nip, i.e. the local value of nip load in each nip was taken equal to the average value of nip load for that nip.

As the calender rolls forming a nip may differ in diameter, the Hertzian average roll radius

$$R = 2(R_i R_{i+1}) / (R_i + R_{i+1}) \quad [\text{Eq. 6.9}]$$

was used in the calendering equation.

When all the input data listed above are available for each nip, the simulation can start. The reduction of local paper bulk is calculated for each nip. If a particular nip is formed by two rolls, neither of which is used for CD control, the permanent version of the calendering equation, Equations 6.1 and 6.2, is used to calculate bulk reduction directly.

When only one of the two rolls is used for CD control the calculation procedure is more complicated. First the in-nip strain at time zero, ϵ_{n0} , is calculated for the given calendering parameters using the in-nip calendering equation, Equations 6.3 and 6.4, while the local thermal deformation of the calender roll as a function of time, $\Delta r(t)$, is determined from Equation 6.7. As the change in local roll deformation is equal and opposite to the change of in-nip paper thickness, then for a given time the new local in-nip strain is calculated as:

$$\epsilon_n(t) = \epsilon_{n0} - \Delta r(t) / (B_i BW) \quad [\text{Eq. 6.10}]$$

where:

t - time, min

B_i - initial bulk, cm^3/g

BW - paper basis weight, g/m^2

The in-nip calendering equation is then rearranged to yield the new local nip load, $L(t)$, which results from the change in the local pressure distribution caused by the change in local shape of the nip:

if $B_i < (1 - A_n) / 2\mu_n$

$$\log_{10} L(t) = ((\epsilon_n(t) - A_n) - B_i \mu_n^*) / B_i a_{Ln}$$

[Eq. 6.11]

if $B_i > (1 - A_n) / 2\mu_n$

$$\log_{10} L(t) = [(1 - A_n)^2 / 4B_i a_{Ln} \epsilon_n(t)] - \mu_n^* / a_{Ln}$$

where:

$$\mu_n^* = a_{0n} + a_{Sn} \log_{10} S + a_{Rn} \log_{10} R + a_{\Theta n} \Theta + a_{Mn} M$$

Average nip load, L_{avg} , remains the same before and after the control action, thus the resulting new CD profile of nip load can be estimated as:

$$L_{avg} = \frac{1}{W} \int_0^W L(t) dW \quad [\text{Eq. 6.12}]$$

The new local $L(t)$ is then used, along with other calendering variables, to calculate the final paper bulk using the permanent version of the calendering equation, Equation 6.1, this final bulk becoming the initial bulk for the next nip.

For the case of only one of the two rolls being used for CD control, if this control is exercised on one of the inner rolls of the calender stack the thermal deformation of this roll affects two nips. In this case the above procedure must be used for the next nip as well.

6.3 Simulation of single nip calendering

6.3.1 Effect of calendering parameters on control response

The first single-nip calender simulations were performed with two identical rolls. Internally heated rolls of radius 250 mm and shell thickness 120 mm were chosen, consistent with common practice in industry. The paper response to calendering was based on experimental data for a TMP newsprint, as reported in Chapters 3 and 4. The coefficients for the in-nip and permanent versions of the calendering equation are those listed in Tables 4.1 and 4.3. CD thickness control was simulated for the use of a cooling control jet installed on either of the identical rolls. The detailed configuration of the simulated control system is given in Section 5.1.

For this demonstration it is assumed that paper contacts the calender rolls only in the nip, which minimizes the effect on the average paper temperature and moisture content from heat transfer between the rolls and paper. Thus the initial values of these two paper

Table 6.1: Parameters for simulation of single-nip calendering

<i>Paper properties:</i>		<i>Process parameters:</i>	
TMP newsprint		S = 500 m/min	
BW = 48.8 g/m ²		L = 25 to 210 kN/m	
Θ = 30, 50, 80 °C		W = 6 m	
M = 2, 6, 8, 10, 12 %			
B _i = t _i /BW			
t _i = t ₀ + t _M M + t _Θ Θ [Eq. 4.9, Table 4.8]			
<i>Configuration of single-nip calender:</i>			
roll number	roll radius	shell thickness	roll type
1	R ₁ = 0.250 m	s ₁ = 120 mm	heated roll
2	R ₂ = 0.250 m	s ₁ = 120 mm	heated roll

properties are used as the input parameters for the calendering equation, regardless of the roll surface temperature. A detailed specification of the process is given in Table 6.1.

For a fixed step change in the control action coming from the local roll heating/cooling control device, the following calendering simulations illustrate the effect on paper response from three calendering parameters: nip load, paper temperature and moisture content. These tests were made for 9 combinations of those three influential calendering parameters in order to examine which combination gives the best control. For paper temperature and moisture content of 30 °C and 8%, five tests were performed with nip load varied from 25 to 210 kN/m. Results of these simulations are presented on Figure 6.3 in terms of change of a variable, thereby providing a clearer illustration of how the same step input control action affects paper response for various cases.

These results show that paper response to the step change in control action depends greatly on nip load. By inspection of the curve of each of the five simulations it is apparent that for any specific change of in-nip paper thickness, the associated change in

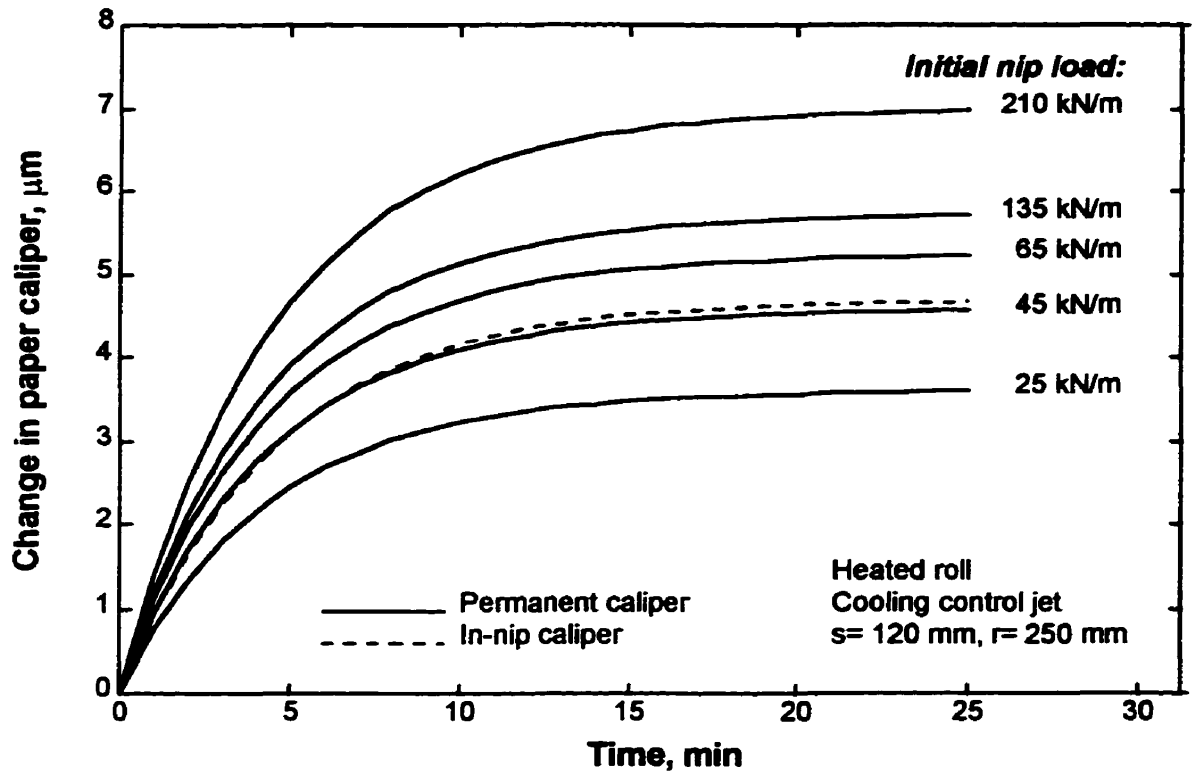


Figure 6.3: Effect of initial nip load on paper response: single nip control action

$L= 25$ to 210 kN/m, $\Theta= 30$ °C, $M= 8\%$, other parameters as listed in Table 6.1.

permanent thickness increases significantly with increasing local nip load. This sensitivity of the response to the level of nip load is however not constant over the range investigated. As shown in Figure 6.4, the change in permanent paper caliper after 25 minutes varies linearly with the logarithm of nip load over the entire range of nip loads investigated. At low nip loads the response is quite small ($3.6 \mu\text{m}$ at 25 kN/m), but the increase in this response with an increase in nip load is large ($0.5 \mu\text{m}$ increase per 10 kN/m). Conversely, at the top end of the nip load range the response is large ($6.6 \mu\text{m}$ at 135 kN/m) but the increase in this response with increasing nip load is small ($0.07 \mu\text{m}$ increase per 10 kN/m). For control purposes an intermediate nip load such as 65 kN/m might be optimal as both the response and the change in response to change in nip load are moderately high.

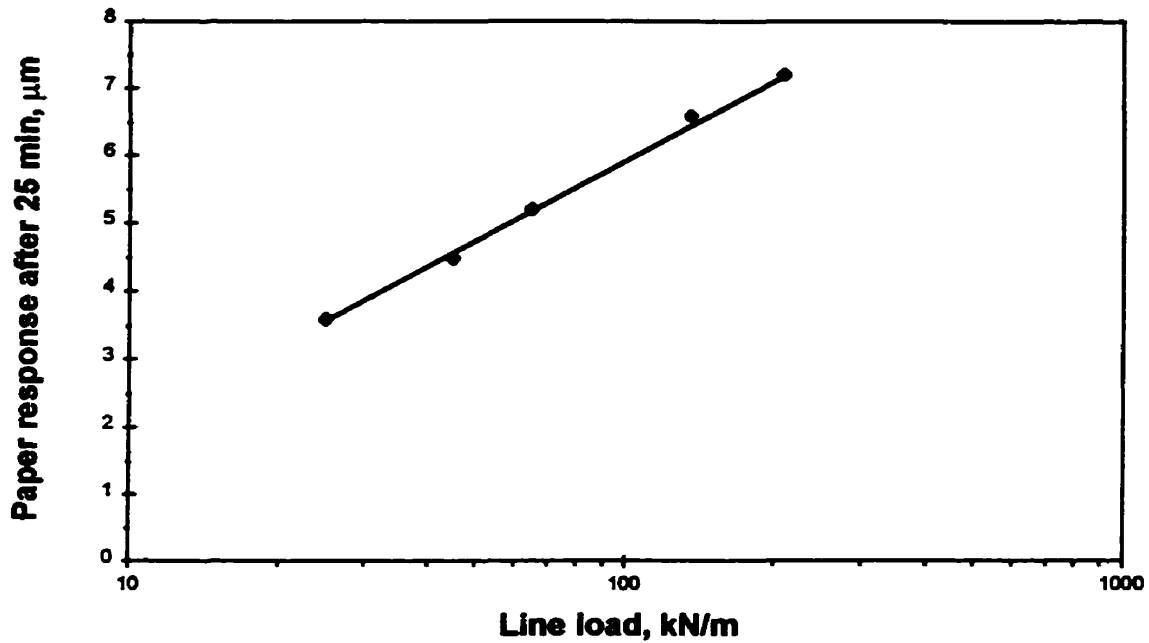


Figure 6.4: Effect of initial nip load on paper response after 25 minutes: single nip control action. $L= 25$ to 210 kN/m, $\Theta= 30$ °C, $M= 8\%$, other parameters as listed in Table 6.1.

The more sensitive paper response to a change in control action at higher nip loads derives from the visco-elastic behaviour of paper in the calender nip. Recent work from this laboratory by Browne et al. [6, 7] and the present study (Chapter 4) establishes that although the relationship between permanent paper strain and logarithm of nip load is essentially linear over the industrially relevant range of loads, this is not so for in-nip strain. For loads lighter than industrial practice the in-nip compression of paper is mostly elastic, hence the paper subsequently recovers most of its thickness. For heavy nip loads, with paper compression in the nip as high as 55% - 65%, further compression is more permanent.

Nip loads are chosen to satisfy paper quality requirements. Results presented on Figures 6.3 and 6.4 show that over the entire range of nip load considered, effective control can be achieved. Provided paper quality requirements are satisfied, for achieving

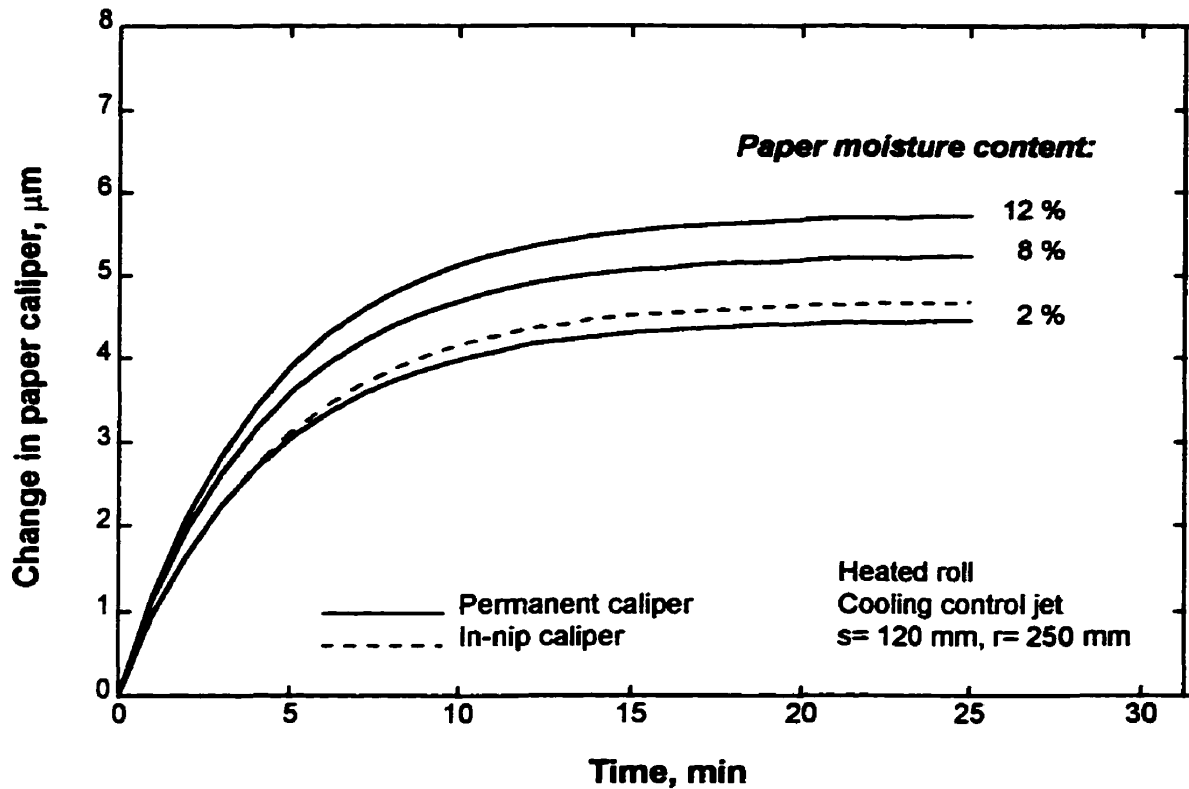


Figure 6.5: Effect of moisture content on paper response: single nip control action

$L = 65 \text{ kN/m}$, $\Theta = 30 \text{ }^\circ\text{C}$, $M = 2 \text{ to } 12\%$, other parameters as listed in Table 6.1.

CD uniformity of paper caliper effectively a load of approximately 65 kN/m would be desirable, i.e. high enough to provide in-nip compression which exceeds the elastic behaviour but low enough to prevent reduction in product quality from excessive calendering.

Paper temperature and moisture content are effective for influencing paper compressibility because increasing either parameter makes the fibers more pliable and plastically deformable. Figure 6.5 gives the results of simulating the response of $30 \text{ }^\circ\text{C}$ paper to a control action for nip load of 65 kN/m over the moisture content range 2 to 12%. The paper response both at short times and the steady state limit are seen to increase with paper moisture content over this range. For calendering at this temperature and nip load the change in permanent paper thickness after 25 minutes is 4.2, 5.2 and 5.8 μm for paper moisture content respectively of 2, 8 and 12%. This response is seen on

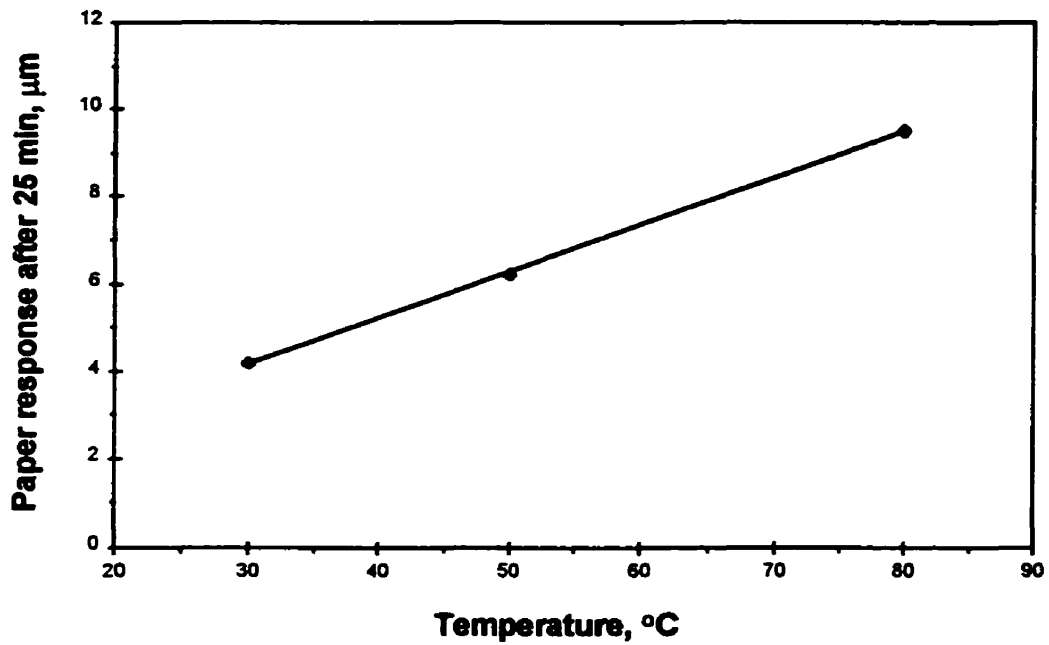
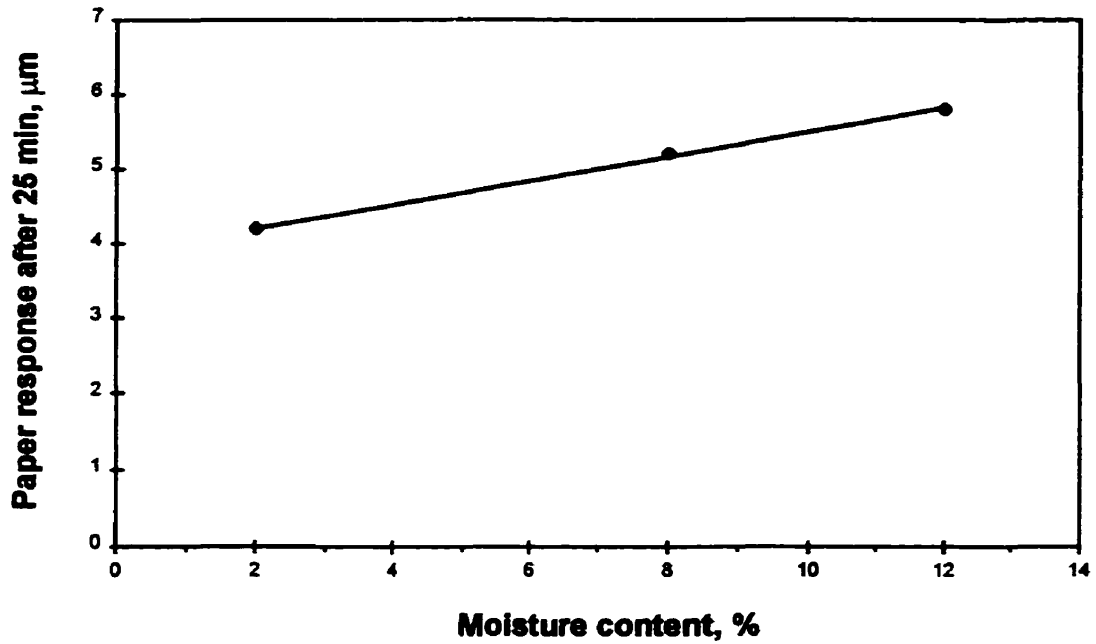


Figure 6.6: Effect of moisture content and temperature on paper response after 25 minutes: single nip control action.

a) $\Theta = 30^{\circ}\text{C}$, $M = 2$ to 12% ,

b) $\Theta = 30$ to 80°C , $M = 2\%$,

$L = 65 \text{ kN/m}$, other parameters as listed in Table 6.1.

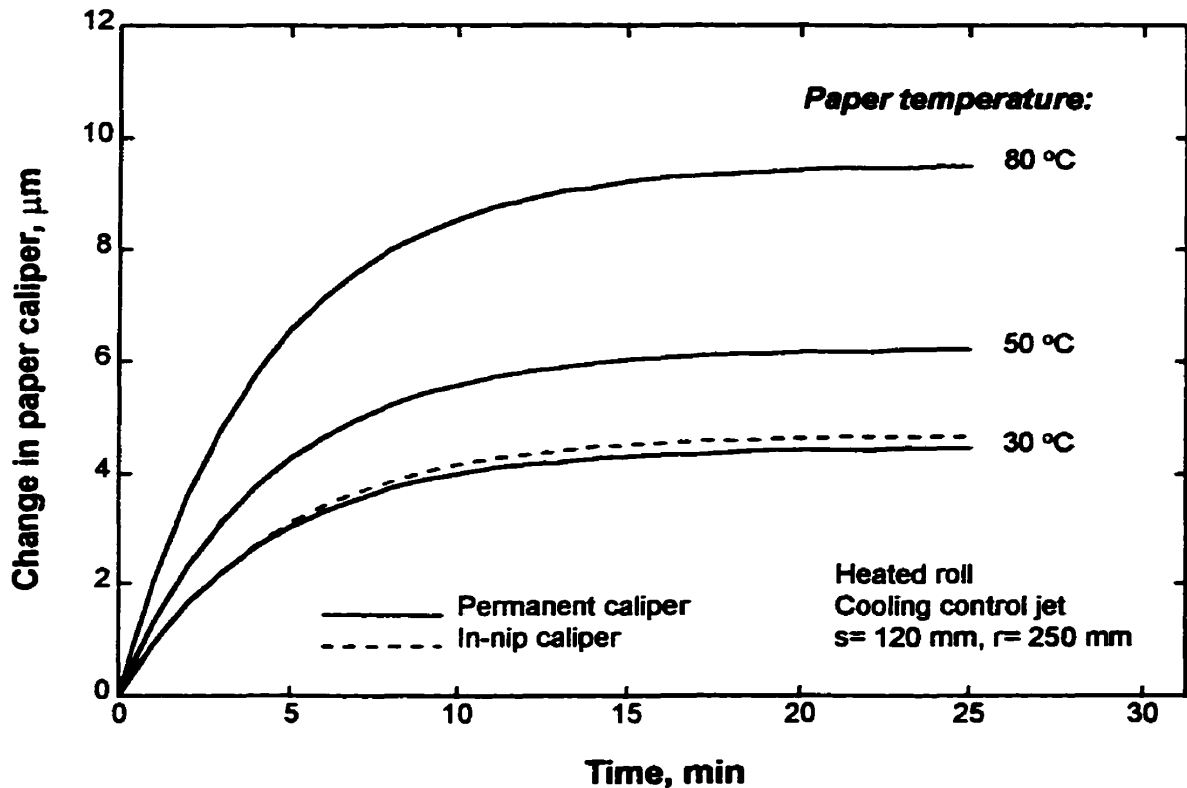


Figure 6.7: Effect of temperature on paper response: single nip control action

$L = 65 \text{ kN/m}$, $\Theta = 30 \text{ to } 80 \text{ }^\circ\text{C}$, $M = 2\%$, other parameters as listed in Table 6.1.

Figure 6.6a to be linear with moisture content, with a slope of $0.16 \text{ } \mu\text{m}$ per percentage point of moisture content. As the $4.2 \text{ } \mu\text{m}$ change in permanent paper thickness which requires 65 kN/m nip load for calendering paper of 2% moisture content, as noted above, could be obtained with only a 45 kN/m nip load for paper of 8% moisture content, Figure 6.4, the high effectiveness of increased moisture content is apparent. Another such comparison is that to obtain the same $5.2 \text{ to } 5.8 \text{ } \mu\text{m}$ increase in paper response under 65 kN/m nip load through increasing the moisture content from $8 \text{ to } 12\%$, as noted above, would have required a major nip load increase, from $65 \text{ to approximately } 95 \text{ kN/m}$, had moisture content remained at 8% . Obtaining the same calendering control action response through reducing the nip load but increasing the paper moisture content is advantageous because lower load may eliminate the degradation of paper quality caused by excessive nip load.

The simulation results shown on Figure 6.7 indicate that, as for the case of increasing moisture content, increasing the paper temperature improves the paper response to a control action at a specific nip load. As the temperature for paper of 2% moisture content is increased from 30 to 50 to 80 °C, both the short term and steady state paper response is seen on Figure 6.6b to increase dramatically: the response 25 minutes after a step change in control action is changed from 4.2 μm for 30 °C paper, to 6.1 μm for 50 °C paper, to 9.5 μm for 80 °C paper, a change of 1.1 μm per 10 °C. Although these results demonstrate the effect, use of such a low moisture content is uneconomic, with moisture contents of 6 to 8% being normal practice. In the other direction, previous studies showed that increasing paper moisture content higher than 15 to 20%, depending on paper temperature, eventually causes permanent strain to decrease, not increase. The Chapter 4 experimental results showed that with other calendering conditions fixed, the permanent deformation increases with paper moisture content only up to about 14% moisture content.

Such behaviour for permanent deformation is even more evident for in-nip behaviour. For 30 °C paper the in-nip deformation actually passes through a maximum at about 8% moisture content. As for permanent deformation, the evidence is that with increasing temperature the moisture content for the occurrence of the maximum in in-nip deformation shifts to lower values. Thus the use of high paper temperature and high moisture content can be beneficial for improving the local paper response to a control action, but this may also require using undesirably high nip loads in order to maintain the required overall reduction of paper bulk. Furthermore, high paper temperature and moisture content also increases paper sensitivity to such disturbances as temperature and moisture streaks. An attractive compromise is use of a combination of moderately higher moisture content and temperature. Figure 6.8 shows the simulation results for 50 °C paper at two moisture contents, 6 and 10%. Such combinations give a strong response of the paper to the standard step change in control action, this response after 25 minutes reaching 6.8 μm for 6% moisture, 7.2 μm for 10% moisture. However, as is the case with nip load, process and paper quality considerations generally govern the operating levels of

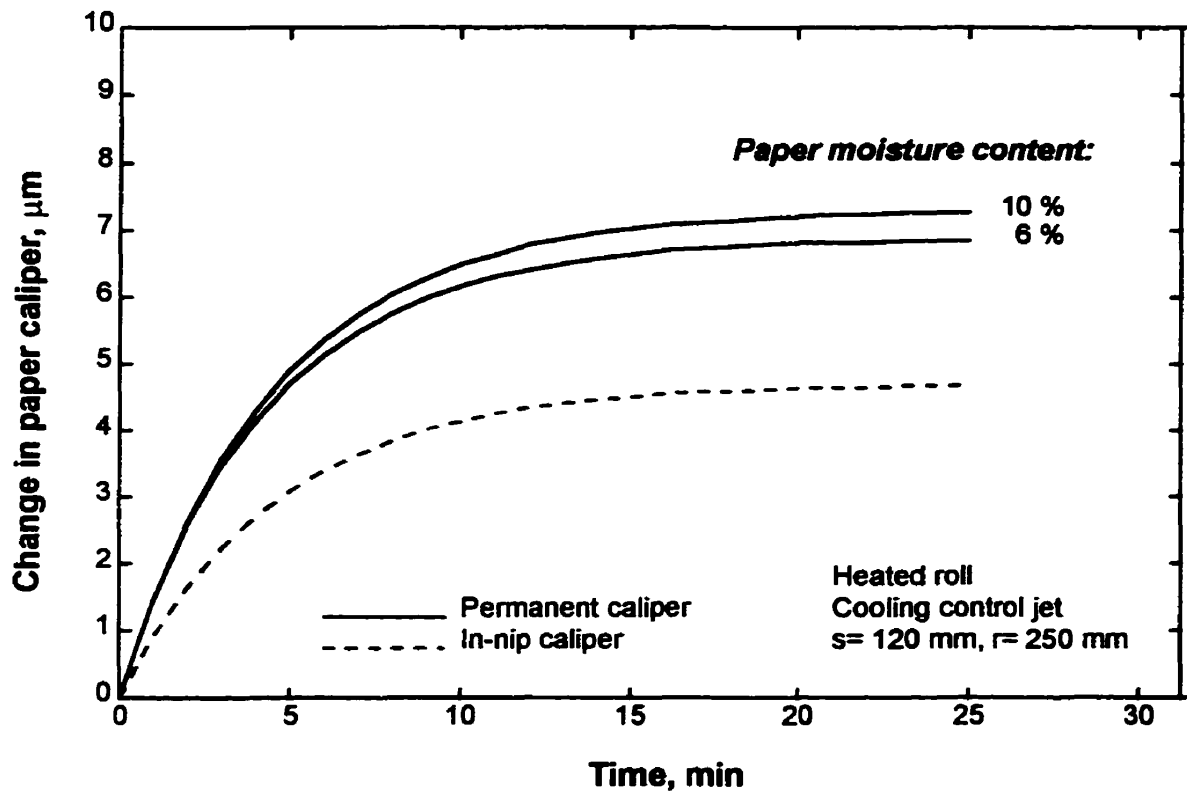


Figure 6.8: Effect of temperature and moisture content on paper response: single nip control action.

$L = 65 \text{ kN/m}$, $\Theta = 50 \text{ }^\circ\text{C}$, $M = 6 \text{ to } 10\%$, other parameters as listed in Table 6.1.

paper temperature and moisture content. The choice of actuator location will be facilitated by knowing how these variables affect the control action.

This sensitivity to changes in temperature and moisture content also creates a problem in calender control, as the most common disturbances that require action by the control system are temperature and/or moisture streaks. Such streaks must be compensated for by the control system, using adjustments in the cross-direction nip load profile and to some extent, the temperature profile. Fortunately there is some synergy in the control effects of nip load, temperature and moisture content. A hot streak in the paper from overdrying at that position will be associated with a lower caliper. Cooling the calender rolls serves both to reduce the paper temperature and the nip load. Both will

contribute to achieving a higher caliper after calendering. A moisture streak will often be cooler than the dryer paper. Local heating of the calender roll will then compensate for the effect of the moisture streak. However, the best way to deal with moisture streaks is to eliminate them ahead of the calender. Such correction should be done well before the calender as a moisture correction system in the immediate vicinity of the calender could interfere seriously with the control system, particularly since the dynamics of the two systems are very different. Thus taking advantage of the fast response from using moisture correction for calender control is likely to create paper quality problems (i.e. roll structure and print quality problems).

6.3.2 Model Predictive Control: Single nip calendering

Although the steady state response of paper to a control action must be large in a good CD control system, another important control performance characteristic is the speed of response. So far, all simulations illustrated here were performed for a single step change in control action, thus the time required to reach a 95% approach to steady state is the same for each case, approximately 25 minutes. To improve the response time a more powerful control action is required. Thus simulation of paper response to a two-step control action is presented on Figure 6.9 for nip load of 65 kN/m, paper moisture content and temperature of 6% moisture and 50 °C. The value of the peak roll deformation at steady state was assumed to be proportional to the strength of control action.

Figure 6.9 shows the change in control action normalised relative to the single step change used for the previous simulations. The strength of the first step control action was doubled from that used previously in order to decrease the time required to bring the system to steady state. As paper response approached the target value, the strength of this simulated control action was reduced by half to maintain this desirable change in permanent caliper. The simulation results indicate that initial doubling of the control action improves the speed of paper response substantially, with the time required to reach a 95%

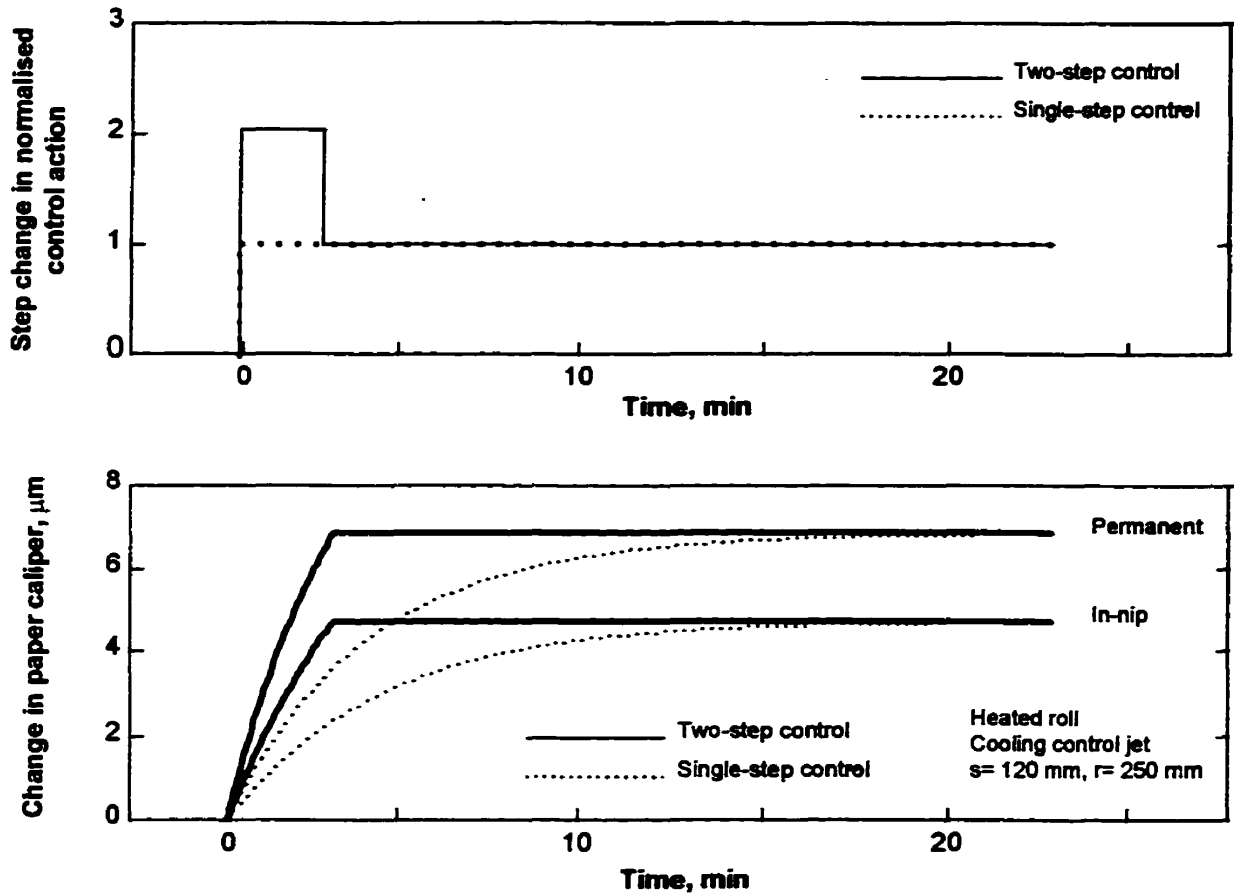


Figure 6.9: Comparison of single and two-step actuator change on speed of paper response: single nip control action

$L= 65 \text{ kN/m}$, $\Theta= 50 \text{ }^\circ\text{C}$, $M= 6\%$, other parameters as listed in Table 6.1.

approach to steady state reduced from 25 minutes for single step control, to 3.2 minutes for two-step control.

The sharp change in the paper response curves at the change from high to low actuator strength is due to the simulation procedure, which does not account for the thermal inertia of the system. Thermal inertia would cause a smoother transition than indicated in Figure 6.9. To take thermal inertia into account would however require use of the full numerical solution to calculate roll deformation, which would add considerable complexity for a small gain in fidelity. The essential conclusion is that a creative

application of model predictive control for calendering has been demonstrated for the first time, and that this basis of control is shown to reduce dramatically the response time for CD control of calendering.

6.4 Simulation of multi-nip calendering

6.4.1 Single calender stack

In the performance of a system for local CD calender control of paper thickness the effect of actuator position within a calender stack is a major parameter. The technical literature on this subject contains divergent recommendations as to the optimum position for CD control actuators. Based on experimental measurements on commercial calenders Lyne et al. [57] and Mitchel and Sheahan [61] concluded that the best placement of the CD control system is on the bottom (king) roll. Fjeld and Hickey [23] speculated that from the viewpoint of feedback control theory the location where the thickness correction takes place is irrelevant, and that the optimal place for CD thickness control is then on the second roll from the top. Kahoun et al. [44] suggested that the best way to control the CD uniformity of paper thickness is by altering the CD temperature profile of the paper web entering the calender stack. None of these recommendations takes into consideration the effect of either roll design, thermal conditions or the stress-strain relationships for paper in the nip or its rheological behaviour after the nip. The preferred location in industrial practice has been on the third or fourth roll from the bottom [43].

The measurements most relevant to this question are those of Journeaux et al. [42, 43] giving paper response to a step change in control action, with the control action coming from local heating/cooling jets on the rolls of an industrial newsprint calender. The nature of the control actuator, i.e. whether it provides local heating or cooling, or whether with air jets or electrically, is relevant to the basic question. With the control jets installed on a different roll for each test, the objective of their work was to determine the location for best control. Those measurements showed that effecting CD control on the second roll from the bottom of the calender stack (queen roll), or the roll immediately above,

produces respectively the strongest and second strongest response to a control action, both short term and steady state. The king roll and the top roll in the stack were found to be the two poorest choices. Thus their work disproved recommendations from some of the earlier literature. They also showed, for two identical calender stacks used in series, the ineffectiveness of the second stack which provided very little control over local paper thickness. Thus the Journeaux et al. measurements on an industrial calender provide a broad insight into expected trends with CD control of calendering.

The dynamic model of calendering obtained in the present study was used to simulate the calendering of newsprint, the grade of paper used for the Journeaux et al. measurements [42, 43]. The first three simulations were carried out on a single calender stack, Figure 6.10, with eight rolls. The first simulation, for the specifications shown in Table 6.2, was performed for a stack having rolls all of the same design and thermal parameters, and with the same values of initial load in each nip. Such a case, which never occurs in practice, serves to show how the location of the control device affects the paper response to a specific control action, independent of differences in roll design and thermal conditions. The calender roll dimensions chosen (250 mm radius, 120 mm shell thickness) are however commonly found in industry.

Paper response was based on experimental data obtained here for a TMP newsprint, Chapters 3 and 4. The coefficients for the in-nip and permanent versions of the calendering equation are listed in Tables 4.1 and 4.3. CD thickness control was simulated for a heating control jet installed on one of the calender rolls; a detailed configuration of the control system simulated is given in Section 5.1. Using procedures outlined in Section 6.2 the final paper response to the standard step change in control action was calculated for control effected on each of the eight positions.

Figure 6.11 shows that the largest effect is obtained with the control jet installed on the second roll from the bottom, the queen roll, the response becoming progressively less for each higher position. The small response for the actuator on the king roll (number 8) is similar to that with the control actuator installed on a roll near the middle of the stack. Thus a thickness correction made on any roll near the bottom of the stack, with the

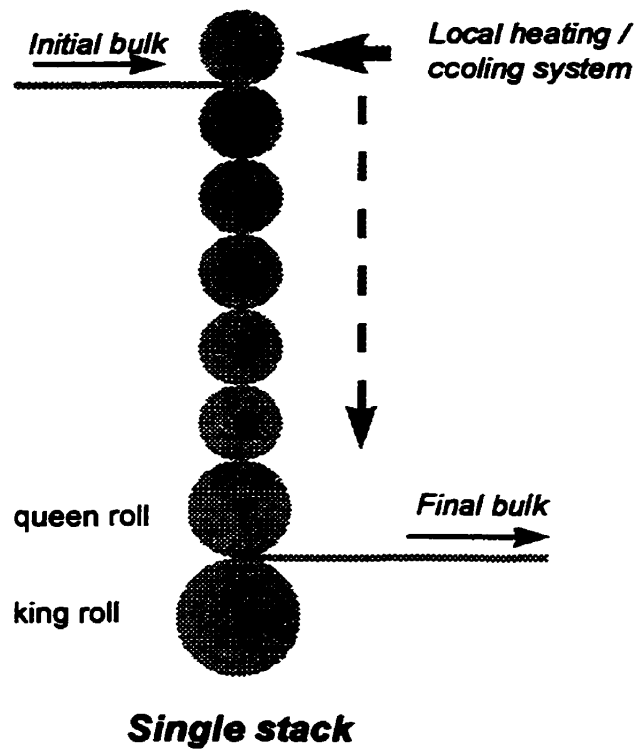


Figure 6.10: Single calender stack for simulation

Table 6.2: Parameters for single calender stack simulation, Case 1.

<i>Paper properties:</i>	<i>Process parameters:</i>		
$B_{i0} = 2.23 \text{ cm}^3/\text{g}$	$S = 500 \text{ m/min}$		
$BW = 48.8 \text{ g/m}^2$	<i>Initial nip load from top to bottom of the stack:</i>		
$\Theta = 55 \text{ }^\circ\text{C}$	$L_i = 65 \text{ kN/m}, i= 1 \text{ to } 7$ for the 1 st through 7 th nip		
$M = 6 \%$			
<i>Calender stack configuration from top roll (1) to bottom roll (8):</i>			
radius	shell thickness	roll type	roll temperature
$R_i = 0.250 \text{ m}$ for $i= 1 \text{ to } 8$	$s_i = 120 \text{ mm}$ for $i= 1 \text{ to } 8$	heated roll	$\Theta_i = 55 \text{ }^\circ\text{C}$ for $i= 1 \text{ to } 8$

exception of the lowest roll, is much more effective than if made on the upper nips. This trend reflects the very non-linear behaviour of paper in the nip of a calender, as documented in Chapter 4. Rolls number 1 and 8 are special cases. Whereas for all other locations of a control actuator there are two nips affected (nips with the roll above and below that with the control device) a control action on the top or bottom rolls of the stack affects only a single nip.

With control exercised on rolls 2 and 3 the Figure 6.11 response curves clearly have two sections, a very low response at short times, then a much larger response subsequently. For the relatively low compression experienced by paper in the nips near the top of the stack this break point in behaviour is a consequence of paper deformation being linear and elastic for the low strain during the period immediately following the control action. By contrast, paper deformation becomes quite nonlinear and inelastic with the higher strains reached later. The predominantly elastic deformation represented by the linear part of the calendering equation produces the low response seen on Figure 6.11 at short times. When at larger times the deformation becomes less elastic, more permanent, the Figure 6.11 curves for control on rolls 2 and 3 are seen to provide more effective control. With the level of nip load increasing from rolls 2 to 3 to 4, the region over which paper behaviour is quite elastic and described by the linear part of the calendering equation is largest for roll 2, smaller for roll 3, and is disappearing for roll 4. As the control system is moved down the stack the paper deformation caused by the same control action becomes mostly permanent, which in turn makes caliper control more effective. The ineffectiveness of the upper nips for control is even more striking because these nip loads, as used in this simulation, are much higher than in industrial practice.

One effect not taken into consideration is transport of heat from local heating/cooling control down the stack with the paper. Results from Journeaux [42] show that the local roll surface temperature peak, depending on roll radius and shell thickness, can reach 3 to 5.5 °C for a heated roll, 6 to 8 °C for an unheated roll. This local temperature disturbance is passed down the stack by the paper, causing local cooling or heating of the rolls. As this effect moves down the stack it spreads axially along length of the roll, thus introducing very long dynamics. However as a relatively small change in

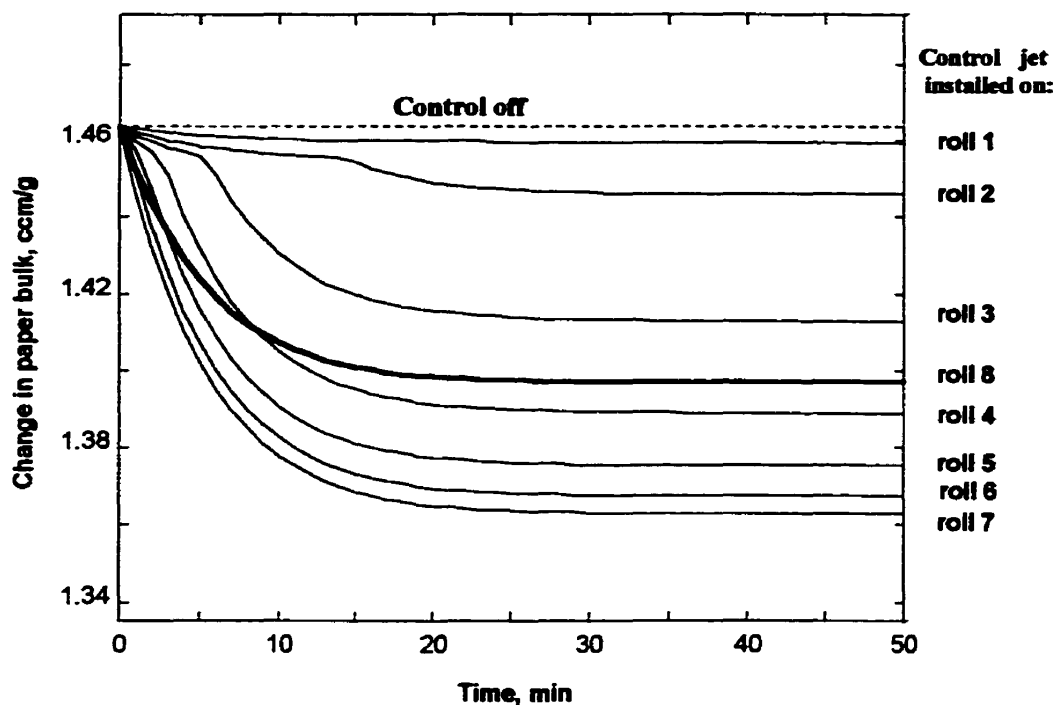


Figure 6.11: Effect on final paper bulk of location of control actuator, Case 1

local roll temperature compared to that induced by the control actuator, in the order of 20 °C change at steady state for the system used by Journeaux, this effect can be neglected.

Further to the speed of response aspect of control performance characteristics, the Figure 6.11 simulations indicate that, with the control jet located on any of the top four rolls, 50% of the steady state response occurs within 6 to 9 minutes. When the control jet is installed on any of the bottom four rolls, it takes less than 5 minutes to achieve 50% of the steady state response. This response time improvement for control on the lower rolls reflects the absence here of the ineffective time when paper in the upper nips is in its primarily elastic behaviour.

Paper response to a corrective control action depends on two parameters: location of the control device within the stack, and the roll geometric and thermal conditions. The first simulation, Figure 6.11, tested only the first aspect, actuator location, and this with the line load constant in all nips. The Case 2 simulation is for the more realistic calender

Table 6.3: Parameters for single calender stack simulation, Cases 2 and 3.

Paper properties:

$$B_{i0} = 2.23 \text{ ccm/g}$$

$$BW = 48.8 \text{ g/m}^2$$

$$\Theta = 55 \text{ }^\circ\text{C}$$

$$M = 6 \%$$

Process parameters:

$$S = 500 \text{ m/min}$$

Initial nip load from top to bottom of the stack:

$$L_1 = 13.3 \text{ kN/m}$$

$$L_2 = 26.6 \text{ kN/m}$$

$$L_3 = 39.9 \text{ kN/m}$$

$$L_4 = 53.2 \text{ kN/m}$$

$$L_5 = 66.5 \text{ kN/m}$$

$$L_6 = 79.8 \text{ kN/m}$$

$$L_7 = 99.5 \text{ kN/m}$$

Calender stack configuration from top roll (1) to bottom roll (8):

radius	shell thickness	roll type	roll temperature
$R_1 = 0.178 \text{ m,}$	$s_1 = 128 \text{ mm,}$	unheated roll	$\Theta_1 = 55 \text{ }^\circ\text{C}$
$R_i = 0.178 \text{ m,}$ for $i= 2 \text{ to } 5$	$s_i = 128 \text{ mm,}$ for $i= 2 \text{ to } 5$	heated roll	$\Theta_i = 55 \text{ }^\circ\text{C}$ for $i= 2 \text{ to } 5$
$R_6 = 0.178 \text{ m,}$	$s_5 = 128 \text{ mm,}$	heated roll - Case 2 unheated roll - Case 3	$\Theta_5 = 55 \text{ }^\circ\text{C}$
$R_7 = 0.238 \text{ m,}$	$s_5 = 178 \text{ mm,}$	heated roll	$\Theta_5 = 55 \text{ }^\circ\text{C}$
$R_8 = 0.355 \text{ m,}$	$s_5 = 355 \text{ mm,}$	solid roll	$\Theta_5 = 55 \text{ }^\circ\text{C}$

stack configuration given in Table 6.3, one resembling the calender of the Journeaux et al. [42, 43] measurements. The paper response was again calculated as outlined in Section 6.2, based on data obtained in the present study, Chapter 4. For all positions of the heating control jet Figure 6.12 shows the response to a fixed step change in control action.

As for the first simulation, the paper response for Case 2 again becomes both stronger and faster with the control effected lower in the stack. The very small response

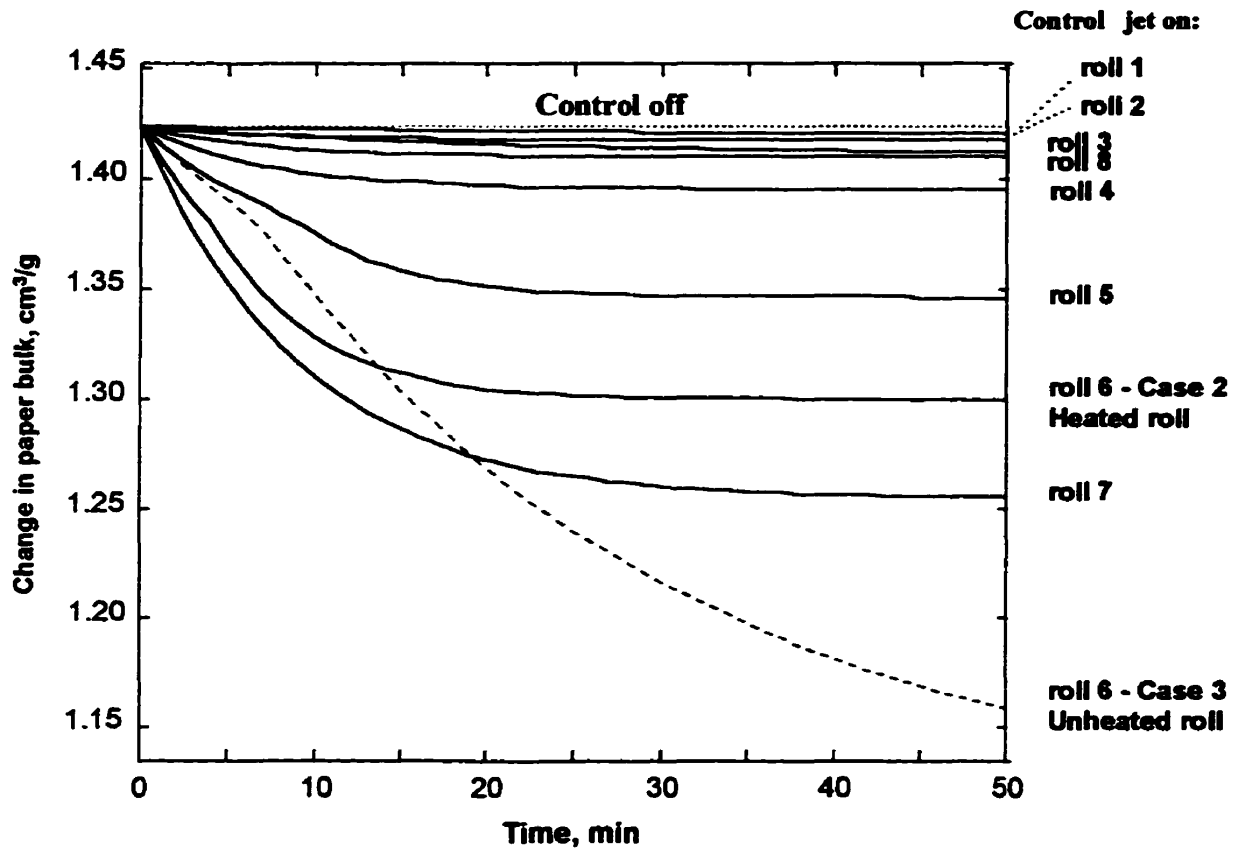


Figure 6.12: Effect on final paper bulk of location of control actuator, Cases 2 and 3

obtained with the control installed on any of the top four rolls, apparent on Figure 6.12, is caused by the low line loads, with the stress-strain behaviour of paper even more predominantly in the elastic domain than for the previous simulation. For the industrial calender conditions used for Case 2, the effect of actuator location is much more significant than for Case 1, Figure 6.11. The response recorded on Figure 6.12 for control on any of the top four rolls or on the king roll is simply negligible. Between rolls 4 and 7, as the control jet is moved down the stack, roll by roll, there is a big improvement in both the short term and steady state response.

It is worth examining why the response with control on the king roll is much worse yet for Case 2 than the Case 1 simulation. Figure 6.12 shows that, even with the high line load, the response for roll 8 is essentially as insignificant as that for the light line load of

roll 3. There are two causes, both relating to roll geometry: the Case 2 king roll radius is larger (60% larger than the queen roll, more than twice that of the other rolls and more than 40% larger than the Case 1 king roll), and it is the only solid roll in the stack. It was shown by Journeaux [42] and again here in Chapter 5 that for a fixed shell thickness the steady state thermal deformation decreases with increasing roll radius. It is the pressure to which paper is subjected that causes its deformation, and for a specific line load the pressure decreases with increasing roll radius as the line load is distributed over a wider nip. The deformation time constant is also much larger for solid than hollow shell rolls. Thus the much better king roll response in the Case 1 simulation derives from two roll design differences: a small, hollow shell king roll (Case 1) vs. a large solid one (Case 2). Of these two effects the dominant one is obviously roll diameter, thereby giving the greatly reduced steady state response of Figure 6.12, which is only 20% of that for Case 1, Figure 6.11.

Although the steady state response of paper is significantly higher when control action is located on the queen roll than on the roll just above, by contrast there is a small difference in the dynamic response over the first 10 minutes for rolls 6 and 7, Figure 6.12 - Case 2 simulation. For longer than 10 minutes after the control action the larger steady state deformation from the higher line load of the queen roll determines the larger response of roll 7. The smaller difference over the first 10 minutes results from the effect of roll design. Of the two rolls, both heated, the queen roll is of larger radius: 238 mm compared to 178 mm, and of larger shell thickness, 178 mm vs. 128 mm. For an internally heated roll, the deformation time constant is much less sensitive to roll radius than to shell thickness, increasing substantially with increasing shell thickness, Figure 5.4 (Chapter 5). Thus the short response time for control on these rolls is subject to two effects: the queen roll has the higher nip load, giving it a faster response, but has the thicker shell, giving a slower response. For about the first 10 minutes after a control action the slower response from the thicker shell of the queen roll is seen on Figure 6.12 to be the more important of these two effects, giving a slower response of roll 7 than roll 6.

Based on their theoretical study Journeaux [42] concluded that locating control on an unheated thin-walled roll situated above a heated queen roll would give local CD

control superior to that performed on a thick-walled queen roll. Their prediction was tested here using the Case 3 configuration of the stack, that modified from Case 2 by changing roll 6, the roll just above the queen roll, from internally heated to an unheated roll, Table 6.3, all else remaining the same. With the control action the same as for Cases 1 and 2, Figure 6.12 shows the results of this test as the Case 3 simulation.

The steady state paper response with the control jet on unheated roll 6 is shown to be far superior, by about 50%, than that obtained for control on the queen roll. However it takes about 20 minutes for control on roll 6 to surpass that on the queen roll. After 10 minutes for example, the response with control on the unheated roll 6 is only about $\frac{2}{3}$ of that with control on the thicker-walled, heated roll 7. Thus for the specifications of rolls 6 and 7 used for this test, paper deformation with the thicker-walled, heated queen roll is better for the first 20 minutes after the control action, but control on the thinner-walled, unheated roll above the queen roll is substantially better thereafter.

Experimental results from Journeaux et al. [42, 43] on change in paper caliper for the effect of control jet position within the stack of an industrial calender are given in Figure 6.13b. They measured paper response to a step change in control action with control coming from a cooling jet placed successively on four of the rolls. For comparison, the dynamic model of calendering obtained in the present study was used to recreate their measurements. The simulation was carried out for the calender stack configuration given in Table 6.3 (Case 2), one approximating the calender of their experiments. For clarity the Journeaux et al. roll notation is related to that used here as follows: their roll A1 stands for roll 8 here (king roll), C1 for roll 6, D1 for roll 5, and F1 for roll 3. The paper response was again calculated as outlined in Section 6.2, based on data obtained in the present study, Chapter 4. For all positions of the cooling control jet Figure 6.13a shows the response to a fixed step change in control action in the form of change in final paper caliper.

In both cases the largest effect, both short term and steady state, was with the control jet on roll 6 (C1), with progressively smaller effects on rolls 5 (D1) and 3 (F1).

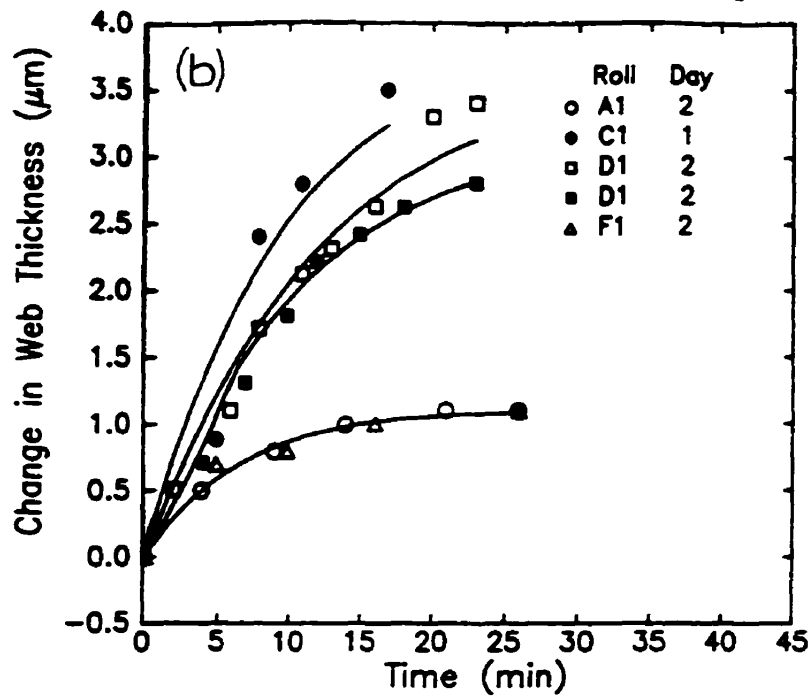
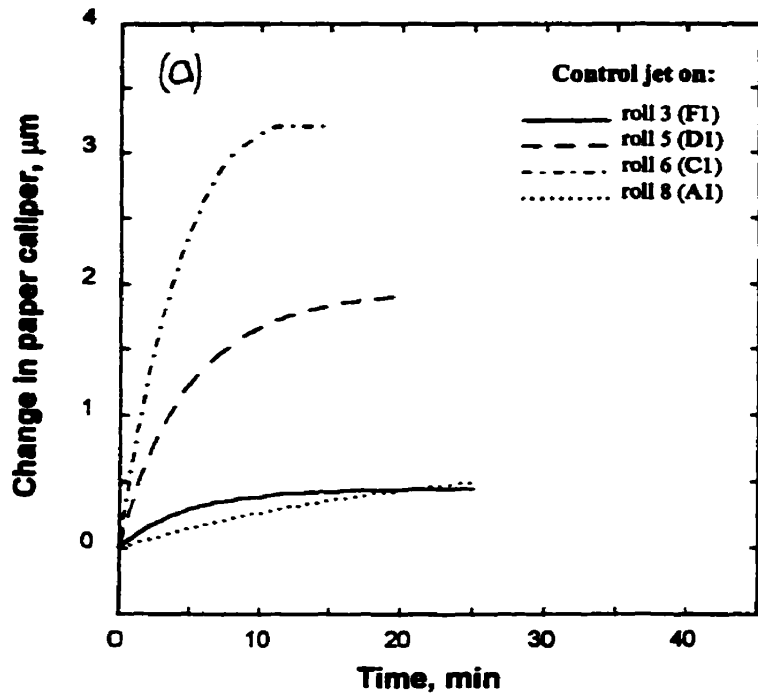


Figure 6.13: Measured and predicted effect of control actuator position: single stack

a) simulation results, present study

b) experimental results, industrial calender, Journeaux et al. [42, 43]

The solid king roll, roll 8 (A1), shows a very weak response to the control jet, effectively indistinguishable from that of roll 3 located near the top of the stack. The general trends and magnitude of these responses, as predicted on Figure 6.13a, as measured on Figure 6.13b, are remarkably close, given some difference in operating conditions and the paper used. The demonstrated consistency between the results measured and simulated for an industrial calender provides validation of the correctness of the dynamic model of calendering developed in the present study.

6.4.2 Double calender stack

The next simulation is for the double calender stack of Figure 6.14. The two stacks are identical, each being the configuration used in the Case 2 simulation, Table 6.3. The permanent paper response to a specific step change in control action for a heating control jet was calculated for two alternatives: first, control on the queen roll on both stacks; second, control on the queen roll of the first stack only.

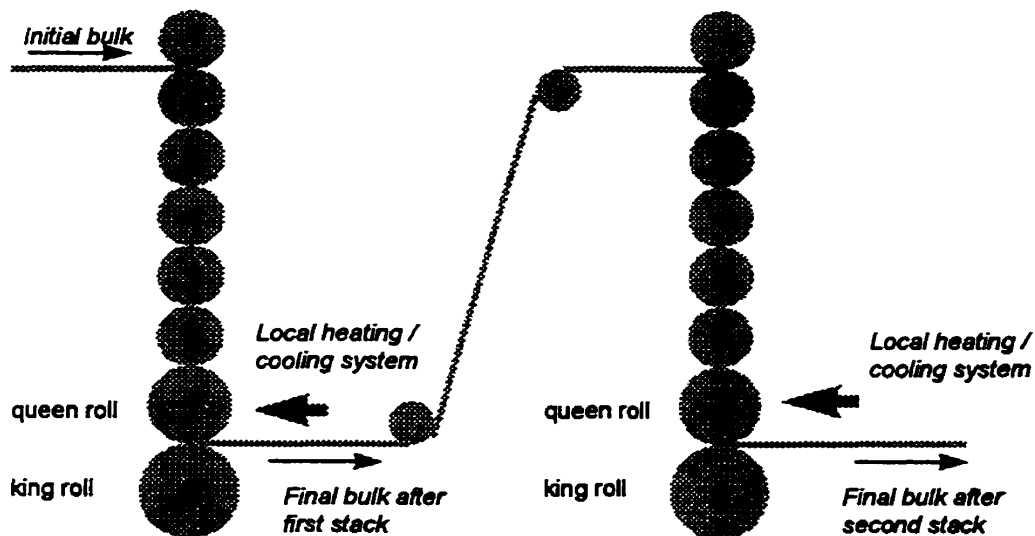


Figure 6.14: Double calender stack for simulation

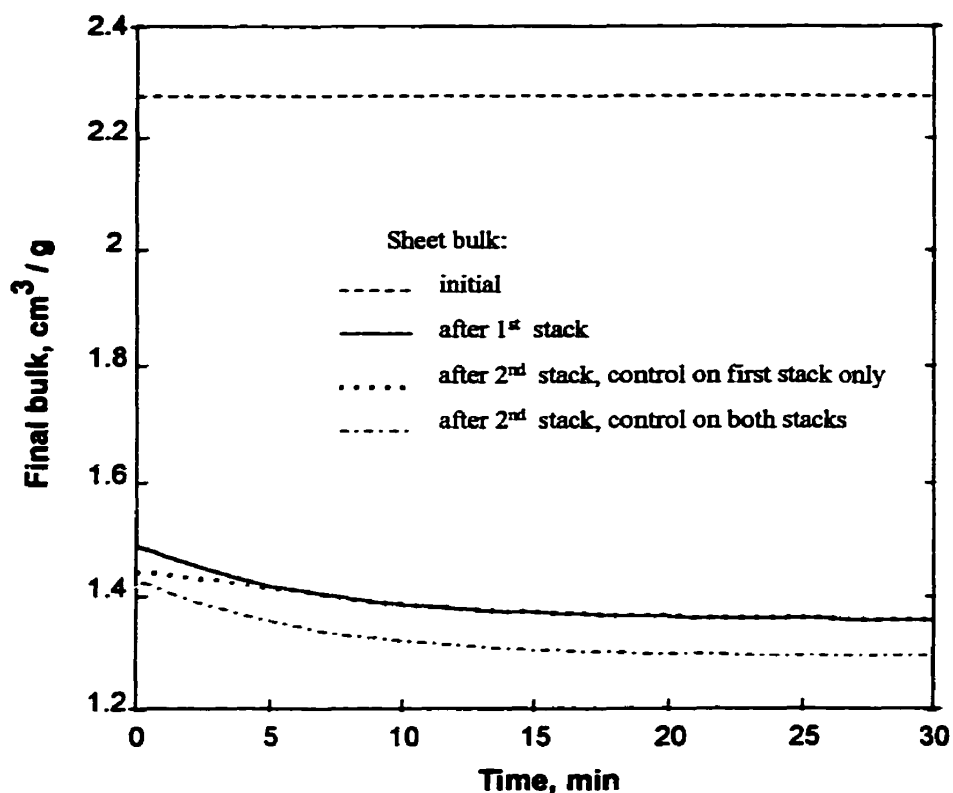


Figure 6.15: Simulation of effectiveness of calendering: double calender stack

The results on Figure 6.15 clearly establish the negligible role of the second stack, both for calendering and for control. Before the control action the first of the identical stacks delivers approximately 94% of the bulk reduction from two stacks. Moreover, in response to a step change in control action the change of paper bulk is seen to be almost completely due to thermal deformation of the queen roll on the first stack. The same thermal deformation of the queen roll on the second stack has only a very small effect on the final bulk. The Figure 6.15 results indicate that when the local thickness control is carried out only on the first stack, the second stack provides only an insignificant increase in paper final deformation. The complete agreement between these results from this simulation and the industrial calender measurements of Journeaux et al. [42, 43] constitutes further validation of the model developed here.

This weak response obtained in the second stack results from the small potential for further deformation of the paper passing through this stack. Since paper leaving the

first stack is already compressed by 30 to 40%, it would require a substantial increase in nip loads in the second stack to achieve any further significant bulk reduction. Such heavy calendering is avoided because of possible loss in paper strength.

6.4.3 Model Predictive Control: Multi-nip calendering

The last simulation was carried out to demonstrate the use of model predictive control to compare single and two-step control action for the single calender stack of 8 rolls, Figure 6.10. This is the configuration of the Case 2 simulation, Table 6.3. The paper final response to a single and two-step control action was calculated for a heating control jet installed on the queen roll. The value of the peak roll deformation at steady state was assumed to be proportional to the strength of the control action.

Figure 6.16 shows the change in normalised control action, defined as in Section 6.3. As for the single nip simulation (Figure 6.9), the strength of control action on the queen roll of the 8-roll stack was doubled for an initial period so as to decrease the time required to bring the system to the target specification, then reduced by half to just maintain this desirable change in permanent paper bulk. The simulation results on Figure 6.16 indicate that varying the strength of the control action in this way substantially improves the speed of paper response, with the time required to 95% of the steady state value from a 8-roll stack reduced dramatically from approximately 50 minutes for single step control, to 6.5 minutes for two-step control.

All the tests reported in this chapter indicate that the results of the simulation developed here are reliable, with the minor exception that the transition in paper bulk at the time of the second step is in reality smooth rather than sharp as shown on Figures 6.9 and 6.16. The approximation that is the source of this effect was noted in connection with Figure 6.9 of Section 6.3. The results of the Figure 6.16 simulation extend the demonstration of the use of model predictive control as developed in the present study from the single-nip case presented first, Figure 6.9, to the industrially relevant case of a 8-roll calender stack.

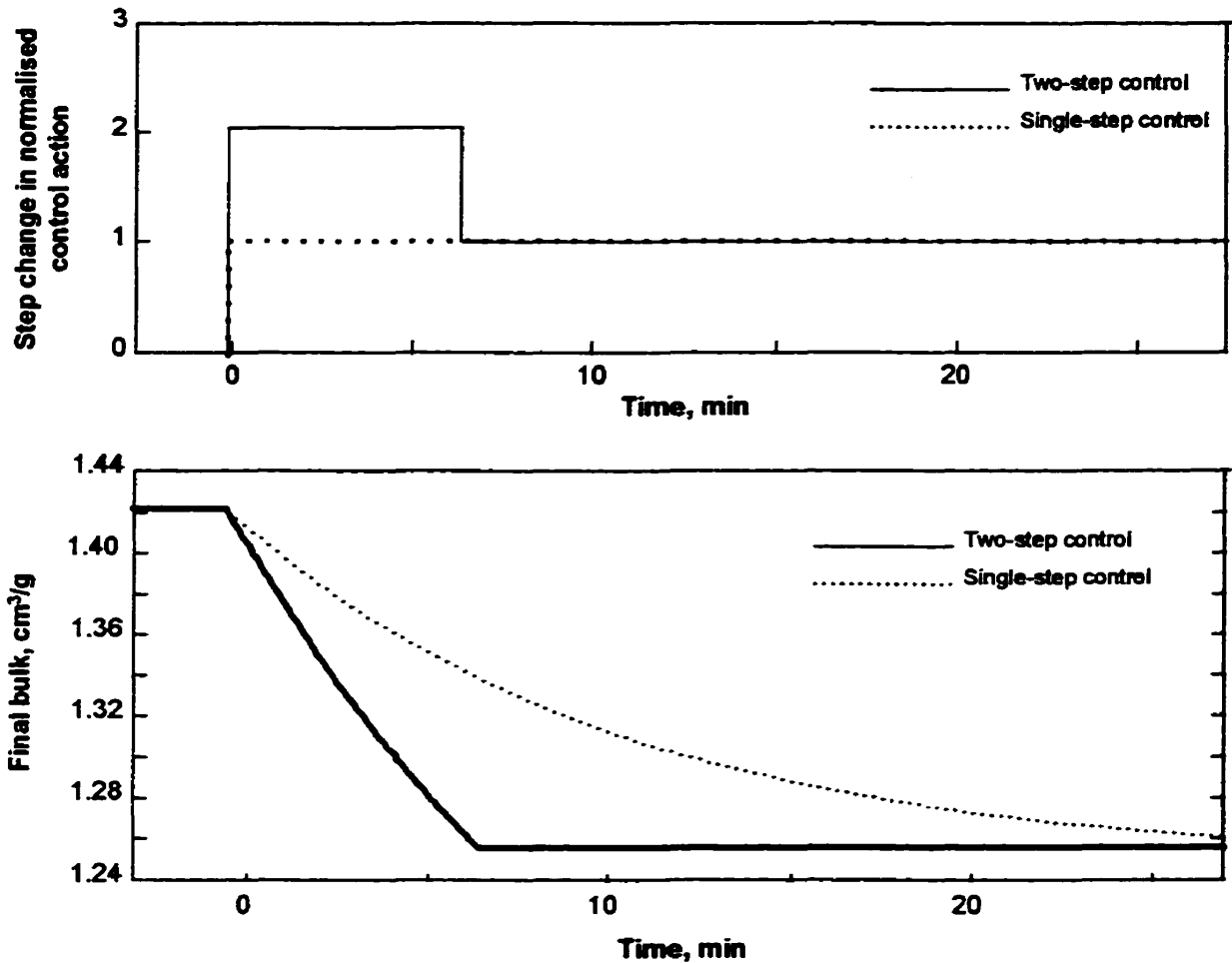


Figure 6.16: Comparison of single and two-step actuator change on speed of paper response: multi-nip calender stack.

6.5 Summary and conclusions

A dynamic model of the calendering process can be developed by combining the calendering equation used to estimate the in-nip strain at a specific CD position, given the permanent strain measured at that position (Chapter 4), with dynamic model of a calender roll deformation (Chapter 5). This model was then used to simulate the paper response to a specific step change in the control action for a variety of process parameters and to

determine the optimal location of the control actuator within the calender stack for the best control of local paper thickness.

Simulation of single nip calendering shows that the paper response to a specific step change in control action is highly sensitive to the local value of initial nip load and to local properties of the paper entering the nip: local paper temperature and moisture content. Increasing either nip load, paper temperature or moisture content increases the potential for paper thickness control.

The dynamic model of calendering developed in the present study was used to predict the results of the industrial calender for which Journeaux et al. reported measurements. The effect of three roll design variables was simulated: radius and shell thickness, and whether the roll is internally heated. Also simulated was the control sensitivity of the calender stack to two position variables: which stack, and which roll within the stack, is used to effect the CD control.

Paper response to a standard control action was shown to be very sensitive to the position of the control device within the stack. With the notable exception of the lowest (king) roll, the lower the control is effected in the stack, the stronger and faster is the paper response. Simulation of a single calender stack indicates that as the control actuator position is moved from the top to bottom roll, the paper response to a step change in the control action is both the largest and the fastest for control effected on the second lowest roll, the queen roll, and is second best for control on the roll just above. When two identical calenders are used in series, the first stack was shown to be by far the most effective place for control, with the second stack providing only a marginal effect on both the average and the local paper thickness.

Paper response for control on the king roll was shown to be very small, comparable with that for the three top rolls. The disadvantage of affecting only one nip is more significant than any anticipated higher control potential of the higher nip load of the king roll. Moreover as the king roll has typically the largest diameter by far, the proportionally wider nip reduces the pressure to which the paper is subjected in the nip, so the potential for paper deformation is thereby substantially reduced.

The excellent agreement between the simulation results and those measured by Journeaux et al. [42, 43] on an industrial calender provides key validation of the dynamic model of calendering contributed by the present study.

The suggestion of Journeaux that a thin-walled unheated roll situated above the queen roll could provide superior control to the commonly used internally heated queen roll was tested. Simulation results showed that although response obtained with control on a thin-walled unheated roll above the queen roll is the stronger by far at the steady state, exercising control on a thick-shelled internally heated queen roll provides much better paper response for about the first 20 minutes after the control action. As the industrial objective is to maintain the time the paper is off specification to well under 20 minutes, this application of the dynamic model of calendering developed and validated in the present study illustrates the value of such a model.

The dynamic model of calendering, subsequent to the validation tests, was used to demonstrate its application in model predictive control of calendering. This was done through simulation of paper response to two-step control action with the first step at twice the strength of the second. The simulation results show a dramatic increase in response speed, with the response time for two-step control only about 1/8 that for single-step control. This advantage was demonstrated for both single nip calendering and for a multi-roll calender stack of industrial specification. These results provide strong evidence of the large improvement in control of calendering possible through application of the model predictive approach developed in the present study. An important advantage of the dynamic model of calendering presented here is the short time (seconds) required to compute the future paper response to a control action, making this technique applicable for real-time CD control of calendering. This model may therefore be used with confidence to start the introduction of model predictive control to the difficult industrial problem of CD control of calendering.

7 Conclusions

7.1 Contributions to knowledge

The contributions of the present study may first be summarized in three distinct categories. The rheological behaviour of paper in calendering depends sensitively on its temperature and moisture content. In the experimental part of the study therefore, the in-nip behaviour of paper was determined over a wide range of temperature and moisture content, thus substantially extending the knowledge of the stress-strain behaviour of paper in the high speed calender nip. Secondly, a simplified model for the transient deformation of a calender roll in response to a local CD control action was determined, then validated by testing against the results for the complete numerical solution for a variety of roll designs and thermal boundary conditions. Finally, a dynamic model of calendering which incorporates relationships for both roll thermal deformation and the stress-strain behaviour of paper in and after the nip was developed and validated, then used to predict future paper response to control action. This final stage demonstrated the application of this work to model predictive control of calendering paper. These contributions are now detailed.

Determination of the effect of initial paper properties and process parameters on the stress-strain behaviour of paper in the nip of a calender produced the following contributions:

1. The in-nip version of the calendering equation for relating local in-nip strain to local values of the calendering variables, as introduced by Browne et al., has now been shown to give a satisfactory description of paper deformation in the calender nip over a wide range of paper temperature and moisture content, industrially important parameters which had not previously been investigated.

2. Increased moisture content is shown to have a strong nonlinear effect on in-nip paper strain. Permanent strain is also affected but, for industrially relevant moisture contents, a linear relationship can be used. The effect of temperature on

paper deformation both in and after a calender nip is similar to that for moisture content.

3. As a consequence of the above, a linear type of calendering equation is shown to be inadequate to provide a comprehensive prediction of the moisture and temperature effects on sheet behaviour in the nip.

4. The coefficients of the calendering equation are found to be sensitive to the range of in-nip strain for which it is applied because the linear part of the calendering equation, which is from 0 to 18% of the total, is fitted to the data of lowest strain. Thus for different sets of in-nip data, covering different ranges of strain, different in-nip coefficients apply.

5. The logarithmic relationship between permanent and in-nip strain proposed by Browne et al. is verified for estimating local in-nip strain for a given local permanent strain. However this relationship is now shown to be a function not only of line load, but of paper temperature and moisture content as well.

6. Uncalendered paper thickness is found to be a linear function of both paper temperature and moisture content over the range 20 to 80 °C, 1 to 14% moisture.

7. The conclusion by Browne et al. that the Kerekes approximation (radius coefficient a_R taken as the average of the load and speed coefficients) can be used in the in-nip case has now been verified.

Contributions pertaining to the development of a model for calender roll thermal deformation appropriate for use in real-time CD control of calendering are:

8. A simplified model of dynamic roll deformation in response to a CD local control action has been obtained and validated successfully against the full finite element and finite volume solution of Journeaux.

9. The very short time this method requires for computation of the dynamic deformation of calender rolls makes this model the appropriate tool for use in improved methods of CD real-time control of calendering.

10. This roll deformation model may be used with confidence to examine the effects of roll geometry and the difference between unheated and heated shell rolls over the range of conditions for which it was obtained and validated.

11. This dynamic model for thermal deformation was shown to be a valuable tool in seeking the choice between unheated and heated rolls and roll geometry variables which provide a satisfactory compromise between three sometimes conflicting objectives - the potential for large roll deformation, for fine CD resolution and for fast control response time.

The modeling of calendering led to the following contributions:

12. The dynamic model of calendering that was developed was validated with results measured by Journeaux et al. on an industrial calender. The excellent agreement between predicted and measured results establishes the reliability of this model for use in improving the CD control of calendering by enabling the adoption of model-based predictive control.

13. Simulations of single nip calendering established that paper response to a control action is highly sensitive to local values of the nip load and to local properties of the paper entering the nip: local paper temperature and moisture content.

14. This dynamic model of calendering was demonstrated to be a valuable tool for determining optimal conditions for CD control of local paper thickness.

15. The suggestion of Journeaux that a thin-walled unheated roll situated above the queen roll could provide superior control to the commonly used internally heated queen roll was tested. Simulation results showed that with control on a thin-walled unheated roll above the queen roll the paper response starts to be

stronger only after 20 minutes from the control action, while control on a thick-shelled internally heated queen roll provides much better paper response for the first 20 minutes. As the industrial objective is to maintain the time the paper is off specification to well under 20 minutes, this application of the dynamic model of calendering developed here illustrates the value of such a model.

16. Simulations of paper response to a two-step control action with the strength of the first step twice that of the second showed that the response time for the two-step control was only about 1/8 that for single-step control.

17. With the above demonstration of the application of the dynamic model of calendering, this model may now be used to introduce model predictive control for CD control of calendering.

7.2 Suggestions for future study

The present study has also been useful in raising interesting new questions.

1. The nonlinear effect of moisture content and temperature on paper behaviour in the nip needs to be further examined for higher levels of these two calendering variables.

2. The effect of furnish on the coefficients of the in-nip calendering equation was not examined in either the present study or that of Browne et al., as both studies used a TMP newsprint. Therefore the in-nip calendering equation for grades of paper made from furnishes other than TMP should be determined.

3. The stress-strain behaviour of paper in and after the nip was investigated for the standard machine calender only. The usefulness of the various relationships for relating local in-nip strain to local values of the calendering variables remains to be determined for soft calendering and supercalendering.

4. The internal heat flux from heated shell rolls has been shown to have a large impact on both the dynamic and steady state characteristics of local roll deformation. This effect should therefore be investigated for varying conditions in the heated core, including the temperature of the internal heating fluid.

5. The effect on local roll deformation of varying the heat transfer rate from a control actuator should be investigated and incorporated into the model of thermal roll deformation.

6. The local deformation response to local heating/cooling control action of various designs of variable crown rolls used for fine resolution CD control of calendering should be investigated and their usefulness in fine resolution CD control of calendering evaluated.

7. The effect of roll bending should be incorporated into the dynamic model of calendering.

8. The dynamic model of calendering developed here needs to be tested for use in industrial calender CD control architectures.

REFERENCES

1. ALBLAS, J.B., KUIPERS, M., "The contact problem of a rigid cylinder rolling on a thin viscoelastic layer", *Int. J. Engng. Sci.* 8(5): 363-380 (1970).
2. BAUMGARTEN, H.L., "Changes of web dimensions during calendering and supercalendering", *Symp. on Calendering and Supercalendering*, UMIST, Manchester, England (1975).
3. BREWSTER, D.B., "Profile control by DCS: dream or reality?", *TAPPI Control Conf. Proc.*:27-34 (1989).
4. BROWNE, T.C., "Design and construction of an experimental paper calender", MEng thesis, McGill University, Montreal, 1991.
5. BROWNE, T.C., CROTOGINO, R.H., and DOUGLAS, W.J.M., "An experimental calender for in-nip paper caliper measurements", *JPPS* 19(2):J92-96 (1992).
6. BROWNE, T.C., CROTOGINO, R.H., and DOUGLAS, W.J.M., "Measurement of paper strain in the nip of an experimental calender", *JPPS* 20(9):J266-271 (1994).
7. BROWNE, T.C., "Viscoelastic properties of paper in a calender nip", Ph.D. thesis, McGill University, Montreal, 1995.
8. BROWNE, T.C., CROTOGINO, R.H., and DOUGLAS, W.J.M., "The effect of paper structure on behaviour in a calender nip", *JPPS* 21(10): J343-J347 (1995).
9. BROWNE, T.C., CROTOGINO, R.H., and DOUGLAS, W.J.M., "Viscoelastic modeling of paper in a calender nip", *JPPS* 22(5): J170-J173 (1996).
10. BROWNE, T.C., KAWKA, D.W., "Effect of initial bulk on in-nip z-direction strain in a calender", *Pulp and Paper Report (PPR 1270)*, published by Pulp and Paper Research Institute of Canada (March 1997).
11. CHAPMAN, D.L.T., PEEL, J.D., "Calendering processes and the compressibility of paper (part one)", *Paper Technol.* 10(2):T116-T124 (1969).

12. COLLEY, J., PEEL, J.D., "Calendering processes and the compressibility of paper (part two)", *Paper Technol.* 13(5):T166-T173 (1972).
13. CROTOGINO, R.H., "Supercalendered and conventionally calendered newsprint - A comparison of surface and printing properties", *TAPPI* 63(11):101-105 (1980).
14. CROTOGINO, R.H., "Towards a comprehensive calendering equation", *Trans. Tech. Sect. CPPA* 6(4):TR89-TR94 (1980).
15. CROTOGINO, R.H., "Machine calendering - recent advances in theory and practice", *Trans. Tech. Sect. CPPA*, 7(4): TR75-TR87 (1981).
16. CROTOGINO, R.H., GENDRON, S., "Control systems for calenders and supercalenders - potential and limitations", *Pulp & Paper Can.* 88(11):T396-T401 (1987).
17. CROTOGINO, R.H., HUSSAIN, S.M. and McDONALD, J.D., "Mill application of the calendering equation", *JPPS* 9(5):TR128-TR133 (1983).
18. CROTOGINO, R.H., "Making a good impression", *Pulp Paper Can.* 90(7):T230-235 (July 1989).
19. DEREZINSKI, S.J., "Digital Computer Simulation of Paper Calendering", *Proc. TAPPI Paper Finishing and Converting Conf.*, [1981].
20. DUNCAN, S.R., "Estimating the response of actuators in a cross-directional control systems", *Pulp and Paper Canada* 98(4): 61-63 (1997).
21. EVANS, R., VIGH, D., SAARINEN, K., "TMP refiner control using adaptive predictive model based control"
22. EVANS, R., SUTINEN, R., SAARINEN, K., "Refiner control effectively accomplished through adaptive control", *Control Systems '92*, pp.267-270
23. FJELD, M., HICKEY, W.P., "Die Querprofilregelung am Kalandar: Praxisbezogene Betrachtungen uber den Einstaz von Luftdusen", *Das Papier* 30(1): 4-13 (1984).
24. FLETCHER, R., "FORTRAN subroutines for minimization by Quasi-Newton methods", *Report AERE R7125, Theoretical Physiscs Division, Atomic Energy Research Establishment, Harwell, Berkshire, England* (1972).

25. FORSETH, T., HELLE, T., "Effect of moistening on cross-sectional details of calendered paper containing mechanical pulp", *JPPS* 23(3): J95-J100 (1997).
26. GARCIA, C.E., PRETT, D.M., MORARI, M., "Model Predictive Control: Theory and Practice - a Survey", *Automatica*, Vol.25(3):335-348 (1989)
27. GAY, J.P., RANTANEN, R., NYKANEN, I., "A solution to calender sheet bubbling problems", *Pulp and Paper Canada* 94(2): T32-T35 (1993).
28. GOUGH, B., SEEBACH, G., "Adoptive control applications in pulp and paper: universal adaptive controller solves difficult problems", *Pulp and Paper Canada*, Vol.95(6):51-43 (1994)
29. GRATTON, M.F., "Three-dimensional web deformations from calendering in a hard nip", *TAPPI* 80(4): 210-218 (1997).
30. HAGLUND, L., ROBERTSON, G., "Local Thickness Reduction in a Calender Nip - An Experimental Study", *Svensk Papperstidning* 77(14):521-530 (1974).
31. HAGLUND, L., "Profile Model for a Calender Nip", *Proc. Sump. on Calendering and Supercalendering of Paper*, UMIST, Manchester, England, Paper 5.1 (1975).
32. HALL, R.C., "Coordinated cross machine control", *TAPPI Process Control Conf. Proc.*:11-19 (1989).
33. HAMEL, J., CROTOGINO, R.H. and GRATTON, M.F., " A design procedure for machine calenders", *TAPPI Finishing and Converting Conf.*, Richmond, Virginia (October 1988).
34. HAMEL, J., CROTOGINO, R.H. and GRATTON, M.F., "Measurement of nip load distribution in calenders using uncalendered paper", *JPPS* 18(1):17-23 (1992).
35. HAMEL, J., DOSTIE, M., "Convective heat transfer in calendering", *JPPS* 23(2): J77-J85 (1997).
36. HASHEMI, S.J., GOMES, V.G., CROTOGINO, R.H., DOUGLAS, W.J.M., " In-plane diffusivity of moisture in paper ", *Drying Technology* 15: 265-294 (1997)

37. HEAVEN, M., GORINEVSKY, D., HAGART-ALEXANDER, C., URQUHART, S., VYSE, R., "Applications of model-based tuning and analysis tools for paper machine control", *Pulp and Paper Canada* 98(7): 54-58 (1997).
38. HOLIK, H., HEB, H., SCHUWERK, W., "CD caliper control in calenders", *TAPPI Engineering Conference Proc.*:95-105 (1989).
39. HUNTER, S.C., "The rolling contact of a rigid cylinder with a viscoelastic half-space", *J. Appl. Mechanics Trans. ASME*, 611-617 (1961).
40. IONIDES, G.N., MITCHEL, J.G., CURZON, F.L., "A theoretical model of paper response to compression", *Trans. Tech. Sect. CPPA* 7(1): TR1-TR5 (1981).
41. JACKSON, M., GAVELIN, G., "The role of nip temperature and surface moisture in the calendering and supercalendering processes", *Svensk Papperstidning* --(5):151-158 (15 May 1966).
42. JOURNEAUX, I.A., "Impinging jet heat transfer and thermal deformation for rotating calender rolls", Ph.D. Thesis, McGill University (1990).
43. JOURNEAUX, I.A., CROTOGINO, R.H., and DOUGLAS, W.J.M., "Effect of actuator position on performance of a CD (Cross-machine Direction) calender control system: experimental study on a commercial calender", *Pulp Paper Can.* 93(1):42-46 (1992).
44. KAHOUN, J.B., ZUROWITCH, W., NEWBY, L., "System for the on-machine measurement and control of paper caliper", *TAPPI* 48(7): 60A-65A (1958).
45. KELLER, S., "Heat transfer in a calender nip", *JPPS* 20(1): J33-J37 (1994)
46. KELLER, S., "Heat transfer in a calender nip (ERRATUM)", *JPPS* 20(6): J160 (1994)
47. KERKES, R.J., PYE, I.T., "Newsprint calendering: an experimental comparison of temperature and loading effects", *Pulp and Paper Canada* 75(11):65-72 (1974).
48. KERKES, R.J., "Pressure distribution on a thin viscoelastic strip rolling between two rigid cylinders", *Trans. CSME* 4(1): 27-32 (1976).
49. KERKES, R.J., "Speed and loading effects in a calender nip", *Trans. Tech. Sect. CPPA* 2(3):TR88-TR91 (1976).

50. KEREKES, R.J., "Heat transfer in calendering", Trans. Tech. Sect. 5(3): TR66-TR76 (1979).
51. KEREKES, R.J., "A simple method for determining the thermal conductivity and contact resistance of paper", TAPPI 63(9): 137-140 (1980).
52. KNECHT, W., "Fast response CD caliper control", TAPPI Finishing & Converting Conf. Proc.:199-203 (1988).
53. LARIVE, R., LINDSTROM, R., "The CalCoil: a new approach for better cross-machine control", Pulp & Paper Can. 87(3):T125-T127 (1986).
54. LIF, J.O., WIKSTROM, M., FELLERS, C., RIGDAHL, M., "Deformation of paper structure during calendering as measured by electronic speckle photography", JPPS 23(10): J481- J486 (1997).
55. LIN, S.H., "Moisture absorption in cellulosic materials", Int. J. Engng Sci. 28(11): 1151-1156 (1990)
56. LIN, S.H., "Moisture desorption in cellulosic materials", Ind. Eng. Chem. Res., 30(8): 1833-1836 (1991).
57. LYNE, M.B., HAGLUND, L., BJELKHAGEN, H., "Control of machine calender roll diameter with air showers - an experimental investigation", Svensk Papperstidning 79(8):251-284 (1976).
58. MALIKIA, H., "Process control and automation of supercalenders", TAPPI J. 69(2): 52-55 (1986)
59. MARDON, J., MONAHAN, R.E., CARTER, R.A., WILDER, J.E., "Dynamic Consolidation of Paper During Calendering and Dynamic Compressibility of Paper", Trans. Symp. Sect. Brit. Paper and Board Makers Assn. (1965).
60. MAY, W.D., MORRIS, E.L., ATTACK, D., "Rolling friction of a hard cylinder over a viscoelastic material", J. Appl. Phys. 30(11): 1713-1724 (1959).
61. MITCHEL, J.G., SHEAHAN, D.K., "The control of reel building with calender stack air showers", CPPA Tech. Sect., Spring Conf. Jasper, Alberta, Canada (1978).

62. de MONTMORENCY, W.H., "The calendering of newsprint: a laboratory study of temperature and pressure effects", *Pulp & Paper Mag. Can.* 68(7):T326-T345 (1967).
63. MURRAY, D.F., "Caliper control by impinging hot or cold air", *Pulp & Paper Can.* 79(4):T136-T138 (1978).
64. O'NEILL, R., "Function minimization using a simplex procedure", AS47, *Applied Statistics Algorithms* (P. Griffiths and L.D. Hill, eds.), Ellis Horwood Limited for a Royal Statistical Society, London (1985).
65. OSAKI, J.M., RHEINBOLDT, W.C., "Iterative solutions of nonlinear equations in several variables", Academic Press, New York (1970).
66. OSAKI, J.M., FUJII, Y., KIICHI, T., "Z-direction compressive properties of paper", *Report on Progress in Polymer Physics in Japan* 23: 375-378 (1980).
67. PELLETIER, L., "Impingement heat transfer on a rotating cylinder - an experimental study of calender cooling", Master's thesis, McGill University (1984).
68. PELLETIER, L., DOUGLAS, W.J.M., and CROTOGINO, R.H., "CD calender control with air jets - an experimental study of impingement heat transfer", *JPPS* 13(2):49-55 (1987).
69. POWELL, R., HEAVEN, M., KING, J., VYSE, R., "Advanced, open control for existing measurement systems", *Pulp and Paper Canada* 97(10): 65-69 (1996).
70. RODAL, J.A., "Soft-nip calendering of paper and paperboard", *TAPPI* 72(5): 177-186 (1989).
71. SCHWEIDER, C.A, RUDD, J.B., "Prediction and control of paper machine parameters using adaptive technologies in process modelling", *TAPPI J.*, Vol.77(11):201-208 (1994)
72. SEBORG, D.E, MELLICHAMP, D.A., "Process dynamics and control", *Wiley Series in Chemical Engineering*, John Wiley & Sons Inc., p:3-20,183-199,387-412 (1989).

73. SLOWIK, A.M., "Cross-machine control experiences", TAPPI J. --(6):57-60 (June 1989).
74. TIMMS, D.G., "Laboratory calendering: a potential troubleshooting tool", Appita 46(2):127-130 (March 1993).
75. VERKASALO, M., "Thermo rolls in newsprint calendering", Valmet Application Notes (1984).
76. WELLSTEAD, P.E., ZARROP, M.B., HEATH, W.P., "Two-dimensional methods for MD and CD estimation and control: recent progress", Pulp and Paper Canada 98(9): 72-76 (1997).
77. WILHELM, R.G., Jr., "On the controllability of cross-direction variations of sheet properties", TAPPI Eng. Conf. Proc.:621-628 (1984).

APPENDIX A1: Raw data and results of non-linear regression analysis

Table A1.1: Paper sorption and desorption, TMP newsprint (Figure 3.2, Chapter 3)

Table A1.2: Command log input to SYSTAT

Table A1.3: SYSTAT output

Table A1.4: Summary of experimental data

**Table A1.1: Paper sorption and desorption,
TMP newsprint (Figure 3.2, Chapter 3)**

**M1, M2 - sorption experiments
M2, M4 - desorption experiments**

time min	M1 %	M2 %	M3 %	M4 %
0	3.63	8.00	2.26	11.50
0.17		7.00	4.36	9.43
0.33	5.89		6.08	8.47
0.50	6.79	5.30	7.22	7.55
0.67			7.94	6.90
0.83			8.45	6.40
1.0	8.29	4.20	8.81	5.98
1.5	9.10	3.60	9.60	4.82
2.0	9.57	3.25	9.96	4.14
2.5	9.95	3.05	10.10	3.61
3.0	10.30	2.90	10.20	3.36
3.5	10.60	2.82	10.10	3.15
4.0	10.80	2.74	10.10	2.99
4.5	10.90	2.67	10.30	2.88
5.0	11.10	2.64	10.60	2.69
5.5	11.20	2.59	10.80	2.65
6.0	11.20	2.55	11.10	2.61
6.5	10.90	2.52	11.20	
7.0	11.10	2.48	10.80	2.55
7.5	11.20	2.47	10.50	2.51
8.0	11.40	2.46	11.00	2.48
8.5	11.50	2.45	11.30	2.48
9.0	11.60	2.44	11.40	2.41
9.5	11.70	2.42	11.60	2.40
10.0	11.80	2.41	11.70	2.39
10.5	11.90	2.39	11.90	2.36
11.0	11.90	2.37	11.90	2.33
11.5	12.00	2.35	12.10	2.34
12.0	12.10	2.35	12.20	2.33
12.5	12.10	2.32	12.20	2.31
13.0	12.10	2.32	12.30	2.30
13.5	12.20	2.31	12.30	2.30
14.0	12.30	2.30	12.40	2.27
14.5	12.30	2.32	12.00	2.27
15.0	12.40	2.29	12.00	2.26
15.5	12.40			
16.0	12.40			
16.5	12.50			
17.0			12.40	

time min	M1 %	M2 %	M3 %	M4 %
17.5			12.50	
18.0			12.60	
18.5			12.60	

Table A1.2: Command log input to SYSTAT, calendring equation

By
Select
Weight
Use 'c:\dariusz\phd\data\enep.sys"
By
Select
Weight
Nonlin

Model EN = (A + B * (A0 + AL * LL + AS * LS + AR * LR + AT * T + AM * M)),
*(B < 0.5 * (1 - A) / (A0 + AL * LL + AS * LS + AR * LR + AT * T + AM * M)),
+(1-0.25*(1 - A)^2 / (B * (A0 + AL * LL + AS * LS + AR * LR + AT * T + AM * M))),
*(B >= 0.5 * (1 - A) / (A0 + AL * LL + AS * LS + AR * LR + AT * T + AM * M))

Format 9
Print = Long
Estimate /Simplex, Iter=500, Tolerance=1e-15, Start=-.3, -.03, .18, -.01, -.05, .0008, .003

By
Select
Weight
Use 'c:\dariusz\phd\data\enep.sys"
By
Select
Weight
Nonlin

Model EP = (A + B * (A0 + AL * LL + AS * LS + AR * LR + AT * T + AM * M)),
*(B < 0.5 * (1 - A) / (A0 + AL * LL + AS * LS + AR * LR + AT * T + AM * M)),
+(1-0.25*(1 - A)^2 / (B * (A0 + AL * LL + AS * LS + AR * LR + AT * T + AM * M))),
*(B >= 0.5 * (1 - A) / (A0 + AL * LL + AS * LS + AR * LR + AT * T + AM * M))

Format 9
Print = Long
Estimate /Simplex, Iter=500, Tolerance=1e-15, Start= -.4, .06, .1, -.02, -.04, .001, .005

Table A1.3: SYSTAT output, calendring equation

DEPENDENT VARIABLE IS		EN		
SOURCE	SUM-OF-SQUARES	DF	MEAN-SQUARE	
REGRESSION	.258011E+03	7	.368587E+02	
RESIDUAL	0.634492196	709	0.000894911	
TOTAL	.258495E+03	716		
CORRECTED	2.695851113	715		
RAW R-SQUARED (1-RESIDUAL/TOTAL)		= 0.997545440		
CORRECTED R-SQUARED (1-RESIDUAL/CORRECTED)		= 0.764641232		
PARAMETER	ESTIMATE	A.S.E.	LOWER <95%>	UPPER
A	-0.310059640	0.023984106	-0.357148023	-0.262971257
A0	-0.027216367	0.012546509	-0.051849131	-0.002583603
AL	0.176948810	0.008578737	0.160106037	0.193791583
AS	-0.012647153	0.004159703	-0.020813965	-0.004480340
AR	-0.048484065	0.012615274	-0.073251836	-0.023716293
AT	0.003346414	0.000109465	0.003131499	0.003561328
AM	0.002884097	0.000374341	0.002149147	0.003619047

DEPENDENT VARIABLE IS		EP		
SOURCE	SUM-OF-SQUARES	DF	MEAN-SQUARE	
REGRESSION	.525675E+02	7	7.509639609	
RESIDUAL	0.416722729	723	0.000576380	
TOTAL	.529842E+02	730		
CORRECTED	3.875110137	729		
RAW R-SQUARED (1-RESIDUAL/TOTAL)		= 0.992134962		
CORRECTED R-SQUARED (1-RESIDUAL/CORRECTED)		= 0.892637801		
PARAMETER	ESTIMATE	A.S.E.	LOWER <95%>	UPPER
A	-0.418576264	0.059784343	-0.290814009	-0.533929350
A0	0.064182781	0.027920252	0.013921878	0.114292945
AL	0.097337064	0.002012262	0.093335834	0.119236987
AS	-0.021799218	0.001244960	-0.023679188	-0.018790851
AR	-0.035103791	0.004063393	-0.043830655	-0.027875734
AT	0.000972998	0.000000093	0.000972652	0.000973216
AM	0.006071144	0.000162950	0.005735177	0.006395000

Table A1.4: Experimental results: TMP newsprint

Exp. number	Initial caliper μm	Basis weight g/m^2	Initial bulk cm^3/g	Roll radius m	Calen. speed m/min	Line Load kN/m	Moisture content %	Paper temp. deg C	In-nip strain	Perm. strain
Ex. No	t_i	BW	Bi	R	S	L	M	T	en	ep
1 a	108.3	48.8	2.22	0.355	98	94	4.3	23.3	0.41	0.22
1 b	108.3	48.8	2.22	0.355	97	129	4.2	23.4	0.46	0.24
1 c	108.3	48.8	2.22	0.355	101	31	4.2	23.3	0.33	0.14
1 d	108.3	48.8	2.22	0.355	98	21	4.2	23.5	0.27	0.11
1 e	108.3	48.8	2.22	0.355	94	95	4.2	23.4	0.43	0.21
1 f	108.3	48.8	2.22	0.355	186	94	4.1	24.6	0.43	0.20
1 g	108.3	48.8	2.22	0.355	189	129	4.1	24.6	0.47	0.24
1 h	108.3	48.8	2.22	0.355	186	165	4.1	24.6	0.49	0.24
1 i	108.3	48.8	2.22	0.355	191	132	4.2	24.6	0.47	0.24
1 j	108.3	48.8	2.22	0.355	197	31	4.2	24.6	0.33	0.12
1 k	108.3	48.8	2.22	0.355	321	93	4.0	24.6	0.43	0.19
1 l	108.3	48.8	2.22	0.355	318	129	4.0	24.6	0.47	0.21
1 m	108.3	48.8	2.22	0.355	320	166	4.0	24.6	0.49	0.24
1 n	108.3	48.8	2.22	0.355	327	133	4.0	24.5	0.48	0.22
1 o	108.3	48.8	2.22	0.355	325	96	3.9	24.6	0.44	0.20
1 p	108.3	48.8	2.22	0.355	574	95	4.1	24.6	0.43	0.18
1 q	108.3	48.8	2.22	0.355	528	129	4.0	24.6	0.47	0.21
1 r	108.3	48.8	2.22	0.355	535	165	4.0	24.7	0.48	0.23
1 s	108.3	48.8	2.22	0.355	531	207	4.0	24.6	0.50	0.25
1 t	108.3	48.8	2.22	0.355	539	170	4.1	24.7	0.49	0.23
1 u	108.3	48.8	2.22	0.355	539	133	4.1	24.6	0.47	0.22
1 v	108.3	48.8	2.22	0.355	983	133	4.1	24.6	0.47	0.19
1 w	108.3	48.8	2.22	0.355	956	166	4.0	24.6	0.50	0.22
1 x	108.3	48.8	2.22	0.355	954	206	4.0	24.6	0.51	0.23
1 y	108.3	48.8	2.22	0.355	966	169	4.0	24.8	0.50	0.21
1 z	108.3	48.8	2.22	0.355	964	168	4.0	25.6	0.51	0.22
1 za	108.3	48.8	2.22	0.355	958	206	4.0	25.5	0.52	0.23
2 a	113.9	48.8	2.33	0.356	97	94	12.5	25.0	0.51	0.34
2 b	113.9	48.8	2.33	0.356	96	132	12.5	25.1	0.56	0.37
2 c	113.9	48.8	2.33	0.356	98	31	12.5	25.1	0.43	0.25
2 d	113.9	48.8	2.33	0.356	96	20	12.4	25.0	0.36	0.22
2 e	113.9	48.8	2.33	0.356	95	95	12.5	25.1	0.51	0.35
2 f	113.9	48.8	2.33	0.356	187	95	12.5	25.0	0.51	0.33
2 g	113.9	48.8	2.33	0.356	186	131	12.5	25.2	0.54	0.36
2 h	113.9	48.8	2.33	0.356	186	170	12.5	25.1	0.57	0.38
2 i	113.9	48.8	2.33	0.356	190	134	12.5	25.7	0.53	0.36
2 j	113.9	48.8	2.33	0.356	188	31	12.5	25.4	0.42	0.23
2 k	113.9	48.8	2.33	0.356	321	94	12.3	25.1	0.50	0.31
2 l	113.9	48.8	2.33	0.356	318	132	12.4	25.1	0.54	0.34
2 m	113.9	48.8	2.33	0.356	318	170	12.6	25.2	0.57	0.36

Table A1.4: Experimental results: TMP newsprint (continued)

Ex. no	t _i	BW	Bi	R	S	L	M	T	en	ep
2 n	113.9	48.8	2.33	0.356	325	135	12.6	25.1	0.53	0.33
2 o	113.9	48.8	2.33	0.356	323	96	12.4	25.1	0.50	0.30
2 p	113.9	48.8	2.33	0.356	532	96	12.6	25.1	0.49	0.29
2 q	113.9	48.8	2.33	0.356	533	132	12.5	25.1	0.51	0.31
2 r	113.9	48.8	2.33	0.356	532	170	12.5	25.1	0.56	0.34
2 s	113.9	48.8	2.33	0.356	533	209	12.4	25.1	0.59	0.36
2 t	113.9	48.8	2.33	0.356	540	174	12.2	25.1	0.55	0.34
2 u	113.9	48.8	2.33	0.356	538	135	12.4	25.1	0.55	0.32
2 v	113.9	48.8	2.33	0.356	982	135	12.8	24.2	0.53	0.30
2 w	113.9	48.8	2.33	0.356	957	170	12.9	24.1	0.56	0.31
2 x	113.9	48.8	2.33	0.356	953	208	12.7	24.2	0.59	0.34
2 y	113.9	48.8	2.33	0.356	963	173	12.6	24.2	0.56	0.32
2 z	113.9	48.8	2.33	0.356	960	208	12.6	24.2	0.58	0.33
2 za	113.9	48.8	2.33	0.356	973	96	12.5	24.2	0.49	0.25
3 a	110.8	48.8	2.31	0.356	98	95	8.0	21.9	0.51	0.28
3 b	110.8	48.8	2.31	0.356	98	132	8.0	21.8	0.54	0.31
3 c	110.8	48.8	2.31	0.356	98	29	7.9	21.7	0.38	0.18
3 d	110.8	48.8	2.31	0.356	98	19	8.0	21.8	0.34	0.14
3 e	110.8	48.8	2.31	0.356	97	96	7.9	21.7	0.51	0.28
3 f	110.8	48.8	2.31	0.356	98	132	7.9	21.8	0.54	0.32
3 g	110.8	48.8	2.31	0.356	190	97	7.9	21.7	0.50	0.27
3 h	110.8	48.8	2.31	0.356	188	132	7.9	21.7	0.54	0.31
3 i	110.8	48.8	2.31	0.356	188	171	8.0	21.7	0.55	0.33
3 j	110.8	48.8	2.31	0.356	190	135	8.0	21.7	0.54	0.31
3 k	110.8	48.8	2.31	0.356	187	29	8.0	21.7	0.38	0.17
3 l	110.8	48.8	2.31	0.356	321	95	8.0	21.7	0.50	0.27
3 m	110.8	48.8	2.31	0.356	321	132	8.0	21.7	0.54	0.29
3 n	110.8	48.8	2.31	0.356	322	170	7.8	21.7	0.56	0.31
3 o	110.8	48.8	2.31	0.356	325	135	8.0	21.7	0.54	0.29
3 p	110.8	48.8	2.31	0.356	325	97	7.9	21.8	0.49	0.25
3 q	110.8	48.8	2.31	0.356	536	96	7.8	21.7	0.50	0.24
3 r	110.8	48.8	2.31	0.356	530	132	7.7	21.7	0.54	0.27
3 s	110.8	48.8	2.31	0.356	530	169	7.8	21.7	0.56	0.29
3 t	110.8	48.8	2.31	0.356	532	209	7.8	21.7	0.56	0.31
3 u	110.8	48.8	2.31	0.356	538	174	7.7	21.7	0.56	0.30
3 v	110.8	48.8	2.31	0.356	527	130	7.6	21.7	0.53	0.28
3 w	110.8	48.8	2.31	0.356	984	130	7.6	21.8	0.52	0.25
3 x	110.8	48.8	2.31	0.356	963	167	7.5	21.8	0.55	0.28
3 y	110.8	48.8	2.31	0.356	952	208	7.6	21.7	0.56	
3 z	110.8	48.8	2.31	0.356	960	172	7.4	21.8	0.54	0.28
3 za	110.8	48.8	2.31	0.356	964	208	7.5	21.8	0.55	0.29
3 zb	110.8	48.8	2.31	0.356	965	97	7.4	21.8	0.46	0.22
4 a	114.7	48.8	2.39	0.356	98	97	13.9	23.9	0.55	0.36
4 b	114.7	48.8	2.39	0.356	99	136	13.7	23.8	0.58	0.39
4 c	114.7	48.8	2.39	0.356	97	26	13.7	23.9	0.42	0.24
4 d	114.7	48.8	2.39	0.356	98	17	13.6	23.9	0.39	0.21

Table A1.4: Experimental results: TMP newsprint (continued)

Ex. no	t ₁	BW	Bi	R	S	L	M	T	en	ep
4 e	114.7	48.8	2.39	0.356	99	98	13.6	23.8	0.55	0.36
4 f	114.7	48.8	2.39	0.356	189	98	13.6	23.9	0.55	0.33
4 g	114.7	48.8	2.39	0.356	189	135	13.6	23.8	0.57	0.36
4 h	114.7	48.8	2.39	0.356	189	175	13.6	23.9	0.60	0.39
4 i	114.7	48.8	2.39	0.356	190	138	13.7	23.8	0.57	0.36
4 j	114.7	48.8	2.39	0.356	190	27	13.7	23.9	0.42	0.22
4 k	114.7	48.8	2.39	0.356	326	97	13.7	25.1		0.33
4 l	114.7	48.8	2.39	0.356	322	134	13.8	25.0		0.35
4 m	114.7	48.8	2.39	0.356	322	173	13.8	24.8	0.61	0.37
4 n	114.7	48.8	2.39	0.356	325	136	13.8	24.8	0.58	0.34
4 o	114.7	48.8	2.39	0.356	323	97	13.7	24.8	0.54	0.31
4 p	114.7	48.8	2.39	0.356	525	97	13.9	23.9	0.54	0.30
4 q	114.7	48.8	2.39	0.356	537	133	13.6	23.8	0.57	0.33
4 r	114.7	48.8	2.39	0.356	537	172	13.7	23.9	0.61	0.34
4 s	114.7	48.8	2.39	0.356	534	210	13.9	23.9	0.61	0.35
4 t	114.7	48.8	2.39	0.356	540	176	13.8	23.8	0.58	0.34
4 u	114.7	48.8	2.39	0.356	537	137	13.7	23.9	0.56	0.32
4 v	114.7	48.8	2.39	0.356	741	135	13.7	23.9	0.56	0.30
5 a	107.1	48.8	2.23	0.356	98	93	2.2	24.8	0.46	0.16
5 b	107.1	48.8	2.23	0.356	98	129	2.2	25.8	0.47	0.19
5 c	107.1	48.8	2.23	0.356	98	31	2.2	25.6	0.38	0.10
5 d	107.1	48.8	2.23	0.356	98	166	2.2	25.7	0.48	0.21
5 e	107.1	48.8	2.23	0.356	98	95	2.3	25.7	0.47	0.17
5 f	107.1	48.8	2.23	0.356	190	95	2.2	27.1	0.47	0.16
5 g	107.1	48.8	2.23	0.356	190	129	2.1	27.1	0.47	0.17
5 h	107.1	48.8	2.23	0.356	190	166	2.2	27.1	0.48	0.20
5 i	107.1	48.8	2.23	0.356	189	132	2.2	27.1	0.47	0.18
5 j	107.1	48.8	2.23	0.356	188	33	2.1	27.1	0.37	0.09
5 k	107.1	48.8	2.23	0.356	323	32	2.1	27.1	0.36	0.08
5 l	107.1	48.8	2.23	0.356	322	129	2.1	27.0	0.48	0.17
5 m	107.1	48.8	2.23	0.356	324	166	2.2	28.0	0.48	0.19
5 n	107.1	48.8	2.23	0.356	323	207	2.2	28.0	0.50	0.20
5 o	107.1	48.8	2.23	0.356	320	95	2.1	28.0	0.46	0.15
5 p	107.1	48.8	2.23	0.356	529	95	2.2	28.0	0.45	0.14
5 q	107.1	48.8	2.23	0.356	536	129	2.1	28.0	0.47	0.17
5 r	107.1	48.8	2.23	0.356	531	166	1.9	28.0	0.47	0.19
5 s	107.1	48.8	2.23	0.356	535	207	1.9	27.9	0.50	0.19
5 t	107.1	48.8	2.23	0.356	540	169	2.0	28.0	0.48	0.17
5 u	107.1	48.8	2.23	0.356	535	132	2.1	28.0	0.48	0.17
5 v	107.1	48.8	2.23	0.356	977	132	1.9	28.1	0.48	0.16
5 w	107.1	48.8	2.23	0.356	952	166	2.1	28.1	0.48	0.18
5 x	107.1	48.8	2.23	0.356	959	206	2.1	28.0	0.50	0.18
5 y	107.1	48.8	2.23	0.356	966	168	2.2	28.0	0.47	0.18
5 z	107.1	48.8	2.23	0.356	958	206	2.1	28.0	0.51	0.18
6 a	107	48.8	2.23	0.356	92	93	1.7	29.1	0.47	0.13
6 b	107	48.8	2.23	0.356	92	130	1.8	29.2	0.49	0.16

Table A1.4: Experimental results: TMP newsprint (continued)

Ex. no	t _i	BW	Bi	R	S	L	M	T	en	ep
6 c	107	48.8	2.23	0.356	94	32	1.9	29.1	0.40	0.07
6 d	107	48.8	2.23	0.356	89	168	1.9	29.1	0.53	0.17
6 e	107	48.8	2.23	0.356	93	95	1.8	29.2	0.45	0.14
6 f	107	48.8	2.23	0.356	184	95	1.8	29.4	0.46	0.13
6 g	107	48.8	2.23	0.356	181	130	1.8	30.1	0.49	0.15
6 h	107	48.8	2.23	0.356	184	171	1.9	30.1	0.51	0.16
6 i	107	48.8	2.23	0.356	187	134	1.9	30.1	0.47	0.14
6 j	107	48.8	2.23	0.356	184	32	1.8	30.1	0.40	0.06
6 k	107	48.8	2.23	0.356	315	32	1.8	30.1	0.40	0.05
6 l	107	48.8	2.23	0.356	312	130	1.9	30.1	0.50	0.14
6 m	107	48.8	2.23	0.356	315	167	1.9	30.1	0.53	0.16
6 n	107	48.8	2.23	0.356	314	208	1.8	30.1	0.55	0.17
6 o	107	48.8	2.23	0.356	325	95	1.9	30.1	0.45	0.11
6 p	107	48.8	2.23	0.356	533	95	1.9	30.1	0.45	0.11
6 q	107	48.8	2.23	0.356	519	130	1.8	30.1	0.48	0.13
6 r	107	48.8	2.23	0.356	530	167	2.0	30.1	0.52	0.16
6 s	107	48.8	2.23	0.356	536	207	1.9	30.1	0.56	0.16
6 t	107	48.8	2.23	0.356	530	170	1.9	30.1	0.51	0.16
6 u	107	48.8	2.23	0.356	535	133	1.9	30.1	0.46	0.13
6 v	107	48.8	2.23	0.356	976	133	1.8	31.0	0.46	0.13
6 w	107	48.8	2.23	0.356	960	167	1.8	31.0	0.51	0.14
6 x	107	48.8	2.23	0.356	944	207	1.7	31.0	0.55	0.16
6 y	107	48.8	2.23	0.356	953	170	1.9	31.0	0.51	0.15
6 z	107	48.8	2.23	0.356	958	207	1.7	31.0	0.55	0.14
6 za	107	48.8	2.23	0.356	962	95	1.8	31.0	0.43	0.08
6 zb	107	48.8	2.23	0.356	180	208	1.9	30.1	0.55	0.18
7 a	112.3	48.8	2.34	0.356	92	93	9.2	28.0	0.52	0.30
7 b	112.3	48.8	2.34	0.356	92	132	9.2	28.0	0.55	0.33
7 c	112.3	48.8	2.34	0.356	91	32	9.1	28.4	0.45	0.21
7 d	112.3	48.8	2.34	0.356	93	172	9.2	29.2	0.58	0.36
7 e	112.3	48.8	2.34	0.356	92	95	9.2	29.2	0.50	0.30
7 f	112.3	48.8	2.34	0.356	182	95	9.1	27.9	0.50	0.29
7 g	112.3	48.8	2.34	0.356	180	132	9.1	27.9	0.55	0.32
7 h	112.3	48.8	2.34	0.356	183	171	9.0	27.9	0.58	0.34
7 i	112.3	48.8	2.34	0.356	179	131	9.0	29.1	0.54	0.32
7 j	112.3	48.8	2.34	0.356	189	32	9.1	29.2	0.44	0.19
7 k	112.3	48.8	2.34	0.356	322	32	9.1	27.9	0.45	0.18
7 l	112.3	48.8	2.34	0.356	322	131	9.0	27.9	0.55	0.32
7 m	112.3	48.8	2.34	0.356	313	170	8.9	27.9	0.58	0.33
7 n	112.3	48.8	2.34	0.356	315	209	8.9	27.9	0.62	0.35
7 o	112.3	48.8	2.34	0.356	324	95	9.0	28.0	0.50	0.29
7 p	112.3	48.8	2.34	0.356	513	95	9.1	27.9	0.50	0.27
7 q	112.3	48.8	2.34	0.356	529	132	8.9	27.9	0.55	0.30
7 r	112.3	48.8	2.34	0.356	529	170	9.0	27.9	0.58	0.33
7 s	112.3	48.8	2.34	0.356	531	209	8.9	27.9	0.62	0.34
7 t	112.3	48.8	2.34	0.356	534	174	9.0	27.9	0.58	0.31

Table A1.4: Experimental results: TMP newsprint (continued)

Ex. no	t _i	BW	Bi	R	S	L	M	T	en	ep
7 u	112.3	48.8	2.34	0.356	534	135	8.9	27.9	0.54	0.29
7 v	112.3	48.8	2.34	0.356	977	135	8.9	28.0	0.54	0.28
7 w	112.3	48.8	2.34	0.356	950	170	8.8	28.0	0.58	0.30
7 x	112.3	48.8	2.34	0.356	948	208	8.9	27.9	0.62	0.32
7 y	112.3	48.8	2.34	0.356	960	173	9.0	28.0	0.57	0.30
7 z	112.3	48.8	2.34	0.356	958	208	8.9	27.9	0.62	0.32
7 za	112.3	48.8	2.34	0.356	964	95	8.7	28.0	0.50	0.23
8 a	108.8	48.8	2.27	0.356	91	92	5.0	39.8	0.59	0.25
8 a'	108.8	48.8	2.27	0.356	92	92	5.6	39.0	0.57	0.29
8 b	108.8	48.8	2.27	0.356	90	128	5.0	39.9	0.63	0.28
8 b'	108.8	48.8	2.27	0.356	91	125	5.6	38.8	0.59	0.31
8 c	108.8	48.8	2.27	0.356	96	32	5.0	39.8	0.54	0.15
8 c'	108.8	48.8	2.27	0.356	91	33	5.6	38.9	0.53	0.18
8 d	108.8	48.8	2.27	0.356	93	164	5.0	39.8	0.64	0.30
8 d'	108.8	48.8	2.27	0.356	92	160	5.6	38.8	0.62	0.33
8 e	108.8	48.8	2.27	0.356	95	94	4.9	39.7	0.60	0.25
8 e'	108.8	48.8	2.27	0.356	90	94	5.6	38.8	0.59	0.25
8 f	108.8	48.8	2.27	0.356	184	92	5.5	40.0	0.58	0.27
8 g'	108.8	48.8	2.27	0.356	181	126	5.5	40.0	0.60	0.29
8 h'	108.8	48.8	2.27	0.356	183	160	5.5	40.0	0.61	0.31
8 i'	108.8	48.8	2.27	0.356	184	129	5.3	39.9	0.61	0.29
8 j'	108.8	48.8	2.27	0.356	183	32	5.5	37.9	0.52	0.16
8 k	108.8	48.8	2.27	0.356	316	93	5.0	38.7	0.54	0.24
8 l	108.8	48.8	2.27	0.356	315	32	5.0	38.8	0.51	0.14
8 m	108.8	48.8	2.27	0.356	314	129	5.0	38.8	0.60	0.26
8 n	108.8	48.8	2.27	0.356	316	166	5.1	38.8	0.62	0.29
8 o	108.8	48.8	2.27	0.356	315	207	5.0	38.7	0.64	0.30
8 p	108.8	48.8	2.27	0.356	535	93	5.0	38.7	0.57	0.23
8 q	108.8	48.8	2.27	0.356	525	129	5.2	38.8	0.59	0.25
8 r	108.8	48.8	2.27	0.356	526	166	5.1	38.8	0.60	0.28
8 s	108.8	48.8	2.27	0.356	527	207	5.0	38.8	0.63	0.30
8 t	108.8	48.8	2.27	0.356	533	170	5.2	38.8	0.63	0.27
8 u	108.8	48.8	2.27	0.356	532	133	5.1	38.8	0.61	0.25
8 v	108.8	48.8	2.27	0.356	987	127	5.1	37.8	0.60	0.24
8 w	108.8	48.8	2.27	0.356	965	163	5.2	37.8	0.62	0.26
8 x	108.8	48.8	2.27	0.356	944	205	5.3	37.8	0.63	0.28
8 y	108.8	48.8	2.27	0.356	944	168	5.2	37.7	0.62	0.26
8 z	108.8	48.8	2.27	0.356	950	205	5.3	37.8	0.62	0.28
8 za	108.8	48.8	2.27	0.356	962	94	5.1	37.7	0.58	0.20
8 zb	108.8	48.8	2.27	0.356	956	167	5.0	37.8	0.62	0.26
9 a	109.3	48.8	2.28	0.356	92	100	2.2	49.5	0.59	0.20
9 b	109.3	48.8	2.28	0.356	93	138	2.1	50.5	0.60	0.23
9 c	109.3	48.8	2.28	0.356	91	39	2.0	50.4	0.53	0.13
9 d	109.3	48.8	2.28	0.356	92	174	2.1	50.4	0.64	0.25
9 e	109.3	48.8	2.28	0.356	94	109	2.1	50.4	0.61	0.21
9 f	109.3	48.8	2.28	0.356	188	100	1.9	50.6	0.59	0.22

Table A1.4: Experimental results: TMP newsprint (continued)

Ex. no	t _i	BW	Bi	R	S	L	M	T	en	ep
9 g	109.3	48.8	2.28	0.356	187	138	2.0	50.5	0.62	0.23
9 h	109.3	48.8	2.28	0.356	187	173	2.0	49.3	0.64	0.25
9 i	109.3	48.8	2.28	0.356	188	141	2.0	49.3	0.62	0.24
9 j	109.3	48.8	2.28	0.356	192	40	1.9	48.9	0.54	0.12
10 a	109.3	48.8	2.28	0.356	528	137	1.9	46.0	0.59	0.25
10 b	109.3	48.8	2.28	0.356	540	107	2.0	46.1	0.57	0.22
10 c	109.3	48.8	2.28	0.356	519	172	2.0	45.2	0.62	0.27
10 d	109.3	48.8	2.28	0.356	508	212	1.8	45.2	0.61	0.28
10 e	109.3	48.8	2.28	0.356	576	176	1.9	45.2	0.61	0.25
10 f	109.3	48.8	2.28	0.356	534	142	1.9	45.3	0.60	0.25
10 g	109.3	48.8	2.28	0.356	566	136	1.9	48.3	0.60	0.24
10 h	109.3	48.8	2.28	0.356	530	106	2.0	48.2	0.57	0.21
10 i	109.3	48.8	2.28	0.356	530	171	2.0	48.2	0.62	0.26
10 j	109.3	48.8	2.28	0.356	526	211	2.1	48.4	0.63	0.27
10 k	109.3	48.8	2.28	0.356	539	175	1.9	48.4	0.61	0.26
10 l	109.3	48.8	2.28	0.356	544	142	1.9	48.2	0.61	0.24
10 m	109.3	48.8	2.28	0.356	96	98	1.9	49.3	0.58	0.24
10 n	109.3	48.8	2.28	0.356	96	133	2.0	49.3	0.61	0.27
10 o	109.3	48.8	2.28	0.356	99	42	1.9	49.1	0.51	0.17
10 p	109.3	48.8	2.28	0.356	92	167	1.9	49.0	0.63	0.29
10 q	109.3	48.8	2.28	0.356	95	208	1.9	49.0	0.63	0.30
10 r	109.3	48.8	2.28	0.356	97	106	1.9	49.1	0.58	0.24
10 s	109.3	48.8	2.28	0.356	340	140	1.4	48.1	0.60	0.25
10 t	109.3	48.8	2.28	0.356	280	176	1.4	48.1	0.61	0.27
11 a	110.4	48.8	2.30	0.356	565	137	6.4	48.4	0.61	0.32
11 b	110.4	48.8	2.30	0.356	544	108	6.5	48.3	0.62	0.29
11 c	110.4	48.8	2.30	0.356	524	171	6.5	47.1	0.64	0.34
11 d	110.4	48.8	2.30	0.356	528	212	6.5	47.1	0.64	0.36
11 e	110.4	48.8	2.30	0.356	538	177	6.4	47.2	0.62	0.34
11 f	110.4	48.8	2.30	0.356	542	143	6.5	47.1	0.62	0.32
11 g	110.4	48.8	2.30	0.356	321	137	6.5	46.7	0.58	0.33
11 h	110.4	48.8	2.30	0.356	317	170	6.4	46.0	0.62	0.36
11 i	110.4	48.8	2.30	0.356	319	211	6.4	46.0	0.65	0.37
11 j	110.4	48.8	2.30	0.356	339	42	6.5	46.1	0.52	0.22
11 k	110.4	48.8	2.30	0.356	310	100	6.4	46.0	0.59	0.30
11 l	110.4	48.8	2.30	0.356	319	135	6.4	46.0	0.61	0.33
11 m	110.4	48.8	2.30	0.356	186	137	6.4	48.4	0.61	0.35
11 n	110.4	48.8	2.30	0.356	198	106	6.5	48.3	0.58	0.32
11 o	110.4	48.8	2.30	0.356	191	172	6.5	48.3	0.64	0.35
11 p	110.4	48.8	2.30	0.356	202	41	6.4	47.5	0.52	0.22
11 q	110.4	48.8	2.30	0.356	184	136	6.5	47.1	0.61	0.34
11 r	110.4	48.8	2.30	0.356	96	98	6.4	48.2	0.60	0.33
11 s	110.4	48.8	2.30	0.356	96	135	6.5	48.1	0.62	0.36
11 t	110.4	48.8	2.30	0.356	98	42	6.5	48.1	0.54	0.24
11 u	110.4	48.8	2.30	0.356	94	171	6.4	48.1	0.65	0.37
11 v	110.4	48.8	2.30	0.356	98	107	6.4	48.1	0.60	0.32

Table A1.4: Experimental results: TMP newsprint (continued)

Ex. no	t _i	BW	Bi	R	S	L	M	T	en	ep
11 w	110.4	48.8	2.30	0.356	982	171	6.4	43.1	0.63	0.32
11 x	110.4	48.8	2.30	0.356	980	140	6.2	42.9	0.62	0.31
11 y	110.4	48.8	2.30	0.356	956	211	6.2	42.9	0.66	0.32
11 z	110.4	48.8	2.30	0.356	947	176	6.5	43.1	0.64	0.32
11 za	110.4	48.8	2.30	0.356	953	211	6.3	41.9	0.65	0.34
11 zb	110.4	48.8	2.30	0.356	965	109	6.3	40.9	0.59	0.27
12 a	110	48.8	2.29	0.356	566	135	4.0	59.9	0.62	0.30
12 b	110	48.8	2.29	0.356	540	105	3.9	59.9	0.59	0.27
12 c	110	48.8	2.29	0.356	523	170	3.9	59.9	0.63	0.32
12 d	110	48.8	2.29	0.356	525	210	3.9	59.9	0.65	0.33
12 e	110	48.8	2.29	0.356	565	170	3.9	60.6	0.62	0.32
12 f	110	48.8	2.29	0.356	544	140	3.9	59.9	0.62	0.30
12 g	110	48.8	2.29	0.356	986	169	4.0	56.6	0.61	0.31
12 h	110	48.8	2.29	0.356	977	140	3.8	55.7	0.62	0.29
12 i	110	48.8	2.29	0.356	955	210	3.7	55.7	0.64	0.33
12 j	110	48.8	2.29	0.356	957	108	3.8	55.7	0.61	0.26
12 k	110	48.8	2.29	0.356	960	210	3.8	55.7	0.63	0.32
12 l	110	48.8	2.29	0.356	958	174	3.8	55.7	0.62	0.30
12 m	110	48.8	2.29	0.356	317	136	3.8	59.9	0.60	0.33
12 n	110	48.8	2.29	0.356	323	170	3.8	59.9	0.64	0.34
12 o	110	48.8	2.29	0.356	317	210	3.9	59.9	0.64	0.35
12 p	110	48.8	2.29	0.356	330	108	3.8	59.8	0.60	0.28
12 q	110	48.8	2.29	0.356	321	137	3.9	59.9	0.62	0.32
12 r	110	48.8	2.29	0.356	327	41	3.7	59.8	0.56	0.21
12 s	110	48.8	2.29	0.356	194	136	3.9	59.9	0.63	0.33
12 t	110	48.8	2.29	0.356	195	106	3.9	59.9	0.61	0.31
12 u	110	48.8	2.29	0.356	187	171	3.8	59.8	0.64	0.35
12 v	110	48.8	2.29	0.356	204	41	3.8	59.8	0.57	0.21
12 w	110	48.8	2.29	0.356	179	136	3.7	59.0	0.64	0.33
12 x	110	48.8	2.29	0.356	96	99	3.6	59.7	0.61	0.30
12 y	110	48.8	2.29	0.356	90	135	3.7	60.1	0.63	0.31
12 z	110	48.8	2.29	0.356	104	41	3.8	59.7	0.56	0.22
12 za	110	48.8	2.29	0.356	98	170	3.8	59.7	0.65	0.35
12 zb	110	48.8	2.29	0.356	93	106	3.7	59.8	0.62	0.31
12 zc	110	48.8	2.29	0.356	527	169	3.8	59.9	0.63	0.32
13 a	107.6	48.8	2.24	0.356	323	97	1.5	49.3	0.59	0.21
13 b	107.6	48.8	2.24	0.356	306	210	1.6	49.3	0.61	0.28
13 c	107.6	48.8	2.24	0.356	328	139	1.5	49.2	0.57	0.21
13 d	107.6	48.8	2.24	0.356	322	170	1.5	49.3	0.60	0.26
13 e	107.6	48.8	2.24	0.356	331	41	1.6	49.2	0.51	0.14
13 f	107.6	48.8	2.24	0.356	315	134	1.6	49.2	0.59	0.24
14 a	110.3	48.8	2.30	0.356	564	133	1.3	74.9	0.65	0.28
14 b	110.3	48.8	2.30	0.356	533	104	1.3	75.0	0.63	0.26
14 c	110.3	48.8	2.30	0.356	524	167	1.3	74.7	0.66	0.30
14 d	110.3	48.8	2.30	0.356	532	208	1.3	74.9	0.67	0.33
14 e	110.3	48.8	2.30	0.356	540	167	1.2	73.7	0.65	0.29

Table A1.4: Experimental results: TMP newsprint (continued)

Ex. no	t _i	BW	Bi	R	S	L	M	T	en	ep
14 f	110.3	48.8	2.30	0.356	525	138	1.2	72.8	0.64	0.31
14 g	110.3	48.8	2.30	0.356	355	134	1.3	74.8	0.60	0.30
14 h	110.3	48.8	2.30	0.356	307	167	1.2	73.7	0.65	0.33
14 i	110.3	48.8	2.30	0.356	305	208	1.3	73.5	0.67	0.35
14 j	110.3	48.8	2.30	0.356	327	107	1.2	73.6	0.62	0.29
14 k	110.3	48.8	2.30	0.356	320	135	1.2	73.6	0.65	0.31
14 l	110.3	48.8	2.30	0.356	321	42	1.3	73.5	0.57	0.20
14 m	110.3	48.8	2.30	0.356	974	137	1.4	69.7	0.64	0.28
14 n	110.3	48.8	2.30	0.356	189	133	1.1	73.0	0.64	0.34
14 o	110.3	48.8	2.30	0.356	191	104	1.2	72.8	0.64	0.31
14 p	110.3	48.8	2.30	0.356	181	168	1.2	72.5	0.67	0.35
14 q	110.3	48.8	2.30	0.356	201	42	1.2	72.2	0.57	0.21
14 r	110.3	48.8	2.30	0.356	176	133	1.2	72.2	0.65	0.32
14 s	110.3	48.8	2.30	0.356	93	98	1.4	74.2	0.65	0.31
14 t	110.3	48.8	2.30	0.356	90	134	1.3	74.1	0.67	0.33
14 u	110.3	48.8	2.30	0.356	98	42	1.4	73.9	0.59	0.24
14 v	110.3	48.8	2.30	0.356	84	169	1.3	74.0	0.69	0.37
14 w	110.3	48.8	2.30	0.356	95	104	1.4	73.5	0.65	0.32
14 x	110.3	48.8	2.30	0.356	556	134	1.2	74.9	0.64	0.30
14 y	110.3	48.8	2.30	0.356	977	168	1.3	69.7		0.30
15 a	109.5	48.8	2.28	0.356	530	135	3.3	38.7	0.63	0.25
15 b	109.5	48.8	2.28	0.356	523	104	3.4	38.7	0.60	0.23
15 c	109.5	48.8	2.28	0.356	527	171	3.3	38.6	0.65	0.27
15 d	109.5	48.8	2.28	0.356	523	211	3.3	38.6	0.65	0.29
15 e	109.5	48.8	2.28	0.356	529	176	3.4	38.5	0.64	0.27
15 f	109.5	48.8	2.28	0.356	535	141	3.3	38.7	0.63	0.26
15 g	109.5	48.8	2.28	0.356	179	134	3.4	40.8	0.62	0.29
15 h	109.5	48.8	2.28	0.356	193	103	3.3	40.0	0.62	0.26
15 i	109.5	48.8	2.28	0.356	182	170	3.2	39.9	0.64	0.31
15 j	109.5	48.8	2.28	0.356	201	41	3.2	39.8	0.55	0.17
15 k	109.5	48.8	2.28	0.356	177	135	3.3	39.9	0.63	0.29
15 l	109.5	48.8	2.28	0.356	92	99	3.3	39.9	0.62	0.26
15 m	109.5	48.8	2.28	0.356	90	135	3.4	39.9	0.62	0.29
15 n	109.5	48.8	2.28	0.356	97	41	3.4	39.8	0.55	0.18
15 o	109.5	48.8	2.28	0.356	84	171	3.4	39.9	0.65	0.31
15 p	109.5	48.8	2.28	0.356	96	105	3.3	39.8	0.60	0.27
15 q	109.5	48.8	2.28	0.356	298	134	3.4	39.9	0.64	0.28
15 r	109.5	48.8	2.28	0.356	318	169	3.3	39.9	0.63	0.30
15 s	109.5	48.8	2.28	0.356	318	209	3.3	39.9	0.64	0.30
15 t	109.5	48.8	2.28	0.356	319	104	3.3	39.9	0.57	0.24
15 u	109.5	48.8	2.28	0.356	327	41	3.4	39.8	0.55	0.17
15 v	109.5	48.8	2.28	0.356	309	134	3.4	39.9	0.62	0.27
15 w	109.5	48.8	2.28	0.356	218	98	3.2	40.8	0.61	
16 a	108	48.8	2.25	0.356	90	103	7.0	30.1	0.57	0.27
16 a'	108	48.8	2.25	0.356	92	101	6.8	30.2	0.56	0.27
16 b	108	48.8	2.25	0.356	91	135	6.9	30.2	0.58	0.30

Table A1.4: Experimental results: TMP newsprint (continued)

Ex. no	t _i	BW	Bi	R	S	L	M	T	en	ep
16 b'	108	48.8	2.25	0.356	92	135	6.8	30.0	0.58	0.30
16 c	108	48.8	2.25	0.356	97	40	6.9	30.1	0.50	0.18
16 c'	108	48.8	2.25	0.356	93	39	6.9	30.1	0.48	0.17
16 d	108	48.8	2.25	0.356	86	169	7.0	30.3	0.60	0.31
16 d'	108	48.8	2.25	0.356	92	171	6.9	30.0	0.59	0.32
16 e	108	48.8	2.25	0.356	94	105	7.0	30.1	0.56	0.27
16 e'	108	48.8	2.25	0.356	92	106	7.0	30.2	0.55	0.27
16 f	108	48.8	2.25	0.356	186	134	7.0	30.2	0.59	0.29
16 g	108	48.8	2.25	0.356	192	105	6.9	29.2	0.57	0.26
16 h	108	48.8	2.25	0.356	181	168	7.0	29.2	0.60	0.30
16 i	108	48.8	2.25	0.356	202	40	7.0	29.2	0.50	0.17
16 j	108	48.8	2.25	0.356	175	134	7.0	29.2	0.58	0.29
16 k	108	48.8	2.25	0.356	536	138	7.1	28.0	0.59	0.25
16 l	108	48.8	2.25	0.356	536	110	7.1	28.0	0.57	0.23
16 m	108	48.8	2.25	0.356	525	171	7.1	28.0	0.60	0.28
16 n	108	48.8	2.25	0.356	521	210	7.0	27.9	0.61	0.30
16 o	108	48.8	2.25	0.356	529	175	7.1	28.0	0.59	0.28
16 p	108	48.8	2.25	0.356	537	141	7.1	28.0	0.58	0.25
16 q	108	48.8	2.25	0.356	309	134	7.0	29.2	0.56	0.27
16 r	108	48.8	2.25	0.356	319	167	7.0	29.2	0.59	0.29
16 s	108	48.8	2.25	0.356	313	208	7.1	29.3	0.60	0.31
16 t	108	48.8	2.25	0.356	324	108	7.1	29.2	0.54	0.24
16 u	108	48.8	2.25	0.356	315	135	7.0	29.3	0.56	0.25
16 v	108	48.8	2.25	0.356	325	41	7.0	29.2	0.49	0.15
16 w	108	48.8	2.25	0.356	982	167	7.0	28.0	0.59	0.27
16 x	108	48.8	2.25	0.356	974	137	7.0	28.0	0.57	0.25
16 y	108	48.8	2.25	0.356	950	206	7.0	28.0	0.59	0.28
16 z	108	48.8	2.25	0.356	949	108	7.0	28.0	0.55	0.21
16 za	108	48.8	2.25	0.356	958	207	7.2	28.0	0.61	0.27
16 zb	108	48.8	2.25	0.356	951	172	7.1	27.1	0.57	0.24
17 a	110.8	48.8	2.31	0.356	93	103	10.6	27.3	0.59	0.34
17 b	110.8	48.8	2.31	0.356	91	138	10.6	27.3	0.62	0.36
17 c	110.8	48.8	2.31	0.356	95	38	10.6	27.4	0.52	0.25
17 d	110.8	48.8	2.31	0.356	93	174	10.5	27.2	0.64	0.39
17 e	110.8	48.8	2.31	0.356	93	110	10.5	27.4	0.60	0.35
17 f	110.8	48.8	2.31	0.356	179	138	10.3	27.1	0.61	0.36
17 g	110.8	48.8	2.31	0.356	187	108	10.2	27.1	0.59	0.32
17 h	110.8	48.8	2.31	0.356	177	172	10.2	27.2	0.62	0.37
17 i	110.8	48.8	2.31	0.356	196	38	10.1	27.1	0.51	0.23
17 j	110.8	48.8	2.31	0.356	172	137	10.2	27.1	0.60	0.35
17 k	110.8	48.8	2.31	0.356	565	137	10.1	25.8	0.60	0.32
17 l	110.8	48.8	2.31	0.356	535	108	10.1	25.8	0.58	0.30
17 m	110.8	48.8	2.31	0.356	520	172	10.2	24.9	0.62	0.33
17 n	110.8	48.8	2.31	0.356	525	210	10.0	24.9	0.63	0.35
17 o	110.8	48.8	2.31	0.356	532	176	10.2	24.9	0.62	0.33
17 p	110.8	48.8	2.31	0.356	537	142	10.2	24.8	0.60	0.31

Table A1.4: Experimental results: TMP newsprint (continued)

Ex. no	t _i	BW	Bi	R	S	L	M	T	en	ep
17 q	110.8	48.8	2.31	0.356	322	137	10.4	27.1	0.59	0.32
17 r	110.8	48.8	2.31	0.356	306	172	10.3	27.1	0.61	0.34
17 s	110.8	48.8	2.31	0.356	330	39	10.3	25.8	0.50	0.21
17 t	110.8	48.8	2.31	0.356	305	212	10.4	25.7	0.62	0.36
17 u	110.8	48.8	2.31	0.356	316	108	10.4	25.7	0.57	0.29
17 v	110.8	48.8	2.31	0.356	322	141	10.5	25.7	0.60	0.31
17 w	110.8	48.8	2.31	0.356	974	166	10.1	22.7	0.60	0.30
17 x	110.8	48.8	2.31	0.356	971	137	10.0	22.8	0.59	0.27
17 y	110.8	48.8	2.31	0.356	940	205	9.4	22.8	0.62	0.29
18 a	104.1	48.8	2.17	0.356	92	97	1.1	28.0	0.52	0.14
18 b	104.1	48.8	2.17	0.356	92	129	1.1	28.1	0.53	0.17
18 c	104.1	48.8	2.17	0.356	95	41	1.1	28.2	0.46	0.07
18 d	104.1	48.8	2.17	0.356	87	163	1.0	28.0	0.56	0.19
18 e	104.1	48.8	2.17	0.356	94	103	1.0	28.0	0.53	0.15
18 f	104.1	48.8	2.17	0.356	184	132	1.1	28.0	0.53	0.17
18 g	104.1	48.8	2.17	0.356	186	104	1.1	28.0	0.52	0.16
18 h	104.1	48.8	2.17	0.356	177	164	1.1	28.1	0.55	0.19
18 i	104.1	48.8	2.17	0.356	194	41	1.1	28.1	0.46	0.08
18 j	104.1	48.8	2.17	0.356	171	130	1.1	28.1	0.54	0.17
18 k	104.1	48.8	2.17	0.356	560	130	1.2	28.1	0.55	0.17
18 l	104.1	48.8	2.17	0.356	536	103	1.2	28.1	0.53	0.15
18 m	104.1	48.8	2.17	0.356	518	163	1.2	28.1	0.57	0.19
18 n	104.1	48.8	2.17	0.356	520	204	1.2	28.0	0.59	0.20
18 o	104.1	48.8	2.17	0.356	530	167	1.2	28.0	0.57	0.19
18 p	104.1	48.8	2.17	0.356	538	135	1.2	28.2	0.55	0.17
18 q	104.1	48.8	2.17	0.356	978	162	1.6	27.1	0.56	0.18
18 r	104.1	48.8	2.17	0.356	979	133	1.4	27.1	0.54	0.16
18 s	104.1	48.8	2.17	0.356	950	165	1.8	27.1	0.58	0.19
18 t	104.1	48.8	2.17	0.356	942	203	1.4	27.1	0.58	0.19
18 u	104.1	48.8	2.17	0.356	959	103	1.4	27.1	0.53	0.13
18 v	104.1	48.8	2.17	0.356	960	203	1.5	27.1	0.57	0.19
18 w	104.1	48.8	2.17	0.356	948	167	1.5	27.1	0.56	0.17
19 a	106.7	48.8	2.22	0.356	92	98	4.5	27.2	0.55	0.23
19 b	106.7	48.8	2.22	0.356	90	132	4.5	27.0	0.57	0.26
19 c	106.7	48.8	2.22	0.356	97	40	4.5	27.1	0.49	0.14
19 d	106.7	48.8	2.22	0.356	87	167	4.5	27.1	0.61	0.29
19 e	106.7	48.8	2.22	0.356	96	104	4.4	27.1	0.56	0.23
19 f	106.7	48.8	2.22	0.356	177	132	4.5	28.1	0.56	0.24
19 g	106.7	48.8	2.22	0.356	187	102	4.5	28.0	0.55	0.22
19 h	106.7	48.8	2.22	0.356	176	166	4.5	28.1	0.60	0.27
19 i	106.7	48.8	2.22	0.356	197	40	4.5	28.0	0.48	0.14
19 j	106.7	48.8	2.22	0.356	170	132	4.5	28.0	0.57	0.25
19 k	106.7	48.8	2.22	0.356	556	131	4.5	28.1	0.57	0.23
19 l	106.7	48.8	2.22	0.356	533	102	4.4	28.0	0.54	0.21
19 m	106.7	48.8	2.22	0.356	520	165	4.5	28.1	0.58	0.25
19 n	106.7	48.8	2.22	0.356	532	206	4.4	27.1	0.61	0.27

Table A1.4: Experimental results: TMP newsprint (continued)

Ex. no	t _i	BW	Bi	R	S	L	M	T	en	ep
19 o	106.7	48.8	2.22	0.356	532	169	4.5	27.2	0.59	0.24
19 p	106.7	48.8	2.22	0.356	533	136	4.5	27.2	0.57	0.23
19 q	106.7	48.8	2.22	0.356	319	131	4.6	28.1	0.56	0.23
19 r	106.7	48.8	2.22	0.356	315	164	4.5	28.1	0.56	0.25
19 s	106.7	48.8	2.22	0.356	328	40	4.4	28.1	0.48	0.14
19 t	106.7	48.8	2.22	0.356	302	207	4.5	28.1	0.60	0.28
19 u	106.7	48.8	2.22	0.356	320	102	4.5	28.1	0.53	0.21
19 v	106.7	48.8	2.22	0.356	321	132	4.5	28.1	0.56	0.23
19 w	106.7	48.8	2.22	0.356	985	164	4.4	27.2	0.61	0.24
19 x	106.7	48.8	2.22	0.356	979	134	4.5	27.2	0.59	0.22
19 y	106.7	48.8	2.22	0.356	957	205	4.5	27.1	0.62	0.26
19 z	106.7	48.8	2.22	0.356	948	102	4.5	27.2	0.54	0.19
19 za	106.7	48.8	2.22	0.356	956	205	4.5	27.2	0.59	0.25
19 zb	106.7	48.8	2.22	0.356	951	168	4.4	27.1	0.57	0.23
20 a	106.4	48.8	2.22	0.356	92	97	3.4	28.1	0.54	0.22
20 b	106.4	48.8	2.22	0.356	90	130	3.5	28.1	0.55	0.24
20 c	106.4	48.8	2.22	0.356	97	41	3.5	28.3	0.47	0.15
20 d	106.4	48.8	2.22	0.356	86	164	3.5	28.1	0.58	0.27
20 e	106.4	48.8	2.22	0.356	95	103	3.5	28.0	0.54	0.22
20 f	106.4	48.8	2.22	0.356	176	130	3.5	28.1	0.55	0.22
20 g	106.4	48.8	2.22	0.356	188	103	3.6	28.1	0.54	0.21
20 h	106.4	48.8	2.22	0.356	177	162	3.6	28.0	0.57	0.24
20 i	106.4	48.8	2.22	0.356	197	40	3.5	28.1	0.46	0.12
20 j	106.4	48.8	2.22	0.356	171	129	3.6	28.1	0.56	0.23
20 k	106.4	48.8	2.22	0.356	550	128	3.6	28.0	0.53	0.20
20 l	106.4	48.8	2.22	0.356	521	101	3.6	28.1	0.53	0.20
20 m	106.4	48.8	2.22	0.356	520	162	3.5	28.1	0.56	0.23
20 n	106.4	48.8	2.22	0.356	524	203	3.5	28.0	0.57	0.26
20 o	106.4	48.8	2.22	0.356	532	167	3.5	28.1	0.55	0.24
20 p	106.4	48.8	2.22	0.356	538	134	3.6	28.2	0.55	0.21
20 q	106.4	48.8	2.22	0.356	337	129	3.5	29.4	0.55	0.23
20 r	106.4	48.8	2.22	0.356	303	161	3.6	29.4	0.54	0.24
20 s	106.4	48.8	2.22	0.356	326	40	3.6	29.4	0.48	0.13
20 t	106.4	48.8	2.22	0.356	304	204	3.5	29.3	0.59	0.26
20 u	106.4	48.8	2.22	0.356	321	102	3.4	28.4	0.52	0.19
20 v	106.4	48.8	2.22	0.356	320	131	3.5	28.1	0.55	0.22
21 a	106	48.8	2.21	0.356	92	98	1.2	47.9	0.59	0.17
21 b	106	48.8	2.21	0.356	92	130	1.3	48.3	0.61	0.20
21 c	106	48.8	2.21	0.356	98	40	1.3	48.5	0.54	0.08
21 d	106	48.8	2.21	0.356	85	164	1.3	48.2	0.61	0.24
21 e	106	48.8	2.21	0.356	96	103	1.2	48.5	0.58	0.18
21 f	106	48.8	2.21	0.356	190	131	1.2	47.1	0.61	0.20
21 g	106	48.8	2.21	0.356	191	101	1.3	47.1	0.59	0.17
21 h	106	48.8	2.21	0.356	182	165	1.3	47.1	0.62	0.23
21 i	106	48.8	2.21	0.356	202	40	1.3	47.1	0.54	0.11
21 j	106	48.8	2.21	0.356	191	131	1.3	47.1	0.60	0.20

Table A1.4: Experimental results: TMP newsprint (continued)

Ex. no	t _i	BW	Bi	R	S	L	M	T	en	ep
21 k	106	48.8	2.21	0.356	567	131	1.3	48.3	0.58	0.19
21 l	106	48.8	2.21	0.356	537	103	1.3	48.3	0.57	0.16
21 m	106	48.8	2.21	0.356	517	164	1.3	48.4	0.59	0.20
21 n	106	48.8	2.21	0.356	519	205	1.3	48.3	0.60	0.23
21 o	106	48.8	2.21	0.356	530	169	1.2	48.3	0.59	0.20
21 p	106	48.8	2.21	0.356	539	136	1.2	48.4	0.58	0.19
21 q	106	48.8	2.21	0.356	316	130	1.4	47.6	0.58	0.21
21 r	106	48.8	2.21	0.356	312	164	1.4	47.1	0.58	0.22
21 s	106	48.8	2.21	0.356	330	40	1.3	47.1	0.53	0.10
21 t	106	48.8	2.21	0.356	303	206	1.4	46.1	0.62	0.23
21 u	106	48.8	2.21	0.356	317	102	1.4	46.2	0.56	0.17
21 v	106	48.8	2.21	0.356	322	132	1.4	46.2	0.59	0.19
21 w	106	48.8	2.21	0.356	977	165	1.3	46.2	0.60	0.20
21 x	106	48.8	2.21	0.356	973	134	1.3	46.2	0.59	0.18
21 y	106	48.8	2.21	0.356	954	206	1.4	46.2	0.61	0.22
21 z	106	48.8	2.21	0.356	949	102	1.2	46.2	0.58	0.15
21 za	106	48.8	2.21	0.356	955	206	1.4	46.2	0.61	0.21
21 zb	106	48.8	2.21	0.356	952	169	1.3	46.2	0.59	0.19
22 a	109.9	48.8	2.29	0.356	93	102	2.9	61.7	0.60	0.26
22 b	109.9	48.8	2.29	0.356	92	134	2.9	61.5	0.60	0.28
22 c	109.9	48.8	2.29	0.356	95	38	2.9	61.5	0.55	0.16
22 d	109.9	48.8	2.29	0.356	88	168	3.0	61.6	0.62	0.30
22 e	109.9	48.8	2.29	0.356	95	103	2.9	61.6	0.60	0.26
22 f	109.9	48.8	2.29	0.356	186	135	3.0	62.4	0.62	0.28
22 g	109.9	48.8	2.29	0.356	187	103	3.0	62.4	0.61	0.25
22 h	109.9	48.8	2.29	0.356	177	170	3.1	62.2	0.62	0.30
22 i	109.9	48.8	2.29	0.356	199	38	3.1	62.1	0.55	0.15
22 j	109.9	48.8	2.29	0.356	171	134	3.2	61.8	0.61	0.29
22 k	109.9	48.8	2.29	0.356	547	134	3.1	60.4	0.62	0.26
22 l	109.9	48.8	2.29	0.356	522	103	3.1	60.5	0.59	0.24
22 m	109.9	48.8	2.29	0.356	521	168	3.1	60.7	0.61	0.28
22 n	109.9	48.8	2.29	0.356	525	209	3.2	60.4	0.62	0.30
22 o	109.9	48.8	2.29	0.356	533	172	3.2	60.5	0.62	0.28
22 p	109.9	48.8	2.29	0.356	538	138	3.1	60.4	0.61	0.26
22 q	109.9	48.8	2.29	0.356	309	133	3.2	60.5	0.62	0.27
22 r	109.9	48.8	2.29	0.356	317	167	3.3	60.4	0.61	0.29
22 s	109.9	48.8	2.29	0.356	329	38	3.3	60.4	0.56	0.15
22 t	109.9	48.8	2.29	0.356	305	209	3.4	60.2	0.64	0.31
22 u	109.9	48.8	2.29	0.356	317	103	3.4	60.1	0.59	0.23
22 v	109.9	48.8	2.29	0.356	322	134	3.3	60.3	0.62	0.27
22 w	109.9	48.8	2.29	0.356	980	169	3.5	57.2	0.63	0.27
22 x	109.9	48.8	2.29	0.356	977	137	3.4	57.2	0.62	0.26
22 y	109.9	48.8	2.29	0.356	957	209	3.5	57.2	0.63	0.28
22 z	109.9	48.8	2.29	0.356	949	103	3.3	57.2	0.61	0.23
22 za	109.9	48.8	2.29	0.356	955	209	3.5	57.1	0.64	0.28
22 zb	109.9	48.8	2.29	0.356	953	173	3.6	56.2	0.64	0.26

Table A1.4: Experimental results: TMP newsprint (continued)

Ex. no	t _i	BW	Bi	R	S	L	M	T	en	ep
23 a	108.6	48.8	2.26	0.356	92	98	4.6	46.1	0.59	0.27
23 b	108.6	48.8	2.26	0.356	91	132	4.8	46.0	0.60	0.32
23 c	108.6	48.8	2.26	0.356	97	39	4.6	46.0	0.54	0.19
23 d	108.6	48.8	2.26	0.356	88	167	4.6	46.1	0.63	0.34
23 e	108.6	48.8	2.26	0.356	94	103	4.5	46.2	0.60	0.29
23 f	108.6	48.8	2.26	0.356	182	132	4.7	48.3	0.61	0.31
23 g	108.6	48.8	2.26	0.356	187	102	4.7	48.2	0.60	0.28
23 h	108.6	48.8	2.26	0.356	176	167	4.8	48.3	0.62	0.32
23 i	108.6	48.8	2.26	0.356	197	39	4.8	47.2	0.55	0.19
23 j	108.6	48.8	2.26	0.356	171	132	4.8	47.0	0.61	0.31
23 k	108.6	48.8	2.26	0.356	543	132	4.9	45.2	0.62	0.28
23 l	108.6	48.8	2.26	0.356	530	101	5.1	45.1	0.60	0.26
23 m	108.6	48.8	2.26	0.356	524	167	4.9	44.0	0.63	0.31
23 n	108.6	48.8	2.26	0.356	521	208	5.0	44.0	0.64	0.33
23 o	108.6	48.8	2.26	0.356	527	172	5.1	44.0	0.63	0.31
23 p	108.6	48.8	2.26	0.356	537	137	4.9	44.0	0.63	0.28
23 q	108.6	48.8	2.26	0.356	353	132	5.2	47.0	0.64	0.29
23 r	108.6	48.8	2.26	0.356	314	167	5.2	46.7	0.63	0.31
23 s	108.6	48.8	2.26	0.356	320	39	5.1	46.1	0.57	0.17
23 t	108.6	48.8	2.26	0.356	309	208	5.1	46.2	0.65	0.33
23 u	108.6	48.8	2.26	0.356	314	103	5.2	46.1	0.60	0.26
23 v	108.6	48.8	2.26	0.356	321	134	5.1	42.6	0.63	0.28
24 a	110.6	48.8	2.30	0.202	97	99	2.2	30.1	0.61	0.21
24 b	110.6	48.8	2.30	0.202	94	128	2.2	30.1	0.63	0.25
24 c	110.6	48.8	2.30	0.202	108	45	2.2	30.1	0.57	0.11
24 d	110.6	48.8	2.30	0.202	85	173	2.2	30.2	0.65	0.29
24 e	110.6	48.8	2.30	0.202	104	104	2.2	30.6	0.61	0.22
24 f	110.6	48.8	2.30	0.202	187	128	2.2	30.2	0.60	0.24
24 g	110.6	48.8	2.30	0.202	193	103	2.2	30.2	0.59	0.21
24 h	110.6	48.8	2.30	0.202	177	172	2.1	30.2	0.62	0.27
24 i	110.6	48.8	2.30	0.202	210	45	2.1	30.1	0.49	0.11
24 j	110.6	48.8	2.30	0.202	171	128	2.1	30.1	0.60	0.24
24 k	110.6	48.8	2.30	0.202	321	131	2.1	30.1	0.61	0.22
24 l	110.6	48.8	2.30	0.202	314	175	2.1	30.1	0.65	0.25
24 m	110.6	48.8	2.30	0.202	346	45	2.0	30.0	0.55	0.10
24 n	110.6	48.8	2.30	0.202	294	207	2.0	30.1	0.65	0.28
24 o	110.6	48.8	2.30	0.202	331	105	2.1	30.1	0.61	0.20
24 p	110.6	48.8	2.30	0.202	323	131	2.2	30.1	0.62	0.22
24 q	110.6	48.8	2.30	0.202	544	129	2.0	30.1	0.62	0.22
24 r	110.6	48.8	2.30	0.202	540	104	2.1	30.2	0.60	0.20
24 s	110.6	48.8	2.30	0.202	527	172	2.0	30.1	0.65	0.25
24 t	110.6	48.8	2.30	0.202	527	206	2.1	30.1	0.65	0.27
24 u	110.6	48.8	2.30	0.202	538	177	2.2	30.1	0.65	0.24
24 v	110.6	48.8	2.30	0.202	546	134	2.2	30.1	0.62	0.22
24 w	110.6	48.8	2.30	0.202	971	170	2.1	30.2	0.64	0.25
24 x	110.6	48.8	2.30	0.202	972	132	2.3	30.3	0.62	0.21

Table A1.4: Experimental results: TMP newsprint (continued)

Ex. no	t _i	BW	Bi	R	S	L	M	T	en	ep
24 y	110.6	48.8	2.30	0.202	948	203	2.2	30.3	0.64	0.26
24 z	110.6	48.8	2.30	0.202	970	105	2.2	30.2	0.61	0.19
24 za	110.6	48.8	2.30	0.202	953	204	2.5	30.2	0.64	0.25
24 zb	110.6	48.8	2.30	0.202	955	175	2.1	30.2	0.64	0.23
25 a	114.7	48.8	2.39	0.202	97	99	12.3	30.2	0.61	0.39
25 b	114.7	48.8	2.39	0.202	95	126	12.3	30.5	0.63	0.42
25 c	114.7	48.8	2.39	0.202	101	45	12.3	31.0	0.58	0.24
25 d	114.7	48.8	2.39	0.202	97	167	12.1	31.0	0.64	0.45
25 e	114.7	48.8	2.39	0.202	102	104	12.1	31.1	0.61	0.39
25 f	114.7	48.8	2.39	0.202	194	128	12.1	31.1	0.63	0.39
25 g	114.7	48.8	2.39	0.202	197	103	12.1	31.0	0.61	0.36
25 h	114.7	48.8	2.39	0.202	185	168	12.1	31.0	0.64	0.42
25 i	114.7	48.8	2.39	0.202	213	45	12.0	31.1	0.58	0.22
25 j	114.7	48.8	2.39	0.202	179	128	12.0	31.0	0.62	0.39
25 k	114.7	48.8	2.39	0.202	321	129	12.0	31.1	0.62	0.38
25 l	114.7	48.8	2.39	0.202	316	170	12.2	31.2	0.64	0.41
25 m	114.7	48.8	2.39	0.202	345	45	11.9	31.1	0.57	0.21
25 n	114.7	48.8	2.39	0.202	298	202	11.9	31.0	0.65	0.43
25 o	114.7	48.8	2.39	0.202	331	104	11.9	31.1	0.61	0.35
25 p	114.7	48.8	2.39	0.202	323	130	11.8	31.0	0.62	0.38
25 q	114.7	48.8	2.39	0.202	537	130	12.1	30.3	0.62	0.36
25 r	114.7	48.8	2.39	0.202	541	103	11.8	30.2	0.60	0.33
25 s	114.7	48.8	2.39	0.202	528	172	12.0	30.1	0.63	0.39
25 t	114.7	48.8	2.39	0.202	524	204	11.8	30.2	0.65	0.42
25 u	114.7	48.8	2.39	0.202	537	176	11.9	30.2	0.63	0.39
25 v	114.7	48.8	2.39	0.202	544	134	12.1	30.2	0.61	0.35
25 w	114.7	48.8	2.39	0.202	971	176	11.5	30.1	0.62	0.39
25 x	114.7	48.8	2.39	0.202	969	135	11.4	30.0	0.61	0.36
25 y	114.7	48.8	2.39	0.202	953	207	11.2	30.1	0.63	0.40
25 z	114.7	48.8	2.39	0.202	968	106	11.1	30.1	0.59	0.31
25 za	114.7	48.8	2.39	0.202	951	207	10.5	30.1	0.63	0.40
25 zb	114.7	48.8	2.39	0.202	950	180	10.3	30.1	0.63	0.37
26 a	109.7	48.8	2.28	0.202	98	103	2.1	60.4	0.63	0.27
26 b	109.7	48.8	2.28	0.202	95	129	2.1	60.2	0.64	0.32
26 c	109.7	48.8	2.28	0.202	109	42	2.1	60.3	0.55	0.11
26 d	109.7	48.8	2.28	0.202	83	167	2.2	60.3	0.65	0.35
26 e	109.7	48.8	2.28	0.202	104	102	2.2	60.2	0.63	0.28
26 f	109.7	48.8	2.28	0.202	188	124	2.1	60.3	0.72	0.29
26 g	109.7	48.8	2.28	0.202	193	101	2.1	60.4	0.70	0.26
26 h	109.7	48.8	2.28	0.202	179	160	2.0	60.4	0.74	0.32
26 i	109.7	48.8	2.28	0.202	210	43	2.2	60.6	0.63	0.12
26 j	109.7	48.8	2.28	0.202	173	123	2.2	60.3	0.72	0.30
26 k	109.7	48.8	2.28	0.202	322	122	2.1	61.0	0.65	0.30
26 l	109.7	48.8	2.28	0.202	317	157	2.1	60.9	0.66	0.33
26 m	109.7	48.8	2.28	0.202	344	43	2.1	60.7	0.56	0.13
26 n	109.7	48.8	2.28	0.202	296	191	2.2	60.6	0.66	0.34

Table A1.4: Experimental results: TMP newsprint (continued)

Ex. no	t _i	BW	Bi	R	S	L	M	T	en	ep
26 o	109.7	48.8	2.28	0.202	334	102	2.1	60.9	0.63	0.26
26 p	109.7	48.8	2.28	0.202	322	124	2.2	60.7	0.65	0.29
26 q	109.7	48.8	2.28	0.202	545	123	2.2	61.0	0.66	0.30
26 r	109.7	48.8	2.28	0.202	541	101	2.1	60.9	0.65	0.26
26 s	109.7	48.8	2.28	0.202	525	159	2.1	61.0	0.68	0.32
26 t	109.7	48.8	2.28	0.202	527	192	2.2	60.4	0.69	0.34
26 u	109.7	48.8	2.28	0.202	538	165	2.3	61.0	0.68	0.32
26 v	109.7	48.8	2.28	0.202	544	127	2.0	61.0	0.67	0.29
26 w	109.7	48.8	2.28	0.202	971	160	2.4	58.8	0.66	0.31
26 x	109.7	48.8	2.28	0.202	972	126	2.3	58.9	0.65	0.28
26 y	109.7	48.8	2.28	0.202	956	191	2.4	58.2	0.67	0.33
26 z	109.7	48.8	2.28	0.202	967	102	2.5	57.6	0.64	0.26
26 za	109.7	48.8	2.28	0.202	956	191	2.4	57.8	0.68	0.33
26 zb	109.7	48.8	2.28	0.202	956	164	2.7	57.6	0.67	0.31
26 zc	109.7	48.8	2.28	0.202	532	194	2.2	60.9	0.69	0.34
27 a	112.7	48.8	2.35	0.202	98	99	8.5	32.3	0.63	0.37
27 b	112.7	48.8	2.35	0.202	95	126	8.4	32.3	0.64	0.42
27 c	112.7	48.8	2.35	0.202	108	44	8.4	32.3	0.52	0.21
27 d	112.7	48.8	2.35	0.202	83	169	8.5	32.3	0.65	0.45
27 e	112.7	48.8	2.35	0.202	104	102	8.5	32.3	0.62	0.37
27 f	112.7	48.8	2.35	0.202	189	126	8.5	32.3	0.63	0.38
27 g	112.7	48.8	2.35	0.202	193	101	8.5	32.3	0.62	0.36
27 h	112.7	48.8	2.35	0.202	179	167	8.4	32.3	0.65	0.43
27 i	112.7	48.8	2.35	0.202	210	44	8.4	32.3	0.52	0.18
27 j	112.7	48.8	2.35	0.202	172	126	8.5	32.3	0.63	0.40
27 k	112.7	48.8	2.35	0.202	325	122	8.5	31.1	0.63	0.36
27 l	112.7	48.8	2.35	0.202	318	161	8.4	31.1	0.65	0.39
27 m	112.7	48.8	2.35	0.202	343	44	8.2	30.9	0.53	0.17
27 n	112.7	48.8	2.35	0.202	301	195	8.5	31.1	0.66	0.42
27 o	112.7	48.8	2.35	0.202	331	101	8.2	31.1	0.62	0.33
27 p	112.7	48.8	2.35	0.202	323	126	8.4	31.1	0.63	0.35
27 q	112.7	48.8	2.35	0.202	537	124	8.5	31.8	0.63	0.34
27 r	112.7	48.8	2.35	0.202	530	161	8.3	31.1	0.65	0.37
27 s	112.7	48.8	2.35	0.202	545	101	8.3	31.1	0.62	0.31
27 t	112.7	48.8	2.35	0.202	527	197	8.2	31.2	0.66	0.39
27 u	112.7	48.8	2.35	0.202	527	169	8.1	31.2	0.65	0.38
27 v	112.7	48.8	2.35	0.202	545	130	8.3	31.1	0.63	0.34
27 w	112.7	48.8	2.35	0.202	972	162	8.4	31.2	0.65	0.36
27 x	112.7	48.8	2.35	0.202	970	127	8.2	31.1	0.63	0.32
27 y	112.7	48.8	2.35	0.202	957	194	8.2	31.0	0.66	0.37
27 z	112.7	48.8	2.35	0.202	966	101	8.3	31.1	0.62	0.28
27 za	112.7	48.8	2.35	0.202	961	193	8.3	31.1	0.66	0.37
27 zb	112.7	48.8	2.35	0.202	953	166	8.4	31.1	0.65	0.33
28 a	106.7	48.8	2.22	0.202	98	99	5.2	29.3	0.59	0.25
28 b	106.7	48.8	2.22	0.202	94	129	5.2	29.3	0.61	0.30
28 c	106.7	48.8	2.22	0.202	109	45	5.2	29.3	0.49	0.30

Table A1.4: Experimental results: TMP newsprint (continued)

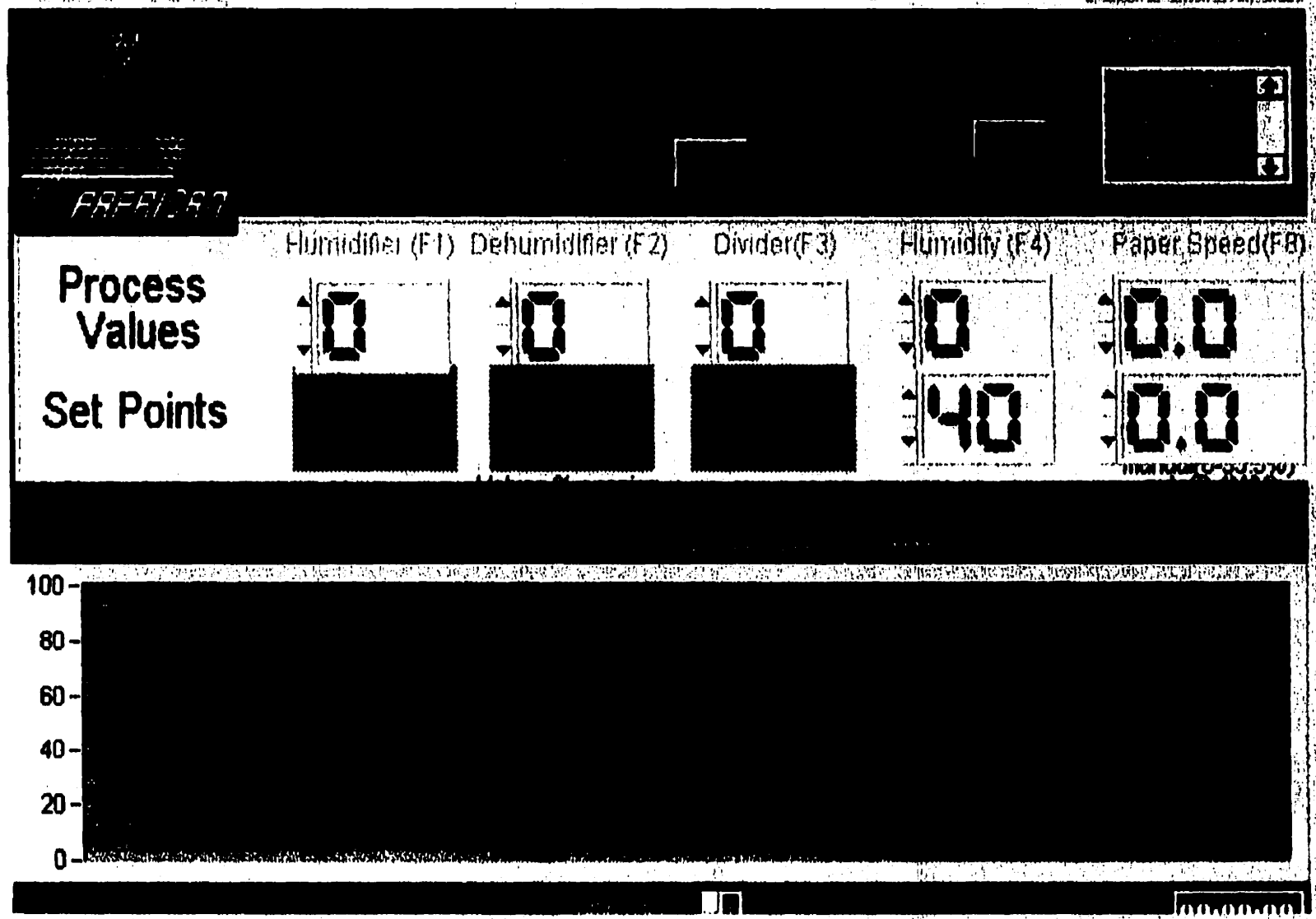
Ex. no	t _i	BW	Bi	R	S	L	M	T	en	ep
28 d	106.7	48.8	2.22	0.202	82	174	5.2	29.3	0.63	0.33
28 e	106.7	48.8	2.22	0.202	104	102	5.2	29.3	0.59	0.26
28 f	106.7	48.8	2.22	0.202	189	129	5.3	29.3	0.61	0.28
28 g	106.7	48.8	2.22	0.202	194	102	5.3	29.3	0.58	0.24
28 h	106.7	48.8	2.22	0.202	177	173	5.1	29.3	0.63	0.32
28 i	106.7	48.8	2.22	0.202	211	45	5.2	29.4	0.49	0.11
28 j	106.7	48.8	2.22	0.202	171	129	5.2	29.3	0.60	0.28
28 k	106.7	48.8	2.22	0.202	321	129	5.2	29.4	0.62	0.28
28 l	106.7	48.8	2.22	0.202	315	174	5.2	29.3	0.64	0.31
28 m	106.7	48.8	2.22	0.202	348	45	5.2	29.4	0.50	0.11
28 n	106.7	48.8	2.22	0.202	294	207	5.2	29.3	0.65	0.32
28 o	106.7	48.8	2.22	0.202	336	102	5.2	29.3	0.60	0.23
28 p	106.7	48.8	2.22	0.202	323	131	5.2	29.3	0.62	0.26
28 q	106.7	48.8	2.22	0.202	547	129	5.2	29.3	0.61	0.25
28 r	106.7	48.8	2.22	0.202	547	101	5.2	29.3	0.58	0.22
28 s	106.7	48.8	2.22	0.202	526	174	5.2	29.3	0.63	0.28
28 t	106.7	48.8	2.22	0.202	522	208	5.2	29.4	0.64	0.31
28 u	106.7	48.8	2.22	0.202	537	179	5.2	29.4	0.63	0.29
28 v	106.7	48.8	2.22	0.202	547	134	5.3	29.3	0.61	0.24
29 a	107.5	48.8	2.24	0.202	97	98	2.7	31.1	0.54	0.19
29 b	107.5	48.8	2.24	0.202	95	130	2.7	31.1	0.57	0.23
29 c	107.5	48.8	2.24	0.202	105	45	2.7	31.4	0.46	0.09
29 d	107.5	48.8	2.24	0.202	96	177	2.8	31.1	0.59	0.27
29 e	107.5	48.8	2.24	0.202	106	90	2.7	32.3	0.56	0.18
29 f	107.5	48.8	2.24	0.202	189	129	2.7	32.4	0.57	0.22
29 g	107.5	48.8	2.24	0.202	194	100	2.7	32.4	0.54	0.18
29 h	107.5	48.8	2.24	0.202	177	172	2.6	32.4	0.60	0.24
29 i	107.5	48.8	2.24	0.202	212	45	2.6	32.4	0.45	0.08
29 j	107.5	48.8	2.24	0.202	171	127	2.6	32.4	0.57	0.22
29 k	107.5	48.8	2.24	0.202	322	129	2.6	32.4	0.55	0.21
29 l	107.5	48.8	2.24	0.202	315	175	2.5	32.4	0.57	0.24
29 m	107.5	48.8	2.24	0.202	346	44	2.5	32.4	0.42	0.08
29 n	107.5	48.8	2.24	0.202	322	208	2.7	32.4	0.59	0.25
29 o	107.5	48.8	2.24	0.202	339	102	2.8	32.3	0.51	0.18
29 p	107.5	48.8	2.24	0.202	319	130	2.7	32.4	0.54	0.21
29 q	107.5	48.8	2.24	0.202	538	129	2.7	33.3	0.57	0.20
29 r	107.5	48.8	2.24	0.202	540	100	2.7	33.4	0.54	0.18
29 s	107.5	48.8	2.24	0.202	526	175	2.5	33.4	0.60	0.24
29 t	107.5	48.8	2.24	0.202	524	208	2.7	33.4	0.61	0.26
29 u	107.5	48.8	2.24	0.202	541	180	2.5	33.3	0.60	0.24
29 v	107.5	48.8	2.24	0.202	548	135	2.4	33.3	0.57	0.21
29 w	107.5	48.8	2.24	0.202	973	175	2.6	33.2	0.58	0.22
29 x	107.5	48.8	2.24	0.202	974	134	2.7	33.2	0.56	0.20
29 y	107.5	48.8	2.24	0.202	957	207	2.6	33.3	0.60	0.24
29 z	107.5	48.8	2.24	0.202	968	102	2.8	33.2	0.54	0.17
29 za	107.5	48.8	2.24	0.202	954	207	2.4	33.2	0.60	0.24

Table A1.4: Experimental results: TMP newsprint (continued)

Ex. no	t _i	BW	Bi	R	S	L	M	T	en	ep
29 zb	107.5	48.8	2.24	0.202	952	179	2.5	33.2	0.59	0.22
29 zc	107.5	48.8	2.24	0.202	323	202	2.6	32.4	0.59	0.25
30 a	110.5	48.8	2.30	0.202	97	99	3.5	60.0	0.64	
30 b	110.5	48.8	2.30	0.202	95	132	3.5	59.6	0.66	
30 c	110.5	48.8	2.30	0.202	108	45	3.6	59.6	0.52	
30 d	110.5	48.8	2.30	0.202	97	180	3.5	60.0	0.67	
30 e	110.5	48.8	2.30	0.202	104	102	3.5	59.7	0.64	
30 f	110.5	48.8	2.30	0.202	188	132	3.5	59.7	0.64	
30 g	110.5	48.8	2.30	0.202	193	102	3.5	59.4	0.62	
30 h	110.5	48.8	2.30	0.202	177	179	3.6	59.4	0.66	
30 i	110.5	48.8	2.30	0.202	212	45	3.5	59.5	0.50	
30 j	110.5	48.8	2.30	0.202	173	132	3.5	59.2	0.64	
30 k	110.5	48.8	2.30	0.202	322	131	3.5	59.1	0.63	
30 l	110.5	48.8	2.30	0.202	316	178	3.5	59.0	0.65	
30 m	110.5	48.8	2.30	0.202	347	44	3.6	59.2	0.49	
30 n	110.5	48.8	2.30	0.202	293	210	3.6	59.2	0.66	
30 o	110.5	48.8	2.30	0.202	340	102	3.6	58.8	0.61	
30 p	110.5	48.8	2.30	0.202	321	132	3.5	58.8	0.63	
30 q	110.5	48.8	2.30	0.202	539	130	3.6	58.7	0.64	
30 r	110.5	48.8	2.30	0.202	539	100	3.6	58.8	0.61	
30 s	110.5	48.8	2.30	0.202	526	178	3.5	58.7	0.65	
30 t	110.5	48.8	2.30	0.202	524	209	3.6	58.7	0.66	
30 u	110.5	48.8	2.30	0.202	537	181	3.4	58.6	0.65	
30 v	110.5	48.8	2.30	0.202	546	133	3.5	58.7	0.63	
30 w	110.5	48.8	2.30	0.202	973	176	3.5	56.4	0.64	
30 x	110.5	48.8	2.30	0.202	973	134	3.5	55.6	0.63	
30 y	110.5	48.8	2.30	0.202	958	209	3.7	55.6	0.66	
30 z	110.5	48.8	2.30	0.202	965	102	3.6	55.5	0.61	
30 za	110.5	48.8	2.30	0.202	961	209	3.5	55.5	0.66	
30 zb	110.5	48.8	2.30	0.202	956	181	3.7	55.5	0.65	

APPENDIX A2: Computer programs for data acquisition and control: facility for controlled air humidity and temperature, preconditioning chamber (detailed specifications concerning system software and hardware are available from electronics shop at Pulp and Paper Research Institute, Pointe Claire)

Temperature & Humidity control



/*

Novembre 1994

rev: Mars 1995 Heater PID
rev: Avril 1995 Speed Paper PID
rev: Mai 1995 5 temperature PID ajoutes

HUMPID2.C PID control humidity paper speed and temperature

Charge#: 358

Programmation: M. Drainville

Analog Inputs: ch0. position of humidifier valve; valve1 0-100%
ch1. position of dehumidifier valve; valve2 0-100%
ch2. position of divider valve; valve3 0-100%
ch3. temperature 0-100 C
ch4. humidity 0-100%
ch5. vitesse encodeur
ch6: temp1
ch7: temp2
ch8: temp3
ch9: temp4
ch10:temp5

Digital Outputs A: do0. close humidifier valve logique positive
do1. open humidifier valve 1=actif
do2. close dehumidifier valve
do3. open dehumidifier valve
do4. close divider valve
do5. open divider valve
do6. duct heater
do7. temp1 heater

Digital Outputs B: do0. temp2 heater
do1. temp3 heater
do2. temp4 heater
do3. temp5 heater
do4.
do5.
do6. P23, +10v REF
do7. P10, +5v

Analog Outputs: Ao0. motor control

*/

```
#include<stdio.h>
#include<conio.h>
#include<string.h>
#include<graph.h>
#include<stdlib.h>
#include<time.h>
#include<math.h>
#include<dos.h>
```

```
#include "michel.h"
#include "humpid2.h"
```

```
#define DELAY_VALVES 20
#define BASE 0x300
#define ENABLED 1
#define DISABLED 0
#define AUTO 1
#define MANUAL 0
#define REV 0
#define FWD 1
#define ON 1
#define OFF 0
#define LOW 0x08
#define MIDDLE 0x1008
#define HIGH 0x2008
#define LOAD 0x3008
#define SIMULATION ON
```

```
short panel, panel_temp, calibration, set, handle, cptr_duct=0, mode_speed=MANUAL;
short mode=AUTO, heater, id, cptr_temp1=0, cptr_temp2=0, cptr_temp3=0, cptr_temp4=0;
short cptr_temp5=0, acq=OFF, val, x, y, pointeur_array[5420];
short qty_point=1, time_chart=1, cptr_moy=0, intervale;
short point[9], deadband_manual=50, cptr_array=0;
long sp_v1, pv_v1, sp_v2, pv_v2, sp_v3, pv_v3, sp_h, pv_h, min_v1, min_v2, min_v3;
long sp_duct, pv_duct, sp_temp1, pv_temp1, max_v1, max_v2, max_v3;
long sp_temp2, pv_temp2, sp_temp3, pv_temp3, tableau_moy[20], moy_hum;
long sp_temp4, pv_temp4, sp_temp5, pv_temp5, pv_dp=0, sp_speed;
double ratio_v1=1, ratio_v2=1, ratio_v3=1, b0_h, b1_h, b2_h, p_h=0, i_h=0, d_h=0;
double error_h[]={0,0,0,0}, value_duct=0, temp_duty, p_s, i_s, d_s, output_h=0;
double value_temp1=0, value_temp2=0, value_temp3=0, value_temp4=0, value_temp5=0;
double b0_t, b1_t, b2_t, p_t=0, i_t=0, d_t=0, output_t=0, error_t[]={0,0,0,0};
double b0_s, b1_s, b2_s, output_s=0, error_s[]={0,0,0,0}, pv_speed, sp_speedf;
double b0_t1, b1_t1, b2_t1, output_t1=0, error_t1[]={0,0,0,0}, p_t1, i_t1, d_t1;
double b0_t2, b1_t2, b2_t2, output_t2=0, error_t2[]={0,0,0,0}, p_t2, i_t2, d_t2;
double b0_t3, b1_t3, b2_t3, output_t3=0, error_t3[]={0,0,0,0}, p_t3, i_t3, d_t3;
double b0_t4, b1_t4, b2_t4, output_t4=0, error_t4[]={0,0,0,0}, p_t4, i_t4, d_t4;
double b0_t5, b1_t5, b2_t5, output_t5=0, error_t5[]={0,0,0,0}, p_t5, i_t5, d_t5;
double temp1_duty, temp2_duty, temp3_duty, temp4_duty, temp5_duty, val_f;
char *setup_file="humpid2.cfg", *selection, *DATA_FILE;
FILE *fichier;
time_t tstart, tend;
```

```
void close_v1(void);
void close_v2(void);
void close_v3(void);
void open_v1(void);
void open_v2(void);
void open_v3(void);
void stop_v1(void);
void stop_v2(void);
void stop_v3(void);
void heater_duct_on(void);
void heater_duct_off(void);
void heater_temp1_on(void);
void heater_temp1_off(void);
void heater_temp2_on(void);
void heater_temp2_off(void);
void heater_temp3_on(void);
void heater_temp3_off(void);
void heater_temp4_on(void);
```

```

void heater_temp4_off(void);
void heater_temp5_on(void);
void heater_temp5_off(void);
void getvalue_main(void);
void getvalue_setup(void);
void humidity_loop(void);
void duct_loop(void);
void duct_pid(void);
void temp1_loop(void);
void temp1_pid(void);
void temp2_loop(void);
void temp2_pid(void);
void temp3_loop(void);
void temp3_pid(void);
void temp4_loop(void);
void temp4_pid(void);
void temp5_loop(void);
void temp5_pid(void);
void position_valves(void);
long acquire(long);
void ad7542(short);
void motor_loop(void);

#pragma check_pointer(off)
#pragma check_stack(off)

main()
{
panel=LoadPanel("humpid2.uir",hum);
calibration=LoadPanel("humpid2.uir",cal);
set=LoadPanel("humpid2.uir",setup);
panel_temp=LoadPanel("humpid2.uir",temp);
DisplayPanel(panel);
SetCtrlVal(panel,hum_text,"Prog.M.Drainville");
SetActiveCtrl(hum_panel_select);
RecallPanelState(set,setup_file);
SetCtrlVal(set,setup_led_acq,OFF);
SetActiveCtrl(set,setup_p_h);
outp(BASE+0x3006,0x89); /* port A,B en sortie C en entree */
outp(BASE+0x06,0x00); /* reset le port, stop valves et heater */
ad7542(0); /* initialise Ao0 a 0v */
InstallPopup(calibration);
SetCtrlVal(calibration,cal_text_box,"Strike a key when both valves will"
" be closed\n\n");
close_v1();
close_v2();
close_v3();
time(&tstart);
time(&tend);
while(!(kbhit() || (difftime(tend,tstart)>DELAY_VALVES)))time(&tend);
if(difftime(tend,tstart)<=DELAY_VALVES)
getch();
stop_v1();
stop_v2();
stop_v3();
min_v1=acquire(0);
min_v2=acquire(1);
min_v3=acquire(2);
SetCtrlVal(calibration,cal_text_box,"Strike a key when both valves will"
" be fully open");
open_v1();

```

```

open_v2();
open_v3();
time(&tstart);
time(&tend);
while(!kbhit() || (difftime(tend,tstart)>DELAY_VALVES));time(&tend);
if(difftime(tend,tstart)<=DELAY_VALVES)
    getch();
stop_v1();
stop_v2();
stop_v3();
max_v1=acquire(0);
max_v2=acquire(1);
max_v3=acquire(2);
if(!SIMULATION)
    {
    if((max_v1<=min_v1) || (max_v2<=min_v2) || (max_v3<=min_v3))
        {
        printf("\n\n\n\n\n\n\a\a\a * * * ERROR * * *   Something is wrong with the
"
                " valves.");
        printf("\n\n\nStrike any key to end program.");
        while(!kbhit());
        getch();
        exit(0);
        }
ratio_v1=(double)4095/(max_v1-min_v1);
ratio_v2=(double)4095/(max_v2-min_v2);
ratio_v3=(double)4095/(max_v3-min_v3);
}
RemovePopup(0);
SetActiveCtrl(hum_panel_select);
getvalue_main();
getvalue_setup();
time(&tstart);

do
{
GetUserEvent(0,&handle,&id);
if(handle==panel_temp)
{
switch(id)
{
case temp_exit:
HidePanel(panel_temp);
DisplayPanel(panel);
SetActiveCtrl(hum_panel_select);
break;
case temp_sp_duct:
GetCtrlVal(panel_temp,temp_sp_duct,&sp_duct);
sp_duct=((double)sp_duct/100)*4095;
break;
case temp_sp_temp1:
GetCtrlVal(panel_temp,temp_sp_temp1,&sp_temp1);
sp_temp1=((double)sp_temp1/100)*4095;
break;
case temp_sp_temp2:
GetCtrlVal(panel_temp,temp_sp_temp2,&sp_temp2);
sp_temp2=((double)sp_temp2/100)*4095;
break;
case temp_sp_temp3:
GetCtrlVal(panel_temp,temp_sp_temp3,&sp_temp3);
sp_temp3=((double)sp_temp3/100)*4095;
}
}
}

```

```

        break;
    case temp_sp_temp4:
        GetCtrlVal(panel_temp,temp_sp_temp4,&sp_temp4);
        sp_temp4=((double)sp_temp4/100)*4095;
        break;
    case temp_sp_temp5:
        GetCtrlVal(panel_temp,temp_sp_temp5,&sp_temp5);
        sp_temp5=((double)sp_temp5/100)*4095;
        break;
    }
}
if(handle==panel)
{
    switch(id)
    {
        case hum_mode_speed:
            GetCtrlVal(panel,hum_mode_speed,&mode_speed);
            if(mode_speed==AUTO)
            {
                sp_speed=pv_speed;
                SetCtrlVal(panel,hum_sp_speed,((double)sp_speed/4095)*4);
            }
            else
            {
                sp_speed=0;
                SetCtrlVal(panel,hum_sp_speed,(double)sp_speed);
            }
            SetActiveCtrl(hum_panel_select);
            break;
        case hum_mode:
            GetCtrlVal(panel,hum_mode,&mode);
            if(mode==AUTO)
            {
                stop_v1();
                stop_v2();
                stop_v3();
                SetCtrlAttribute(panel,hum_sp_v1,15,DISABLED);
                SetCtrlAttribute(panel,hum_sp_v2,15,DISABLED);
                SetCtrlAttribute(panel,hum_sp_v3,15,DISABLED);
                SetCtrlAttribute(panel,hum_sp_humidity,15,ENABLED);
            }
            if(mode==MANUAL)
            {
                stop_v1();
                stop_v2();
                stop_v3();
                SetCtrlAttribute(panel,hum_sp_v1,15,ENABLED);
                SetCtrlAttribute(panel,hum_sp_v2,15,ENABLED);
                SetCtrlAttribute(panel,hum_sp_v3,15,ENABLED);
                SetCtrlAttribute(panel,hum_sp_humidity,15,DISABLED);
            }
            SetActiveCtrl(hum_panel_select);
            break;

        case hum_pb_v1:          /* push button */
            if(mode==MANUAL)
                SetActiveCtrl(hum_sp_v1);
            break;
        case hum_pb_v2:
            if(mode==MANUAL)
                SetActiveCtrl(hum_sp_v2);
            break;
    }
}

```

```

case hum_pb_v3:
    if(mode==MANUAL)
        SetActiveCtrl(hum_sp_v3);
    break;
case hum_pb_humidity:
    if(mode==AUTO)
        SetActiveCtrl(hum_sp_humidity);
    break;
case hum_pb_mode:
    SetActiveCtrl(hum_mode);
    break;
case hum_pb_speed:
    SetActiveCtrl(hum_sp_speed);
    break;
case hum_pb_mode_speed:
    SetActiveCtrl(hum_mode_speed);
    break;
case hum_panel_select:
    GetCtrlVal(panel,hum_panel_select,selection);
    if(!(strcmp(selection,"exit")))
    {
        if(ConfirmPopup("Exit software ?"))
        {
            outp(BASE+0x06,0x00); /* reset le port */
            exit(0);
        }
    }
    if(!(strcmp(selection,"setup")))
    {
        HidePanel(panel);
        DisplayPanel(set);
        SetActiveCtrl(setup_filename);
    }
    if(!(strcmp(selection,"temperature")))
    {
        HidePanel(panel);
        DisplayPanel(panel_temp);
        SetActiveCtrl(temp_exit);
    }
    break;
case hum_sp_humidity:
case hum_sp_v1:
case hum_sp_v2:
case hum_sp_v3:
case hum_sp_speed:
    getvalue_main();
    SetActiveCtrl(hum_panel_select);
    break;
}
}
if(handle==set)
{
switch(id)
{
case setup_acq:
    if(acq==OFF)
    {
        SetCtrlVal(set,setup_led_acq,ON);
        acq=ON;
    }
    else
    {

```

```

        SetCtrlVal(set,setup_led_acq,OFF);
        acq=OFF;
    }
    break;
case setup_exit_setup:
    getvalue_setup();          /* valeurs dans variables et */
    HidePanel(set);           /* sauve sur disque */
    DisplayPanel(panel);
    SetActiveCtrl(hum_panel_select);
    break;
case setup_save_to_disk:
    GetCtrlVal(set,setup_filename,DATA_FILE);
    fichier=fopen(DATA_FILE,"w");
    if(!fichier)
    {
        printf("\a\a\a");
        printf("\nerror opening file");
        exit(0);
    }
    intervale=6*time_chart; /* time_chart=1@12HRS*/
    fprintf(fichier,"
    " SYSTEM\n\n");
    fprintf(fichier," %s",_strdate());
    fprintf(fichier," %s",_strtime());
    fprintf(fichier,"\n\nAcquisition rate: %d sec.",intervale);
    fprintf(fichier,"\n\n
    "Tduct T1 T2 T3 T4 T5 SPD "
    "HUM DEW POINT");
    val=round(((double)sp_duct*100)/4095); /* sauve setpoints */
    fprintf(fichier,"\n\nSETPOINTS %3d ",val);
    val=round(((double)sp_temp1*100)/4095);
    fprintf(fichier,"%3d ",val);
    val=round(((double)sp_temp2*100)/4095);
    fprintf(fichier,"%3d ",val);
    val=round(((double)sp_temp3*100)/4095);
    fprintf(fichier,"%3d ",val);
    val=round(((double)sp_temp4*100)/4095);
    fprintf(fichier,"%3d ",val);
    val=round(((double)sp_temp5*100)/4095);
    fprintf(fichier,"%3d ",val);

    if(mode_speed==MANUAL)
    {
        val=round((sp_speed*100)/4095);
        fprintf(fichier,"%3d ",val);
    }
    else
    {
        val_f=((double)sp_speed*4)/4095;
        fprintf(fichier,"%3.11f ",val_f);
    }
    val=round(((double)sp_h*100)/4095);
    fprintf(fichier,"%3d\n\n",val);
    fprintf(fichier,"PROCESS VAL.");
    x=0;
    while(x<(cptr_array-1)) /* save data */
    {
        fprintf(fichier,"\n
        ");
        for(y=0;y<6;y++)
        {
            val=round(((float)(* (pointeur_array+x))/4095)*100);
            fprintf(fichier,"%3d ",val);
            x++;
        }
    }

```

```

    }
    val_f=((*(pointeur_array+x))/4095)*4;
    fprintf(fichier,"%3.1f ",val_f);
    x++;
    val=round(((float)*(pointeur_array+x))/4095)*100;
    fprintf(fichier,"%3d",val);
    x++;
}

fclose(fichier);
cptr_array=0;
break;
}

pv_v1=acquire(0);
pv_v1=(pv_v1-min_v1)*ratio_v1;
if(pv_v1<0)
    pv_v1=0;
if(pv_v1>4095)
    pv_v1=4095;
pv_v2=acquire(1);
pv_v2=(pv_v2-min_v2)*ratio_v2;
if(pv_v2<0)
    pv_v2=0;
if(pv_v2>4095)
    pv_v2=4095;
pv_v3=acquire(2);
pv_v3=(pv_v3-min_v3)*ratio_v3;
if(pv_v3<0)
    pv_v3=0;
if(pv_v3>4095)
    pv_v3=4095;
pv_duct=acquire(3);
pv_h=acquire(4);
pv_speed=acquire(5);
pv_temp1=acquire(6);
pv_temp2=acquire(7);
pv_temp3=acquire(8);
pv_temp4=acquire(9);
pv_temp5=acquire(10);

if(qty_point>1)
{
    for(cptr_moy=qty_point;cptr_moy>1;cptr_moy--) /* decale le tableau */
        tableau_moy[qty_point-cptr_moy]=tableau_moy[qty_point-cptr_moy+1];
    tableau_moy[qty_point-1]=pv_h; /* nouvelle lect. a la fin */
    moy_hum=tableau_moy[0];
    for(cptr_moy=1;cptr_moy<qty_point;cptr_moy++) /* fait la moyenne */
        moy_hum=moy_hum+tableau_moy[cptr_moy];
    moy_hum=moy_hum/qty_point;
}
else
    moy_hum=pv_h;
SetCtrlVal(panel,hum_pv_v1,(long)(((double)pv_v1/4095)*100));
SetCtrlVal(panel,hum_pv_v2,(long)(((double)pv_v2/4095)*100));
SetCtrlVal(panel,hum_pv_v3,(long)(((double)pv_v3/4095)*100));
SetCtrlVal(panel,hum_pv_humidity,(long)(((double)pv_h/4095)*100));
SetCtrlVal(panel,hum_pv_speed,((double)pv_speed/4095)*4);
time(&tend);

```

```

if (difftime(tend, tstart) >= 6 * time_chart) /* chart variable 1-12# */
{
    if ((acq == ON) && (cptr_array < 4800))
    {
        *(pointeur_array + cptr_array) = pv_duct;
        cptr_array++;
        *(pointeur_array + cptr_array) = pv_temp1;
        cptr_array++;
        *(pointeur_array + cptr_array) = pv_temp2;
        cptr_array++;
        *(pointeur_array + cptr_array) = pv_temp3;
        cptr_array++;
        *(pointeur_array + cptr_array) = pv_temp4;
        cptr_array++;
        *(pointeur_array + cptr_array) = pv_temp5;
        cptr_array++;
        *(pointeur_array + cptr_array) = pv_speed;
        cptr_array++;
        *(pointeur_array + cptr_array) = pv_h;
        cptr_array++;
        /* *(pointeur_array + cptr_array) = pv_dp; dew point
        cptr_array++; */
    }
    point[0] = ((short) (((double) moy_hum / 4095) * 100));
    point[1] = ((short) (((double) sp_h / 4095) * 100));
    point[2] = ((short) ((pv_speed / 4095) * 40));
    PlotStripChart(panel, hum_strip, point, 3, 0, 0, 1);
    point[0] = ((short) (((double) pv_duct / 4095) * 100));
    SetCtrlVal(panel_temp, temp_duct_digit, pv_duct / 4095 * 100);
    PlotStripChart(panel_temp, temp_strip_duct, point, 1, 0, 0, 1);
    point[0] = ((short) (((double) pv_temp1 / 4095) * 100));
    SetCtrlVal(panel_temp, temp_t1_digit, pv_temp1 / 4095 * 100);
    PlotStripChart(panel_temp, temp_strip_temp1, point, 1, 0, 0, 1);
    point[0] = ((short) (((double) pv_temp2 / 4095) * 100));
    SetCtrlVal(panel_temp, temp_t2_digit, pv_temp2 / 4095 * 100);
    PlotStripChart(panel_temp, temp_strip_temp2, point, 1, 0, 0, 1);
    point[0] = ((short) (((double) pv_temp3 / 4095) * 100));
    SetCtrlVal(panel_temp, temp_t3_digit, pv_temp3 / 4095 * 100);
    PlotStripChart(panel_temp, temp_strip_temp3, point, 1, 0, 0, 1);
    point[0] = ((short) (((double) pv_temp4 / 4095) * 100));
    SetCtrlVal(panel_temp, temp_t4_digit, pv_temp4 / 4095 * 100);
    PlotStripChart(panel_temp, temp_strip_temp4, point, 1, 0, 0, 1);
    point[0] = ((short) (((double) pv_temp5 / 4095) * 100));
    SetCtrlVal(panel_temp, temp_t5_digit, pv_temp5 / 4095 * 100);
    PlotStripChart(panel_temp, temp_strip_temp5, point, 1, 0, 0, 1);

    time(&tstart);
}
if (mode == AUTO)
{
    humidity_loop();
}
duct_loop();
temp1_loop();
temp2_loop();
temp3_loop();
temp4_loop();
temp5_loop();
motor_loop();
position_valves();
duct_pid();
temp1_pid();

```

```

temp2_pid();
temp3_pid();
temp4_pid();
temp5_pid();
SetCtrlVal(panel,hum_text_time,time_chart); /* temps du graph :-12h */
SetCtrlVal(panel,hum_display_time,_strtime()); /* affiche heure */
}
while(1);
}

```

```

void getvalue_main(void)
{
GetCtrlVal(panel,hum_sp_v1,&sp_v1);
sp_v1=((double)sp_v1/100)*4095;
GetCtrlVal(panel,hum_sp_v2,&sp_v2);
sp_v2=((double)sp_v2/100)*4095;
GetCtrlVal(panel,hum_sp_v3,&sp_v3);
sp_v3=((double)sp_v3/100)*4095;
GetCtrlVal(panel,hum_sp_humidity,&sp_h);
sp_h=((double)sp_h/100)*4095;
GetCtrlVal(panel,hum_sp_speed,&sp_speedf);
if(mode_speed==MANUAL)
{
sp_speed=round((sp_speedf/100)*4095);
}
else
{
sp_speed=round((sp_speedf/4)*4095);
}
}

```

```

void getvalue_setup(void)
{
GetCtrlVal(set,setup_p_h,&p_h);
GetCtrlVal(set,setup_i_h,&i_h);
GetCtrlVal(set,setup_d_h,&d_h);
GetCtrlVal(set,setup_p_t,&p_t);
GetCtrlVal(set,setup_i_t,&i_t);
GetCtrlVal(set,setup_d_t,&d_t);
GetCtrlVal(set,setup_p_s,&p_s);
GetCtrlVal(set,setup_i_s,&i_s);
GetCtrlVal(set,setup_d_s,&d_s);
GetCtrlVal(set,setup_p_temp1,&p_t1);
GetCtrlVal(set,setup_i_temp1,&i_t1);
GetCtrlVal(set,setup_d_temp1,&d_t1);
GetCtrlVal(set,setup_p_temp2,&p_t2);
GetCtrlVal(set,setup_i_temp2,&i_t2);
GetCtrlVal(set,setup_d_temp2,&d_t2);
GetCtrlVal(set,setup_p_temp3,&p_t3);
GetCtrlVal(set,setup_i_temp3,&i_t3);
GetCtrlVal(set,setup_d_temp3,&d_t3);
GetCtrlVal(set,setup_p_temp4,&p_t4);
GetCtrlVal(set,setup_i_temp4,&i_t4);
GetCtrlVal(set,setup_d_temp4,&d_t4);
GetCtrlVal(set,setup_p_temp5,&p_t5);
GetCtrlVal(set,setup_i_temp5,&i_t5);
GetCtrlVal(set,setup_d_temp5,&d_t5);
GetCtrlVal(set,setup_time_chart,&time_chart);
GetCtrlVal(set,setup_qty_point,&qty_point);
GetCtrlVal(set,setup_filename,DATA_FILE);
}

```

```

    SavePanelState(set, setup_file);
}

void humidity_loop(void)
{
    b0_h=p_h+i_h+d_h;
    b1_h=-(p_h+(2*d_h));
    b2_h=d_h;

    error_h[3]=error_h[2];
    error_h[2]=error_h[1];
    error_h[1]=(double)((pv_h-sp_h)*100)/4095; /* reverse action */
    output_h=output_h+b0_h*error_h[1]+b1_h*error_h[2]+b2_h*error_h[3];
    if(output_h<0)
        output_h=0;
    if(output_h>100)
        output_h=100;
    sp_v1=(output_h*4095)/100;
}

void duct_loop(void)
{
    b0_t=p_t+i_t+d_t;
    b1_t=-(p_t+(2*d_t));
    b2_t=d_t;

    error_t[3]=error_t[2];
    error_t[2]=error_t[1]; /* foward action */
    error_t[1]=(double)((sp_duct-pv_duct)*100)/4095;
    output_t=output_t+b0_t*error_t[1]+b1_t*error_t[2]+b2_t*error_t[3];
    if(output_t<0)
        output_t=0;
    if(output_t>100)
        output_t=100;
    temp_duty=(output_t*30)/100;
}

void temp1_loop(void)
{
    b0_t1=p_t1+i_t1+d_t1;
    b1_t1=-(p_t1+(2*d_t1));
    b2_t1=d_t1;

    error_t1[3]=error_t1[2];
    error_t1[2]=error_t1[1]; /* foward action */
    error_t1[1]=(double)((sp_temp1-pv_temp1)*100)/4095;
    output_t1=output_t1+b0_t1*error_t1[1]+b1_t1*error_t1[2]+b2_t1*error_t1[3];
    if(output_t1<0)
        output_t1=0;
    if(output_t1>100)
        output_t1=100;
    temp1_duty=(output_t1*30)/100;
}

void temp2_loop(void)
{
    b0_t2=p_t2+i_t2+d_t2;
    b1_t2=-(p_t2+(2*d_t2));
    b2_t2=d_t2;

    error_t2[3]=error_t2[2];
    error_t2[2]=error_t2[1]; /* foward action */
    error_t2[1]=(double)((sp_temp2-pv_temp2)*100)/4095;
}

```

```

output_t2=output_t2+b0_t2*error_t2[1]+b1_t2*error_t2[2]+b2_t2*error_t2[3];
if(output_t2<0)
    output_t2=0;
if(output_t2>100)
    output_t2=100;
temp2_duty=(output_t2*30)/100;
}

void temp3_loop(void)
{
    b0_t3=p_t3+i_t3+d_t3;
    b1_t3=-(p_t3+(2*d_t3));
    b2_t3=d_t3;

    error_t3[3]=error_t3[2];
    error_t3[2]=error_t3[1];
    error_t3[1]=(double)((sp_temp3-pv_temp3)*100)/4095; /* foward action */
    output_t3=output_t3+b0_t3*error_t3[1]+b1_t3*error_t3[2]+b2_t3*error_t3[3];
    if(output_t3<0)
        output_t3=0;
    if(output_t3>100)
        output_t3=100;
    temp3_duty=(output_t3*30)/100;
}

void temp4_loop(void)
{
    b0_t4=p_t4+i_t4+d_t4;
    b1_t4=-(p_t4+(2*d_t4));
    b2_t4=d_t4;

    error_t4[3]=error_t4[2];
    error_t4[2]=error_t4[1];
    error_t4[1]=(double)((sp_temp4-pv_temp4)*100)/4095; /* foward action */
    output_t4=output_t4+b0_t4*error_t4[1]+b1_t4*error_t4[2]+b2_t4*error_t4[3];
    if(output_t4<0)
        output_t4=0;
    if(output_t4>100)
        output_t4=100;
    temp4_duty=(output_t4*30)/100;
}

void temp5_loop(void)
{
    b0_t5=p_t5+i_t5+d_t5;
    b1_t5=-(p_t5+(2*d_t5));
    b2_t5=d_t5;

    error_t5[3]=error_t5[2];
    error_t5[2]=error_t5[1];
    error_t5[1]=(double)((sp_temp5-pv_temp5)*100)/4095; /* foward action */
    output_t5=output_t5+b0_t5*error_t5[1]+b1_t5*error_t5[2]+b2_t5*error_t5[3];
    if(output_t5<0)
        output_t5=0;
    if(output_t5>100)
        output_t5=100;
    temp5_duty=(output_t5*30)/100;
}

void duct_pid(void) /* duty cycle pour PID */
{
    if(cptr_duct==30)
    {
        cptr_duct=0;
    }
}

```

```

        value_duct=temp_duty;
    }
    if((value_duct>0)&&(value_duct>cptr_duct))
        heater_duct_on();
    else
        heater_duct_off();
    cptr_duct++;

}
void temp1_pid(void)      /* duty cycle pour PID */
{
    if(cptr_temp1==30)
    {
        cptr_temp1=0;
        value_temp1=temp1_duty;
    }
    if((value_temp1>0)&&(value_temp1>cptr_temp1))
        heater_temp1_on();
    else
        heater_temp1_off();
    cptr_temp1++;
}
void temp2_pid(void)      /* duty cycle pour PID */
{
    if(cptr_temp2==30)
    {
        cptr_temp2=0;
        value_temp2=temp2_duty;
    }
    if((value_temp2>0)&&(value_temp2>cptr_temp2))
        heater_temp2_on();
    else
        heater_temp2_off();
    cptr_temp2++;
}
void temp3_pid(void)      /* duty cycle pour PID */
{
    if(cptr_temp3==30)
    {
        cptr_temp3=0;
        value_temp3=temp3_duty;
    }
    if((value_temp3>0)&&(value_temp3>cptr_temp3))
        heater_temp3_on();
    else
        heater_temp3_off();
    cptr_temp3++;
}
void temp4_pid(void)      /* duty cycle pour PID */
{
    if(cptr_temp4==30)
    {
        cptr_temp4=0;
        value_temp4=temp4_duty;
    }
    if((value_temp4>0)&&(value_temp4>cptr_temp4))
        heater_temp4_on();
    else
        heater_temp4_off();
    cptr_temp4++;
}

```

```

}
void temp5_pid(void)      /* duty cycle pour PID */
{
    if(cptr_temp5==30)
    {
        cptr_temp5=0;
        value_temp5=temp5_duty;
    }
    if((value_temp5>0)&&(value_temp5>cptr_temp5))
        heater_temp5_on();
    else
        heater_temp5_off();
    cptr_temp5++;
}

void position_valves(void)
{
    if(((pv_v1>=sp_v1)&&(pv_v1<(sp_v1+deadband_manual)))) ||
        ((pv_v1>(sp_v1-deadband_manual))&&(pv_v1<=sp_v1)))
        stop_v1();
    else
    {
        if(sp_v1<(pv_v1-deadband_manual))
            close_v1();
        if(sp_v1>(pv_v1+deadband_manual))
            open_v1();
    }
    if(((pv_v2>=sp_v2)&&(pv_v2<(sp_v2+deadband_manual)))) ||
        ((pv_v2>(sp_v2-deadband_manual))&&(pv_v2<=sp_v2)))
        stop_v2();
    else
    {
        if(sp_v2<(pv_v2-deadband_manual))
            close_v2();
        if(sp_v2>(pv_v2+deadband_manual))
            open_v2();
    }
    if(((pv_v3>=sp_v3)&&(pv_v3<(sp_v3+deadband_manual)))) ||
        ((pv_v3>(sp_v3-deadband_manual))&&(pv_v3<=sp_v3)))
        stop_v3();
    else
    {
        if(sp_v3<(pv_v3-deadband_manual))
            close_v3();
        if(sp_v3>(pv_v3+deadband_manual))
            open_v3();
    }
}

long acquire(long channel)
{
    long data,data1;

    if(channel<8)
        outp(BASE,0x21+(channel*2)); /* select channel */
    else
        outp(BASE,0x30+((channel-8)*2));
    for(data=0;data<200;data++);

    outp(BASE+03,00); /* debute conversion */
    for(data=0;data<1000;data++);
}

```

```

    data1=inp(BASE+03);
    data=((data1<<4)&0x0FF0)|((inp(BASE+02)>>4)&0x000F);
    return(data);
}

void close_v1(void)
{
    outp(BASE+0x06,(inp(BASE+0x06)|0x02)&0xFE); /* REV v1 */
}

void close_v2(void)
{
    outp(BASE+0x06,(inp(BASE+0x06)|0x08)&0xFB); /* REV v2 */
}

void close_v3(void)
{
    outp(BASE+0x06,(inp(BASE+0x06)|0x20)&0xEF); /* REV v3 */
}

void open_v1(void)
{
    outp(BASE+0x06,(inp(BASE+0x06)|0x01)&0xFD); /* FWD v1 */
}

void open_v2(void)
{
    outp(BASE+0x06,(inp(BASE+0x06)|0x04)&0xF7); /* FWD v2 */
}

void open_v3(void)
{
    outp(BASE+0x06,(inp(BASE+0x06)|0x10)&0xDF); /* FWD v3 */
}

void stop_v1(void)
{
    outp(BASE+0x06,inp(BASE+0x06)&0xFC); /* arrete valve 1 */
}

void stop_v2(void)
{
    outp(BASE+0x06,inp(BASE+0x06)&0xF3); /* arrete valve 2 */
}

void stop_v3(void)
{
    outp(BASE+0x06,inp(BASE+0x06)&0xCF); /* arrete valve 3 */
}

void heater_duct_on(void)
{
    outp(BASE+0x06,inp(BASE+0x06)|0x40); /* turn on heater */
    SetCtrlVal(panel_temp,temp_led_duct,ON);
}

void heater_duct_off(void)
{
    outp(BASE+0x06,inp(BASE+0x06)&0xBF); /* turn off heater */
    SetCtrlVal(panel_temp,temp_led_duct,OFF);
}

void heater_temp1_on(void)

```

```

    {
        outp(BASE+0x06, inp(BASE+0x06) | 0x80);          /* turn on heater */
        SetCtrlVal(panel_temp, temp_led_temp1, ON);
    }

void heater_temp1_off(void)
{
    outp(BASE+0x06, inp(BASE+0x06) & 0x7F);          /* turn off heater */
    SetCtrlVal(panel_temp, temp_led_temp1, OFF);
}

void heater_temp2_on(void)
{
    outp(BASE+0x1006, inp(BASE+0x1006) | 0x01);      /* turn on heater */
    SetCtrlVal(panel_temp, temp_led_temp2, ON);
}

void heater_temp2_off(void)
{
    outp(BASE+0x1006, inp(BASE+0x1006) & 0xFE);      /* turn off heater */
    SetCtrlVal(panel_temp, temp_led_temp2, OFF);
}

void heater_temp3_on(void)
{
    outp(BASE+0x1006, inp(BASE+0x1006) | 0x02);      /* turn on heater */
    SetCtrlVal(panel_temp, temp_led_temp3, ON);
}

void heater_temp3_off(void)
{
    outp(BASE+0x1006, inp(BASE+0x1006) & 0xFD);      /* turn off heater */
    SetCtrlVal(panel_temp, temp_led_temp3, OFF);
}

void heater_temp4_on(void)
{
    outp(BASE+0x1006, inp(BASE+0x1006) | 0x04);      /* turn on heater */
    SetCtrlVal(panel_temp, temp_led_temp4, ON);
}

void heater_temp4_off(void)
{
    outp(BASE+0x1006, inp(BASE+0x1006) & 0xFB);      /* turn off heater */
    SetCtrlVal(panel_temp, temp_led_temp4, OFF);
}

void heater_temp5_on(void)
{
    outp(BASE+0x1006, inp(BASE+0x1006) | 0x08);      /* turn on heater */
    SetCtrlVal(panel_temp, temp_led_temp5, ON);
}

void heater_temp5_off(void)
{
    outp(BASE+0x1006, inp(BASE+0x1006) & 0xF7);      /* turn off heater */
    SetCtrlVal(panel_temp, temp_led_temp5, OFF);
}

void ad7542(short value)          /* 0-4095 */
{
    outp(BASE+LOW, value);
    outp(BASE+MIDDLE, (value>>4));
    outp(BASE+HIGH, (value>>8));
}

```

```

void motor_loop(void)
{
    if(mode_speed==AUTO)
    {
        b0_s=p_s+i_s+d_s;
        b1_s=-(p_s+(2*d_s));
        b2_s=d_s;

        error_s[3]=error_s[2];
        error_s[2]=error_s[1];
        error_s[1]=(double)((sp_speed-pv_speed)*100)/4095; /* foward action */
        output_s=output_s+b0_s*error_s[1]+b1_s*error_s[2]+b2_s*error_s[3];
        if(output_s<0)
            output_s=0;
        if(output_s>100)
            output_s=100;
        ad7542((output_s*4095)/100);
    }
    else
        ad7542(sp_speed);
}

#pragma check_pointer(on)
#pragma check_stack(on)

```

**APPENDIX A3: Computer programs for data acquisition and control: environment
controlled calender**

```

/* Data Acquisition and control program for World's Narrowest Calender */
/*      Written by Miles Sherman, August 1990      */
/* This version includes averaging and conversion routines from TX.C */
/*      Modified for 2 A/D boards, May 1992, by Thomas Browne      */
/* Automatic trim control installed, June/July 1992, by Thomas Browne */
/* Counters for draw installed July 1992, by Thomas Browne      */
/* Modified for Dariusz Kawka by Thomas Browne, March 1993      */
/* Modified for new sensors, Dariusz Kawka 1994      */
/* Global variable definitions are in the file DAQSUBS2.C      */

```

```

#include <doslbdrv.h>
#include <conio.h>
#include <stdio.h>
#include <stdlib.h>
#include <dos.h>
#include <malloc.h>
#include <graph.h>
#include <ctype.h>
#include <float.h>
#include <math.h>
#include <time.h>
#include "daqsubs2.c"

```

```

main()
{
    FILE      *outfbin,          /* data file */
             *inftxt,          /* parameter file */
             *outftxt;
    double el_time;
    int      cont,
            ascii,             /* ascii value */
            i,j,
            press,            /* value read from nip load cell */
            errNum,
            pdest,
            length,
            overflow,
            cr;               /* carriage return */
    char      quit,            /* first character entered for vel */
            vel_char,         /* next character entered for vel */
            vel_temp[100],    /* temporary velocity as char string */
            firstdta[5] = "f:\\";
    time_t tstart,
            tstop;
    float DeltaVFact;

    _clearscreen(_GCLEARSCREEN);
    num_samples = num_scans*num_chans;    /* allocate data buffers */
    exp_buff1 = NULL;
    exp_buff2 = NULL;
    if (!(exp_buff1=(int huge *) malloc ((unsigned
long)num_samples,sizeof(int))))
    {
        perror ("error allocating memory for buffer 1");
        printf("ending program....");
        exit(1);
    }
    if (!(exp_buff2=(int huge *) malloc ((unsigned
long)num_samples,sizeof(int))))
    {
        perror ("error allocating memory for buffer 2");
        printf("ending program....");
        exit(1);
    }

    if ((inftxt=fopen(par_file,"rt")) != NULL)
    {

```

```

fscanf(inftxt, "%f", &data.dry_bulb);      /* Open and read INFO2.TXT */
fscanf(inftxt, "%f", &data.dew_pt);
fscanf(inftxt, "%f", &data.baro);
fscanf(inftxt, "%f", &data.rel_hum);
fscanf(inftxt, "%f", &data.calroll_d1);
fscanf(inftxt, "%d", &data.calroll_n1);
fscanf(inftxt, "%f", &data.calroll_d2);
fscanf(inftxt, "%d", &data.calroll_n2);
fscanf(inftxt, "%f", &data.bas_wt);
fscanf(inftxt, "%s", data.pap_type);
fscanf(inftxt, "%lf", &data.s_rate);
fscanf(inftxt, "%lf", &data.scan_rate);
for (i=0; i<num_chans; i++)
    fscanf(inftxt, "%d", &data.chan_seq1[i]);
for (i=0; i<num_chans; i++)
    fscanf(inftxt, "%d", &data.gain_seq1[i]);
for (i=0; i<num_chans; i++)
    fscanf(inftxt, "%d", &data.chan_seq2[i]);
for (i=0; i<num_chans; i++)
    fscanf(inftxt, "%d", &data.gain_seq2[i]);
for (i=0; i<num_chans-1; i++)
    fscanf(inftxt, "%d", &data.sens_seq[i]);
for (i=0; i<num_chans-1; i++)
    fscanf(inftxt, "%f", &data.volt_seq[i]);
fscanf(inftxt, "\n%f", &data.i_vel);
fscanf(inftxt, "\n%d", &data.file_no);
fclose(inftxt);
}
else
{
    perror("error opening DINFO2.TXT");
    exit(1);
}
if ((inftxt=fopen(calibr_file, "rt")) != NULL)
{
    for (i=0; i<3; i++)
    {
        for (j=0; j<num_chans; j++)
            fscanf(inftxt, "%f", &cons[i][j]);
    }
    for (i=0; i<3; i++)
    {
        for (j=num_chans; j<(2*num_chans); j++)
            fscanf(inftxt, "%f", &cons[i][j]);
    }
}
else
{
    perror("error opening DCALIBR2.TXT");
    exit(1);
}

if ((inftxt=fopen(control_file, "rt")) != NULL)
{
    fscanf(inftxt, "%f", &Tp);      /* Open and read CONTROL.TXT */
    fscanf(inftxt, "%f", &Ti);
    fscanf(inftxt, "%f", &Td);
    fscanf(inftxt, "%f", &Lp);
    fscanf(inftxt, "%f", &Li);
    fscanf(inftxt, "%f", &Ld);
    fscanf(inftxt, "%f", &deltaT);
    fclose(inftxt);
}
else
{
    perror("error opening DCONTROL.TXT");
    exit(1);
}

```

```

}
tensadj[0] = Tp + 0.5*Ti*deltaT + Td/deltaT;      /* PID constants */
tensadj[1] = -Tp + 0.5*Ti*deltaT - 2*Td/deltaT;
tensadj[2] = Td*deltaT;
loadadj[0] = Lp + 0.5*Li*deltaT + Ld/deltaT;
loadadj[1] = -Lp + 0.5*Li*deltaT - 2*Ld/deltaT;
loadadj[2] = Ld/deltaT;
for (i=0; i<3; i++)
{
    tenserr[i] = 0;
    loaderr[i] = 0;
}

_dos_getdate(&ddate);
_dos_gettime(&dtime);
if ((AQerrNum = AO_Config(board1,0,1,10.0,0))!=0)
    DAQ_error("AO_Config 1, channel 0",10);
if ((AQerrNum = AO_Config(board1,1,1,10.0,0))!=0)
    DAQ_error("AO_Config 1, channel 1",20);
if ((AQerrNum = AO_Config(board2,0,1,10.0,0))!=0)
    DAQ_error("AO_Config 2, channel 0",30);
if ((AQerrNum = AO_Config(board2,1,1,10.0,0))!=0)
    DAQ_error("AO_Config 2, channel 1",40);
if ((AQerrNum = AI_Config(board1,0,5,0))!=0)
    DAQ_error("AI_Config 1",50);
if ((AQerrNum = AI_Config(board2,0,10,1))!=0)
    DAQ_error("AI_Config 2",60);
if ((AQerrNum = DIG_Prt_Config(board1,0,0,0))!=0)
    DAQ_error("DIG_Prt_Config 1",70);
if ((AQerrNum = DIG_Prt_Config(board1,1,0,1))!=0)
    DAQ_error("DIG_Prt_Config 1",80);
if ((AQerrNum = DIG_Prt_Config(board2,0,0,0))!=0)
    DAQ_error("DIG_Prt_Config 2",90);
if ((AQerrNum = DIG_Prt_Config(board2,1,0,1))!=0)
    DAQ_error("DIG_Prt_Config 2",100);

motor_bits = 0;
trim_bits = 0;
load_bits = 0;
DeltaVFact = DRollOut*NumEdgeIn/(DRollIn*NumEdgeOut);
if ((AQerrNum = AO_Write(board1,0,motor_bits))!=0) /* Main motor off */
    DAQ_error("AO_Write Main",110);
if ((AQerrNum = AO_Write(board1,1,load_bits))!=0) /* load off */
    DAQ_error("AO_Write Load",120);
if ((AQerrNum = AO_Write(board2,0,trim_bits))!=0) /* Trim motor off */
    DAQ_error("AO_Write Trim",130);
mask = mask & 11; /* leave load alone */
if ((AQerrNum = DIG_Out_Port(board1,1,mask))!=0) /* Release brake */
    DAQ_error("DIG_Out_Port",140);

data_screen(); /* displays current parameters */
_settextposition(22,1);
printf("    Enter choice:\n\t>");
cr = getche();
while ((cr != 'c') && (cr != 'C'))
{
    change(cr); /* change selected parameter */
    clear(23,10,2);
    cr = getche();
}

_settextposition(24,1);
printf("Lowering roll . . .");
mask = raise_load_mask; /* lower roll . . . (raise_load_mask for larger
rolls or smaller cylinders) */
load_bits = 500; /* using less pressure than required to lift; 500
bits for larger rolls */

```

```

/* 1575 bits, small cyl, small rolls */
if ((AQerrNum = AO_Write(board1,1,load_bits))!=0)
    DAQ_error("AO_Write",150);
if ((AQerrNum = DIG_Out_Port(board1,1,mask))!=0) /* pressure . . . */
    DAQ_error("DIG_Out_Port",160);
do
    if ((AQerrNum = AI_Read
(board1,loadchan,data_gain_seq1[loadchan],&press))!=0)
        DAQ_error("AI_Read",170);
    while ((press > contactload) && (!kbhit())); /* . . . until contact or
keypress. */
    mask = 0;
    if ((AQerrNum = DIG_Out_Port(board1,1,mask))!=0) /* then release */
        DAQ_error("DIG_Out_Port",180);
    if ((AQerrNum = AO_Write(board1,1,0))!=0)
        DAQ_error("AO_Write",190);

    _clearscreen( GCLEARSCREEN);
    _settextposition(10,1);
    printf(" T0   T1  dt2   dt3   t4     t5    L6   V7  N10  N11  C12  C13  T14
H15  T16  M17\n");
    printf("  C   C    C    C  N/m   N/m  kN/m  m/m  um   um   um   um   C
RH   C   % ");

do /* experiment loop begins here */
{
    cont = 1;
    _settextposition(2,1);
    printf(" \"C\" - CONTINUE ");
    _settextposition (4,52);
    printf("Velocity: %8.2f m/min",data.i_vel);
    _settextposition (5,52);
    printf("Load:      %6d kN/m",load_array[load_sel]);
    _settextposition(4,1);
    printf("Press V for Velocity, L for Load; ");
    _settextposition(5,1);
    printf("Press GREY + or - to increment or decrement:");
    quit = 0;
    while (quit != 'C') /* Get new sheet speed and load */
    {
        while (!kbhit())
        {
            get_last_data(); /* read latest data */
            display_last_data(); /* display */
            if (firstrun > 1)
            {
                trim_control(0); /* control */
            }
        }
        quit = getch(); /* key has been hit */
        ascii = toupper(quit); /* get the key */
        /* convert to upper case */
        quit = ascii;
        if ((ascii == 'L') || (ascii == 'V'))
        { /* increment or decrement */
            _settextposition (5,45);
            printf("%1c",ascii);
            while (!kbhit())
            {
                get_last_data(); /* read latest data */
                display_last_data(); /* display */
                if (firstrun > 1) /* while waiting for second key */
                    trim_control(0); /* control */
            }
            /* key has been hit */
            /* get the key */
            quit = getch();
            if (quit == '+')
            {
                _settextposition (5,46);

```

```

printf ("+");
if (ascii == 'L')
{
    load_sel++;
    if (load_sel > load_sel_max) load_sel = load_sel_max;
}
else
{
    vel_sel++;
    if (vel_sel > vel_sel_max) vel_sel = vel_sel_max;
    data.i_vel = vel_array[vel_sel];
    data.scan_rate =
20*ceil(0.05*num_scans*data.i_vel/(3.1416*60*data.calroll_dl*minrevs));
}
}
else if (quit == '-')
{
    _settextposition (5,46);
    printf("-");
    if (ascii == 'L')
    {
        load_sel--;
        if (load_sel < load_sel_min) load_sel = load_sel_min;
    }
    else
    {
        vel_sel--;
        if (vel_sel < vel_sel_min) vel_sel = vel_sel_min;
        data.i_vel = vel_array[vel_sel];
        data.scan_rate =
20*ceil(0.05*num_scans*data.i_vel/(3.1416*60*data.calroll_dl*minrevs));
    }
}
_settextposition (4,52);
printf("Velocity: %8.2f m/min    ",data.i_vel);
_settextposition (5,52);
printf("Load:      %6d kN/m    ",load_array[load_sel]);
_settextposition (5,45);
printf("    ");
}
}
/* End get sheet speed and load*/
load_bits = load_array_bin[load_sel];

clearl (4,1,45);
clearl (5,1,45);
_dos_gettime(&dttime);
/* gets current time*/
_settextposition (1,1);
printf("\nESC\n - EMERGENCY EXIT");
_settextposition(7,1);
printf("File number: %4d; Run: %4d    \n",data.file_no,firstrun);
printf("Acq. rate:   %8.2lf Hz    \n",data.scan_rate);
_settextposition (20,1);
printf("starting motor....");
errNum = 0;
mask = apply_load_mask;
/* if (load_dir[load_start] == 1)
load_bits =
load_bits_per_kN*log(load_array[load_start])+load_bits_offset;
else
load_bits =
relief_bits_per_kN*log(load_array[load_start])+relief_bits_offset;
*/ if ((AQerrNum = AO_Write(board1,1,load_array_bin[load_sel]))!=0)
DAQ_error("AO_Write",280);
if ((AQerrNum = DIG_Out_Port(board1,1,mask))!=0)
DAQ_error("DIG_Out_Port",290);
/*
_settextposition (18,1);
printf("%5d %5d %5d %6.6f    ",VinCount,VoutCount,ClockCount,deltaV);

```



```

    fwrite (&ClockCount, sizeof(ClockCount), 1, outfbn);
    for (i=0; i<4; i++)
        fwrite (&endblock, sizeof(endblock), 1, outfbn);
    fwrite (&exp_buff1[0], sizeof(exp_buff1[0]), num_samples, outfbn);
    fwrite (&exp_buff2[0], sizeof(exp_buff2[0]), num_samples, outfbn);
    fclose(outfbn);
}
clear(20,1,1);
firstrun++;
}
if (!errNum)
{
    _settextposition(1,1);
    printf(" \E\ " - END \n");
    printf(" \C\ " - CHANGE VELOCITY OR LOAD AND CONTINUE");
    while ((cont != 69) && (cont != 67))
    {
        /* if E or C has not been pressed */
        get_last_data();
        trim_control(0);
        display_last_data();
        if (kbhit())
        {
            cont = getch();
            ascii = toascii(cont);
            if (ascii == 27)
            {
                cont = 69;          /* ASCII 69 = 'E', for exit */
                errNum = eexit(5);
            }
            else
                cont = toupper(cont);
        }
    }
    } else cont = 69;          /* force exit if errNum */
} while (cont == 67);      /* end experiment loop unless C pressed */

data.file_no++;
write_data();
if (firstrun>1)          /* If this is not the first run */
{
    outfbn = fopen(file_name,"ab");
    for (i=0; i<8; i++)
        fwrite(&endfile,sizeof(endfile),1,outfbn);
    fclose(outfbn);
}

if (errNum)          /* If emergency exit . . . */
{
    do {} while (!kbhit()); /* don't release brake until keypressed */
    cont = getch();
}
else          /* Otherwise normal exit, lift roll */
{
    _settextposition(21,1);
    printf("Raising upper roll . . . \n");
    time (&tstart);
    if ((AQerrNum = DIG_Out_Port(board1,1,(raise_load_mask)))!=0)
        DAQ_error("DIG OuE Prt",480);
    if ((AQerrNum = AO_Write(board1,1,4000))!=0)
        DAQ_error("AO_Write",490);
    do          /* Wait */
    {
        time (&tstop);
        el_time = difftime(tstop,tstart);
    }
    while (el_time < lift_time);
}
}

```

```

if ((AQerrNum = AO_Write(board1,0,0)) !=0)      /* Main motor off */
    DAQ_error("AO_Write Main",500);
if ((AQerrNum = AO_Write(board1,1,0)) !=0)      /* Load off */
    DAQ_error("AO_Write Load",510);
if ((AQerrNum = AO_Write(board2,0,0)) !=0)      /* Trim motor off */
    DAQ_error("AO_Write Trim",520);
if ((AQerrNum = DIG_Out_Port(board1,1,0)) !=0)
    DAQ_error("DIG_Out_Prt 1",530);
if ((AQerrNum = DIG_Out_Port(board2,1,0)) !=0)
    DAQ_error("DIG_Out_Prt 2",540);
if ((AQerrNum = AI_Clear(board1)) !=0)
    DAQ_error("AI_Clear 1",570);
if ((AQerrNum = AI_Clear(board2)) !=0)
    DAQ_error("AI_Clear 2",580);
data.file_no--;
txconvert(data.file_no);

if ((outftxt = fopen(control_file,"wt")) != NULL)
{
    fprintf(outftxt,"%10.8f\n",Tp);
    fprintf(outftxt,"%10.8f\n",Ti);
    fprintf(outftxt,"%10.8f\n",Td);
    fprintf(outftxt,"%10.8f\n",Lp);
    fprintf(outftxt,"%10.8f\n",Li);
    fprintf(outftxt,"%10.8f\n",Ld);
    fprintf(outftxt,"%10.8f\n",deltaT);
    fclose(outftxt);
}
hfree(exp_buff1);          /* frees allocated memory */
hfree(exp_buff2);
printf("\n");
}                          /* END MAIN PROGRAM */

/*****

/* Global definitions */
/* and subroutines */
/* for DAQ2.C */
/* Last modification: 27 February 1992 */
/* Modified for 2 A/D boards, May 1992 */

#define apply_load_mask 1      /* digital output to apply load */
#define raise_load_mask 8     /* digital output to relieve load */
#define brake_reel_mask 4     /* digital output to apply brake */
#define emerg_stop_mask 12    /* relieve load and apply brake */
#define num_chans 8           /* 8 channels per board */
#define num_scans 2048        /* read each channel 2048 times */
#define num_avg 4             /* continuous averaging parameter */
#define num_saved 512         /* num_scans/num_avg */
#define tenschan 5            /* winder tension is board 1, channel 5 */
#define loadchan 6            /* nip load is board 1, channel 6 */
#define contactload 525      /* load cell output when roll contacts;
525 for 711 rolls and 4" cylinder,
-50 for 404 rolls and 4" cylinder,
120 for 404 rolls and 2" cylinder*/

#define trigger 0             /* initiate A/D; 1 for hardware trigger */
#define board1 1              /* board addresses */
#define board2 2
#define lift_time 3.0
/*time in sec to lift at end of exprmnt; longer for large rolls or small
cylinder */
#define motor_bits_per_vel 2.143033 /* 4.043256 bits/(m/min), 60:30 */
#define motor_bits_offset -20.45419 /* 14.19529 bits, 60:30 */
#define trim_bits_per_vel 44.045435 /* trim bits/(m/min) */

```

```

#define trim_bits_offset 249.16481 /* trim bits offset */
#define load_bits_per_kN 2235.597 /* bits/kN/m, loading, log fit */ /*
for 711 rolls only */
#define load_bits_offset -9574.39 /* bits, loading, log fit */
#define relief_bits_per_kN -325.18 /* bits/kN/m, lifting, log fit */
#define relief_bits_offset 1578.596 /* bits, lifting, log fit */
#define min_load_bits 0 /* limits on analog output */
#define max_load_bits 2500
#define load_sel_min 0 /* indices for load select array */
#define load_sel_max 5
#define load_start 2 /* initial load selection */
#define vel_sel_min 0 /* indices for velocity select
array*/
#define vel_sel_max 4
#define min_trim_bits 0 /* limits on analog output */
#define max_trim_bits 4095
#define d_v 1 /* vel increment, bits */
#define d_t 110 /* time increment, ms */
#define minrevs 25 /* min acq time in roll revs */
#define xerror 15 /* x, y coords for error messages */
#define yerror 60
#define TMid 950 /* target winder tension in bits */
/* #define LMid -200 */
/* target load in bits; converted to variable */
#define smoothfact 0.4 /* filtering for tension control */
#define gain_adjust 1.50 /* factor to alter gains on the fly
*/
#define ctrl 1 /* counter addresses */
#define ctr5 5
#define source1 6
#define source5 10
#define NumEdgeIn 10 /* number of rising edges */
#define NumEdgeOut 10

int huge *exp_buff1, /* raw data buffers */
huge *exp_buff2;
double outbuff1[num_saved][num_chans], /* converted data buffers */
outbuff2[num_saved][num_chans],
avg_data1[num_chans],
avg_data2[num_chans];
int motor_bits, /* main motor output, bits */
trim_bits, /* trim motor output, bits */
load_bits, /* load control output, bits */
LMid,
vel_array[6] = {90,175,300,500,900,1100},
vel_sel = 0, /* index for velocities */
load_array[6] = {15,25,95,135,175,210},
/* for 404 rolls and 2" cylinder: {10,20,40,65,15,50}*/
/* for 404 rolls and 4" cylinder: {70,80,95,135,175,175}, */
load_array_bin[6] = {875,550,750,1500,2000,2500},
/* for 404 rolls and 2" cylinder:1450,600,1100,3000,1250,1825},*/
/* for 404 rolls and 4" cylinder:
{700,971,1253,1865,2346,2346},*/
load_dir[6] = {8,8,1,1,1,1}, /* 8 for relief, 1 for load */
load_sel = 2, /* index for loading */
mask = 0, /* digital output mask */
firstrun = 1, /* number of runs saved in a file */
num_samples, /* num_scans * num_channels */
endfile = 11111, /* flag at the end of a file */
endblock = 10000, /* flag at the end of a block */
AQStatus, /* end of acquisition flag */
AQerrNum, /* error handling */
tenserr[3], /* winder tension deviation from setpoint */
avg_tens = 0, /* continuous averaging for tension control */
loaderr[3],
monitor_buff[2*num_chans]; /* most recent block of data */

```

```

unsigned int buff_index,      /* index to most recent block of data */
          VinCount,          /* count from ingoing speed square wave */
          VoutCount,         /* count from outgoing speed square wave */
          ClockCount;        /* count in ms from clock */
char      file_name[50],     /* data file name */
          par_file[15] = "dinfo2.txt", /* parameter file name */
          calibr_file[15] = "dcalibr2.txt",
          control_file[15] = "dcontrol.txt", /* PID gains */
          firstprn[50] = "c:\\dariusz\\data\\experime", /*converted data
files*/
          prn[5] = ".prn", /* converted data files */
          dta[5] = ".dta", /* raw data files */
          sum[5] = ".sum"; /* summary file */
float     cons[3][16],      /* calibration constants */
          Tp,                /* PID controller coefficients */
          Ti,
          Td,
          Lp,
          Li,
          Ld,
          deltaT,            /* PID control dt */
          deltaV,            /* speed change due to stretch */
          tensadj[3],        /* PID controller coefficients */
          loadadj[3],
          DRollIn = 0.06335, /* idler roll diameters */
          DRollOut = 0.06334;

struct    dosdate_t ddate;
struct    dostime_t dtime;
struct    {
          float dry_bulb, /* laboratory ambient temp */
              dew_pt, /* laboratory dew point */
              baro, /* laboratory barometric pressure */
              rel_hum, /* laboratory relative humidity */
              bas_wt, /* basis weight */
              volt_seq[7], /* sequence of supply voltages */
              calroll_d1,
              calroll_d2, /* calender reel diameters in m */
              i_vel; /* velocity in meters/min */
          int   file_no, /* file identification number */
              calroll_n1,
              calroll_n2, /* calender roll id numbers */
              chan_seq1[8], /* sequence channels read */
              gain_seq1[8], /* sequence of gains */
              chan_seq2[8], /* sequence channels read */
              gain_seq2[8], /* sequence of gains */
              sens_seq[7]; /* sequence of sensor connections */
          char  pap_type[30]; /* type of paper */
          double s_rate, /* rate between channels, Hz */
              scan_rate; /* rate between consecutive scans, Hz */
        } data;

/*****
/*          Subroutines begin here          */
*****/

int motor() /* ramp motor up to desired speed */
{
    int dd_v,
        exitNum = 0,
        eltime, /* time spent in loop */
        over,
        old_time, /* time when loop starts */
        new_time, /* time when loop finishes */
        new_motor_bits; /* desired velocity in bits */

    new_motor_bits = (data.i_vel*motor_bits_per_vel+motor_bits_offset) * 1;

```

```

if (new_motor_bits>4095) new_motor_bits=4095;
if (motor_bits>new_motor_bits) dd_v = -d_v;
else dd_v = d_v;
while ((motor_bits <= (new_motor_bits-d_v))
|| (motor_bits >= (new_motor_bits+d_v))
&& (exitNum != 27))
{
    eltime=0;
    if ((AQerrNum = CTR_EvCount(board1,5,4,1))!=0) /* starts timer */
        DAQ_error("CTR_EvCount",1000);
    if ((AQerrNum = CTR_EvRead(board1,5,&over,&old_time))!=0)
        DAQ_error("CTR_EvRead",1010);
    while ((eltime<d_t) && (exitNum != 27))
    {
        if (kbhit())
            exitNum = getch();
        if (exitNum != 27)
        {
            get_last_data();
            display_last_data();
            trim_control(exitNum);
            load_control(exitNum);
            exitNum = 0;
        }
        /*
        _settextposition(22,23);
        printf("motor %6.2f ",((motor_bits-
motor_bits_offset)/motor_bits_per_vel));
        */
        if ((AQerrNum = CTR_EvRead(board1,5,&over,&new_time))!=0)
            DAQ_error("CTR_EvRead",1020);
        eltime = new_time-old_time;
    }
    motor_bits=motor_bits+dd_v;
    if (abs(motor_bits-new_motor_bits)>0.01*new_motor_bits)
        motor_bits=motor_bits+dd_v;
    if (abs(motor_bits-new_motor_bits)>0.1*new_motor_bits)
        motor_bits=motor_bits+dd_v;
    if ((AQerrNum = AO_Write(board1,0,motor_bits))!=0)
        DAQ_error("AO_Write",1030);
}
if ((AQerrNum = CTR_Stop(board1,5))!=0) /* stop the timer */
    DAQ_error("CTR_Stop",1040);
if ((AQerrNum = AO_Write(board1,0,new_motor_bits))!=0)
    DAQ_error("AO_Write",1050);
/*
_settextposition(22,23);
printf("motor %6.2f ",((new_motor_bits-
motor_bits_offset)/motor_bits_per_vel));
*/
return exitNum;
}

/*****

int wait() /* wait for a keypress while reading and controlling */
{
    int exitNum=0;
    _settextposition(2,1);
    printf(" \nA\n - begin ACQUISITION ");

    _settextposition(20,1);
    printf("requested speed reached of %6.2f m/min ",data.i_vel);
    while ((exitNum!=27) && (exitNum!=97) && (exitNum!=65))
    {
        if (kbhit()) exitNum = getch();
        else exitNum = 0;
        get_last_data();
        display_last_data();
        trim_control(exitNum);
        load_control(exitNum);
    }
}

```

```

    }
    return exitNum;
}

/*****
int exprmnt()          /* acquire the data and store in two arrays */
{
    int exitNum = 0,
        scan_int;

    if ((AQerrNum = AI_Clear(board1))!=0)
        DAQ_error("AI_Clear 1",1120);
    if ((AQerrNum = AI_Clear(board2))!=0)
        DAQ_error("AI_Clear 2",1130);
    if ((AQerrNum = DAQ_Config(board1,trigger,0))!=0)
        DAQ_error("DAQ_Config 1",1140);
    if ((AQerrNum = DAQ_Config(board2,trigger,0))!=0)
        DAQ_error("DAQ_Config 2",1150);
    if ((AQerrNum = DAQ_DB_Config(board1,0))!=0)
        DAQ_error("DAQ_DB_Config 1",1160);
    if ((AQerrNum = DAQ_DB_Config(board2,0))!=0)
        DAQ_error("DAQ_DB_Config 2",1170);
    buff_index = 1;
    _settextposition(20,1);
    printf("acquiring data . . . .");
    scan_int = 1000000.0/data.scan_rate;
    if ((AQerrNum = SCAN_Setup(board1,num_chans,data.chan_seq1,
        data.gain_seq1))!=0)
        DAQ_error("SCAN_Setup 1",1180);
    if ((AQerrNum = SCAN_Setup(board2,num_chans,data.chan_seq2,
        data.gain_seq2))!=0)
        DAQ_error("SCAN_Setup 2",1190);
    if ((AQerrNum = SCAN_Start(board1,exp_buff1,num_samples,1,50,1,
        scan_int)) != 0)
    {
        DAQ_error("SCAN_Start 1",1200);
        exitNum=4;
        return exitNum;
    }
    if ((AQerrNum = SCAN_Start(board2,exp_buff2,num_samples,1,50,1,
        scan_int)) != 0)
    {
        DAQ_error("SCAN_Start 2",1210);
        exitNum=4;
        return exitNum;
    }
    while (buff_index < 2*num_chans)
        if ((AQerrNum = DAQ_Check(board1, &AQStatus,&buff_index))!=0)
            DAQ_error("DAQ_Check",1220);
    do
        /* Check acquisition progress, display and control */
    {
        if((AQerrNum = DAQ_Monitor(board1,-1,0,num_chans,monitor_buff,
            &buff_index,&AQStatus))!=0)
            DAQ_error("DAQ_Monitor 1",1230);
        if((AQerrNum = DAQ_Monitor(board2,-1,0,num_chans,&monitor_buff[num_chans],
            &buff_index,&AQStatus))!=0)
            DAQ_error("DAQ_Monitor 2",1240);
        if (kbhit()) exitNum=getch();
        display_last_data();
        trim_control(exitNum);
        load_control(exitNum);
        if (exitNum != 27) exitNum = 0;
    } while (!(AQStatus) && (exitNum != 27));
    if ((AQerrNum = DAQ_Clear(board1))!=0)
        DAQ_error("DAQ_Clear 1",1250);
    if ((AQerrNum = DAQ_Clear(board2))!=0)

```

```

    DAQ_error("DAQ_Clear 2",1260);
    return exitNum;
}

/*****/

int trim_control(Num)      /* adjust trim as necessary */
int Num;
{
    int ii;
    if (Num > 0)
    {
        switch (Num)
        {
            case 56:
                Tp *= gain_adjust;
                tensadj[0] = Tp + 0.5*Ti*deltaT + Td/deltaT;
                tensadj[1] = -Tp + 0.5*Ti*deltaT - 2*Td/deltaT;
                tensadj[2] = Td*deltaT;
                break;
            case 53:
                Tp /= gain_adjust;
                tensadj[0] = Tp + 0.5*Ti*deltaT + Td/deltaT;
                tensadj[1] = -Tp + 0.5*Ti*deltaT - 2*Td/deltaT;
                tensadj[2] = Td*deltaT;
                break;
            case 57:
                Ti *= gain_adjust;
                tensadj[0] = Tp + 0.5*Ti*deltaT + Td/deltaT;
                tensadj[1] = -Tp + 0.5*Ti*deltaT - 2*Td/deltaT;
                tensadj[2] = Td*deltaT;
                break;
            case 54:
                Ti /= gain_adjust;
                tensadj[0] = Tp + 0.5*Ti*deltaT + Td/deltaT;
                tensadj[1] = -Tp + 0.5*Ti*deltaT - 2*Td/deltaT;
                tensadj[2] = Td*deltaT;
                break;
        }
        _settextposition (23,40);
        printf("Trim gains: Tp= %f, Ti = %f",Tp,Ti);
    }
    avg_tens = smoothfact*avg_tens + (1-smoothfact)*monitor_buff[tenschan];
    tenserr[0] = TMid - avg_tens;          /* compute deviation */
    for (ii=0;ii<3;ii++)
        trim_bits -= tensadj[ii]*tenserr[ii];    /* compute corection */
    if (trim_bits > max_trim_bits) trim_bits = max_trim_bits;
    else if (trim_bits < min_trim_bits) trim_bits = min_trim_bits;
    tenserr[2] = tenserr[1];              /* save current deviation . . . */
    tenserr[1] = tenserr[0];              /* . . . for next loop */
    if ((AQerrNum = AO_Write(board2, 0, trim_bits))!=0)
        DAQ_error("AO_Write",1300);      /* Output new value to trim */
    _settextposition(22,62);
    printf("trimming %d bits    ",trim_bits);
}

/*****/

int load_control(Num)      /* adjust load as necessary */
int Num;
{
    int ii;
    float load_corr = 0.0250;

    if (Num > 0 )
    {

```

```

switch (Num)
{
  case 43:
    if (load_dir[load_sel] == 1)          /* adjust gains if neccessary */
      load_bits *= (1+load_corr);        /* remove once controller is fully
*/
    else                                  /* debugged. */
      load_bits *= (1-load_corr);
    break;
  case 45:
    if (load_dir[load_sel] == 1)
      load_bits *= (1-load_corr);
    else
      load_bits *= (1+load_corr);
    break;
}
_settextposition(22,40);
printf("loading %d bits; ",load_bits);
}
/*
loaderr[0] = LMid - monitor_buff[loadchan];
if (load_dir[load_sel] = 8)
{
  for (ii=0;ii<3;ii++)
    load_bits -= loadadj[ii]*loaderr[ii];
}
if (load_bits > max_load_bits) load_bits = load_bits;
else if (load_bits < min_load_bits) load_bits = min_load_bits;
loaderr[2] = loaderr[1];
loaderr[1] = loaderr[0];
*/
if ((AQerrNum = AO_Write(board1, 1, load_bits))!=0)
  DAQ_error("AO_Write",1350);
}

/*****/

get_last_data()
{
  int ii;
  for (ii=0; ii<num_chans;ii++)
    if ((AQerrNum = AI_Read(board1,ii,data.gain_seq1[ii],
      &monitor_buff[ii]))!=0)
      DAQ_error("AI_Read 1",1420);          /* read 8 channels from each
board */
  for (ii=num_chans; ii<(2*num_chans);ii++)
    if ((AQerrNum = AI_Read(board2,(ii-num_chans),
      data.gain_seq2[ii-num_chans],&monitor_buff[ii]))!=0)
      DAQ_error("AI_Read 2",1430);
  return;
}

/*****/

display_last_data()      /* convert and display latest data */
{
  int ii;
  _settextposition(13,1);
  for (ii=0; ii<(2*num_chans);ii++)
    printf("%4.0f ",(cons[0][ii]+monitor_buff[ii]*(cons[1][ii]
      +cons[2][ii]*monitor_buff[ii]));
  /* _settextposition (14,1);
  for (ii=0; ii<(2*num_chans);ii++)
    printf("%4d ",monitor_buff[ii]);
*/
  _settextposition(21,30);
  printf("%6u",buff_index);
  return;
}

```

```

}
/*****/
write_data()          /* update parameter file */
{
    FILE *x;
    int i,
        j,
        endblock = 10000;

    if ((x=fopen(par_file,"wt")) != NULL)
    {
        fprintf(x,"%5.3f\n",data.dry_bulb);
        fprintf(x,"%5.3f\n",data.dew_pt);
        fprintf(x,"%5.3f\n",data.baro);
        fprintf(x,"%5.3f\n",data.rel_hum);
        fprintf(x,"%5.3f\n",data.calroll_d1);
        fprintf(x,"%d\n",data.calroll_n1);
        fprintf(x,"%5.3f\n",data.calroll_d2);
        fprintf(x,"%d\n",data.calroll_n2);
        fprintf(x,"%5.3f\n",data.bas_wt);
        fprintf(x,"%s\n",data.pap_type);
        fprintf(x,"%8.2lf\n",data.s_rate);
        fprintf(x,"%8.2lf\n",data.scan_rate);
        for (i=0; i<num_chans; i++)
            fprintf(x,"%1d\t",data.chan_seq1[i]);
        fprintf(x,"\n");
        for (i=0; i<num_chans; i++)
            fprintf(x,"%3d\t",data.gain_seq1[i]);
        fprintf(x,"\n");
        for (i=0; i<num_chans; i++)
            fprintf(x,"%1d\t",data.chan_seq2[i]);
        fprintf(x,"\n");
        for (i=0; i<num_chans; i++)
            fprintf(x,"%3d\t",data.gain_seq2[i]);
        fprintf(x,"\n");
        for (i=0; i<7 ; i++)
            fprintf(x,"%1d\t",data.sens_seq[i]);
        fprintf(x,"\n");
        for (i=0; i<7 ; i++)
            fprintf(x,"%5.2f\t",data.volt_seq[i]);
        fprintf(x,"\n%6.2f",data.i_vel);
        fprintf(x,"\n%4d\n",data.file_no);
    }
    else
    {
        perror("write error: can't open DINFO2.TXT for writing");
        exit(1);
    }
    fclose(x);
    return;
}
/*****/

data_screen()        /* display parameters */
{
    _clearscreen(_GCLEARSCREEN);
    printf(" World's Narrowest Calender Data Acquisition Program Version 936.51b\n");
    printf("C. THESE VALUES ARE CORRECT\n");
    printf("1. Dry bulb temperature           \t\t\t%5.3f\n",data.dry_bulb);
    printf("2. Dew point temperature           \t\t\t%5.3f\n",data.dew_pt);
    printf("3. Barometric pressure           \t\t\t%5.3f \n",data.baro);
}

```

```

printf("4. Relative humidity                \t\t\t%5.3f\n",data.rel_hum);
printf("5. top calender reel - diameter (cm): \t\t\t%5.3f\n",data.calroll_d1);
printf("6.                                - id #: \t\t\t %d\n",data.calroll_n1);
printf("7. bottom calender reel -diameter (cm): \t\t\t%5.3f\n",data.calroll_d2);
printf("8.                                -id #: \t\t\t %d\n",data.calroll_n2);
printf("9. basis weight (Kg):                \t\t\t%5.3f\n",data.bas_wt);
printf("10. paper type:                       \t\t\t %s\n",data.pap_type);
printf("11. scan rate-one channel (scan/sec): \t\t\t%8.2lf\n",data.s_rate);
printf("12.                                -all channels (scan/sec):\n",data.scan_rate);
printf("\n--      Edit INFO.TXT to alter Gain vector      --\n\n");
printf("17. initial velocity (m/min):          \t\t\t%6.2f\n",data.i_vel);
printf("18. file number:                          \t\t\t %4d\n",data.file_no);
_settextposition(22,1);
return;
}

```

/*-----*/

```

int change(ch1)          /* alter selected parameter */
char ch1;               /* first character of inputted choice */
{
    int  ascii,         /* ascii value */
        x,
        i;
    char temp[100],
        y[3];          /* final choice to input data */

    strcpy(y, &ch1);
    ch1 = getche();
    ascii = toascii(ch1);
    if (ascii != 13)
    {
        strcpy (y + 1, &ch1);
        ch1 = getch();
    }
    x=atoi(y);
    if ((x>0) && (x<=18))
    {
        clrhl((x+2),40,38);
        _settextposition((x+2),66);
        if ((x!=11) && (x!=12))
            scanf("%s", temp );
        if (x==1)
            data.dry_bulb=atof( temp );
        else if (x==2)
            data.dew_pt = atof( temp );
        else if (x==3)
            data.baro = atof( temp );
        else if (x==4)
            data.rel_hum = atof( temp );
        else if (x==5)
            data.calroll_d1 = atof( temp );
        else if (x==6)
            data.calroll_n1 = atoi( temp );
        else if (x==7)
            data.calroll_d2 = atof( temp );
        else if (x==8)
            data.calroll_n2 = atoi( temp );
    }
}

```

```

else if (x==9)
    data.bas_wt = atoi( temp );
else if (x==10)
    strcpy(data.pap_type, temp);
else if (x==11)
    scanf("%lf",&data.s_rate);
else if (x==12)
    scanf("%lf",&data.scan_rate);
else if (x==17)
{
    data.i_vel = atof( temp );
    data.scan_rate =
20*ceil(0.05*num_scans*data.i_vel/(3.1416*60*data.calroll_d1*minrevs));
    clearl((14),40,38);
    _settextposition((14),66);
    printf("%8.2lf",data.scan_rate);
}
else if (x==18)
    data.file_no = atoi( temp );
}
return;
}

/*****/

int txconvert (filenum)          /* convert raw binary file . . . */
int filenum;                    /* . . . to .PRN files */
{
    FILE *dtabin;
    int i,
        end,
        temp,
        trial = 0,
        ch = 96;
    char file_[10];

    _settextposition (21,1);
    printf("Reading file: %s",file_name);
    if ((dtabin = fopen(file_name, "rb")) == NULL)
    {
        printf("error opening file");
        exit(1);
    }
    itoa(filenum,file_,10);
    for (i=0;i<8;i++)
    {
        fread (&end, sizeof(end), 1, dtabin);
    }
    do
    {
        trial++;
        ch++;
        clearl(22,1,78);
        printf("Reading trial %d; ",trial);
        fread (&ddate, sizeof(ddate), 1, dtabin);
        fread (&dtime, sizeof(dtime), 1, dtabin);
        fread (&data, sizeof(data), 1, dtabin);
        fread (cons, sizeof(cons), 1, dtabin);
        fread (&deltaV, sizeof(deltaV), 1, dtabin);
        fread (&VinCount, sizeof(VinCount), 1, dtabin);
        fread (&VoutCount, sizeof(VoutCount), 1, dtabin);
        fread (&ClockCount, sizeof(ClockCount), 1, dtabin);
        for (i=0; i<4; i++)
            fread (&temp, sizeof(temp), 1, dtabin);
        fread (&exp_buff1[0], sizeof(exp_buff1[0]), num_samples, dtabin);
        fread (&exp_buff2[0], sizeof(exp_buff2[0]), num_samples, dtabin);
        for (i=0;i<8;i++)

```

```

    {
        fread (&end, sizeof(end), 1, dtabin);
    }
    average();
    svetxt(file_,ch);
} while (end != 11111);
fclose(dtabin);
}

/*****/

average()          /* average and de-multiplex data */
{
    int divisor,
        ch,
        sc,
        i;
    float tempC12 = 0.0,
          tempC13 = 0.0;

    printf ("adding; ");
    sc = 0;
    for (ch=0;ch<num_chans;ch++)          /* First channel scan */
    {
        outbuff1[sc][ch]=0.0;
        outbuff2[sc][ch]=0.0;
        avg_data1[ch]=0.0;
        avg_data2[ch]=0.0;
        for (i=0;i<num_avg+1;i++)        /* add data from first num_avg+1 scans */
        {
            outbuff1[sc][ch] += exp_buff1[i*num_chans+ch];
            outbuff2[sc][ch] += exp_buff2[i*num_chans+ch];
            avg_data1[ch] += exp_buff1[i*num_chans+ch];
            avg_data2[ch] += exp_buff2[i*num_chans+ch];
        }
    }

    for (sc=1;sc<(num_saved-1);sc++)      /* Scans 2 through 2047 */
    {
        for (ch=0;ch<num_chans;ch++)
        {
            outbuff1[sc][ch]=0.0;
            outbuff2[sc][ch]=0.0;
            for (i=-num_avg;i<num_avg+1;i++) /* add data from 9 scans about the
current one */
            {
                outbuff1[sc][ch] += exp_buff1[(num_avg*sc+i)*num_chans+ch];
                outbuff2[sc][ch] += exp_buff2[(num_avg*sc+i)*num_chans+ch];
                avg_data1[ch] += exp_buff1[i*num_chans+ch];
                avg_data2[ch] += exp_buff2[i*num_chans+ch];
            }
        }
    }

    sc = num_saved-1;
    for (ch=0;ch<num_chans;ch++)          /* last channel scan */
    {
        outbuff1[sc][ch]=0;
        outbuff2[sc][ch]=0;
        for (i=-num_avg;i<num_avg+1;i++)  /* add data from last scans */
        {
            outbuff1[sc][ch] += exp_buff1[(num_avg*sc+i)*num_chans+ch];
            outbuff2[sc][ch] += exp_buff2[(num_avg*sc+i)*num_chans+ch];
            avg_data1[ch] += exp_buff1[i*num_chans+ch];
            avg_data2[ch] += exp_buff2[i*num_chans+ch];
        }
    }
}

```

```

printf ("averaging; ");          /* divide sums by appropriate divisors
*/
divisor = num_avg+1;
sc = 0;
for (ch=0;ch<num_chans;ch++)    /* and convert to real variables */
{
    outbuff1[sc][ch] = cons[0][ch]
        +outbuff1[sc][ch]*(cons[1][ch]+
        cons[2][ch]*outbuff1[sc][ch]/divisor)/divisor;
    outbuff2[sc][ch] = cons[0][ch+num_chans]
        +outbuff2[sc][ch]*(cons[1][ch+num_chans]+
        cons[2][ch+num_chans]*outbuff2[sc][ch]/divisor)/divisor;
    avg_data1[ch] = avg_data1[ch]/num_scans;
    avg_data2[ch] = avg_data2[ch]/num_scans;
}
tempC12 += outbuff2[sc][2];      /* compute average for C12 and C13 */
tempC13 += outbuff2[sc][3];

divisor = 2*num_avg+1;
for (sc=1;sc<(num_saved-1);sc++)
{
    for (ch=0;ch<num_chans;ch++)
    {
        outbuff1[sc][ch] = cons[0][ch]
            +outbuff1[sc][ch]*(cons[1][ch]+
            cons[2][ch]*outbuff1[sc][ch]/divisor)/divisor;
        outbuff2[sc][ch] = cons[0][ch+num_chans]
            +outbuff2[sc][ch]*(cons[1][ch+num_chans]+
            cons[2][ch+num_chans]*outbuff2[sc][ch]/divisor)/divisor;
    }
    tempC12 += outbuff2[sc][2];
    tempC13 += outbuff2[sc][3];
}

divisor = 2*num_avg;
sc = num_saved-1;
for (ch=0;ch<num_chans;ch++)
{
    outbuff1[sc][ch] = cons[0][ch]
        +outbuff1[sc][ch]*(cons[1][ch]+
        cons[2][ch]*outbuff1[sc][ch]/divisor)/divisor;
    outbuff2[sc][ch] = cons[0][ch+num_chans]
        +outbuff2[sc][ch]*(cons[1][ch+num_chans]+
        cons[2][ch+num_chans]*outbuff2[sc][ch]/divisor)/divisor;
}
tempC12 += outbuff2[sc][2];
tempC13 += outbuff2[sc][3];
tempC12 /= num_saved;
tempC13 /= num_saved;
/*
for (sc=0;sc<num_saved;sc++)
{
    tempC12 = smoothfact*tempC12 + (1-smoothfact)*outbuff2[sc][2];
    tempC13 = smoothfact*tempC13 + (1-smoothfact)*outbuff2[sc][3];
    outbuff2[sc][2] = tempC12;
    outbuff2[sc][3] = tempC13;
}
*/
}

/*****/

svetxt(file1,chext)              /* save converted data after averaging */
char file1[50];
char chext;
{

```

```

FILE *dtatxt;
int length,
    pdest,
    divisor,
    ch,
    sc,
    j, k;
char ext[5],
    file[50];

strcpy (firstprn,"c:\\dariusz\\data\\experime");
strcpy (prn,".prn");
strcpy(file,file1);

pdest = strcpy( firstprn + 16, file );
length = strlen(firstprn);
pdest = strcpy( firstprn + length, &chext );
length = strlen(firstprn);
pdest = strcpy( firstprn + length, prn );
pdest = strcpy( file , firstprn);

dtatxt = fopen(file, "wt");
save_data(file,chext,dtatxt);

for (sc=0;sc<num_saved;sc++)
{
    for (ch=0;ch<num_chans;ch++)
        fprintf(dtatxt,"%4.8f, ",outbuff1[sc][ch]);
    for (ch=0;ch<num_chans;ch++)
        fprintf(dtatxt,"%4.8f, ",outbuff2[sc][ch]);
    fprintf (dtatxt,"\n");
}
fclose(dtatxt);
}

/*****

save_data(file,ext,dtatxt)      /* save parameters with converted data */
char file[50],
    ext;
FILE *dtatxt;
{
int j, k;

printf("writing file: %s\n",file);
fprintf(dtatxt,"\"DATE: \"\"%u/%u/%u\" \"TIME: \"\"%u/%u/%u\" \"\n",ddate.day,
    ddate.month,ddate.year, dtime.hour, dtime.minute,dtime.second);
fprintf(dtatxt,"\"Dry bulb \"      %5.3f  \n",data.dry_bulb);
fprintf(dtatxt,"\"Dew point \"      %5.3f  \n",data.dew_pt);
fprintf(dtatxt,"\"Barometer \"      %5.3f  \n",data.baro);
fprintf(dtatxt,"\"R.H. \"          %5.3f  \n",data.rel_hum);
fprintf(dtatxt,"\"TrollD \"       %5.3f  \n",data.calroll_d1);
fprintf(dtatxt,"\"id \"           %d  \n",data.calroll_n1);
fprintf(dtatxt,"\"BrollD \"      %5.3f  \n",data.calroll_d2);
fprintf(dtatxt,"\"id \"           %d  \n",data.calroll_n2);
fprintf(dtatxt,"\"BW \"           %5.3f  \n",data.bas_wt);
fprintf(dtatxt,"\"paper type\" \"  %s\" \"\n",data.pap_type);
fprintf(dtatxt,"\"CRate \"       %8.2lf\n",data.s_rate);
fprintf(dtatxt,"\"SRate \"       %8.2lf,
%8.2lf\n",data.scan_rate,data.scan_rate/num_avg);
fprintf(dtatxt,"\"channel v:\"");
for (j=0; j<8 ; j++)
    fprintf(dtatxt,"%1d      ",data.chan_seq1[j]);
for (j=0; j<8 ; j++)
    fprintf(dtatxt,"%1d      ",data.chan_seq2[j]);
fprintf(dtatxt,"\"gain v: \"");
for (j=0; j<8 ; j++)

```

```

    fprintf(dtatxt, "%3d      ", data.gain_seq1[j]);
    for (j=0; j<8 ; j++)
        fprintf(dtatxt, "%3d      ", data.gain_seq2[j]);
    fprintf(dtatxt, "\n\"sensor v: \"");
    for (j=0; j<7 ; j++)
        fprintf(dtatxt, "%1d      ", data.sens_seq[j]);
    fprintf(dtatxt, "\n\"Vin,Vout,Clock,DeltaV:\" %5u %5u %5u %6.6f",
            VinCount,VoutCount,ClockCount,deltaV);
    fprintf(dtatxt, "\n\"Vel\"          %6.2f %6.2f", data.i_vel, data.i_vel);
    fprintf(dtatxt, "\n\"file:\" %4d \" %c \"\n", data.file_no, ext);
    fprintf(dtatxt, "\n\"calibration \" \n");
    for (j=0; j<3; j++)
    {
        for (k=0; k<(2*num_chans); k++)
            fprintf(dtatxt, "%8f, ", cons[j][k]);
        fprintf(dtatxt, "\n");
    }

fprintf(dtatxt, "\n\"T0\" \"T1\" \"dT2\" \"dT3\" \"t4\" \"t5\" \"L6\" \"t\"
V7\" \"t");

fprintf(dtatxt, "\"N10\" \"N11\" \"C12\" \"C13\" \"X14\" \"X15\" \"T16\" \"
t\" \"M17\" \"t\n");
}

/*****/

int DAQ_error(err_msg, location) /* general error message handler */
char err_msg[30];
int location;
{
    _settextposition(xerror, yerror);
    printf("%s error # %d at %d", err_msg, AQerrNum, location);
    return;
}

/*****/

int eexit(int x) /* emergency exit subroutine */
{
    time_t etstart, etstop;
    float emerg_time;
    if ((AQerrNum = DIG_Out_Port(board1, 1, emerg_stop_mask)) != 0)
        DAQ_error("DIG_Out_Port", 3000);
    if ((AQerrNum = AO_Write(board1, 0, 0)) != 0)
        DAQ_error("AO_Write 1", 3010);
    if ((AQerrNum = AO_Write(board1, 1, 4000)) != 0)
        DAQ_error("AO_Write 1", 3020);
    if ((AQerrNum = AO_Write(board2, 0, 0)) != 0)
        DAQ_error("AO_Write 2", 3030);
    if ((AQerrNum = AO_Write(board2, 1, 4000)) != 0)
        DAQ_error("AO_Write 2", 3040);
    motor_bits = 0;
    _settextposition(xerror, yerror);
    printf ("Emergency stop");
    _settextposition(xerror+1, yerror);
    printf ("error # %d", x);
    _settextposition(xerror+2, yerror);
    if (x==1)
        printf("subroutine EXPRMNT");
    else if (x==2)
        printf("subroutine WAIT");
    else if (x==3)
        printf("subroutine MOTOR");
    else if (x==4)
        printf("subroutine SCAN_Start");
    else if (x==5)

```

```

    printf("subroutine MAIN");
    _settextposition (xerror+3,yerror);

    time (&etstart);
    do
        /* Wait */
        {
            time (&etstop);
            emerg_time = difftime(etstop,etstart);
        }
        while (emerg_time < lift_time);

        if((AQerrNum = AO_Write(board1,1,brake_reel_mask)) !=0) /* Load off,
leave brake on */
            DAQ_error("AO_Write Load",3050);

        printf("Press a key to exit:");
        return x;
    }

/*****/

int clear(row,column,num) /* Clear n lines */
int row,
    column,
    num;
{
    int i,j;
    _settextposition(row,column);
    for (j=column;j<79;j++)
        printf(" ");
    printf("\n");
    for (i=1;i<num;i++)
    {
        for (j=0;j<79;j++)
            printf(" ");
        printf("\n");
    }
    _settextposition(row,column);
    return;
}

/*****/

int clearl(row,column,num) /* Clear n spaces */
int row,
    column,
    num;
{
    int i;
    _settextposition(row,column);
    for (i=0;i<num;i++)
        printf(" ");
    _settextposition(row,column);
    return;
}

/*****/

```